ISSN (1230-0322)
2026, Vol. 76, No. 3

Food

Polish Journal of Food and Nutrition Sciences

formerly Acta Alimentaria Polonica

Published
by InLife Institute of Animal Reproduction and Food Research, Polish Academy of Sciences, Olsztyn

Published since 1957 as
Roczniki Chemii i Technologii Żywności and Acta Alimentaria Polonica (1975–1991)

SCOPE: The Journal covers fundamental and applied research in food area and nutrition sciences with a stress on interdisciplinary studies in the areas of food, nutrition and related subjects.

POLICY: Editors select submitted manuscripts in relation to their relevance to the scope. Reviewers are selected from the Advisory Board and from Polish and international scientific centres. Identity of reviewers is kept confidential.

AUTHORSHIP FORMS referring to Authorship Responsibility, Conflict of Interest and Financial Disclosure, Copyright Transfer and Acknowledgement, and Ethical Approval of Studies are required for all authors.

FREQUENCY: Quarterly – one volume in four issues (March, June, September, December).

COVERED by Web of Science, Current Contents/Agriculture, Biology & Environmental Sciences, Journal Citation Reports and Science Citation Index Expanded, BIOSIS (Biological Abstracts), SCOPUS, FSTA (formerly: Food Science and Technology Abstracts), CAS (Chemical Abstracts), AGRICOLA, AGRO-LIBREX data base, EBSCO, FOODLINE, Leatherhead FOOD RA data base FROSTI, AGRIS, Biblioteka Nauki ICM, Biblioteka Narodowa – POLONA, and any www browser; ProQuest: The Summon, Bacteriology Abstracts, Immunology Abstracts.

EDITORIAL AND BUSINESS CORRESPONDENCE: Submit contributions (see Instructions to Authors) and address all communications regarding subscriptions, changes of address, etc. to:

CORRESPONDENCE TO: Ms. Joanna Molga
Polish Journal of Food and Nutrition Sciences
InLife Institute of Animal Reproduction and Food Research,
Polish Academy of Sciences,
ul. Trylińskiego 18, 10-683 Olsztyn, Poland
e-mail: pjfns@pan.olsztyn.pl; http://journal.pan.olsztyn.pl

Polish Journal of Food and Nutrition Sciences

ADVISORY BOARD OF PJFNS 2023–2026

Contents

ORIGINAL PAPERS

Subscription
Since 2025, PJFNS is published only on-line. Past issues can be ordered as previously. One volume,
four issues per volume. Annual subscription rates are: Poland 150 PLN, all other countries 80 EUR.
Prices are subject to exchange rate fluctuation. Subscription payments should be made by direct bank transfer to
Bank Gospodarki Żywnościowej, Olsztyn, Poland, account No 17203000451110000000452110 SWIFT code: GOPZPLWOLA
with corresponding banks preferably. Subscription and advertising offices at the Institute of Animal Reproduction
and Food Research of Polish Academy of Sciences, ul. Trylińskiego 18, 10-683 Olsztyn, Poland, tel./fax (48 89) 5003245,
e-mail: pjfns@pan.olsztyn.pl; http://journal.pan.olsztyn.pl

Wersja pierwotna (referencyjna) kwartalnika PJFNS: wersja on-line (eISSN 2083-6007)
Ark. wyd. 18
Skład: ITEM

ORIGINAL ARTICLE
http://journal.pan.olsztyn.pl

Polish Journal of Food and Nutrition Sciences
2026, Vol. 76, No. 3, 228–241
DOI: 10.31883/pjfns/225064
ISSN 1230-0322, e-ISSN 2083-6007

Impact of Osmotic Dehydration and Lactic Acid Fermentation of Onion on the Physiological Effects in Rats

Jerzy Juśkiewicz[1]*, Katarzyna Grzelak-Błaszczyk[2], Dorota Napiórkowska[1], Sylwia Ścieszka[3], Lidia Piekarska-Radzik[3], Elżbieta Klewicka[3], Katarzyna Jaworska[1], Joanna Fotschki[4], Michał Sójka[2], Robert Klewicki[2], Maria Grzegorzewska[5], Bartosz Fotschki[4]

[1]Biological Function of Food Team, InLife Institute of Animal Reproduction and Food Research, Polish Academy of Sciences, Trylińskiego 18, 10-683 Olsztyn, Poland
[2]Institute of Food Technology and Analysis, Lodz University of Technology, Stefanowskiego 2/22, 90-537 Łódź, Poland
[3]Institute of Fermentation Technology and Microbiology, Lodz University of Technology, Wólczańska 171/173, 90-530 Łódź, Poland
[4]Immunology and Food Microbiology Team, InLife Institute of Animal Reproduction and Food Research, Polish Academy of Sciences, Trylińskiego 18, 10-683 Olsztyn, Poland
[5]The National Institute of Horticultural Research, Konstytucji 3 Maja 1/3, 96-100 Skierniewice, Poland

This study investigated the effects of four different dietary onion (*Allium cepa* L.) preparations from the new Allurion variety on body composition, metabolic parameters, hepatic gene expression, and gut microbial activity in healthy male Wistar rats. Fifty 7-week old rats were randomly assigned to five dietary groups and fed semi-purified diets for four weeks: control, untreated onion, osmotically dehydrated onion with a glucose-fructose syrup, and dehydrated onion further subjected to lactic acid fermentation with *Levilactobacillus brevis* ŁOCK 944 and *Lactiplantibacillus plantarum* P27. Body weight, feed intake, and body composition were monitored, and blood, liver, and cecal samples were collected for biochemical, enzymatic activity, bile acid, short-chain fatty acid, and gene expression analyses. Dietary onion preparations reduced hepatic expression of lipogenic genes *Hif1a*, *Scd1*, and *Acly*, indicating anti-lipogenic effects. Osmotic dehydration boosted these benefits by suppressing inflammatory and lipogenic genes (*Nfkb1*, *Srebf1*, *Tlr4*) and improving plasma markers of liver function and lipid metabolism. Fermentation had a preparation-specific impact on liver genes that regulate fatty acid oxidation, bile acid metabolism, and inflammation. The percentage of lean tissue decreased in dehydrated onion-fed rats, yet there were no changes in their overall body weight, and fermentation did not further affect their body composition. Cecal enzyme activities and bile acid profiles were modulated, reflecting favorable gut microbial activity. These findings demonstrate that dietary onion, particularly when processed *via* osmotic dehydration and selective fermentation, can beneficially modulate hepatic gene expression, plasma biochemistry, and gut microbial function, supporting its potential as a functional dietary component to promote metabolic health.

Keywords: intestine, liver, microbial acidification, onion, osmotic drying, rat

ABBREVIATIONS

AC, atherogenic coefficient; AIP, atherogenic index of plasma; BA, bile acid; C, control diet (group); G, diet (group) with 2% (*w/w*) of untreated onion preparation; GD, diet (group) with 2% (*w/w*) of onion preparation obtained by osmotic dehydration in a glucose-fructose syrup; GDFa, diet (group) with 2% (*w/w*) of onion preparation obtained by osmotic dehydration in a glucose-fructose syrup and fermentation with *Levilactobacillus brevis* ŁOCK 944; GDFb, diet (group) with 2% (*w/w*) of onion preparation obtained by osmotic dehydration in a glucose-fructose syrup

***Corresponding Author:**
E-mail: **j.juskiewicz@pan.olsztyn.pl** (Prof. J. Juśkiewicz)

Submitted: 2 April 2026
Accepted: 25 June 2026
Published on-line: 7 July 2026

and fermentation with *Lactiplantibacillus plantarum* P27; PSCFA, putrefactive short-chain fatty acids; SCFA, short-chain fatty acids.

INTRODUCTION

Onion (*Allium cepa* L.) is a widely consumed vegetable rich in vitamins and bioactive compounds, including flavonoids (such as quercetin), sulfur-containing compounds, and prebiotic fibers, which together exert diverse health-promoting effects. Regular intake of onion has been associated with improvements in cardiometabolic risk factors, including reductions in body weight, waist circumference, blood lipid levels, and markers of glucose metabolism in humans, particularly with longer supplementation periods or higher daily doses (>300 mg/day), as shown in randomized trials and meta-analyses [Hejazi *et al*., 2023]. This metabolic modulation likely reflects potent antioxidant and anti-inflammatory effects of onion, which support cardiovascular health through lipid and blood pressure reduction, endothelial function improvement, as well as potential antidiabetic effects *via* enhanced glycemic control [Li *et al*., 2020]. Onions also contain significant levels of prebiotic fructans that favorably influence gut microbiota composition and short-chain fatty acid production, contributing to digestive health and systemic metabolic benefits, and their flavonoid content has been linked to reduced oxidative stress [Benítez *et al*., 2011; Gupta *et al*., 2025].

Osmotic dehydration is a mild food processing technique in which plant tissues are partially dehydrated in a hypertonic solution, leading to water removal while limiting high-temperature exposure and preserving key quality attributes of fruits and vegetables. Compared with conventional high-heat drying methods, osmotic dehydration can help retain important bioactive compounds, including phenolic compounds [Yazidi *et al*., 2024]. Studies on onion have shown that significant amounts of flavonols, such as quercetin derivatives, can be preserved or stabilized during osmotic dehydration, suggesting that this process may enhance the functional value of dried onion preparations while improving their texture and shelf stability [Grzelak-Błaszczyk *et al*., 2021]. Despite several studies on osmotic dehydration and compositional changes in plant foods, in the current scientific literature there are no published *in vivo* animal or human trials testing health endpoints (*e.g.*, blood cholesterol and triglyceride content, liver enzyme activity) specifically after consumption of osmotically dehydrated vegetables or fruit.

Osmotic dehydration prior to further processing has been shown to affect the retention and stability of bioactive compounds, indicating that careful selection of dehydration conditions can help maintain nutritional quality of dried onion products. Subsequent lactic acid fermentation of osmodehydrated onion allows for the development of fermented products with potentially enhanced functional properties. It has been shown that fermentation does not adversely affect phenolic content and may even improve the profile of beneficial organic acids without compromising the availability of fructooligosaccharides [Grzelak-Błaszczyk *et al*., 2023]. Fermentation processes are also known to increase the bioavailability of phenolic compounds and modify carbohydrate profiles in plant foods, which can lead to increased antioxidant activity and greater potential for modulating gut health [Nowak *et al*., 2025].

The goal of this study was to thoroughly evaluate the efficacy of osmotic dehydration techniques utilizing a glucose-fructose syrup solution. This was done both as a standalone method and in combination with lactic acid fermentation processes. The aim was to develop innovative preparations from onion of the Allurion variety with enhanced functional properties. The research also focused on investigating the *in vivo* effects of these specially formulated preparations on large intestinal function and various metabolic parameters in rats, providing a comprehensive understanding of their potential health benefits.

MATERIALS AND METHODS

Onion preparation

The preparations were made from red-skinned onion of the Allurion variety grown at the Institute of Horticulture in Skierniewice, Poland. After harvest, the bulbs were stripped of inedible parts and cut lengthwise into eight pieces. Then, five times the amount of the hypertonic solution was added. Osmoconcentration was carried out using a 50% glucose-fructose syrup (Kemikals, Gdynia, Poland) and a 5% sodium chloride (Chempur, Piekary Śląskie, Poland) solution, in a water bath with a shaker (GFL 1086, Lauda GFL, Burgwedel, Germany) at 25°C and a shaking frequency of 150 cycles/min for 2 h. After osmotic dehydration, the onion samples were double-rinsed with water for 5 s, blotted dry, and then one-third of the samples were lyophilized using an Alpha 1-2 LDplus lyophilizer (Christ, Osterode am Harz, Germany) at a vacuum of 0.26 mbar for 48 h. The remaining samples were immersed in sterile water at a ratio of 50 g of the material *per* 100 mL and divided into two parts. Each experimental variant was inoculated separately with a monoculture prepared from an overnight culture of either *Lactiplantibacillus plantarum* P27 [Ścieszka *et al*., 2025] or *Levilactobacillus brevis* ŁOCK 944 [Klewicka *et al*., 2013]. In each case, the inoculum was added at 10% (*v/v*), providing approximately 10^7 cells/mL. Fermentation was conducted at 30°C for 96 h. After fermentation, the onion was separated from the broth, and the obtained fermented samples were lyophilized under the same conditions as described earlier.

Analysis of onion preparations

The proximate composition of the preparations was determined by AOAC International methods using the following procedures: protein content – 920.152; crude fat – 930.09; dry matter and ash content – 940.26, total dietary fiber (TDF) – 985.29 [Horwitz & Latimer, 2007].

Phenolic compound profile was determined according to the method described by Grzelak-Błaszczyk *et al*. [2020]. Onion preparations weighing 0.5 g (±0.0001 g) were extracted with 70% (*v/v*) methanol for 15 min at room temperature in an IS 4 ultrasonic cleaner (Intersonic S.C., Olsztyn, Poland). The process was repeated three times, and the filtrates from each step were

combined. The extracts were analyzed by the high-performance liquid chromatography (HPLC) method using a Dionex Ultimate 3000 system with a photodiode array (PDA) detector and Chromeleon software (Thermo Fisher Scientific Inc., Waltham, MA, USA). A Kinetex C18 column (100 Å, 150 mm×2.1 mm, 2.6 µm; Phenomenex, Torrance, CA, USA) was used. The mobile phase consisted of solvent A (0.1% formic acid in H_2O, *v/v*) and solvent B (0.1% formic acid in 90% acetonitrile, *v/v*), which were applied in the following gradient program: 0–1 min 5% B; 1–15 min 5%–35% B; 15–17 min 35%–80% B; 17–21 min 80% B; 21–22 min 80–5% B; and 22–30 min 5% B. The injection volume was 5 µL, and the mobile phase flow rate was 0.5 mL/min. Separation was carried out at 35°C. Chromatograms were recorded at a wavelength of 360 nm for flavonols and 520 nm for anthocyanins. The quantification was based on the following standards: quercetin 3,4'-diglucoside, quercetin 4'-glucoside, quercetin 3-*O*-glucoside, quercetin, and cyanidin 3-glucoside chloride (Extrasynthese, Genay, France). The total content of identified phenolic compounds was calculated as the sum of flavonols and anthocyanins and expressed in g/100 g of preparation.

The composition of mono-, di-, and oligosaccharides was determined according to the method described by Grzelak *et al*. [2009] with modifications. An onion preparation of 0.5 g (±0.0001 g) was extracted three times for 15 min using: 2, 1.5, and 1.5 mL of 70% (*v/v*) methanol. This process was carried out in an IS 4 ultrasonic cleaner (Intersonic S.C.) at room temperature. The combined extracts were concentrated using a speed-vacuum centrifuge (ScanSpeed 40, Denmark). Finally, the concentrated solution was diluted with 1 mL of 50% (*v/v*) acetonitrile and analyzed using a Knauer HPLC Smartline system (Berlin, Germany) equipped with a ClarityChrome 5.0.5. data acquisition system and a Knauer refractive index detector (K-2301). Separation was carried out under isocratic conditions on a Shodex NH_2P column (250×4 mm; Shodex, Tokyo, Japan). The mobile phase consisted of acetonitrile and water (68:32, *v/v*) and was used at a flow rate of 0.7 mL/min. The column temperature was maintained at 25°C. The following standards were used: fructose, glucose, sucrose, kestose, and nystose (Merck, Darmstadt, Germany). The total content of identified fructooligosaccharides was calculated as the sum of kestose, nystose, and frutosyl nystose and expressed in g/100 g of preparation.

To enumerate lactic acid bacteria (LAB) in the onion preparation, 1 g of the sample was aseptically transferred into 9 mL of sterile physiological saline (0.9% NaCl) and homogenized thoroughly to obtain the initial 10^{-1} dilution. Serial tenfold dilutions were subsequently prepared using the same diluent. Then, 1-mL dilutions were surface-plated in duplicate onto de Man, Rogosa, and Sharpe (MRS) agar (Merck, Darmstadt, Germany), a selective medium for the cultivation of LAB. The inoculated plates were incubated at 30±1°C for 48 h under anaerobic conditions. After incubation, plates containing 30-300 colonies were selected for enumeration, and the bacterial counts were expressed as $\log_{10}$ colony-forming units *per* gram (log CFU g^{-1}) of onion preparation.

Animals and diet

The experiment included 50 healthy male Wistar (Cmdb: WI) rats, aged 49 days and weighing 183.5 g on average (standard error of the mean: 3.447). This study was conducted in accordance with the approval granted by the Local Institutional Animal Care and Use Committee (Approval No. 41/2022; Olsztyn, Poland, June 15, 2022). We took every precaution to minimize suffering and enhance the welfare of the experimental animals, following the principles outlined in the European Convention for the Protection of Vertebrate Animals Used for Experimental and Other Scientific Purposes, Directive 2010/63/EU. The four-week feeding experiment involved five distinct experimental groups, each with 10 animals (n=10). The group size was calculated to ensure reliable research findings suitable for rigorous statistical analysis, adhering to the 3R principle – replacement, reduction, refinement – for ethical animal research. The rats were randomly assigned and housed individually in stainless steel cages within a controlled environment. Temperature was maintained at 21–22°C with a relative humidity of 60±10%. The facility featured a 12-h day-night cycle and a ventilation system providing 15 air changes *per* hour.

For four weeks, the rats were given unrestricted access to tap water and semi-purified diets. These diets were prepared and subsequently stored at 4°C in airtight containers until the termination of the experiment (details are provided in **Table S1** in Supplementary Materials). The diets were adapted from a casein diet for laboratory rodents as recommended by the American Institute of Nutrition. Five experimental treatments were utilized to assess the effects of four different onion preparations, each added at a 2% (*w/w*) dietary level, replacing an equivalent amount of maize starch (**Table S1**). The control diet was devoid of any onion supplementation. In the experimental onion groups, four lyophilized onion preparations were evaluated: (i) untreated, (ii) osmotically dehydrated using a glucose-fructose syrup solution, (iii) osmotically dehydrated in a glucose-fructose syrup solution followed by lactic acid fermentation using *Lev. brevis* ŁOCK 944 (stain 944), and (iv) osmotically dehydrated with a glucose-fructose syrup solution followed by lactic acid fermentation with *Lb. plantarum* P27 (strain P27).

Sample collection and analyses

The individual feed consumption and body weight gains of the rats were assessed. At the termination of the experiment, the rats were fasted for 8 h before being subjected to time-domain nuclear magnetic resonance (NMR) analysis using a minispec LF 90II analyzer (Bruker, Karlsruhe, Germany) to determine fat and lean tissue mass. The minispec emitted various radio frequency pulse sequences into soft tissues to realign the nuclear magnetic spins of hydrogen and subsequently detected the radio frequency signals generated by these hydrogen spins from the tissues. The contrast in relaxation times of hydrogen spins between adipose tissue and water-rich tissues was utilized to estimate fat and lean body mass. Following the NMR procedure, the rats were anesthetized intraperitoneally using ketamine

(100 mg/kg body weight) and xylazine (10 mg/kg body weight), in accordance with established guidelines for the anesthesia and euthanasia of laboratory rodents. After performing a laparotomy, blood samples were collected from the caudal vena cava into heparinized and ethylenediaminetetraacetic acid tubes, after which the animals were euthanized by cervical dislocation. Blood plasma was obtained through centrifugation at 350×*g* for 10 min at 4°C and stored at −70°C until analysis. Selected internal organs and tissues were then dissected and weighed.

Cecal samples were promptly analyzed for contents of ammonia, dry matter, bile acids, and short-chain fatty acids (SCFA). The remaining digesta were stored at −70°C. Ammonia was extracted using boric acid in Conway dishes and measured through titration with sulfuric acid [Conway, 1957]. The dry matter content was determined by drying to constant weight at 105°C. SCFA profile was analyzed by gas chromatography, where 0.2-g samples were mixed with formic acid, diluted with deionized water, and then centrifuged [Mikulski *et al*., 2024]. The supernatant was injected into a capillary column (SGE BP21; Trajan Scientific and Medical, Melbourne, Australia) and separated according to a specified temperature program: the initial oven temperature was 85°C, it was raised to 180°C at 8°C/min and held for 3 min. The temperature of the flame ionization detector and the injector was 180°C and 85°C, respectively. Identification and quantification of SCFAs were based on standards sourced from Sigma-Aldrich (Saint Louis, MO, USA). Contents of individual compounds were expressed as µmol *per* g of cecal digesta. In addition, the cecal putrefactive SCFA (PSCFA) content was calculated as the sum of isobutyric, isovaleric, and valeric acids. Analysis was performed in duplicate. The bile acids (BA) in the cecum were determined by liquid chromatography-mass spectrometry (LC-MS) using a system consisting of an Agilent 1200 chromatograph (Stockport, United Kingdom) and an AB Sciex 4000 QTrap triplequadrupole mass spectrometer (Warrington, UK). A Supelco Ascentis Express C18 column (15×4.6 mm, 2.7µm; Sigma Aldrich) maintained at 40°C was used for compound separation. Elution was carried out in a gradient system of solvent A (5 mM ammonium acetate in water) and solvent B (0.012% (*v/v*) formic acid in methanol) according to the following program: 0–2 min, 50% (*v/v*) B; 2–20 min, 50–95% (*v/v*) B; 20–22 min, 95% (*v/v*) B; 22–23 min, 95–50% (*v/v*) B; and 23–40 min, 50% (*v/v*) B. The injection volume was 5 µL, and the mobile phase was pumped at the flow rate of 0.6 mL/min. Mass data acquisition was performed using Analyst 1.6.2 software (SCIEX, Marlborough, MA, USA). The internal standards: d4-cholic, d4-glycochenodeoxycholic, d4-glycocholic, d4-litocholic, d4-deoxycholic, and d4-chenodeoxycholic acids, and the relative response factor, were used to quantify the BA. Content of individual BA was expressed as mg *per* g of cecal digesta.

Bacterial extracellular enzyme activity in cecal digesta was evaluated by measuring the release rates of *p*- or *o*-nitrophenol from nitrophenylglucosides [Juśkiewicz *et al*., 2024]. This assessment focused on enzymes, such as α- and β-glucosidase, α- and β-galactosidase, β-glucuronidase, α-arabinopyranidase, and β-xylosidase. The reaction mixtures were incubated at 37°C with *p*-nitrophenol and *o*-nitrophenol being quantified by absorbance measurement at 400 and 420 nm, respectively, following the addition of sodium carbonate. The enzymatic activity was expressed as µmol of product released *per* hour *per* gram of digesta. To measure the total enzyme activity, the cecal digesta was vortexed with glass beads and centrifuged, and the resulting supernatant was analyzed in the same manner as for extracellular activity. Intracellular enzyme activity was derived by comparing total activity against secreted (extracellular) enzyme activities. Standard curves for *p*-nitrophenol and *o*-nitrophenol were used for calculations, and analyses were conducted in duplicate.

In whole blood, hematological parameters were measured, including total white blood cell count (WBC), lymphocytes (LYM), granulocytes (GRA), red blood cell count (RBC), hemoglobin (HGB), hematocrit (HCT), and platelet count (PLT), using the ABACUS Jr VET Analyzer (DIATRON MI PLC, Budapest, Hungary). Blood plasma analysis included triglycerides (TG), total cholesterol (TC), HDL cholesterol (HDL), urea, glucose, albumin, and the activity of aspartate aminotransferase (AST), alkaline phosphatase (ALP), and alanine aminotransferase (ALT), and was performed with a biochemical analyzer (Pentra C200, Horiba, Tokyo, Japan). Based on blood plasma parameters, atherogenic coefficient (AC) and atherogenic index of plasma (AIP) were calculated according to Equations (1) and (2), respectively:

$$AC = (TC - HDL)/HDL \quad (1)$$

$$AIP = lg(TG/HDL) \quad (2)$$

Liver lipids were extracted according to the method of Folch *et al*. [1957]. The cholesterol and triglyceride contents in the extract were determined with the spectrophotometric method using commercial kits (cholesterol DST, triglycerides DST, Alpha Diagnostics, Ltd., San Antonio, TX, USA). Total RNA was isolated from liver tissue fragments weighing approximately 30 mg using the MagnifiQ 16 Total RNA Plus instant kit (A&A Biotechnology, Gdańsk, Poland) on an NPA-32P automated nucleic acid extractor, following the manufacturer's instructions. Samples were first homogenized in 400 µL of a Phenozol Plus reagent using a TissueLyser II homogenizer (Qiagen, Hilden, Germany), and the resulting lysates were processed automatically according to the programmed isolation protocol. RNA concentration and purity were determined with a NanoDrop Lite spectrophotometer (Thermo Fisher Scientific, Waltham, MA, USA). All RNA samples were normalized to a concentration of 10 ng/µL using a TE buffer (Thermo Fisher Scientific, Cat. No. 12090015) prior to reverse transcription. cDNA was synthesized using the High-Capacity cDNA Reverse Transcription Kit (Thermo Fisher Scientific) according to the manufacturer's user guide (Pub. No. MAN0017977). Reverse transcription reactions (20 µL) were performed under the following thermal profile: 25°C for 10 min, 37°C for 120 min, and 85°C for 5 min, followed by storage at 4°C. The resulting cDNA was pre-amplified using the Fluidigm

PreAmp Master Mix (PN 100-5744) with a custom pool of TaqMan Gene Expression Assays. Pre-amplification was conducted on a QuantStudio 5 Real-Time PCR System (Thermo Fisher Scientific) following the Fluidigm protocol (PN 100-5876), with the following cycling conditions: 95°C for 2 min; 14 cycles of 95°C for 15 s and 60°C for 4 min. The pre-amplified products were diluted (1:5, *w/v*) in a Dilution Reagent (Fluidigm PN 100-8726) before quantitative PCR (qPCR) analysis. Quantitative gene expression analysis was carried out using the Biomark HD System and Juno Controller (Fluidigm Corporation, South San Francisco, CA, USA) with the 192.24 Dynamic Array Integrated Fluidic Circuit (IFC), following the manufacturer's guidelines (PN 100-6170). Each reaction contained diluted, preamplified cDNA combined with TaqMan Universal PCR Master Mix (2X), TaqMan Assay, GE Sample Loading Reagent and GE Assay Loading Reagent. The IFC was loaded using the Juno Load Mix 192.24 GE script, and qPCR was performed on the Biomark HD using the GE 192×24 Standard v1 protocol. Data was acquired using the Fluidigm Real-Time PCR Analysis Software, with default baseline and threshold settings applied. Gene expression data were expressed relative to the reference gene (glyceraldehyde-3-phosphate dehydrogenase, GAPDH) and were presented as relative fold gene.

Plasma samples were analyzed utilizing the Olink Target 96 Mouse Exploratory kit (Olink Proteomics, Uppsala, Sweden) in accordance with the manufacturer's recommended protocol. Initially, serum samples were thawed on ice and centrifuged at 4°C to eliminate any particulate matter prior to processing. The samples then underwent an overnight incubation at 4°C with oligonucleotide-labeled antibody pairs specific to the target proteins, facilitating the formation of antigen-antibody complexes and enhancing assay sensitivity and specificity. Following the formation of these immune complexes, proximity extension assay (PEA) technology was employed to promote the hybridization of complementary oligonucleotides, followed by enzymatic extension to generate unique DNA reporter sequences for each target protein. The QuantStudio 5 Real-Time PCR System (Applied Biosystems, Foster City, CA, USA) was used for pre-amplification of these reporter sequences, ensuring they reached detectable levels to enhance signal reliability. Sample loading and integrated fluidic circuit (IFC) priming were performed using the Juno system (Standard BioTools, South San Francisco, CA, USA), strictly adhering to the manufacturer's instructions to maintain optimal fluidic integrity and assay performance. Protein expression signals were quantified using qPCR amplification with the Biomark HD system (Standard BioTools), enabling the simultaneous quantification of multiple targets in a highly multiplexed assay format. Data normalization was conducted with the help of internal and external assay controls provided by the manufacturer, ensuring the quality and consistency of the results. Protein expression values were reported as Normalized Protein eXpression (NPX) units, calculated using the Olink NPX Signature software (Olink Proteomics).

Statistical analysis

The results are presented as average values, complemented by the standard error of the mean (SEM) to provide insight into data variability. To assess the statistical significance of differences among the various experimental treatments, namely the control, untreated onion, dehydrated onion, and dehydrated/fermented onion groups, a one-way analysis of variance (ANOVA) was employed (STATISTICA software, version 14.0; StatSoft Corp., Krakow, Poland). Following this analysis, a Tukey post-hoc test was conducted to identify significant differences among the groups. Additionally, effect sizes were calculated using partial eta squared (ηp^2), which quantifies the proportion of total variance that can be attributed to the specific factor under consideration, while effectively isolating the influence of other factors. Data were tested for normality using the Shapiro-Wilk test prior to ANOVA.

RESULTS AND DISCUSSION

Results showing the effects of the applied technological processes on the chemical composition of onion preparations are presented in **Table 1**. The rate of loss of chemical compounds during osmotic dehydration is affected by process conditions, including the concentration and temperature of the hypertonic solution, immersion time, the sample-to-solution ratio, and the agitation or circulation of the osmotic solution [Revaskar *et al*., 2014; Yazidi *et al*., 2024]. The onion preparations subjected to osmotic concentration followed by lactic acid fermentation exhibited reduced contents of protein, dietary fiber, fructooligosaccharides (FOS), and phenolics. In contrast, the contents of their simple sugars, sucrose, and ash increased. Similar changes have been reported in previous studies on onion subjected to osmotic dehydration in sucrose and sodium chloride solutions [Grzelak-Błaszczyk *et al*., 2021], followed by lactic acid fermentation [Grzelak-Błaszczyk *et al*., 2023].

The effect size analysis revealed that the applied dietary treatments with onion preparations had a moderate to large effect on fat and lean tissue content in the rat's body as well as on relative mass of spleen, liver, kidneys and epididymal white adipose tissue (ηp^2=0.063–0.201; **Table 2**). The one-way ANOVA and Tukey post-hoc test showed a significant increase in the body's lean tissue percentage in rats fed a diet supplemented with osmotically dehydrated onion preparation (p<0.05; GD *vs*. control group). These moderate-to-large effect size values indicate that a substantial proportion of the variance in internal organ weights as well as fat and lean tissue contents can be attributed to the dietary onion intervention, suggesting it has practical significance. In a 12-week randomized, double-blind, placebo-controlled trial, supplementation with an onion peel extract significantly reduced body weight and percentage of body fat in overweight and obese adults compared with placebo [Lee *et al*., 2016]. In Zucker diabetic fatty rats, dietary supplementation with a whole onion extract reduced body weight gain and adipose tissue weight compared with controls [Yoshinari *et al*., 2012]. In our study, we observed that the lean tissue percentage in rats was significantly reduced when they consumed a diet containing dehydrated onion, without any accompanying changes in body weight. The fermentation processing applied to the dietary onion preparation did not yield any additional effects on body fat or lean tissue composition. Some researchers

Table 1. Chemical composition (g/100 g) and count of live lactic acid bacteria (LAB) (log CFU/g) of preparations from onion (v. Allurion) obtained by lyophilization (untreated onion), osmotic dehydration in a glucose-fructose syrup, and a combination of osmotic dehydration and fermentation with *Levilactobacillus brevis* ŁOCK 944 or *Lactiplantibacillus plantarum* P27.

Parameter	Lyophilization	Osmotic dehydration	Osmotic dehydration and fermentation with strain 944	Osmotic dehydration and fermentation with strain P27
Dry matter	84.50±0.03	88.69±0.11	84.23±0.08	84.06±0.20
Protein	11.34±0.28^{a}	4.83±0.07^{b}	5.67±0.32^{b}	4.71±0.19^{b}
F+G+S	43.94±1.28^{c}	62.51±1.61^{a}	54.85±3.04^{b}	55.01±1.93^{b}
Total dietary fiber	12.70±0.30^{a}	4.50±0.11^{c}	9.50±0.33^{b}	8.30±0.00^{b}
Crude fat	0.47±0.04	0.44±0.02	0.64±0.04	0.51±0.04
Ash	4.26±0.34^{b}	7.62±0.33^{a}	9.06±0.11^{a}	8.88±0.08^{a}
FOS	6.72±0.37^{a}	1.78±0.13^{b}	1.61±0.06^{b}	1.29±0.06^{b}
Total phenolics	1.33±0.03^{a}	0.54±0.03^{b}	0.51±0.02^{b}	0.50±0.01^{b}
Live LAB	Not detected	Not detected	8.64±0.14	8.16±0.15

Results are shown as mean ± standard deviation (n=3). Means within a row with unlike superscript letters are shown to be significantly different (p<0.05). F+G+S, sum of fructose, glucose and saccharose; FOS, fructooligosaccharides (kestose, nystose, fructosyl nystose).

have noted that changes in gene expression are consistent with a pattern of decreased hepatic lipid synthesis and fat deposition, establishing a link between onion intake and alterations in liver gene expression related to fat metabolism [Chang *et al*., 2022].

The results in **Table 3** show that the dietary addition of onion preparations determined 6–70% (ηp^2=0.064–0.696) of the variations in the expression of the analyzed genes in the liver tissue of rats. The moderate effect size was noted in the case of genes: *Ldlr*, *Olr1*, *Ptgs2*, *Stat3*, *Cyp8b1*, and *Fasn*. In the case of the remaining analyzed genes, the observed effect size was large. The highest expression of *Ahr* and *Pparg* genes in the liver was observed in the GDFb group (p<0.05 *vs*. all other groups). All four onion dietary treatments caused a significant decrease in hepatic *Hif1a*, *Scd1*, and *Acly* expression compared to changes observed in the control animals (p<0.05). The *Nfkb1* and *Nrlh4* expression was the highest in the onion untreated preparation group (p<0.05 *vs*. GD, GDFa groups and p<0.05 *vs*. other groups, respectively). The *Ppara* hepatic expression was elevated in the GDFb rats (p<0.05 *vs*. control and GDFa groups). The osmotic dehydration with a glucose-fructose syrup as well as subsequent lactic fermentation with selected bacterial strains (groups GD, GDFa, GDFb) caused a significant decrease in the hepatic *Srebf1* and *Tlr4* expression compared to the control groups (*Srebf1*) and control and G groups (*Tlr4*), respectively. The GDFa dietary treatment caused a significant increase in the *Lpl*, *Cyp27a1*, *Cyp7a1* expression in the liver as compared to all other treatments (p<0.05). The GD and GDFa groups excelled the G rats in terms of hepatic *Baat* expression (p<0.05). The G rats had the highest *Cpt1a* and *Fdft1* expressions in the liver (p<0.05 *vs*. GDFa and p<0.05 *vs*. all other groups, respectively).

The applied dietary treatments with onion preparations explained 7–17% of the variance in the liver fat (ηp^2=0.102; moderate effect), total cholesterol (ηp^2=0.065; moderate effect), and triglycerides (ηp^2=0.165; large effect) contents (**Table 4**). A one-way ANOVA analysis showed a near-significant trend to decreased liver TG in the GDFb group (p=0.080). The dietary addition of the dehydrated onion preparation caused a significant decrease in plasma AST activity (p<0.05 *vs*. C), while the GDFa and GDFb groups exhibited decreased ALT activity (in both cases p<0.05 *vs*. C). In the case of plasma ALP, there was a descending tendency in its activity in the plasma in the onion groups (p=0.063). The dietary onion addition explained 18%, 23% and 24% of the variance in ALP, AST, and ALT activity, respectively. In the case of total cholesterol (TC) and glucose concentration, the respective percentages were 20% and 29% (the effect sizes: ηp^2=0.195 and ηp^2=0.286, respectively). The lowest glucose and TC plasma concentrations were determined in the GDFb rats (p<0.05 *vs*. C and GD, and p<0.05 *vs*. C, respectively). The onion dietary treatments exerted moderate effects on HDL concentration in the plasma and the value of atherogenic coefficient (AC; ηp^2=0.068 and ηp^2=0.088, respectively). Such size of the effect on triglycerides (TG) and atherogenic index of plasma (AIP) was noted as a large effect (ηp^2=0.307 and ηp^2=0.247, respectively). The lowest TG concentration and AIP value were determined in the GD group (p<0.05 *vs*. C and GDFa and p<0.05 *vs*. C, respectively).

As demonstrated by the analysis of multiple liver tissue markers, the beneficial changes observed in the rats fed diets containing onion preparations, both directly in the liver tissue and in blood biochemical parameters, should be attributed to the modulation of the expression of several genes essential for metabolic regulation. However, it is necessary to distinguish which genes were activated or suppressed by the onion preparation itself and whether the applied technological processes

Table 2. Final body weight (BW), daily diet intake, and internal organ weight in rats fed diets with onion preparations and a control diet.

Parameter	C	G	GD	GDFa	GDFb	SEM	*p*-Value	Effect size ηp^2
Final BW (g)	327.1	330.2	329.5	334.5	326.4	2.281	0.832	0.031
Diet intake (g/day)	18.70	18.99	19.07	18.86	19.00	0.108	0.834	0.031
Fat (g)	38.55	35.46	30.98	35.43	34.55	0.994	0.203	0.121
Lean (g)	213.6	222.5	223.3	223.4	218.3	1.648	0.260	0.108
Fat (% BW)	11.76	10.72	9.462	10.63	10.57	0.300	0.206	0.121
Lean (% BW)	65.32^{b}	67.42^{ab}	67.77^{a}	66.79^{ab}	66.89^{ab}	0.268	0.034	0.201
eWAT (g/100 g BW)	2.867	2.508	2.632	2.668	2.680	0.065	0.545	0.064
Heart (g/100 g BW)	0.270	0.265	0.265	0.262	0.265	0.002	0.880	0.025
Spleen (g/100 g BW)	0.235	0.218	0.233	0.222	0.202	0.006	0.470	0.074
Liver (g/100 g BW)	3.651	3.614	3.656	3.500	3.467	0.044	0.552	0.063
Testes (g/100 g BW)	1.019	1.018	1.024	0.994	1.030	0.010	0.811	0.033
Kidneys (g/100 g BW)	0.649	0.651	0.671	0.631	0.637	0.007	0.512	0.068

Mean values within a row with unlike superscript letters are shown to be significantly different ($p<0.05$; post-hoc Tukey test); ηp^2, partial eta squared; SEM, pooled standard error of the mean (standard deviation for all rats divided by the square root of rat number, $n=50$); eWAT, epididymal white adipose tissue. Experimental groups: C, control diet; G, diet with 2% (*w/w*) of untreated onion (v. Allurion) preparation; GD, diet with 2% (*w/w*) of onion preparation obtained by osmotic dehydration in a glucose-fructose syrup; GDFa, diet with 2% (*w/w*) of onion preparation obtained by osmotic dehydration in a glucose-fructose syrup and fermentation with *Levilactobacillus brevis* ŁOCK 944; GDFb, diet with 2% (*w/w*) of onion preparation obtained by osmotic dehydration in glucose-fructose syrup and fermentation with *Lactiplantibacillus plantarum* P27.

Table 3. Gene expression in the liver tissue in rats fed diets with onion preparations and a control diet.

Gene	C	G	GD	GDFa	GDFb	SEM	*p*-Value	Effect size ηp^2
Ahr	0.045^{b}	0.031^{b}	0.051^{b}	0.055^{b}	0.325^{a}	0.029	0.002	0.312
Hif1a	0.118^{a}	0.007^{b}	0.013^{b}	0.037^{b}	0.006^{b}	0.009	<0.001	0.432
Ldlr	0.238	0.243	0.304	0.305	0.150	0.032	0.553	0.064
Nfkb1	0.148^{ab}	0.351^{a}	0.118^{b}	0.062^{b}	0.168^{ab}	0.027	0.005	0.273
Nr1h4	0.080^{b}	0.207^{a}	0.043^{b}	0.034^{b}	0.088^{b}	0.014	<0.001	0.389
Olr1	0.071	0.011	0.010	0.061	0.033	0.008	0.061	0.177
Ppara	0.028^{b}	0.145^{ab}	0.036^{ab}	0.022^{b}	0.161^{a}	0.016	0.003	0.299
Pparg	0.178^{b}	0.004^{b}	$<0.001^{b}$	0.145^{b}	1.543^{a}	0.129	<0.001	0.425
Ptgs2	<0.001	<0.001	0.001	0.001	<0.001	<0.001	0.530	0.066
Srebf1	1.021^{a}	0.612^{ab}	0.355^{b}	0.183^{b}	0.228^{b}	0.067	<0.001	0.429
Stat3	0.128	0.177	0.071	0.060	0.112	0.016	0.151	0.136
Tlr4	0.470^{a}	0.475^{a}	$<0.001^{b}$	$<0.001^{b}$	$<0.001^{b}$	0.046	<0.001	0.520
Lpl	0.034^{b}	0.025^{b}	0.024^{b}	0.244^{a}	0.030^{b}	0.019	<0.001	0.435
Scd1	15.653^{a}	3.513^{b}	4.262^{b}	2.708^{b}	3.877^{b}	0.874	<0.001	0.629
Acly	0.339^{a}	$<0.001^{b}$	0.037^{b}	0.015^{b}	0.072^{b}	0.024	<0.001	0.554
Baat	1.718^{ab}	0.847^{b}	2.454^{a}	2.462^{a}	1.196^{ab}	0.203	0.027	0.211
Cpt1a	1.050^{ab}	2.787^{a}	1.509^{ab}	0.540^{b}	1.455^{ab}	0.217	0.013	0.241
Cyp27a1	0.132^{b}	0.203^{b}	0.127^{b}	1.286^{a}	0.185^{b}	0.090	<0.001	0.512
Cyp7a1	0.077^{b}	$<0.001^{b}$	0.031^{b}	0.938^{a}	0.029^{b}	0.079	<0.001	0.431

Table 3 cont. Gene expression in the liver tissue in rats fed diets with onion preparations and a control diet.

Gene	C	G	GD	GDFa	GDFb	SEM	*p*-Value	Effect size ηp^2
Cyp8b1	0.249	0.379	0.264	0.181	0.181	0.035	0.382	0.086
Fasn	0.312	0.285	0.136	0.282	0.092	0.040	0.303	0.099
Fdft1	0.020^{b}	0.520^{a}	0.006^{b}	0.050^{b}	0.024^{b}	0.034	<0.001	0.696

Mean values within a row with unlike superscript letters are shown to be significantly different ($p<0.05$; post-hoc Tukey test); ηp^2, partial eta squared; SEM, pooled standard error of the mean (standard deviation for all rats divided by the square root of rat number, $n=50$). Gene names: *Ahr*, aryl hydrocarbon receptor; *Hif1a*, hypoxia-inducible factor 1-alpha; *Ldlr*, low-density lipoprotein receptor; *Nfkb1*, nuclear factor kappa b subunit 1; *Nr1h4* (*Fxr*), *n*uclear receptor subfamily 1, group H, member 4 (Farsenoid x receptor); *Olr1* (*Lox-1*), oxidized low-density lipoprotein receptor 1 (Lectin-like oxidized LDL receptor-1); *Ppara*, peroxisome proliferator-activated receptor alpha; *Pparg*, peroxisome proliferator-activated receptor gamma; *Ptgs2*, prostaglandin-endoperoxidase synthase 2; *Srebf1*, sterol regulatory element binding transcription factor 1; *Stat3*, signal transducer and activator of transcription 3; *Tlr4*, toll-like receptor 4; *Lpl*, lipoprotein lipase; *Scd1*, steaoryl-CoA desaturase 1; *Acly*, ATP citrate lyase; *Baat*, bile acid-CoA: amino acid N-acyltransferase; *Cpt1a*, carnitine palmitoyltransferase 1a; Cyp27a1, cytochrom P450 family 27 subfamily a member 1; *Cyp7a1*, cytochrom P450 family 7 subfamily a member 1; *Cyp8b1*, cytochrom P450 family 8 subfamily b member 1; *Fasn*, fatty acid synthase; *Fdft1*, farnesyl-diphosphate farnesyltransferase 1. Experimental groups: C, control diet; G, diet with 2% (*w/w*) of untreated onion (v. Allurion) preparation; GD, diet with 2% (*w/w*) of onion preparation obtained by osmotic dehydration in a glucose-fructose syrup; GDFa, diet with 2% (*w/w*) of onion preparation obtained by osmotic dehydration in a glucose-fructose syrup and fermentation with *Levilactobacillus brevis* ŁOCK 944; GDFb, diet with 2% (*w/w*) of onion preparation obtained by osmotic dehydration in a glucose-fructose syrup and fermentation with *Lactiplantibacillus plantarum* P27.

Table 4. Liver fat content and biochemical blood plasma parameters in rats fed diets with onion preparations and a control diet.

Parameter	C	G	GD	GDFa	GDFb	SEM	*p*-Value	Effect size ηp^2
Liver								
Fat (g/100 g)	15.02	13.53	13.18	13.39	14.18	0.298	0.288	0.102
TC (mg/g)	4.457	4.588	4.534	4.269	4.027	0.115	0.543	0.065
TG (mg/g)	15.90	15.83	15.28	15.26	13.21	0.344	0.080	0.165
Plasma								
AST (U/L)	56.80^{a}	51.14^{ab}	48.32^{b}	53.18^{ab}	50.96^{ab}	0.836	0.016	0.232
ALT (U/L)	22.45^{a}	20.43^{ab}	19.87^{ab}	18.01^{b}	18.55^{b}	0.454	0.012	0.241
ALP (U/L)	176.7	166.0	164.7	162.7	156.6	2.218	0.063	0.176
GL (mmol/L)	18.63^{a}	16.40^{ab}	17.72^{a}	17.47^{ab}	15.19^{b}	0.315	0.003	0.286
TC (mmol/L)	2.119^{a}	1.682^{ab}	1.833^{ab}	1.879^{ab}	1.591^{b}	0.059	0.040	0.195
HDL (mmol/L	0.547	0.485	0.507	0.549	0.474	0.017	0.512	0.068
TC/HDL	3.858	3.626	3.695	3.440	3.435	0.077	0.374	0.088
AC	2.858	2.626	2.695	2.440	2.435	0.077	0.374	0.088
TG (mmol/L)	1.733^{a}	1.307^{ab}	1.022^{b}	1.508^{a}	1.295^{ab}	0.061	0.002	0.307
TG/HDL	3.253^{a}	2.791^{ab}	2.124^{b}	2.733^{ab}	2.779^{ab}	0.112	0.027	0.211
AIP	0.500^{a}	0.430^{ab}	0.303^{b}	0.428^{ab}	0.430^{ab}	0.018	0.010	0.247
ALB (µmol/L)	406.8	413.1	412.9	414.3	405.1	3.865	0.927	0.018
Urea (mmol/L)	3.921	4.118	3.726	3.717	4.121	0.080	0.298	0.101

Mean values within a row with unlike superscript letters are shown to be significantly different ($p<0.05$; post-hoc Tukey test); ηp^2, partial eta squared; SEM, pooled standard error of the mean (standard deviation for all rats divided by the square root of rat number, $n=50$); AC, atherogenic coefficient; AIP, atherogenic index; ALB, albumin; ALT, alanine aminotransferase; AST, aspartate aminotransferase; ALP, alkaline phosphatase; GL, glucose; TC, total cholesterol; TG, triglycerides. Experimental groups: C, control diet; G, diet with 2% (*w/w*) of untreated onion (v. Allurion) preparation; GD, diet with 2% (*w/w*) of onion preparation obtained by osmotic dehydration in a glucose-fructose syrup; GDFa, diet with 2% (*w/w*) of onion preparation obtained by osmotic dehydration in a glucose-fructose syrup and fermentation with *Levilactobacillus brevis* ŁOCK 944; GDFb, diet with 2% (*w/w*) of onion preparation obtained by osmotic dehydration in a glucose-fructose syrup and fermentation with *Lactiplantibacillus plantarum* P27.

(osmotic dehydration with a glucose-fructose syrup and subsequent lactic acid fermentation with selected bacterial strains) exerted any additional effects. Accordingly, regardless of further modification of the onion preparation through dehydration and fermentation, a beneficial reduction in the expression of *Hif1a*, *Scd1*, and *Acly* was observed in all dietary groups receiving onion preparations. It is well known that the activation of *Hif1a via* downstream genes, such as *Srebp1* and *Fasn*, promotes lipogenesis, and that *Hif1a* is often excessively activated in pathological conditions, such as non-alcoholic fatty liver disease (NAFLD) [Zeng *et al*., 2025]. In turn, *Scd1* regulates the synthesis of triglycerides, phospholipids, and cholesterol, and increased expression of this gene promotes lipogenesis and may contribute to hepatic steatosis [Yu *et al*., 2025]. Similarly, elevated *Acly* activity enhances lipogenesis and lipid accumulation in hepatocytes [Rauckhorst *et al*., 2025]. Consistent with these findings, Son *et al*. [2024] reported that a dietary onion extract rich in quercetin modulated hepatic gene expression of key regulators of lipid metabolism, including *Srebp1*, *Fasn*, *Ppara*, and *Cpt1a*, and that these changes were accompanied by improved lipid profiles and reduced serum triglyceride and low-density lipoprotein (LDL) levels in rats fed a high-fat diet.

In the present study, the application of osmotic dehydration of onion (v. Allurion) in a glucose-fructose syrup resulted in a health-beneficial reduction in the hepatic expression of the *Nfkb1*, *Srebf1*, and *Tlr4* genes. Increased expression of the first of these genes is observed in chronic inflammatory states associated with non-alcoholic fatty liver disease (NAFLD) and enhanced immune activation; moreover, sustained activation of the *NF-κB* transcriptional complex (including *Nfkb1*) exacerbates liver tissue fibrosis [Cordero-Pérez *et al*., 2025]. In turn, the overexpression of *Srebf1* promotes lipogenesis in response to metabolic signaling and leads to increased lipid storage in hepatocytes [Yang *et al*., 2020]. Elevated *Tlr4* expression may trigger inflammatory responses and activate hepatic stellate cells, which are responsible for collagen production and the progression of liver fibrosis [Ding *et al*., 2025]. In our study, the most favorable changes in plasma biochemical parameters, namely AST activity, triglyceride (TG) concentration, and the atherogenic index of plasma (AIP), were observed in the rats fed the GD diet containing onion prepared by osmotic dehydration with a glucose-fructose syrup. Osmotic dehydration is a low-temperature pretreatment that partially removes water from plant tissues by immersion in a hypertonic solution. As this process does not involve high thermal exposure, it enables better preservation of heat-sensitive nutrients compared with conventional hot-air drying, particularly vitamins, polyphenols, and flavor compounds that are susceptible to degradation under conditions of elevated temperature and oxygen [Galus *et al*., 2025; Yadav & Singh, 2014]. Of course, the literature on the health-promoting effects of consuming fermented fruits and vegetables is extensive. However, these studies do not address the effects of consuming products that were first subjected to osmotic dehydration before fermentation. We aimed to fill this gap in knowledge with the present experiment. The combined application of dehydration and fermentation produced some effects that were not observed in the C, G, or GD groups. Specifically, beneficial changes were observed in hepatic gene expression: *Ahr*, *Ppara*, and *Pparg* (with the preparation fermented using the probiotic strain P27) and *Lpl*, *Cyp27a1*, and *Cyp7a1* (with the preparation fermented using strain 944). As suggested by Shang *et al*. [2023], endogenous *Ahr* activation *via* dietary or microbial ligands can confer hepatoprotection and reduce inflammation. Increased *Ppara* expression is associated with enhanced insulin sensitivity in tissues as well as enhanced fatty acid β-oxidation, decreased plasma triglycerides, anti-inflammatory effects (*e.g.*, inhibition of NF-κB activation), and anti-steatotic action in the liver. Conversely, increased *Pparg* expression can promote hepatic steatosis under certain conditions, such as NAFLD, but it can also attenuate inflammation (through NF-κB inhibition) and exert antifibrotic effects [Sepehri *et al*., 2025]. Indeed, the most favorable changes in parameters, such as liver triglycerides (TG) and plasma levels of alkaline phosphatase (ALP), glucose, and total cholesterol (TC), were observed in our study in the GDFb group.

The counts of total white blood cells (WBC) and lymphocytes (LYM) were affected by the onion dietary treatments in a moderate manner (**Table S2** in Supplementary Materials; ηp^2=0.085–0.117). The neutrophil (NEU) count and percentage were the highest in the G group (p<0.05 *vs*. all other onion groups, and p<0.05 *vs*. GDFb, respectively). The onion treatments explained 30 and 25% of the variance in NEU count and percentage, respectively. The addition of dietary onion preparations to rat diets exerted a moderate to large effect on their red blood cell count, hemoglobin level, hematocrit percentage, and red cell distribution width (ηp^2=0.100–0.140). The size of the effect of the dietary factor on platelet count and mean platelet volume was moderate (ηp^2=0.065–0.086), while a large effect was noted on platelet distribution width (ηp^2=0.175). The above hematological changes should be regarded as a physiological response within normal limits. The increased NEU level observed in group G (untreated onion preparation), in the absence of alterations in other blood parameters, should not be associated with elevated stress levels or infectious conditions [Herrero-Cervera *et al*., 2022].

The dietary addition of onion preparations explained 14% and 20% of the variance in relative cecal digesta mass and cecal digesta pH value, respectively, meaning that dietary manipulation had a strong influence (**Table 5**). The dietary treatment with untreated onion preparation (group G) significantly lowered digesta pH in the cecum as compared to the control rats (p<0.035). The applied dietary onion treatments had a moderate effect (ηp^2=0.068–0.088) on cecal acetic and valeric acid contents, while a large effect was noted for cecal butyric acid level (ηp^2=0.143). The butyric acid percentage in the SCFA profile was significantly higher in the GD group than in the C control animals (p=0.034; ηp^2=0.202). There was a significant difference between the GDFa and GDFb groups in the SCFA pool (31.4 *vs*. 53.3 µmol/100 g of body weight; p=0.033; ηp^2=0.203). The dietary

Table 5. Cecal parameters in rats fed diets with onion preparations and a control diet.

Parameter	C	G	GD	GDFa	GDFb	SEM	*p*-Value	Effect size ηp^2
Cecum								
Cecal tissue (g/100 g BW)	0.240	0.282	0.258	0.257	0.262	0.006	0.349	0.092
Cecal digesta (g/100 g BW)	0.501	0.635	0.600	0.479	0.692	0.031	0.144	0.138
Cecal pH	7.471^{a}	7.191^{b}	7.385^{ab}	7.335^{ab}	7.265^{ab}	0.031	0.035	0.200
SCFA (µmol/g digesta)								
Acetic	42.64	41.06	41.98	39.38	46.33	1.257	0.515	0.068
Propionic	18.01	18.37	18.61	16.68	17.65	0.629	0.894	0.023
Butyric	7.171	8.436	10.50	7.650	7.779	0.407	0.128	0.143
Isovaleric	1.459	1.329	1.470	1.428	1.613	0.061	0.701	0.046
Valeric	2.643	2.055	2.261	1.958	2.101	0.116	0.374	0.088
Isobutyric	1.560	1.376	1.460	1.442	1.498	0.056	0.893	0.023
PSCFA	5.663	4.760	5.191	4.828	5.212	0.206	0.667	0.050
Total SCFA	74.03	72.62	76.28	68.54	76.96	2.094	0.739	0.042
SCFA profile (%)								
Acetic	57.73	56.23	55.45	57.41	60.13	0.656	0.230	0.114
Propionic	24.29	25.60	24.09	24.22	22.96	0.561	0.709	0.045
Butyric	10.39^{ab}	11.41^{ab}	13.68^{a}	11.11^{ab}	10.15^{b}	0.398	0.034	0.202
SCFA pool (µmol/100 g BW)	36.28^{ab}	45.62^{ab}	45.53^{ab}	31.37^{b}	53.32^{a}	2.444	0.033	0.203

Mean values within a row with unlike superscript letters are shown to be significantly different ($p<0.05$; post-hoc Tukey test); ηp^2, partial eta squared; SEM, pooled standard error of the mean (standard deviation for all rats divided by the square root of rat number, $n=50$); BW, body weight; SCFA, short-chain fatty acid; PSCFA, putrefactive short-chain fatty acid. Experimental groups: C, control diet; G, diet with 2% (*w/w*) of untreated onion (v. Allurion) preparation; GD, diet with 2% (*w/w*) of onion preparation obtained by osmotic dehydration in a glucose-fructose syrup; GDFa, diet with 2% (*w/w*) of onion preparation obtained by osmotic dehydration in a glucose-fructose syrup and fermentation with *Levilactobacillus brevis* ŁOCK 944; GDFb, diet with 2% (*w/w*) of onion preparation obtained by osmotic dehydration in a glucose-fructose syrup and fermentation with *Lactiplantibacillus plantarum* P27.

onion preparation factor accounted for 14% to 18% of the variance observed in both the intracellular and total activity of bacterial α- and β-glucosidase in the cecal digesta (**Table S3** in Supplementary Materials). Additionally, a statistical trend indicating an increased release rate of these enzymes from bacterial cells into the cecal environment was noted in the groups fed diets containing onion, with *p*-values of 0.098 and 0.080, respectively. The onion preparation treatments had moderate effects on cecal bacterial extracellular, intracellular and total activities of α- and β-galactosidase (ηp^2=0.072–0.130). The highest extracellular and total activity of cecal bacterial β-glucuronidase was found in the GD group (**Table 6**; $p<0.05$ *vs.* all other groups, and $p<0.05$ *vs.* GDFa and GDFb groups, respectively; ηp^2=0.396 and ηp^2=0.291, respectively). The onion dietary treatments explained 13% of the variance in the percentage value of β-glucuronidase and α-arabinopyranosidase release rates (ηp^2=0.134 and 0.127, respectively). The dietary onion preparation factor had a large effect on intracellular and total α-arabinopyranosidase activity in the aecal digesta of rats (ηp^2=0.174 and 0.168, respectively). There was also a statistical tendency to an increase in intracellular and total α-arabinopyranosidase activity, especially in the G group (p=0.065 and p=0.074, respectively). The dietary addition of onion preparations had a moderate effect on extracellular and total β-xylosidase cecal activity (ηp^2=0.098 and 0.084, respectively), and a large effect on the release rate of that enzyme (ηp^2=0.179). The β-xylosidase release rate tended to increase in the dietary onion treatments as compared to the C rats (p=0.058). The inclusion of onion preparations in the diet did not induce highly significant changes in the metabolic activity of the rat cecal microbiota, indicating good gastrointestinal tolerance of this dietary supplementation. Positive effects entailed the significant acidification of the cecal digesta in the rats fed the diet containing untreated onion preparation, an increase in the butyric acid pool in group GD (dehydrated onion preparation), and an

Table 6. Microbial enzymatic activity in the cecal digesta in rats fed diets with onion preparations and a control diet.

Enzyme	C	G	GD	GDFa	GDFb	SEM	*p*-Value	Effect size ηp^2
β-Glucuronidase								
Extracellular (μmol/h/g digesta)	26.15^{b}	26.42^{b}	37.11^{a}	21.70^{b}	19.56^{b}	1.375	<0.001	0.396
Intracellular (μmol/h/g digesta)	14.22	11.62	12.22	10.58	11.54	0.720	0.603	0.057
Total (μmol/h/g digesta)	40.37^{ab}	38.04^{ab}	49.32^{a}	32.28^{b}	31.10^{b}	1.730	0.003	0.291
Release rate (%)	65.25	69.07	74.79	67.48	64.27	1.446	0.156	0.134
α-Arabinopyranosidase								
Extracellular (μmol/h/g digesta)	2.615	3.075	3.253	3.167	3.199	0.098	0.232	0.114
Intracellular (μmol/h/g digesta)	1.105	1.880	1.209	1.210	1.561	0.099	0.065	0.174
Total (μmol/h/g digesta)	3.720	4.955	4.462	4.377	4.760	0.147	0.074	0.168
Release rate (%)	70.78	63.14	73.06	71.77	68.14	1.407	0.181	0.127
β-Xylosidase								
Extracellular (μmol/h/g digesta)	3.361	3.396	4.362	3.707	4.226	0.189	0.310	0.098
Intracellular (μmol/h/g digesta)	1.843	2.217	1.760	1.385	1.872	0.205	0.808	0.034
Total (μmol/h/g digesta)	4.600	4.276	5.111	4.187	5.039	0.187	0.401	0.084
Release rate (%)	72.79	79.14	84.76	88.00	82.58	1.753	0.058	0.179

Mean values within a row with unlike superscript letters are shown to be significantly different ($p<0.05$; post-hoc Tukey test); ηp^2, partial eta squared; SEM, pooled standard error of the mean (standard deviation for all rats divided by the square root of rat number, $n=50$); Experimental groups: C, control diet; G, diet with 2% (*w/w*) of untreated onion (v. Allurion) preparation; GD, diet with 2% (*w/w*) of onion preparation obtained by osmotic dehydration in a glucose-fructose syrup; GDFa, diet with 2% (*w/w*) of onion preparation obtained by osmotic dehydration in a glucose-fructose syrup and fermentation with *Levilactobacillus brevis* ŁOCK 944; GDFb, diet with 2% (*w/w*) of onion preparation obtained by osmotic dehydration in a glucose-fructose syrup and fermentation with *Lactiplantibacillus plantarum* P27.

increase in the total short-chain fatty acid (SCFA) pool in the group fed a diet containing dehydrated/fermented onion preparation. The increased bacterial β-glucuronidase activity observed in group GD, an enzyme generally associated with less desirable gut microbiota [Rauf *et al*., 2025], can be attributed to the lower fiber content and the higher simple sugar content of the onion osmotic-dehydrated in a glucose-fructose syrup. Fermentation of this preparation led to a reduction in both the total and extracellular activity of this enzyme.

The dietary onion factor had a moderate effect on the cecal hyodeoxycholic, tauro-α-muricholic, tauro-β-muricholic, glycocholic, and taurochenodeoxycholic acids (**Table 7**; $\eta p^2=0.065$–0.129). The GDFa and GDFb treatments caused a significant decrease in the cecal lithocholic acid content as compared to C rats ($p<0.05$; $\eta p^2=0.272$). All onion groups had a significantly lowered β-hyodeoxycholic acid content in the cecal digesta *vs*. control group ($p<0.05$; $\eta p^2=0.481$). The tauro-ω-muricholic level in GDFa significantly excelled the GDFb group ($p<0.05$; $\eta p^2=0.180$). Changes in the bile acid content of the rat cecal digesta in response to dietary supplementation with onion preparations should be considered minor, similar to the case of SCFAs. The observed reduction in cecal lithocholic acid (LCA) in the dehydrated/fermented GDFa and GDFb groups is likely beneficial, as excessive LCA is cytotoxic and genotoxic. Moreover, lower LCA levels may reflect favorable modulation of the gut microbiota and its activity [Chen *et al*., 2025].

The dietary application of onion preparations had a moderate effect size ($\eta p^2=0.065$–0.134; **Table S4** in Supplementary Materials) on the following plasma relative protein expression levels (NPX) related to immunological status of the rat's body: Aryl hydrocarbon receptor (Ahr), C-C motif chemokine 2 (Ccl2), C-X-C motif chemokine 9 (Cxcl9), follistatin (Fst), interleukin-1 alpha (Il1a), interleukin-6 (Il6), interleukin-17A (Il17a), plexin-A4 (Plxna4), tumor necrosis factor receptor superfamily member 11B (Tnfrsf11b), and V-set and immunoglobulin domain-containing protein 2 (Vsig2). A large effect size was noted in the case of transforming growth factor beta receptor type 3 level ($\eta p^2=0.146$). The diet composition factor explained 10% and 15% of the variance in forkhead box protein O1 (Foxo1) and NAD kinase (Nadk) expression levels (**Table S5** in Supplementary Materials). With

Table 7. Cecal bile acid (BA) content (mg/g digesta) in rats fed diets with onion preparations and a control diet.

	C	G	GD	GDFa	GDFb	SEM	*p*-Value	Effect size ηp^2
Primary BA	42.31	43.09	39.27	42.44	41.97	2.602	0.993	0.005
αMCA	12.08	13.17	11.82	15.05	13.25	0.886	0.813	0.033
βMCA	28.44	28.32	25.63	25.72	27.07	1.815	0.980	0.009
CA	1.717	1.457	1.655	1.501	1.460	0.189	0.989	0.006
CDCA	0.068	0.142	0.162	0.172	0.199	0.035	0.820	0.032
Secondary BA	30.41	22.47	26.05	22.06	24.60	2.126	0.800	0.035
ωMCA	7.835	10.33	7.846	8.370	8.474	0.676	0.780	0.037
UDCA	0.506	0.999	0.739	0.662	0.856	0.124	0.780	0.037
HDCA	0.393	0.275	0.259	0.176	0.244	0.037	0.468	0.074
DCA	1.639	1.741	1.487	1.560	1.844	0.183	0.978	0.009
LCA	2.219^{a}	1.600^{ab}	1.661^{ab}	1.103^{b}	0.919^{b}	0.125	0.005	0.272
HCA	16.52	12.35	13.70	10.03	12.07	1.323	0.639	0.053
βHDCA	1.297^{a}	0.162^{b}	0.343^{b}	0.169^{b}	0.200^{b}	0.090	<0.001	0.481
Conjugated BA	0.983	0.750	1.851	1.439	1.367	0.243	0.665	0.050
TαMCA	0.203	0.094	0.193	0.449	0.306	0.054	0.291	0.102
TωMCA	0.104^{ab}	0.156^{ab}	0.134^{ab}	0.421^{a}	0.056^{b}	0.043	0.049	0.180
TβMCA	0.580	0.447	1.444	0.533	0.822	0.179	0.407	0.083
GCA	0.057	0.036	0.061	0.016	0.136	0.023	0.535	0.065
TCDCA	0.040	0.017	0.019	0.020	0.046	0.005	0.172	0.129
Total BA	73.70	71.31	67.17	65.95	67.95	4.546	0.984	0.008

Mean values within a row with unlike superscript letters are shown to be significantly different ($p<0.05$; post-hoc Tukey test); ηp^2, partial eta squared; SEM, pooled standard error of the mean (standard deviation for all rats divided by the square root of rat number, $n=50$); MCA, muricholic acid; CA, cholic acid; HDCA, hyodeoxycholic acid; UDCA, ursodeoxycholic acid; CDCA, chenodeoxycholic acid; DCA, deoxycholic acid; LCA, lithocholic acid; TMCA, tauromuricholic acid; GCA, glycocholic acid; TCDCA, taurochenodeoxycholic acid; HCA, hyocholic acid. Experimental groups: C, control diet; G, diet with 2% (*w/w*) of untreated onion (v. Allurion) preparation; GD, diet with 2% (*w/w*) of onion preparation obtained by osmotic dehydration in a glucose-fructose syrup; GDFa, diet with 2% (*w/w*) of onion preparation obtained by osmotic dehydration in a glucose-fructose syrup and fermentation with *Levilactobacillus brevis* ŁOCK 944; GDFb, diet with 2% (*w/w*) of onion preparation obtained by osmotic dehydration in a glucose-fructose syrup and fermentation with *Lactiplantibacillus plantarum* P27.

regard to carbohydrate metabolism parameters, the plasma expression levels (NPX) of carboxypeptidase E (Cpe), delta-like 1 homolog (Dlk1), enolase 2 (Eno2), and follistatin-related protein 3 (Fstl3) were characterized with a moderate effect size (ηp^2=0.066–0.084). The lipoprotein lipase (Lpl) and perilipin-1 (Plin1) plasma relative expression levels, which are connected with lipid metabolism, were characterized with a moderate effect size (ηp^2=0.070–0.082). The dietary onion treatments explained 11% of the variance in the expression level of epithelial cell adhesion molecule (Epcam). Effect size estimates provide information on the magnitude of biological differences and may be informative even in the absence of statistical significance, particularly in studies with limited power. While our findings should be interpreted with caution, the observed effect sizes suggest that these proteins (connected with moderate to large effect size) may be biologically relevant and warrant further investigation in larger, adequately powered studies, or in dietary scenarios with higher supplementation doses.

CONCLUSIONS

In summary, the observed moderate-to-large effect sizes indicate that dietary onion supplementation plays a significant role in influencing body composition and metabolic response in rats. In all groups fed diets with onion preparations, there was a consistent downregulation of hepatic *Hif1a*, *Scd1*, and *Acly*, suggesting that onion intake exerts an anti-lipogenic effect that

was independent of onion processing methods. Furthermore, osmotic dehydration in a glucose-fructose syrup enhanced these benefits, as evidenced by a reduction in the expression of inflammatory and lipogenic genes (*Nfkb1*, *Srebf1*, *Tlr4*) and improvement in plasma markers related to liver function and lipid metabolism. The subsequent fermentation process exerted additional, preparation-specific effects on hepatic genes involved in fatty acid oxidation, bile acid metabolism, and inflammatory regulation. Overall, dietary onion preparations appear to be valuable vehicles of these beneficial metabolic impacts, while the technological processing of onions can influence their specificity. These findings highlight the potential of appropriately processed onion preparations as functional dietary components that can promote metabolic health.

RESEARCH FUNDING

The research was funded by National Science Centre, Poland (OPUS, 2022/45/B/NZ9/00550).

CONFLICT OF INTERESTS

The authors declare that they have no conflict of interests.

ADDITIONAL INFORMATION

The animal study was approved by Local Animal Care and Use Committee in Olsztyn, Poland (Approval No. 41/2022; Olsztyn, Poland, 15.06.2022).

SUPPLEMENTARY MATERIALS

The following are available online at **https://journal.pan.olsztyn.pl/Impact-of-Osmotic-Dehydration-and-Lactic-Acid-Fermentation-of-Onion-on-the-Physiological,225064,0,2.html**; **Table S1**. The composition of control and experimental diets (g/100 g diet). **Table S2**. Hematological parameters in rats fed diets with onion preparations and control diet. **Table S3**. Microbial enzymatic activity in the cecal digesta in rats fed diets with onion preparations and control diet. **Table S4**. Plasma relative protein levels (normalized protein expression, NPX) related to immunological status in rats fed diets with onion preparations and control diet. **Table S5**. Plasma relative protein levels (normalized protein expression, NPX) related to redox status, glucose/insulin, lipids metabolism and intestinal tissue integrity in rats fed diets with onion preparations and control diet.

ORCID IDs

B. Fotschki **https://orcid.org/0000-0002-9727-7481**
J. Fotschki **https://orcid.org/0000-0002-0116-0909**
K. Grzelak-Błaszczyk **https://orcid.org/0000-0002-2399-4138**
M. Grzegorzewska **https://orcid.org/0000-0003-4499-6404**
K. Jaworska **https://orcid.org/0009-0005-5071-0400**
J. Juśkiewicz **https://orcid.org/0000-0003-0068-5970**
E. Klewicka **https://orcid.org/0000-0002-3958-0407**
R. Klewicki **https://orcid.org/0000-0003-0600-9906**
D. Napiórkowska **https://orcid.org/0009-0002-0497-9968**
L. Piekarska-Radzik **https://orcid.org/0000-0002-9438-0299**
M. Sójka **https://orcid.org/0000-0003-0848-7629**
S. Ścieszka **https://orcid.org/0000-0002-9678-8407**

REFERENCES

1. Benítez, V., Mollá, E., Martín-Cabrejas, M.A., Aguilera, Y., López-Andréu, F.J., Cools, K., Terry, L.A., Esteban, R.M. (2011). Characterization of industrial onion wastes (*Allium cepa* L.): dietary fibre and bioactive compounds. *Plant Foods for Human Nutrition*, *66*(1), 48-57. **https://doi.org/10.1007/s11130-011-0212-x**
2. Chang, W.-L., Liu, P.-Y., Yeh, S.-L., Lee, H.-J. (2022). Effects of dried onion powder and quercetin on obesity-associated hepatic manifestation and retinopathy. *International Journal of Molecular Sciences*, *23*(19), art. no. 11091. **https://doi.org/10.3390/ijms231911091**
3. Chen, L., Ye, Z., Li, J., Wang, L., Chen, Y., Yu, M., Han, J., Huang, J., Li, D., Lv, Y., Xiong, K., Tian, D., Liao, J., Seidler, U., Xiao, F. (2025). Gut bacteria *Prevotellaceae* related lithocholic acid metabolism promotes colonic inflammation. *Journal of Translational Medicine*, *23*(1), art. no. 55. **https://doi.org/10.1186/s12967-024-05873-6**
4. Conway, E.J. (1957). Microdiffusion Analysis and Volumetric Error, 4th edition, Crosby Lockwood and Son, London, UK.
5. Cordero-Pérez, P., Tijerina-Márquez, R., Rivas-Galindo, V.M., Torres-González, L., Rodríguez-Rodríguez, D.R., Mendoza-Hernández, O.H., Espinosa-Cantú, C.B., Solís-Cruz, G.Y., Muñoz-Espinosa, L.E., Pérez-Rodríguez, E., Cura-Esquivel, I., Alarcón-Galván, G., Moreno-Pena, D.P. (2025). Antioxidant and hepatoprotective effect of *Jatropha dioica* against the valproic acid-induced damage in an *in vivo* model. *BMC Complementary Medicine and Therapies*, *25*(1), art. no. 207. **https://doi.org/10.1186/s12906-025-04914-x**
6. Ding, K., Xie, R., Han, B., Zheng, H., Tian, T. (2025). Histone methyltransferase SMYD2 regulates the activation of hepatic stellate cells by activating TLR4 signaling. *Scientific Reports*, *15*(1), art. no. 13166. **https://doi.org/10.1038/s41598-025-96699-9**
7. Folch, J., Lees, M., Stanley, G.H.S. (1957). A simple method for the isolation and purification of total lipids from animal tissues. *Journal of Biological Chemistry*, *226*(1), 497-509. **https://doi.org/10.1016/S0021-9258(18)64849-5**
8. Galus, S., Rybak, K., Dadan, M., Witrowa-Rajchert, D., Nowacka, M. (2025). The effect of the use of unconventional solutions for osmotic dehydration on selected properties of fresh-cut oranges. *Foods*, *14*(3), art. no. 468. **https://doi.org/10.3390/foods14030468**
9. Grzelak, K., Milala, J., Król, B., Adamicki, F., Badełek, E. (2009). Content of quercetin glycosides and fructooligosaccharides in onion stored in a cold room. *European Food Research & Technology*, *228*, 1001-1007. **https://doi.org/10.1007/s00217-009-1018-z**
10. Grzelak-Błaszczyk, K., Czarnecki, A., Klewicki, R., Grzegorzewska, M., Klewicka, E. (2023). Lactic acid fermentation of osmo-dehydrated onion. *Food Chemistry*, *399*, art. no. 133954. **https://doi.org/10.1016/j.foodchem.2022.133954**
11. Grzelak-Błaszczyk, K., Grzegorzewska, M., Klewicki, R. (2021). Retention of flavonols in onions after osmotic dehydration. *LWT – Food Science and Technology*, *150*, art. no. 112067. **https://doi.org/10.1016/j.lwt.2021.112067**
12. Grzelak-Błaszczyk, K., Milala, J., Kołodziejczyk, K., Sójka, M., Czarnecki, A., Kosmala, M., Klewicki, R., Fotschki, B., Jurgoński, B., Juśkiewicz, J. (2020). Protocatechuic acid and quercetin glucosides in onions attenuate changes induced by high fat diet in rats. *Food & Function*, *11*, 3585-3597. **https://doi.org/10.1039/c9fo02633a**
13. Gupta, A.J., Kaldate, S., Valaguthala, S., Mahajan, V. (2025). Onion nutritional and nutraceutical composition and therapeutic potential of its phytochemicals assessed through preclinical and clinical studies. *Journal of Functional Foods*, *129*, art. no. 106889. **https://doi.org/10.1016/j.jff.2025.106889**
14. Hejazi, N., Ghalandari, H., Nouri, M., Askarpour, M. (2023). Onion supplementation and health metabolic parameters: A systematic review and meta-analysis of randomized controlled trials. *Clinical Nutrition ESPEN*, *58*, 1-13. **https://doi.org/10.1016/j.clnesp.2023.08.032**
15. Herrero-Cervera, A., Soehnlein, O., Kenne, E. (2022). Neutrophils in chronic inflammatory diseases. *Cellular & Molecular Immunology*, *19*(2), 177-191. **https://doi.org/10.1038/s41423-021-00832-3**
16. Horwitz, W., Latimer, G.W., Jr. (Eds.). (2007). Official Methods of Analysis of AOAC International (18th ed., Rev. 2). AOAC International. ISBN: 9780935584783.
17. Juśkiewicz, J., Fotschki, B., Stępniowska, A., Cholewińska, E., Napiórkowska, D., Marzec, A., Brzuzan, Ł., Fotschki, J., Żary-Sikorska, E., Ognik, K. (2024). Dietary fiber with functional properties counteracts the thwarting effects of copper nanoparticles on the microbial enzymatic activity and short-chain fatty acid production in the feces of rats. *Polish Journal of Food and Nutrition Sciences*, *74*(4), 363-375. **https://doi.org/10.31883/pjfns/194694**

18. Klewicka, E., Libudzisz, Z., Śliżewska, K., Otlewska, A. (2013). *A new strain of the lactic acid bacterium Lactobacillus brevis*. (Polish Patent No. PL 214504). Polish Patent Office (in Polish).
19. Lee, J.S., Cha, Y.J., Lee, K.H., Yim, J.E. (2016). Onion peel extract reduces the percentage of body fat in overweight and obese subjects: a 12-week, randomized, double-blind, placebo-controlled study. *Nutrition Research and Practice*, *10*(2), 175-181. **https://doi.org/10.4162/nrp.2016.10.2.175**
20. Li, Q., Wang, Y., Mai, Y., Li, H., Wang, Z., Xu, J., He, X. (2020). Health benefits of the flavonoids from onion: constituents and their pronounced antioxidant and anti-neuroinflammatory capacities. *Journal of Agricultural and Food Chemistry*, *68*(3), 799-807. **https://doi.org/10.1021/acs.jafc.9b07418**
21. Mikulski, D., Juśkiewicz, J., Ognik, K., Fotschki, B., Tykałowski, B., Jankowski, J. (2024). Gastrointestinal response to the early administration of antimicrobial agents in growing turkeys infected with *Escherichia coli*. *Poultry Science*, *103*(6), art. no. 103720. **https://doi.org/10.1016/j.psj.2024.103720**
22. Nowak, K.W., Miszczak, I., Pszczółkowski, B., Rejmer, W., Zielińska, M. (2025). Application of ultrasound in convective drying of fermented, frozen-thawed, and osmotically dehydrated beetroot slices. *Polish Journal of Food and Nutrition Sciences*, *75*(3), 221-233. **https://doi.org/10.31883/pjfns/208279**
23. Rauckhorst, A.J., Sheldon, R.D., Pape, D.J., Ahmed, A., Falls-Hubert, K.C., Merrill, R.A., Brown, R.F., Deshmukh, K., Vallim, T.A., Deja, S., Burgess, S.C., Taylor, E.B. (2025). A hierarchical hepatic *de novo* lipogenesis substrate supply network utilizing pyruvate, acetate, and ketones. *Cell Metabolism*, *37*(1), 255-273.e6. **https://doi.org/10.1016/j.cmet.2024.10.013**
24. Rauf, A., Ajaj, R., Akram, Z., Khan, M., Wadood, A., Zulfat, M., Shah, Z.A., Alamri, A.S., Alsanie, W.F., Alhomrani, M., Hussain, H., Formanowicz, D. (2025). Investigation of the inhibitory potential of secondary metabolites isolated from *Fernandoa adenophylla* against Beta-glucuronidase *via* molecular docking and molecular dynamics simulation studies. *PLoS One*, *20*(5), art. no. e0324100. **https://doi.org/10.1371/journal.pone.0324100**
25. Revaskar, V.A., Pisalkar, P.S., Pathare, P.B., Sharma, G.P. (2014). Dehydration kinetics of onion slices in osmotic and air convective drying process. *Research in Agricultural Engineering*, *60*(3), 92-99. **https://doi.org/10.17221/22/2012-RAE**
26. Ścieszka, S., Piekarska-Radzik, L., Klewicki, R., Sójka, M., Juśkiewicz, J., Fotschki, B., Klewicka, E., Grzelak-Błaszczyk, K. (2025). Spontaneously fermented *Allium cepa* L. as a source of lactic acid bacteria with probiotic potential. *Scientific Reports*, *15*(1), art. no. 25970. **https://doi.org/10.1038/s41598-025-10037-7**
27. Sepehri, S., De Win, D., Heymans, A., Van Goethem, F., Rodrigues, R.M., Rogiers, V., Vanhaecke, T. (2025). Next generation risk assessment of hair dye HC yellow no. 13: Ensuring protection from liver steatogenic effects. *Regulatory Toxicology and Pharmacology*, *159*, art. no. 105794. **https://doi.org/10.1016/j.yrtph.2025.105794**
28. Shang, H., Huang, C., Xiao, Z., Yang, P., Zhang, S., Hou, X., Zhang, L. (2023). Gut microbiota-derived tryptophan metabolites alleviate liver injury *via* AhR/Nrf2 activation in pyrrolizidine alkaloids-induced sinusoidal obstruction syndrome. *Cell & Bioscience*, *13*(1), art. no. 127. **https://doi.org/10.1186/s13578-023-01078-4**
29. Son, M.J., Kim, J.T., Lee, G.Y., Zhou, Y., Jeon, D.H., Kwon, J.W., Kim, M.J., Jung, S.K., Kim, Y.J., Kim, J.H., Jo, J.Y., Byun, S., Lee, H.J. (2024). Effect of onion peel extract and quercetin at an equivalent concentration in the extract on the improvement of dyslipidemia induced by high fat diet in rats. *Food Science and Biotechnology*, *34*(4), 1045-1054. **https://doi.org/10.1007/s10068-024-01741-7**
30. Yadav, A.K., Singh, S.V. (2014). Osmotic dehydration of fruits and vegetables: a review. *Journal of Food Science and Technology*, *51*(9), 1654-1673. **https://doi.org/10.1007/s13197-012-0659-2**
31. Yang, B., Zhang, B., Cao, Z., Xu, X., Huo, Z., Zhang, P., Xiang, S., Zhao, Z., Lv, C., Meng, M., Zhang, G., Dong, L., Shi, S., Yang, L., Zhou, Q. (2020). The lipogenic LXR-SREBF1 signaling pathway controls cancer cell DNA repair and apoptosis and is a vulnerable point of malignant tumors for cancer therapy. *Cell Death & Differentiation*, *27*(8), 2433-2450. **https://doi.org/10.1038/s41418-020-0514-3**
32. Yazidi, R., Yeddes, W., Rybak, K., Witrowa Rajchert, D., Aidi Wannes, W., Hammami, M., Hessini, K., Saidani Tounsi, M., Nowacka, M. (2024). Osmotic dehydration of orange fruits in sucrose and prickly pear molasses solutions: Mass transfer and quality of dehydrated products. *Polish Journal of Food and Nutrition Sciences*, *74*(4), 340-349. **https://doi.org/10.31883/pjfns/194785**
33. Yoshinari, O., Shiojima, Y., Igarashi, K. (2012). Anti-obesity effects of onion extract in Zucker diabetic fatty rats. *Nutrients*, *4*(10), 1518-1526. **https://doi.org/10.3390/nu4101518**
34. Yu, H.C., Jin, L., Bai, L., Zhang, Y.J., Yang, Z.X. (2025). C12ORF49 inhibits ferroptosis in hepatocellular carcinoma cells *via* reprogramming SREBP1/SCD1-mediated lipid metabolism. *Cell Death Discovery*, *11*(1), art. no. 178. **https://doi.org/10.1038/s41420-025-02480-2**
35. Zeng, R., Wang, Y., Wen, J., Cen, Z., Wang, T., Duan, M., Huang, X., Zhao, Z., Zhang, Z., Yang, C., Chen, S. (2025). Hypoxia-inducible factor-1α inhibitor promotes non-alcoholic steatohepatitis development and increases hepatocellular lipid accumulation *via* TSKU upregulation. *Archives of Biochemistry and Biophysics*, *765*, art. no. 110313. **https://doi.org/10.1016/j.abb.2025.110313**

ORIGINAL ARTICLE
http://journal.pan.olsztyn.pl

Polish Journal of Food and Nutrition Sciences
2026, Vol. 76, No. 3, 242–250
DOI: 10.31883/pjfns/225254
ISSN 1230-0322, e-ISSN 2083-6007

Fermentation of Bergamot (*Citrus bergamia* Risso) Fruit with *Lactobacillus plantarum*: Phenolic Compound Content, Antioxidant Capacity, and Prebiotic Potential

Ozlem Aslan Bursali[1], Bora Ekinci[2*], Ahmet S. Sonmezdag[2]

[1]Nutrition and Dietetics Msc. Program, Institute of Health Sciences, Mugla Sitki Kocman University, Mentese, Mugla 48000, Turkey
[2]Department of Nutrition and Dietetics, Faculty of Health Sciences, Mugla Sitki Kocman University, Mentese, Mugla 48000, Turkey

Bergamot (*Citrus bergamia* Risso) fruit is rich in flavonoids and health-promoting compounds. However, it is not widely consumed unprocessed because of its bitter taste. In this study, the potential of fermenting the entire bergamot fruit, including its non-consumable fractions, with *Lactobacillus plantarum* was evaluated with respect to bacterial viability, antioxidant capacity, and phenolic compound content. A bergamot homogenate was inoculated with *L. plantarum* and incubated at 30°C for 6 days. Simultaneously, an uninoculated homogenate was incubated as a control. Samples collected on days 0, 2, 3, 4, and 6 were analyzed for total phenolic content, DPPH$^{\bullet}$ and ABTS$^{\bullet+}$ scavenging activity, and contents of individual phenolic compounds, including neoeriocitrin, naringin, neoeriocitrin dioxalate, neohesperidin, neohesperidin dioxalate, and melitidin. The total phenolic content increased from 20.17 to 21.74 mg GAE/mL in the fermentation group, whereas an insignificant change was found in the sample without *L. plantarum* inoculation on day 6. Antioxidant capacity in the ABTS assay increased from 8.56 to 9.72 mmol Trolox/L following fermentation, while it decreased to 7.63 mmol Trolox/L in the control group. The contents of neoeriocitrin, naringin, and neoeriocitrin dioxalate increased significantly on the 4th day, to 297.23 µg/L, 160.37 µg/L, and 55.86 µg/L, respectively. Melitidin content, on the other hand, decreased over the fermentation period. This study provides the first evidence of a change in neoeriocitrin content during bergamot fermentation and demonstrates that the 4th day of fermentation represents the optimal stage for increasing bioactive compound content, while maintaining antioxidant capacity.

Keywords: *Citrus bergamia*, fermentation, *Lactobacillus plantarum*, neoeriocitrin, phenolic compounds

INTRODUCTION

Bergamot (*Citrus bergamia* Risso) is a tree belonging to the Rutaceae family, native to Western India, with fruits resembling yellow oranges in size and shape. Distinguished by health-promoting compounds that are uncommon in other citrus fruits, bergamot is valued for its rich flavonoid profile and volatile organic compound composition, which have led to numerous industrial and functional applications [Baron *et al*., 2021; Dosoky & Setzer, 2018; Forlot & Pevet, 2012; Nogata *et al*., 2006]. However, due to its acidic and bitter taste, bergamot is not widely consumed as a fruit juice, thereby increasing interest has aroused in the alternative utilization of pectin and bioactive compounds derived from its juice and albedo fractions [Ballistreri *et al*., 2021; Capomolla *et al*., 2019; Navarra *et al*., 2020]. Bergamot juice, peel, and albedo contain considerable amounts of health-promoting compounds and pectin with potential prebiotic properties. Nevertheless, the fruit is primarily processed for essential oil extraction from the peel, leaving a substantial portion of the remaining biomass

***Corresponding Author:**
E-mail: **bekinci@mu.edu.tr**, e-mail: **immunbora@gmail.com** (Dr. B. Ekinci)

Submitted: 16 January 2026
Accepted: 30 June 2026
Published on-line: 15 July 2026

underutilized and discarded as waste [Di Donna *et al*., 2020; Gattuso *et al*., 2023].

Among these bioactive compounds, phenolic compounds, particularly flavonoids, have attracted considerable attention due to their significant pharmacological properties. Approximately 61 phenolic compounds have been identified in various parts of the bergamot fruit, including the pulp, peel, flavedo, and albedo [Baron *et al*., 2021]. Most of these compounds are glycosides and acetyl derivatives of flavones and flavanones [Baron *et al*., 2021; Nogata *et al*., 2006; Pernice *et al*., 2009]. Neoeriocitrin, naringin, neohesperidin, naringin dioxalate, and neohesperidin dioxalate constitute nearly 90% of flavanone *O*-glycosides [Delle Monache *et al*., 2013]. The flavonoids present in bergamot exhibit numerous bioactivities, including anticancer, antioxidant, anti-inflammatory, antidiabetic, antibacterial, and antifungal properties as well as protection against the metabolic syndrome [Ortiz *et al*., 2022; Shilpa *et al*., 2023]. Research suggests that the antiproliferative and pro-apoptotic effects observed in cancer cells are associated with the suppression of cyclooxygenase-2 (COX-2) expression, decreased reactive oxygen species (ROS) levels, modulation of oncogenic signaling pathways, and downregulation of nuclear transcription factor kappa B (NF-kB) [Delle Monache *et al*., 2013].

As studies have elucidated the impact of colon health on overall well-being, prebiotics and probiotics used in fermentation technology are gaining increasing importance and are becoming highly researched. Fermentation plays a key role in the food industry by contributing to the production of functional foods and beverages with an enhanced nutritional value and contents of health-promoting compounds, such as bioactive compounds with increased bioavailability and beneficial end products like short-chain fatty acids (SCFAs) [Cecchi *et al*., 2024]. Ongoing studies are aimed at identifying bacterial strains during fermentation that do not reduce the concentrations of key components [Di Donna *et al*., 2020]. Lactobacillus species, particularly *Lactobacillus plantarum*, play a significant role among the bacteria commonly used in lactic acid fermentation. *L. plantarum* is widely used in the fermentation of various food products such as dairy, pickles, fermented beverages, and fermented vegetables. *L. plantarum* is recognized as safe by the Food and Drug Administration (FDA) because of its probiotic features, ability to adapt to environmental conditions, and ability to withstand different pH levels, temperatures, and salt concentrations [Behera *et al*., 2018].

Processing and consumption of the fruit generate considerable amounts of by-products, accounting for nearly half of the total fruit weight and consisting mainly of peels, seeds, pulp, and segment residues. This waste contains substantial quantities of bioactive compounds and exhibits a high biological oxygen demand, thereby contributing to environmental pollution [Di Donna *et al*., 2020]. Limited research has investigated the valorization potential of bergamot fruit, including its albedo, through microbial fermentation, particularly regarding its effects on bioactive compound composition, antioxidant activity, and prebiotic potential. Therefore, this study aimed to evaluate the potential of *L. plantarum* fermentation to enhance the functional properties of bergamot fruit, including the non-consumable albedo fraction, by analyzing total phenolic content, antioxidant capacity, flavonoid composition, and prebiotic characteristics.

MATERIALS AND METHODS

Preparation of a bergamot homogenate

Approximately 10 kg of bergamot fruit commercially sourced from a local grower in the Antalya region in Turkey was used in this study. The fruits were washed with an iodine solution, rinsed, and peeled. The albedo portions were retained. The peeled fruits were homogenized using a Waring 8011 blender (Waring Laboratory Science, Torrington, CT, USA) and stored at –80°C until the completion of the study.

Fermentation process

A commercially obtained probiotic strain of *L. plantarum* (Swanson Health Products, Fargo, ND, USA) was reactivated by inoculating it into De Man, Rogosa, and Sharpe (MRS) broth (Biokar Diagnostics, Beauvais, France) and grown at 36°C for 24 h. A bergamot homogenate (75 mL corresponded to 75 g of fruits) was diluted with sterile distilled water at a 1:4 (*v/v*) ratio (total volume of 300 mL) and adjusted to pH 7.0 using 3 M KOH. Two different experimental setups were implemented: a control group without bacteria addition and a fermentation group inoculated with *L. plantarum*, 10^6 CFU/mL (LP group). The experimental design was adapted from Hashemi & Jafarpour [2020]. To determine the optimal growth conditions, parameters such as temperature and incubation time were optimized, and 30°C for 6 days were identified as optimal for growth.

Samples (300 mL) collected on days 0, 2, 3, 4, and 6 were centrifuged at 2,650×*g* for 30 min using a 5804 R centrifuge (Eppendorf, Hamburg, Germany), and the supernatant was used for future analysis of pH, total phenolic content, antioxidant capacity, and individual phenolic compound content. The fermentation experiments were carried out in three independent batches prepared at different times under identical conditions. Samples collected at each time point were analyzed in triplicate.

Determination of total live bacteria count

For each sampling day, 100 µL of bergamot homogenates from both the control and fermentation groups were taken, serially diluted, and plated on MRS agar for the determination of viable *L. plantarum* counts. The control group was used to verify the absence of contamination by indigenous lactic acid bacteria (LAB). The plates were incubated at 36°C for 48 h [Multari *et al*., 2020]. The visible colonies were enumerated, and the results were presented as log CFU/mL of product.

Determination of antioxidant capacity

2,2-Diphenyl-1-picrylhydrazyl radical scavenging activity determination

A solution of 3.54 mg of 2,2-diphenyl-1-picrylhydrazyl (DPPH) radicals (TCI, Tokyo, Japan) in 150 mL of methanol was prepared

by placing in an ultrasonic bath (VCX 130 PB, Sonics and Materials, Inc., Newtown, CT, USA) for 30 min. After passing through a 0.45 µm filter, supernatants of both control and LP groups were diluted at 1/20, and this dilution was used to calculate the results from the Trolox calibration curve. Sample solutions (0.1 mL) were mixed with 3.9 mL of a DPPH$^{\bullet}$ solution. The absorbances were read at 515 nm after 30 min of incubation in the dark [Brand-Williams *et al.*, 1995]. For the calibration curve, Trolox (Sigma-Aldrich, Saint Louis, MO, USA) solutions at concentrations of 100, 50, 25, 12.5, 6.25, and 3.125 µmol/L were prepared and analyzed under the same conditions. The results were expressed as mmol Trolox/L of supernatant.

2,2′-Azinobis(3-ethylbenzothiazoline-6-sulfonic acid) assay

A mixture of 360.2 mg of 2,2′-azino-bis(3-ethylbenzothiazoline-6-sulfonic acid) (ABTS; Sigma-Aldrich) and 67.5 mg of potassium persulfate (Sigma-Aldrich) was prepared, completed to 100 mL with a methanol and water mixture (80:20, *v/v*), and left for 16 h [Re *et al.*, 1999]. Prior to analysis, 30 mL of this solution with generated ABTS$^{\bullet+}$ was adjusted to an absorbance of 0.7 at 734 nm by adding 300 mL of a methanol and water solution (80:20, *v/v*). The calibration curve was prepared using Trolox solutions with a concentration range from 3.125 to 100 µmol /L. For the reaction, 100 µL of the sample or the standard solution was mixed with 3.9 mL of the ABTS$^{\bullet+}$ solution and left for 15 min in the dark at room temperature, absorbance was then measured at 734 nm. ABTS$^{\bullet+}$ scavenging activity was expressed as mmol Trolox/L of supernatant based on the standard curve.

Determination of total phenolic content

The total phenolic content of the bergamot supernatant was analyzed using the Folin-Ciocalteu reagent [Singleton *et al.*, 1999]. In this method, 300 µL of supernatants were mixed with 1.5 mL of the Folin-Ciocalteu reagent (Merck, Darmstadt, Germany) diluted 10 times and 1.2 mL of a 7.5% (*w/v*) solution of sodium carbonate (Merck). After vortex mixing, the tubes were incubated in the dark at 25°C for 90 min, and absorbances were measured at 760 nm using a spectrophotometer (T80+ UV/VIS spectrometer, PG Instruments, Lutterworth, UK). The total phenolic content was calculated using gallic acid standard curve and expressed as mg gallic acid equivalent (GAE)/mL of supernatant.

Analysis of phenolic compound composition

The phenolic compounds were identified and quantified in the collected samples using liquid chromatography-diode array detection–electrospray ionization-mass spectrometry (LC-DAD-ESI-MS/MS) according to the procedure adapted from Kelebek *et al.* [2020]. An Agilent 1100 HPLC system (Agilent Technologies, Santa Clara, CA, USA) with a diode array detector equipped with Windows NT-based ChemStation software was used for phenolic compound analysis. A reverse-phase Luna C18 column (4.6×250 mm, 5 µm diameter; Phenomenex, Torrance, CA, USA) was employed. Two different solvents were used in the mobile phase: solvent A consisting of water and formic acid (99:1, *v/v*) and solvent B consisting of solvent A and acetonitrile (60:40, *v/v*). Phenolic compounds were eluted under the following conditions: 0–5 min, 0% B; 5–25 min, 0–5% B; 25–43 min, 5–15% B; 43–57 min, 15–25% B; 57–88 min, 25–50% B; and 88–91 min, 50–100% B. The flow rate was set at 0.5 mL/min, and the temperature was maintained at 25°C. Ultraviolet-visible (UV-Vis) spectra (from 200 to 800 nm) were recorded for all the peaks. Samples were also analyzed using an Agilent 6430 LC-MS/MS system (Agilent Technologies) equipped with an electrospray ionization source. Detection was performed in a negative ion mode under optimized conditions: capillary temperature 400°C, capillary voltage −3 V, nebulizer gas flow 1.75 L/min, desolvation gas flow 1 L/min, and spray voltage 5 kV. The identification of neoeriocitrin, naringin, and neohesperidin was performed by comparing their retention times and UV spectra with those of authentic standards, and the identities were further confirmed by LC-ESI-MS/MS analysis in a multiple reaction monitoring (MRM) mode. Neoeriocitrin, naringin, and neohesperidin standards were purchased from Sigma-Aldrich. Neoeriocitrin dioxalate, melitidin, and neohesperidin dioxalate were tentatively identified based on their UV spectra, MS/MS fragmentation patterns, and literature data. These tentatively identified compounds were semi-quantified as equivalents of the structurally closest available standards. Quantification was carried out using calibration curves prepared from the available authentic standards, with regression coefficients consistently exceeding 0.995. The calculated amounts of phenolic compounds were expressed as mg/L of supernatant.

Statistical analysis

The data obtained in this study were analyzed using SPSS Statistics for Windows 25.0 (IBM, Armonk, NY, USA). For quantitative data comparisons in normally distributed datasets, an independent *t*-test was applied for differences between two independent groups, whereas a one-way analysis of variance (ANOVA) was used for comparisons involving more than two independent groups. In cases where a significant difference was found, Duncan's post-hoc test was used to identify the specific group(s) causing the difference. Differences were considered significant at $p<0.05$. Correlation analysis was conducted to examine the relationships between the two variables.

RESULTS AND DISCUSSION

Total live bacteria count and pH

The growth rate of probiotic strains can vary based on the composition and physicochemical properties of the food as well as the metabolic capacity and nutritional requirements of the microorganisms. *L. plantarum* requires a limited number of amino acids compared to other lactic acid bacteria, which may require more than fifteen amino acids for optimal growth [Gokavi *et al.*, 2005]. The growth kinetics of *L. plantarum* and the corresponding pH changes during fermentation of bergamot fruit homogenate are presented in **Figure 1**. *L. plantarum* exhibited a prolonged adaptation phase in the homogenate, characterized by relatively

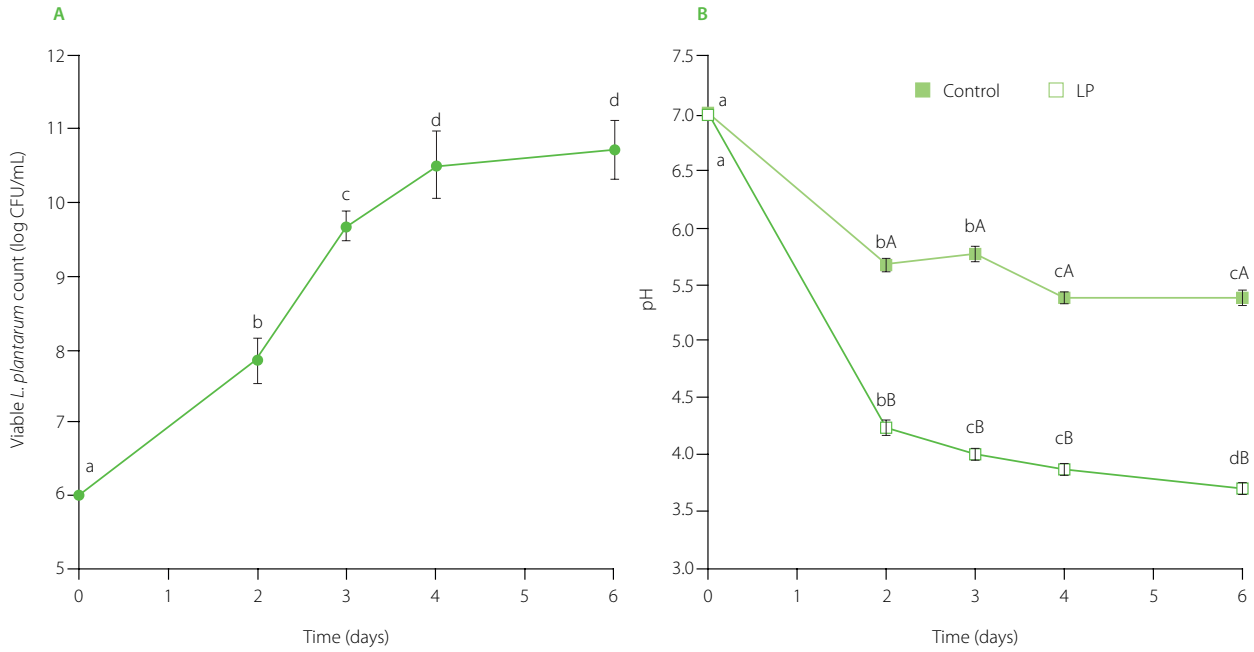

Figure 1. (**A**) Changes in viable *L. plantarum* counts in bergamot homogenate during 6 days of fermentation. No growth was detected in the control group, and therefore it was not illustrated in the figure. (**B**) Changes in pH during fermentation of bergamot homogenate inoculated with *L. plantarum* (LP) and the control group. Different lowercase letters indicate significant differences between fermentation days within the same group, whereas different uppercase letters indicate significant differences between the LP and control group on the same fermentation day ($p<0.05$).

slow growth during the first 48 h, followed by a marked increase in viable cell counts. Growth stabilized on the 4th day and reached 10.7 log CFU/mL (5.3×10^{10} CFU/mL) by the 6th day, at which point fermentation was terminated. Throughout the fermentation period, pH values in the LP group decreased. In the control group, pH also decreased, but reached the equilibrium on day 4. Significant differences were observed between the control and LP groups on each day of fermentation ($p<0.05$). Final pH values were 5.4 for the control group and 3.7 for the LP group, indicating active acid fermentation. In a study by Hashemi & Jafarpour [2020], fermenting bergamot juice with *L. plantarum* subsp. *plantarum* PTCC 1896, *L. plantarum* AF1, and *L. plantarum* LP3 for 72 h resulted in an increase in the live cell count of *L. plantarum* AF1 from 6 log CFU/mL to 8.9 log CFU/mL. Although the overall growth patterns observed in the present study are consistent with previous findings, the relatively slower growth rate may be attributed to the use of a single bacterial strain and the absence of cross-feeding interactions that typically occur in mixed microbial consortia [Hashemi & Jafarpour, 2020]. Owing to the delayed adaptation of *L. plantarum* to the bergamot homogenate medium, fermentation was extended to six days, at which point maximum viable counts were achieved. These findings support the potential of bergamot homogenate as a substrate with prebiotic characteristics capable of sustaining probiotic growth.

Antioxidant capacity

Fermentation may influence the antioxidant properties of plant-based substrates by modifying the composition, availability, and activity of phenolic compounds. Microbial enzymatic activities can promote the release of bound phenolics and facilitate their transformation into compounds with different antioxidant characteristics. Consequently, fermentation has the potential to alter the antioxidant capacity of food matrices, making the assessment of antioxidant activity an important parameter in evaluating the functional properties of fermented products [Hur *et al.*, 2014].

To ensure a reliable determination of the antioxidant capacity, two assays (DPPH and ABTS assays) were used. As depicted in **Figure 2**, the antioxidant capacity of the supernatant from the untreated bergamot homogenate (day 0) was determined as 8.56 mmol Trolox/L using the ABTS assay and 3.25 mmol Trolox/L using the DPPH assay. During the fermentation period, some fluctuations in antioxidant activity were observed in the ABTS assay; it decreased at the beginning of the process and then increased in both groups. Such fluctuations in DPPH radical scavenging activity were negligible. Nevertheless, following six days of fermentation, antioxidant capacity in the LP group increased to 9.72 and 3.55 mmol Trolox/L, respectively, while in the control group, it decreased significantly ($p<0.05$) to 7.63 and 2.80 mmol Trolox/L, respectively.

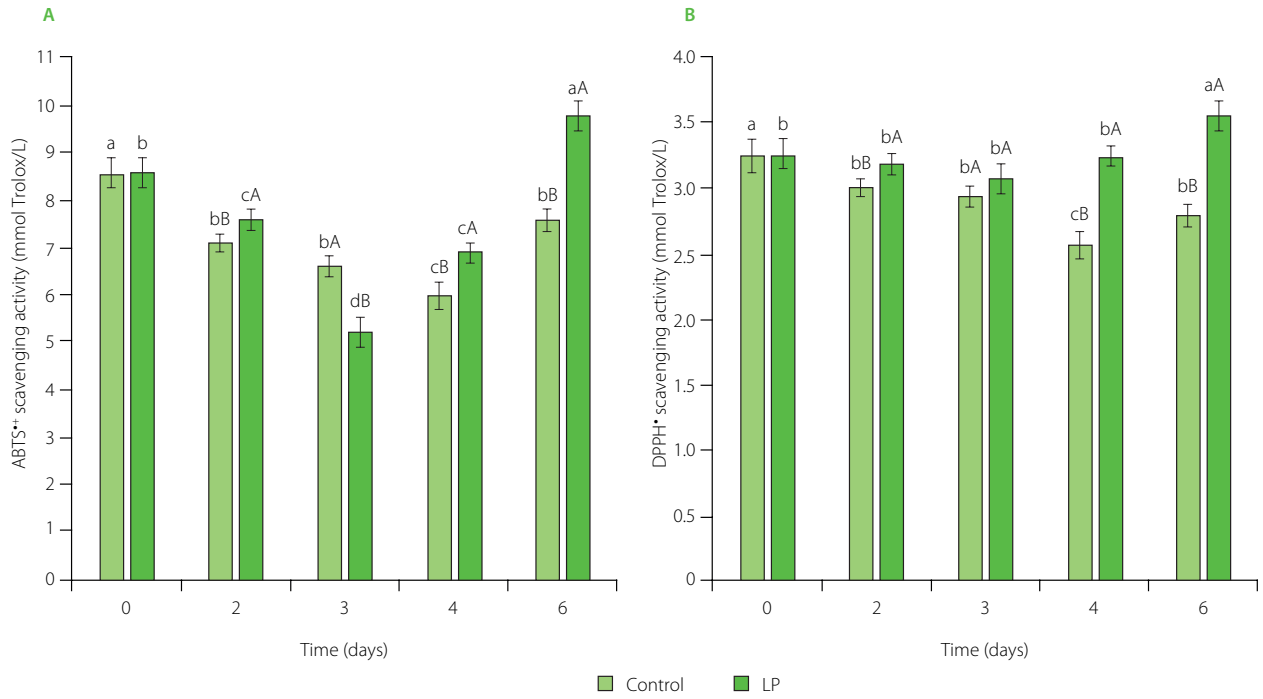

Figure 2. Antioxidant capacity of bergamot homogenate fermented by *L. plantarum* (LP) and control without bacteria over a period of six days determined using (**A**) ABTS assay and (**B**) DPPH assay. Different lowercase letters indicate significant differences between fermentation days within the same group, whereas different uppercase letters indicate significant differences between the LP and control group on the same fermentation day ($p<0.05$).

Mousavi *et al.* [2013] observed a similar increase in the antioxidant activity in the DPPH assay after the 72-h fermentation of pomegranate juice with *L. plantarum* and *L. acidophilus*. In another study in which sweet lemon juice was fermented with *L. plantarum* LS5, a significant increase in DPPH radical scavenging activity and ferric-reducing antioxidant power (FRAP) was reported as a result of lactic acid fermentation [Hashemi *et al.*, 2017]. The increase in antioxidant activity is positively associated with changes in phenolic composition during fermentation [Adebo *et al.*, 2018]. It may be attributed to the enzymatic hydrolysis of glycosidic bonds in phenolic compounds and release of aglycones, which are generally more active than their glycosidic forms, or the generation of other metabolites with higher antioxidant potential [Adebo *et al.*, 2018]. In addition, fermentation-induced structural disruption of plant cell walls may facilitate the release of bound phenolic compounds, thereby contributing to the observed antioxidant effects [Katina *et al.*, 2007; Zhang *et al.*, 2025].

Hashemi & Jafarpour [2020] examined bergamot juice fermented for 72 h using *L. plantarum* subsp. *plantarum* PTCC 1896, *L. plantarum* AF1, and *L. plantarum* LP3. The authors revealed that the juice fermented with *L. plantarum* strains exhibited greater antioxidant potential than the control juice fermented with natural flora. This observation is confirmed by the results of our research; in both antioxidant assays, indicating that antioxidant capacity of LP group homogenates was higher than of the control group homogenates after 6 days of fermentation (**Figure 2**).

Phenolic compound content

Changes in the total phenolic content during the six days of bergamot homogenate fermentation are presented in **Figure 3**. The initial total phenolic content of the bergamot supernatant was determined to be 20.17 mg GAE/mL. At the end of fermentation, the total phenolic content did not change significantly ($p\geq0.05$) in the control group (20.78 mg GAE/mL), however in the LP group it was 21.74 mg GAE/mL and represented a statistically significant increase ($p=0.048$) compared to the initial total phenolic content. During the first days of incubation, the total phenolic content decreased to 7.32 mg GAE/mL (day 4) and 7.40 mg GAE/mL (day 3) in the control and LP groups, respectively, followed by a recovery by day 6 of fermentation. However, no statistically significant ($p\geq0.05$) differences in total phenolic content were observed between the groups on day 6.

Hashemi *et al.* [2017] reported a significant decrease in the total phenolic content during the fermentation of sweet lemon juice with *L. plantarum LS5*, while Guo *et al.* [2019] reported no significant changes in the total phenolic content of ougan juice fermented with *L. plantarum* or *L. paracasei*. In a similar study, Multari *et al.* [2020] reported that the effect of lactic acid bacteria on the total phenolic content was specific to orange varieties. They reported that *L. rhamnosus* increased the phenolic content of 'Washington navel' juice but decreased phenolics in juice from the 'Tarocco' variety.

The fluctuation in the total phenolic content over fermentation time, which decreased and then increased, may be explained by the majority of compounds in the fruit being in a bound form

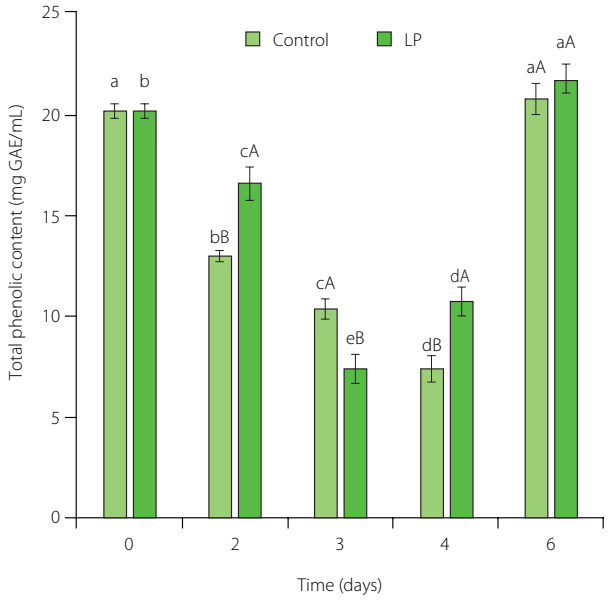

Figure 3. Total phenolic content of bergamot homogenate fermented by *L. plantarum* (LP) and control without bacteria over a period of six days. Different lowercase letters indicate significant differences between fermentation days within the same group, whereas different uppercase letters indicate significant differences between the LP and control group on the same fermentation day ($p<0.05$). GAE, gallic acid equivalent.

initially, becoming soluble over time, or their microbial hydrolysis during fermentation [Yu *et al.*, 2015].

Among phenolic compounds, neoeriocitrin, naringin, neoeriocitrin dioxalate, neohesperidin, melitidin, and neohesperidin dioxalate were identified in the bergamot homogenates by LC-MS/MS method. The LC-MS/MS chromotograms used for identification are presented in **Figure S1** in Supplementary Materials. All these compounds have been previously detected in bergamot fruits and their products [Baron *et al.*, 2021; Delle Monache *et al.*, 2013; Gattuso *et al.*, 2023]. Most of them are typical of the phenolic profiles of citrus fruits, although neoeriocitrin and neohesperidin distinguish bergamot from others [Nogata *et al.*, 2006]. The contents of identified phenolics in the supernatants from the bergamot homogenates at different fermentation times are shown in **Table 1**. The sum of individual phenolic compounds in the supernatant from the untreated bergamot homogenate on day 0 was 608.18 mg/L and in the case of the bergamot fermented with *L. plantarum*, it ranged from 653.70 to 687.92 mg/L, with the highest value ($p<0.05$) obtained on the 4th day, suggesting that a four-day fermentation period may be sufficient to maximize phenolic availability. Neoeriocitrin was the most abundant in all samples, which can be considered important due to its potential cardioprotective properties [Capomolla *et al.*, 2019]. On the 4th day of fermentation, contents of neoeriocitrin and neoeriocitrin dioxalate in the LP group were 297.23 and 55.86 mg/L, respectively, showing a statistically significant increase compared to the supernatant of the untreated homogenate on day 0 and the control group on day 4. In the control group, neoeriocitrin content did not show statistically significant differences between 0, 4, and 6 days of fermentation ($p\geq0.05$), and neoeriocitrin dioxalate showed a numerical increase on day 4, followed by a decrease by day 6; however, these changes were not statistically significant ($p\geq0.05$). The content of naringin, which has been associated with antioxidant and anti-inflammatory activities [Shilpa *et al.*, 2023], was 158.01 mg/L in the control group on the 4th day and 160.37 mg/L in the LP group on the same day. These values were significantly ($p<0.05$) higher than that in the supernatant from raw homogenate (138.26 mg/mL). On the 6th day of fermentation, a statistically significant reduction was noted in naringin content compared to day 4 in LP group ($p<0.05$). The content of melitidin, which showed statin-like activity and cardioprotective effects [Shen *et al.*, 2023; Wang *et al.*, 2026], was observed to significantly ($p<0.05$) decrease in both groups to 44.82 mg/mL (control) and 39.00 mg/mL (LP group) compared to that determined on day zero (49.68 mg/mL). The content of neohesperidin dioxalate in the control group did not differ significantly ($p\geq0.05$) on day 0 and day 6, while in the LP group, it decreased gradually with fermentation time to 72.04 mg/L on the 6th day ($p<0.05$). Overall, a fermentation period of four days was sufficient to enhance the content of main phenolic compounds of bergamot homogenate, including neoeriocitrin and naringin. The 4-day fermentation also promoted increases in neoeriocitrin dioxalate content. However, melitidin content decreased significantly during fermentation with LP.

Fermentation with bacteria exhibiting β-glucosidase activity may lead to a decrease in flavonoid glycosides due to hydrolysis, whereas bacteria possessing esterase activity can promote the release and accumulation of flavonoid compounds [Guo *et al.*, 2019]. Multari *et al.* [2020] reported decreased hesperidin and narirutin contents when orange juice was fermented with *Lactobacillus* strains. In a study on vinegar produced from bergamot wine with *Acetobacter* strains, the levels of neoeriocitrin, neohesperidin, melitidin, and brutieridin decreased, whereas the naringin level increased compared with the levels determined in bergamot wine [Di Donna *et al.*, 2020]. In another study by Tang *et al.* [2022], fermented citrus fruits (grapefruit, kumquat, blood orange) with 10 strains of lactic acid bacteria grapefruit showed an increase in naringin content, while the content of hesperidin and neohesperidin decreased in blood oranges.

Correlation analysis revealed significant associations between specific phenolic compounds within the LP group. Positive correlations were observed between neoeriocitrin and naringin contents (correlation coefficient, $r=0.807$, $p<0.01$), as well as between contents of neoeriocitrin and its dioxalate derivative ($r=0.673$, $p<0.05$), while negative correlations were detected between contents of neoeriocitrin and melitidin ($r=-0.830$, $p<0.01$). A statistically significant positive correlation was detected between levels of naringin and neoeriocitrin dioxalate ($r=0.976$, $p<0.01$), but a negative correlation was observed between naringin and melitidin contents ($r=-0.847$, $p<0.01$). The content of melitidin and neohesperidin dioxalate correlated positively ($r=0.739$, $p<0.01$), and the content of neoeriocitrin dioxalate and melitidin correlated negatively ($r=-0.770$, $p<0.01$).

Table 1. Content of phenolic compounds in the supernatant from the bergamot homogenate fermented by *L. plantarum* (LP) and control without bacteria over a period of six days analyzed by LC-DAD-ESI-MS/MS (mg/L).

Compound	Rt (min)	Control				LP			
		Day 0	Day 2	Day 4	Day 6	Day 0	Day 2	Day 4	Day 6
Neoeriocitrin	46.78	236.71±0.50^{a}	208.83±0.20^{bB}	240.95±0.93^{aB}	237.45±0.83^{aB}	236.71±0.50^{c}	263.07±0.29^{bA}	297.23±0.29^{aA}	278.02±0.27^{bA}
Naringin	50.77	138.26±0.54^{b}	139.58±0.13^{bA}	158.01±0.15^{aA}	163.85±0.42^{aA}	138.26±0.54^{cA}	160.74±0.43^{bB}	160.37±0.15^{bA}	154.40±0.14^{aB}
Neoeriocitrin dioxalate	51.58	47.75±0.29^{a}	45.44±0.04^{aB}	54.75±0.29^{aB}	48.87±0.61^{bB}	47.75±0.29^{b}	57.90±0.07^{aA}	55.86±0.55^{aA}	53.59±0.54^{aA}
Neohesperidin	53.6	55.40±0.32^{a}	40.98±0.03^{bB}	50.29±0.08^{aA}	53.39±0.54^{aA}	55.40±0.32^{a}	53.78±0.61^{aA}	54.05±0.56^{aA}	56.65±0.62^{aA}
Melitidin	56.08	49.68±0.10^{a}	40.15±0.03^{bA}	46.36±0.19^{abB}	44.82±0.59^{bA}	49.68±0.10^{a}	42.03±0.60^{bA}	41.21±0.02^{bA}	39.00±0.60^{bB}
Neohesperidin dioxalate	57.07	80.38±0.19^{a}	67.91±0.06^{bB}	83.34±0.26^{aA}	81.44±0.64^{aA}	80.38±0.19^{a}	77.22±0.64^{aA}	79.20±0.54^{aA}	72.04±0.56^{bB}
Total		608.18±1.60^{a}	542.89±0.47^{bB}	633.70±0.69^{aB}	629.83±2.71^{aB}	608.18±1.60^{c}	654.73±1.22^{bA}	687.92±1.41^{aA}	653.70±1.05^{bA}

Results are presented as mean ± standard deviation. In rows, different lowercase letters followed by values indicated significant differences between fermentation days within the same group, whereas different uppercase letters indicate significant differences between the LP and control group on the same fermentation day ($p<0.05$). Rt, retention time.

A significant positive correlation was also detected between neoeriocitrin content and *L. plantarum* viable counts ($r=0.704$, $p<0.05$), whereas negative correlations were observed between live bacterial counts and melitidin ($r=-0.736$, $p<0.01$) and neohesperidin dioxalate ($r=-0.726$, $p<0.01$) contents. These findings suggest an association between microbial growth dynamics and phenolic transformations during fermentation, although causal relationships cannot be inferred.

Phenolic compounds found in bergamot have been observed to exert beneficial effects on health, providing protection against cancer, diabetes, and neurodegenerative diseases [Ferlazzo *et al*., 2020; Fogacci *et al*., 2023; Navarra *et al.*, 2020]. In an experimental model, the oral administration of bergamot juice to Wistar rats improved blood cholesterol levels [Miceli *et al.*, 2007]. The authors reported that the administration of bergamot juice containing neoeriocitrin, naringin, and neohesperidin decreased cholesterol, triglyceride, and low-density lipoprotein (LDL) cholesterol levels. Moreover, there was an increase in high-density lipoprotein (HDL) cholesterol levels compared to those in hypercholesterolemic controls. In another study conducted by Toth *et al.* [2016], 80 hypercholesterolemic patients received bergamot flavonoids at 150 mg/day for 6 months. The results showed a reduction in the total cholesterol, LDL cholesterol, and triglyceride levels and an increase in HDL cholesterol levels, suggesting a cardioprotective effect.

CONCLUSIONS

The results of this study demonstrate that fermentation of bergamot homogenate with *L. plantarum* led to the stabilization or enhancement of contents of key phenolic compounds, particularly neoeriocitrin and naringin, when compared with the non-fermented control. Fermentation was associated with an increase in ABTS radical scavenging activity, which reached its highest value on day 6 of fermentation. Notably, neoeriocitrin was quantified as the main phenolic compound in bergamot homogenates using LC-DAD-ESI-MS/MS analysis, and its content was positively associated with *L. plantarum* growth during fermentation. Despite its high flavonoid content, bergamot is not widely consumed due to its bitter taste, which points to the need for seeking alternative methods to make its beneficial compounds more accessible. Our study findings suggest that *L. plantarum*-mediated fermentation is a promising approach to enhance the functional value of bergamot, by improving its phenolic composition and antioxidant potential, thereby supporting its potential application in functional food development.

RESEARCH FUNDING

This study was supported by the Muğla Sıtkı Koçman University, Research Support and Funding Office under the grant number 21/127/02/3/5, as part of a Master's Thesis project.

CONFLICT OF INTERESTS

The authors declare that they have no conflict of interest.

SUPPLEMENTARY MATERIALS

The following are available online at **https://journal.pan.olsztyn.pl/Fermentation-of-Bergamot-Citrus-bergamia-Risso-Fruit-with-Lactobacillus-plantarum,225254,0,2.html**; **Figure S1**. LC-ESI-MS/MS chromatograms of phenolic compounds identified in the supernatant from bergamot fruit homogenate.

ORCID IDs

O. Aslan Bursali https://orcid.org/0000-0002-1202-8620
B. Ekinci https://orcid.org/0000-0003-2425-8797
A.S. Sonmezdag https://orcid.org/0000-0001-6360-4037

REFERENCES

1. Adebo, O.A., Njobeh, P.B., Adeboye, A.S., Adebiyi, J.A., Sobowale, S.S., Ogundele, O.M., Kayitesi, E. (2018). Advances in fermentation technology for novel food products. In S. Panda, P. Shetty, (Eds.), *Innovations in Technologies for Fermented Food and Beverage Industries, Food Microbiology and Food Safety*. Springer, Cham, Switzerland, pp. 71-87. https://doi.org/10.1007/978-3-319-74820-7_4
2. Ballistreri, G., Amenta, M., Fabroni, S., Consoli, V., Grosso, S., Vanella, L., Sorrenti, V., Rapisarda, P. (2021). Evaluation of lipid and cholesterol-lowering effect of bioflavonoids from bergamot extract. *Natural Product Research, 35*(23), 5378-5383. https://doi.org/10.1080/14786419.2020.1768085
3. Baron, G., Altomare, A., Mol, M., Garcia, J.L., Correa, C., Raucci, A., Mancinelli, L., Mazzotta, S., Fumagalli, L., Trunfio, G., Tucci, L., Lombardo, E., Malara, D., Janda, E., Mollace, V., Carini, M., Bombardelli, M., Aldini, G. (2021). Analytical profile and antioxidant and anti-inflammatory activities of the enriched polyphenol fractions isolated from bergamot fruit and leave. *Antioxidants*, *10*(2), art. no. 141. https://doi.org/10.3390/antiox10020141
4. Behera, S.S., Ray, R.C., Zdolec, N. (2018). *Lactobacillus plantarum* with functional properties: An approach to increase safety and shelf-life of fermented foods. *BioMed Research International, 2018*, art. no. 9361614. https://doi.org/10.1155/2018/9361614
5. Brand-Williams, W., Cuvelier, M.E., Berset, C. (1995). Use of a free radical method to evaluate antioxidant activity. *LWT – Food Science and Technology, 28*(1), 25-30. https://doi.org/10.1016/S0023-6438(95)80008-5
6. Capomolla, A.S., Janda, E., Paone, S., Parafati, M., Sawicki, T., Mollace, R., Ragusa, S., Mollace, V. (2019). Atherogenic index reduction and weight loss in metabolic syndrome patients treated with a novel pectin-enriched formulation of bergamot polyphenols. *Nutrients, 11*(6), art. no. 1271. https://doi.org/10.3390/nu11061271
7. Cecchi, N., Romanelli, R., Ricevuti, F., Carbone, M.G., Dinardo, M., Cesarano, E., De Michele, A., Messere, G., Morra, S., Scognamiglio, A., Spagnuolo, M.I. (2024). Bioactives in oral nutritional supplementation: a pediatric point of view. *Nutrients, 16*(13), art. no. 2067. https://doi.org/10.3390/nu16132067
8. Delle Monache, S., Sanitá, P., Trapasso, E., Ursino, M.R., Dugo, P., Russo, M., Ferlazzo, N., Calapai, G., Angelucci, A., Navarra, M. (2013). Mechanisms underlying the anti-tumoral effects of *Citrus bergamia* juice. *PLoS ONE, 8*(4), art. no. e61484. https://doi.org/10.1371/journal.pone.0061484
9. Di Donna, L., Bartella, L., De Vero, L., Gullo, M., Giuffrè, A.M., Zappia, C., Capocasale, M., Poian, M., D'Urso, S., Caridi, A. (2020). Vinegar production from *Citrus bergamia* by-products and preservation of bioactive compounds. *European Food Research Technology*, *246*, 1981-1990. https://doi.org/10.1007/s00217-020-03549-1
10. Dosoky, N.S., Setzer, W.N. (2018). Biological activities and safety of *Citrus* spp. essential oils. *International Journal of Molecular Sciences*, *19*(7), art. no. 1966. https://doi.org/10.3390/ijms19071966
11. Ferlazzo, N., Cirmi, S., Maugeri, A., Russo, C., Lombardo, G. E., Gangemi, S., Calapai, G., Mollace, V., Navarra, M. (2020). Neuroprotective effect of bergamot juice in 6-OHDA-induced SH-SY5Y cell death, an *in vitro* model of Parkinson's disease. *Pharmaceutics, 12*(4), art. no. 326. https://doi.org/10.3390/pharmaceutics12040326
12. Fogacci, F., Giovannini, M., Imbalzano, E., Grandi, E., Rizzoli, E., D'Addato, S., Cicero, A.F.G. (2023). Metabolic and vascular effect of a new standardized bergamot phytocomplex: a three-arm, placebocontrolled, double-blind clinical trial. *Archives of Medical Science*, *19*(5),1228–1235. https://doi.org/10.5114/aoms/163368
13. Forlot, P., Pevet, P. (2012). Bergamot (*Citrus bergamia* Risso et Poiteau) essential oil: Biological properties, cosmetic and medical use. *Journal of Essential Oil Research, 24*(2), 195-201. https://doi.org/10.1080/10412905.2012.659527
14. Gattuso, A., Piscopo, A., Romeo, R., De Bruno, A., Poiana, M. (2023). Recovery of bioactive compounds from Calabrian bergamot citrus waste: Selection of best green extraction. *Agriculture*, *13*(5), art. no. 1095. https://doi.org/10.3390/agriculture13051095
15. Gokavi, S., Zhang, L., Huang, M-K., Zhao, X., Guo, M. (2005). Oat-based symbiotic beverage fermented by *Lactobacillus plantarum*, *Lactobacillus paracasei* ssp. *casei*, and *Lactobacillus acidophilus*. *Journal of Food Science*, *70*(4), M216-M223. https://doi.org/10.1111/j.1365-2621.2005.tb07191.x
16. Guo, X., Cao, X., Guo, A., Li, E. (2019). Improving the taste of Ougan (*Citrus reticulate* cv. *Suavissima*) juice by slight fermentation with lactic acid bacteria. *Journal of Food Processing and Preservation*, *43*(9), art. no. e14056. https://doi.org/10.1111/jfpp.14056
17. Hashemi, S.M.B., Jafarpour, D. (2020). Fermentation of bergamot juice with *Lactobacillus plantarum* strains in pure and mixed fermentations: Chemical composition, antioxidant activity and sensorial properties. *LWT – Food Science and Technology*, *131*, art. no. 109803. https://doi.org/10.1016/j.lwt.2020.109803
18. Hashemi, S.M.B., Khaneghah, A.M., Barba, F.J., Nemati, Z., Shokofti, S.S., Alizadeh, F. (2017). Fermented sweet lemon juice (*Citrus limetta*) using *Lactobacillus plantarum* LS5: Chemical composition, antioxidant and antibacterial activities. *Journal of Functional Foods, 38*(A), 409-414. https://doi.org/10.1016/j.jff.2017.09.040
19. Hur, S.J., Lee, S.Y., Kim, Y.C., Choi, I., Kim, G.B. (2014). Effect of fermentation on the antioxidant activity in plant-based foods. *Food Chemistry*, *160*, 346–356. https://doi.org/10.1016/j.foodchem.2014.03.112
20. Katina, K., Liukkonen, K.H., Kaukovirta-Norja, A., Adlercreutz, H., Heinonen, S.M., Lampi, A.M., Pihlava, J.M., Poutanen, K. (2007). Fermentation-induced changes in the nutritional value of native or germinated rye. *Journal of Cereal Science*, *46*(3), 348-355. https://doi.org/10.1016/j.jcs.2007.07.006
21. Kelebek, H., Sonmezdag, A.S., Guclu, G., Cengiz, N., Uzlasir, T., Kadiroglu, P., Selli, S. (2020). Comparison of phenolic profile and some physicochemical properties of Uzun pistachios as influenced by different harvest period. *Journal of Food Processing and Preservation*, *44*, art. no. e14605. https://doi.org/10.1111/jfpp.14605
22. Miceli, N., Mondello, M.R., Monforte, M.T., Sdrafkakis, A., Dugo, P., Crupi, M.L., Taviano, M.F., De Pasquale, R., Trovato, A. (2007). Hypolipidemic effects of *Citrus bergamia* Risso et Poiteau juice in rats fed a hypercholesterolemic diet. *Journal of Agricultural and Food Chemistry*, *55*(26), 10671-10677. https://doi.org/10.1021/jf071772i
23. Mousavi, Z.E., Mousavi, S.M., Razavi, S.H., Hadinejad, M., Emam-Djomeh, Z., Mirzapour, M. (2013). Effect of fermentation of pomegranate juice by *Lactobacillus plantarum* and *Lactobacillus acidophilus* on the antioxidant activity and metabolism of sugars, organic acids and phenolic compounds. *Food Biotechnology, 27*(1), 1-13. https://doi.org/10.1080/08905436.2012.724037
24. Multari, S., Carafa, I., Barp, L., Caruso, M., Licciardello, C., Larcher, R., Tuohy, K., Martens, S. (2020). Effects of *Lactobacillus* spp. on the phytochemical composition of juices from two varieties of *Citrus sinensis* L. Osbeck: 'Tarocco' and 'Washington navel'. *LWT – Food Science and Technology*, *125*, art. no. 109205. https://doi.org/10.1016/j.lwt.2020.109205
25. Navarra, M., Femia, A.P., Romagnoli, A., Katia Tortora, K., Luceri, C., Cirmi, S., Ferlazzo, N., Caderni, G. (2020). A flavonoid-rich extract from bergamot juice prevents carcinogenesis in a genetic model of colorectal cancer, the Pirc rat (F344/NTac-Apc^{am1137}). *European Journal of Nutrition*, *59*, 885-894. https://doi.org/10.1007/s00394-019-01948-z
26. Nogata, Y., Sakamoto, K., Shiratsuchi, H., Ishii, T., Yano, M., Ohta, H. (2006). Flavonoid composition of fruit tissues of *Citrus* species. *Bioscience, Biotechnology & Biochemistry*, *70*(1), 178-192. https://doi.org/10.1271/bbb.70.178
27. Ortiz, A. de C., Fideles, S.O.M., Reis, C.H.B., Bellini, M.Z., Pereira, E.deS.B.M., Pilon, J.P.G., de Marchi, M.Â., Detregiachi, C.R.P., Flato, U.A.P., Trazzi, B.F.deM., Pagani, B.T., Ponce, J.B., Gardizani, T.P., Veronez, F.deS., Bucahim, D.V., Buchami, R.L. (2022). Therapeutic effects of citrus flavonoids neohesperidin, hesperidin and its aglycone, hesperetin on bone health. *Biomolecules*, *12*(5), art. no. 626. https://doi.org/10.3390/biom12050626
28. Pernice, R., Borriello, G., Ferracane, R., Borrelli, R.C., Cennamo, F., Ritieni, A. (2009). Bergamot: A source of natural antioxidants for functionalized fruit juices. *Food Chemistry*, *112*(3), 545-550. https://doi.org/10.1016/j.foodchem.2008.06.004

29. Re, R., Pellegrini, N., Proteggente, A., Pannala, A., Yang, M., Rice-Evans, C. (1999). Antioxidant activity applying an improved ABTS radical cation decolorization assay. *Free Radical Biology and Medicine*, *26*(9-10), 1231-1237. **https://doi.org/10.1016/S0891-5849(98)00315-3**
30. Shen, S., Wang, S., Yang, C., Wang, C., Zhou, Q., Zhou, S., Zhang, R., Li, Y., Wang, Z., Dai, L., Peng, W., Hao, Y., Guo, H., Cao, G., Liu, X., Yao, F., Xu, Q., Fernie, A.R., Luo, J. (2023). Elucidation of the melitidin biosynthesis pathway in pummelo. *Journal of Integrative Plant Biology, 65*(11), 2505–2518. **https://doi.org/10.1111/jipb.13564**
31. Shilpa, V., Shams, R., Dash, K.K., Pandey, V.K., Dar, A.H., Ayaz Mukarram, S., Harsányi, E., Kovács, B. (2023). Phytochemical properties, extraction, and pharmacological benefits of naringin: A review. *Molecules*, *28*(15), art. no. 5623. **https://doi.org/10.3390/molecules28155623**
32. Singleton, V.L., Orthofer, R., Lamuela-Raventós, R.M. (1999). Analysis of total phenols and other oxidation substrates and antioxidants by means of folin-ciocalteu reagent. *Methods in Enzymology*, *299*, 152-178. **https://doi.org/10.1016/S0076-6879(99)99017-1**
33. Tang, R., Yu, H., Qi, M., Yuan, X., Ruan, Z., Hu, C., Xiao, M., Xue, Y., Yao, Y., Liu, Q. (2022). Biotransformation of citrus fruits phenolic profiles by mixed probiotics *in vitro* anaerobic fermentation. *LWT – Food Science and Technology*, *160*, art. no. 113087. **https://doi.org/10.1016/j.lwt.2022.113087**
34. Toth, P.P., Patti, A.M., Nikolic, D., Giglio, R.V., Castellino, G., Biancucci, T., Geraci, F., David, S., Montalto, G., Rizvi, A., Rizzo, M. (2016). Bergamot reduces plasma lipids, atherogenic small dense LDL, and subclinical atherosclerosis in subjects with moderate hypercholesterolemia: a 6 months prospective study. *Frontiers in Pharmacology*, *6*, art. no. 299. **https://doi.org/10.3389/fphar.2015.00299**
35. Wang, Y., Ashfaq, H., Alsaleem, M.A., Alissa, M., Alghamdi, A., Alhegaili, A.S., Al-Emam, A., Hassan, H.M. (2026), Melitidin alleviates escitalopram-induced sub-chronic cardiotoxicity *via* regulating mitochondrial fission-fusion machinery and redox signaling: A biochemical, echocardiographic, and histological study. *Tissue and Cell*, *101*, art. no. 103435. **https://doi.org/10.1016/j.tice.2026.103435**
36. Yu, Y., Xiao, G., Xu, Y., Wu, J., Fu, M., Wen, J. (2015). Slight fermentation with *Lactobacillus fermentium* improves the taste (sugar:acid ratio) of citrus (*Citrus reticulata* cv. chachiensis) juice. *Journal of Food Science*, *80*(11), M2543-M2547. **https://doi.org/10.1111/1750-3841.13088**
37. Zhang, P., Zhang, J., Li, L., Gu, T., Chen, S., Wang, J., Gao, M. (2025). The release of bound phenolics to enhance the antioxidant activity of cornmeal by liquid fermentation with *Bacillus subtilis*. *Foods*, *14*(3), art. no. 499. **https://doi.org/10.3390/foods14030499**

ORIGINAL ARTICLE
http://journal.pan.olsztyn.pl

Polish Journal of Food and Nutrition Sciences
2026, Vol. 76, No. 3, 251–263
DOI: 10.31883/pjfns/225266
ISSN 1230-0322, e-ISSN 2083-6007

Sorghum-Based Instant Rice Analog Enriched with Modified Cassava Flour and Pumpkin Flour Improves Starch Digestibility, Functional Properties, and Sensory Acceptance

Agus Slamet[1]*, Bayu Kanetro[2], Hamidin Rasulu[3]

[1]Department of Agricultural Product Technology, Faculty of Agroindustry, Universitas Mercu Buana Yogyakarta, Jl. Wates Km 10 Yogyakarta, Daerah Istimewa Yogyakarta, 55752, Indonesia
[2]Department of Food Science, Faculty of Agroindustry, Universitas Mercu Buana Yogyakarta, Jl. Wates Km 10 Yogyakarta, Daerah Istimewa Yogyakarta, 55752, Indonesia
[3]Department of Agricultural Product Technology, Faculty of Agriculture, Universitas Khairun, Ternate 9717, Indonesia

Rice analog refers to rice-shaped grains produced from non-rice flours using processing techniques such as extrusion. This study evaluated the influence of partially substituting sorghum flour with modified cassava flour (mocaf) and pumpkin flour on starch digestibility, physicochemical properties, and sensory acceptance of extruded instant rice analogs. Increasing the proportions of mocaf and pumpkin flour led to a significant increase in the contents of crude fiber, β-carotene, total phenolics, and resistant starch in rice analogs, reaching 5.71 g/100 g, 32.66 µg/g, 9.15 mg GAE/g, and 6.84%, respectively, for the formulation containing sorghum flour, mocaf, and pumpkin flour at a ratio of 20:40:40 (*w/w/w*). Conversely, it decreased rapidly digestible starch content, total starch digestibility, bulk density, and texture hardness. Fourier transform infrared (FTIR) spectroscopy revealed no indication of new functional group formation; however, an increase in the amorphous starch fraction indicated structural changes in the starch matrix. This finding was supported by scanning electron microscope (SEM) micrographs showing a more porous matrix. Products of all formulations were generally sensory acceptable, with the rice analog formulated at a 40:30:30 (*w/w/w*) ratio exhibiting the highest aroma and taste scores and one of the highest overall acceptance. These findings suggest that composite flours improve the functional properties of rice analogs by modifying starch architecture while preserving acceptable sensory quality. The results further highlight the potential of rice analogs as functional staple foods produced from locally available ingredients.

Keywords: extrusion cooking, modified cassava flour, pumpkin flour, resistant starch, starch structure

INTRODUCTION

Dependence on rice remains high across many Asian countries, including Indonesia. The increasing prevalence of metabolic disorders has driven the development of carbohydrate-rich foods that not only serve as a source of energy but also provide additional physiological benefits [Nikrad *et al.*, 2023]. Rice analogs have been introduced as a staple food alternative to lessen reliance on conventional rice. Rice analogs are rice-shaped grains produced from non-rice sources and processed using techniques such as extrusion to achieve cooking and sensory properties similar to those of conventional rice [Chaturvedi & Manickavasagan, 2024].

Extrusion technology modifies starch-based matrices through thermomechanical treatment, promoting starch

***Corresponding Author:**
E-mail: **agus@mercubuana-yogya.ac.id** (A. Slamet)

Submitted: 1 March 2026
Accepted: 30 June 2026
Published on-line: 17 July 2026

gelatinization and molecular reorganization, thereby influencing the functional properties of rice analogs. However, most studies on rice analogs have focused on processing feasibility and product characteristics [Bahlawan *et al*., 2023; Kishore *et al*., 2024; Shaikh *et al*., 2025]. In contrast, the influence of formulation on starch digestibility and structural transformations remains insufficiently explored. Structural modification of starch is important from a nutritional perspective because it affects starch digestibility and the proportions of rapidly digestible starch (RDS), slowly digestible starch (SDS), and resistant starch (RS), thereby influencing glycemic control and metabolic regulation [Kim *et al*., 2024; Zheng *et al*., 2026]. These starch fractions differ in their digestion rates and physiological effects, making them important determinants of the nutritional quality of starch-based foods [Jiali *et al*., 2024].

Sorghum fosters considerable potential as the main ingredient for rice analog production because its relatively high amylose content and unique starch characteristics promote the development of a stable matrix during processing [Bahlawan *et al*., 2023]. Sorghum flour forms a compact gel network after gelatinization and cooling, which contributes to the texture and structural integrity of rice analogs by enhancing matrix cohesiveness and hardness [Chiodetti *et al*., 2024]. In addition, its non-starch components, including proteins and lipids, influence intermolecular interactions during thermomechanical processing [Chao *et al*., 2024]. Nevertheless, variations in the physicochemical and functional characteristics of sorghum cultivars, particularly water absorption capacity and structural stability [Adebo & Kesa, 2023], may influence their suitability as raw materials for rice analog production.

Modified cassava flour (mocaf), produced through the fermentation of cassava tubers, has been widely used as an ingredient in composite food formulations due to its favorable processing and quality characteristics [Rahmadani *et al*., 2025]. Its incorporation into extruded rice analogs may improve structural integrity and overall product quality [Sumardiono *et al*., 2021]. Despite these advantages, the effects of mocaf on starch structure and digestibility in composite rice analog formulations remain insufficiently documented.

Pumpkin (*Cucurbita moschata* Duchesne) flour contains substantial amounts of β-carotene and phenolic compounds, which contribute to its antioxidant potential and functional properties [Alija *et al*., 2025; Ninčević Grassino *et al*., 2023]. Pumpkin flour may be incorporated into composite flour formulations to enhance the content of bioactive compounds and improve color attributes [Alija *et al*., 2025]. Its incorporation into food products has also been reported to increase β-carotene content, antioxidant capacity, and sensory quality, as demonstrated in gluten-free egg rolls and instant porridge formulations [Slamet *et al*., 2025, 2026]. However, information regarding the combined use of sorghum flour, mocaf, and pumpkin flour in extruded rice analog products remains scarce. In particular, the effects of this combination on starch digestibility and structural properties have not been comprehensively studied.

Therefore, there is a clear research gap regarding the coupled effects of sorghum, mocaf, and pumpkin flours on starch digestibility, structural characteristics, and overall quality of extrusion-based rice analogs. Accordingly, this study evaluated the influence of partially substituting sorghum flour with mocaf and pumpkin flour on starch digestibility, physicochemical properties, structural characteristics, and sensory acceptance of extruded instant rice analogs.

MATERIALS AND METHODS

Materials and reagents

Sorghum flour, mocaf, and pumpkin flour were supplied by food producers from Sleman, Yogyakarta, Indonesia. Hydrochloric acid, sulfuric acid, boric acid, sodium hydroxide, and petroleum ether used for proximate and crude fiber determinations were analytical-grade reagents obtained from Merck, Darmstadt, Germany. Folin–Ciocalteu reagent, sodium carbonate, and gallic acid used for total phenolic content analysis were obtained from Sigma-Aldrich (St. Louis, MO, USA). Sigma-Aldrich was also a supplier of solvents (acetone, methanol, ethanol, and *n*-hexane), anhydrous sodium sulfate, β-carotene standard, α-amylase, amyloglucosidase, pepsin, sodium acetate, potassium phosphate buffer, 3,5-dinitrosalicylic acid, and glucose standard.

Production of rice analogs

Rice analogs were produced from composite flour formulations consisting of sorghum flour, mocaf, and pumpkin flour in different proportions. Flours were blended at ratios of 100:0:0, 80:10:10, 60:20:20, 40:30:30, and 20:40:40 (*w/w/w*), respectively. The blends underwent hot extrusion using a co-rotating intermeshing twin-screw extruder (Model DS32-II, Jinan Saixin Machinery Co., Ltd., Jinan, China) featuring 32 mm diameter screws with a length-to-diameter (L/D) ratio of 20:1. The screw profile comprised conveying and kneading elements configured to provide sufficient mixing and shear during extrusion. Before extrusion, the flour blends were homogenized and their moisture content was adjusted to 30 g/100 g by manual mixing, followed by equilibration for 30 min. The conditioned feed was then extruded at a barrel temperature profile of 50/65/85/100/95°C, a screw speed of 60 rpm, and a feed rate of approximately 300 g/min. After exiting the 2 mm die, the extrudate was cut into rice-shaped grains and dried at 60°C for 3 h using a hot-air oven (UN55, Memmert GmbH, Schwabach, Germany). Drying proceeded to achieve a final moisture content below 10 g/100 g, which is within the recommended range for dried cereal-based products and contributes to storage stability. After drying, the rice analogs were cooled to room temperature and stored in airtight containers until subsequent analyses.

Proximate composition and crude fiber analysis

Proximate composition and crude fiber content were assessed following AOAC International guidelines [AOAC, 2005], including moisture (method 930.15), ash (method 930.05), fat (method 930.09), protein (method 978.04), and crude fiber (method

978.10). The carbohydrate content of the rice analogs was calculated by difference. Results were expressed as g *per* 100 g of dried rice analog.

Color coordinate measurement

The color of the rice analogs was determined using a CR-400 colorimeter (Konica Minolta, Osaka, Japan) after calibration against a standard white reference tile. The color of the rice analogs was evaluated according to the CIELab system and reported as *L** (lightness), *a** (redness/greenness), and *b** (yellowness/blueness) values. Measurements were recorded at five different locations on each rice analog sample, and the data were presented as mean values.

Analysis of physical and functional properties

Water absorption capacity (WAC) and oil absorption capacity (OAC) of the rice analogs were determined gravimetrically following the procedure described by Beuchat [1977], with slight modifications. An aliquot of 10 mL of distilled water or vegetable oil was mixed with 1.0 g of the instant rice analog in a centrifuge tube. The suspension was mixed using a Genie 2 vortex (Scientific Industries Inc., Bohemia, NY, USA) for 1 min, incubated at room temperature (25±2°C) for 30 min, and subsequently centrifuged at 3,000×*g* for 15 min using a 5804R centrifuge (Eppendorf, Hamburg, Germany). After removal of the supernatant by careful decantation, the residue was weighed. Water and oil absorption capacities were expressed as grams of water or oil retained *per* gram of dry rice analog (g/g).

The bulk density of rice analogs was determined using a standard gravimetric method following the AOAC International method [AOAC, 2016]. The sample was gently introduced into a 100-mL graduated cylinder, and its surface was leveled carefully without applying pressure. The mass was measured using an analytical balance (AUY220, Shimadzu, Kyoto, Japan). Bulk density (g/mL) was determined from the quotient of rice analog mass and the corresponding sample volume.

Water activity (a_w) of rice analogs was determined at 25±1°C using an AquaLab 4TE instrument (METER Group Inc., Pullman, WA, USA), which operates based on the dew-point principle. Prior to analysis, the instrument was calibrated with certified salt solution standards according to the manufacturer's recommendations. Rice analogs were placed in the sample cup, and the measurement was performed until a stable reading was obtained.

The swelling power of rice analogs was determined using a modified procedure based on the method of Leach *et al*. [1959]. A 0.5-g sample (dry basis) was suspended in 10 mL of distilled water and heated at 90°C for 30 min in a water bath (WNB14, Memmert GmbH), with manual stirring every 5 min. Following heat treatment, the suspension was cooled to room temperature before centrifugation at 3,000×*g* for 15 min using a 5804R centrifuge (Eppendorf). After decanting the supernatant, the sediment (gel) was weighed. Swelling power (g/g) was calculated using Equation (1):

$$\text{Swelling power} = \frac{\text{Sediment weight}}{\text{Initial dry weight of rice analog}} \quad (1)$$

Cooking loss was determined using a modified procedure based on the method of Sutrisno *et al*. [2024]. A 5-g portion of rice analog (dry basis) was immersed in 100 mL of boiling distilled water and cooked for 15 min to achieve complete gelatinization. The cooking water was collected and dried in a hot-air oven (UN55, Memmert GmbH) at 105°C until reaching a constant weight. The weight of the residue was used to calculate the cooking loss (%) using Equation (2):

$$\text{Cooking loss (\%)} = \frac{\text{Dried residue weight}}{\text{Initial dry weight of rice analog}} \times 100 \quad (2)$$

Determination of starch fractions with different digestibility

In vitro starch digestibility of rice analogs was assessed using a sequential enzymatic hydrolysis procedure based on the method of Englyst *et al*. [1992] with slight modifications. This procedure mimics gastrointestinal digestion through stepwise enzymatic treatments. To simulate gastric digestion, 1 g of the rice analog was incubated with pepsin at pH 2.0 and 37°C for 30 min. Subsequently, the pH was adjusted to 6.9 for enzymatic hydrolysis performed using pancreatic α-amylase (10 U/mg starch) and amyloglucosidase (3 U/mg starch) at 37°C under continuous agitation. Aliquots were collected at 20 min and 120 min to determine glucose release. Glucose concentration in the hydrolysates was quantified spectrophotometrically by the 3,5-dinitrosalicylic acid (DNS) method [Li & McKee, 2023]. Glucose released after 20 and 120 min of enzymatic hydrolysis was used to calculate the contents of rapidly digestible starch (RDS), slowly digestible starch (SDS), and resistant starch (RS). RDS represented the starch fraction hydrolyzed during the first 20 min of digestion, whereas SDS corresponded to the fraction hydrolyzed between 20 and 120 min. The starch remaining unhydrolyzed after 120 min was classified as RS. Total starch digestibility was expressed as the percentage of hydrolyzed starch relative to the total starch content of the rice analog. The amount of hydrolyzed starch was estimated from the glucose released during enzymatic digestion and converted to starch equivalents using a conversion factor of 0.9. In this study, the total starch digestibility represents the sum of RDS and SDS, corresponding to the starch fraction hydrolyzed within 120 min of digestion.

Determination of β-carotene content and total phenolic content

The β-carotene content of rice analogs was quantified spectrophotometrically after extraction with an acetone and *n*-hexane (4:6, *v/v*) mixture using a modified procedure derived from the method previously used by Bieżanowska-Kopeć *et al*. [2022]. For extraction, 1.0 g of the rice analog (dry basis) was combined with 10 mL of the extraction solvent, homogenized, and then

centrifuged at 3,000×*g* for 10 min. The upper phase was collected as the extract. The absorbance of the extract was measured at 450 nm using a UV–Vis spectrophotometer (UV-1800, Shimadzu). The β-carotene content was calculated from a β-carotene calibration curve and expressed as mg/100 g dry rice analog.

The total phenolic content (TPC) of rice analogs was quantified using the Folin–Ciocalteu reagent according to the method described by Martins *et al*. [2021]. For extraction, the dry sample was mixed with 80% (*v/v*) aqueous ethanol at a sample-to-solvent ratio of 1:10 (*w/v*). The mixture was incubated under agitation at 150 rpm for 30 min at room temperature before centrifugation at 3,000×*g* for 15 min. The resulting supernatant was used as the extract. For TPC analysis, 0.5 mL of the extract was combined with 2.5 mL of a 10% (*v/v*) Folin–Ciocalteu reagent and 2.0 mL of a 7.5% (*w/v*) Na_2CO_3 solution. After standing in the dark at room temperature for 30 min, the absorbance of the reaction mixture was measured at 765 nm with a UV–Vis spectrophotometer (UV-1800, Shimadzu). The total phenolic content was calculated from a gallic acid calibration curve, and the results were reported as mg gallic acid equivalent (GAE)/g dry rice analog.

Texture profile analysis

For texture profile analysis, instant rice analogs were first cooked using a rice-to-water ratio of 1:2 (*w/v*) according to the preparation procedure applied in the sensory evaluation. Following cooking, the rice analogs were cooled to room temperature, and then subjected to measurements of texture properties using a TA.XTplus texture analyzer (Stable Micro Systems Ltd., Surrey, UK) fitted with a cylindrical probe (P/36R). The analysis was conducted using a two-cycle compression test. The pre-test, test, and post-test speeds were 1.0 mm/s. Rice analog samples were compressed to 50% of their original height using a trigger force of 0.05 N. Their texture profile parameters included hardness, cohesiveness, springiness, and chewiness. Hardness (N) was defined as the highest force recorded in the initial compression cycle. Cohesiveness was calculated by dividing the area under the second compression curve by that obtained during the first compression. Springiness described the ability of the rice analog to recover its original height after the compressive force was released. Chewiness (N) was calculated as the product of hardness, cohesiveness, and springiness.

Analysis of structural and microstructural characteristics

Fourier transform infrared (FTIR) spectra of the rice analogs were recorded using an IRTracer-100 spectrometer (Shimadzu) operated in attenuated total reflectance (ATR) mode. Spectral data were acquired over the wavenumber range of 4,000–400 cm^{-1} at a resolution of 4 cm^{-1} using 32 scans for each rice analog sample. The analysis was performed to examine differences in the position and intensity of absorption bands corresponding to O–H, C–H, and C–O functional groups among the rice analog formulations.

Rice analog microstructure was characterized by scanning electron microscopy (SEM) using a JSM-6510LV instrument (JEOL Ltd., Tokyo, Japan). Prior to imaging, rice analog samples were mounted on aluminum stubs and coated with a gold–palladium layer for 60 s using a JEC-3000FC sputter coater (JEOL Ltd.). Micrographs were captured at an accelerating voltage of 10 kV with magnifications of ×500 and ×1,000. The evaluation focused on differences in surface morphology, pore structure, and matrix continuity among the samples.

Sensory preference test

The rice analog preference test was conducted with 30 untrained panelists, namely students of the Agricultural Product Technology Study Program at Universitas Mercu Buana Yogyakarta, Yogyakarta, Indonesia (17 women and 13 men; aged 18–21 years) who did not have allergies to pumpkin, mocaf, or sorghum. All panelists participated voluntarily and provided written informed consent after receiving an explanation of the sensory evaluation procedure. The number of panelists (n=30) was considered sufficient for preliminary assessment of consumer acceptability. The attributes evaluated included color, aroma, taste, texture, and overall acceptance, which were scored using a five-point hedonic scale ranging from 1 (strongly dislike) to 5 (strongly like). Prior to evaluation, rice analog samples were prepared in a rice cooker at a rice-to-water ratio of 1:2 (*w/v*), allowed to equilibrate at room temperature (29±1°C) for 10 min, and served warm in 10-g portions. All samples were coded using randomly generated three-digit numbers before sensory assessment.

Statistical analysis

Data are presented as mean and standard deviation. Three independent production batches were prepared, and each analytical measurement was performed in triplicate for every batch. The reported values represent the means of all measurements obtained from these independent experiments. The experiment was arranged in a completely randomized design (CRD) with a single factor, namely the proportion of sorghum flour, mocaf, and pumpkin flour in the formulations. Statistical differences among treatments were evaluated using one-way analysis of variance (ANOVA), followed by Duncan's multiple range test (DMRT) when significant effects were detected. Differences were considered statistically significant at p<0.05. All analyses were carried out using IBM SPSS Statistics for Windows, version 25.0 (IBM Corp., Armonk, NY, USA).

RESULTS AND DISCUSSION

Proximate composition of raw materials

The compositional profiles of the flours used in the rice analog formulations are summarized in **Table 1**. Sorghum flour exhibited the highest protein (8.29 g/100 g) and fat (2.60 g/100 g) contents among the raw materials, indicating its potential contribution to the nutritional value of the rice analog formulations. Sorghum has been recognized as a cereal with moderate protein and lipid

Table 1. Proximate composition of raw materials.

Raw material	Moisture (g/100 g)	Protein (g/100 g)	Ash (g/100 g)	Fat (g/100 g)	Carbohydrates (g/100 g)
Sorghum flour	7.53±0.42^{b}	8.29±0.94^{a}	1.57±0.07^{b}	2.60±0.06^{a}	80.01±1.14^{c}
Mocaf	9.16±0.97^{a}	1.45±0.07^{b}	0.54±0.01^{c}	0.24±0.03^{c}	88.61±0.98^{a}
Pumpkin flour	6.71±0.53^{c}	1.38±0.01^{b}	5.78±0.93^{a}	0.32±0.00^{b}	85.81±1.05^{b}

Data are reported as mean ± standard deviation. Different letters within a column indicate significant differences (p<0.05).

Table 2. Proximate composition and crude fiber content of instant rice analogs produced from sorghum flour, mocaf, and pumpkin flour blended in various proportions.

Sorghum flour to mocaf and pumpkin flour ratio	Moisture (g/100 g)	Protein (g/100 g)	Ash (g/100 g)	Fat (g/100 g)	Crude fiber (g/100 g)	Carbohydrates (g/100 g)
100:0:0 (*w/w/w*)	6.71±0.98^{a}	10.63±0.15^{a}	1.68±0.09^{e}	3.82±0.85^{a}	2.59±0.17^{e}	77.16±2.06^{c}
80:10:10 (*w/w/w*)	6.74±0.57^{a}	9.24±0.92^{b}	1.73±0.18^{d}	3.10±0.98^{b}	2.77±0.85^{d}	79.19±1.64^{b}
60:20:20 (*w/w/w*)	6.72±0.81^{a}	8.06±0.85^{c}	2.61±0.55^{c}	2.53±0.18^{c}	3.54±0.07^{c}	80.08±1.19^{a}
40:30:30 (*w/w/w*)	6.73±0.90^{a}	7.74±0.72^{d}	2.83±0.15^{b}	2.29±0.09^{d}	4.80±0.95^{b}	80.41±2.73^{a}
20:40:40 (*w/w/w*)	6.65±0.58^{b}	7.13±0.50^{e}	3.47±0.77^{a}	1.87±0.05^{e}	5.71±0.05^{a}	80.88±2.28^{a}

Data are reported as mean ± standard deviation. Different letters within a column indicate significant differences (p<0.05).

contents and has been widely utilized in rice analog production due to its favorable nutritional properties [Kishore *et al*., 2024]. In contrast, mocaf had the highest carbohydrate content (88.61 g/100 g) and relatively low contents of protein, ash, and fat (**Table 1**). Its high carbohydrate content can be attributed to the starch-rich composition of cassava flour [Alamu *et al*., 2017]. Pumpkin flour was characterized by the highest ash content (5.78 g/100 g) (**Table 1**), indicating a higher mineral content than in the other raw materials. These compositional differences among sorghum flour, mocaf, and pumpkin flour were expected to influence the nutritional composition, starch digestibility, physicochemical properties, and sensory characteristics of the resulting rice analogs.

Proximate composition and crude fiber content of rice analogs

The moisture content of instant rice analogs based on sorghum flour, mocaf, and pumpkin flour ranged from 6.65 to 6.74 g/100 g with significant differences found only between the rice analog obtained at a flour ratio of 20:40:40 (*w/w/w*) and other products (p<0.05) (**Table 2**). The relatively narrow range of moisture contents in the rice analogs indicates that variations in formulation had only a limited effect on this parameter. In the case of extrusion-based rice analogs, processing conditions, including extrusion and post-extrusion drying parameters, mainly influence the residual moisture content [Shaikh *et al*., 2025; Sumardiono *et al*., 2021]. The moisture content of the rice analogs produced in this study was less than 12 g/100 g, a level generally regarded as adequate for maintaining the storage stability of dry cereal-based products [Bahlawan *et al*., 2023].

The protein content of the rice analogs produced from blends of sorghum flour, mocaf, and pumpkin flour ranged from 7.13 g/100 g (flour ratio of 20:40:40, *w/w/w*, respectively) to 10.63 g/100 g (100:0:0 formulation) (**Table 2**). Significant differences between the samples indicate that changes in the proportion of raw materials directly affect the protein content in the composite system. This trend is consistent with reports indicating that the protein content of rice analogs is highly determined by the type and ratio of their ingredients [Bahlawan *et al*., 2023; Sumardiono *et al*., 2021]. The decrease in protein content observed in the rice analogs produced from blends with higher proportions of mocaf and pumpkin flour (**Table 2**) was primarily due to the lower protein contents of these ingredients (1.45 and 1.38 g/100 g, respectively) compared to sorghum flour (8.29 g/100 g) (**Table 1**). Protein content gradually declined as the proportion of mocaf and pumpkin flour increased because replacing sorghum flour produced a dilution effect. In addition, the extrusion process might have promoted protein denaturation and modify starch–protein interactions, thereby affecting the protein fraction of the final product [Sumardiono *et al*., 2021; Sun *et al*., 2023; Webb *et al*., 2023]. Nevertheless, protein content of the rice analogs produced in this study was substantially higher than that reported for starch-based rice analogs (0.46–1.25 g/100 g) [Zulfa *et al*., 2023]. These results indicate that the inclusion of sorghum flour contributed to the higher protein content and overall nutritional quality of the rice analog formulations.

Ash content is widely used as an indicator of the mineral content of food products. As presented in **Table 2**, the ash content of the rice analogs increased from 1.68 g/100 g for

the sorghum-only formulation (100:0:0) to 3.47 g/100 g for the formulation containing sorghum flour, mocaf, and pumpkin flour at a ratio of 20:40:40 (*w/w/w*). A successive increase in ash content was observed with increasing proportions of mocaf and pumpkin flour in the formulations. The higher ash content was likely associated with the higher mineral content of pumpkin flour, which is known to be a good source of potassium, magnesium, and phosphorus [Aktaş & Gerçekaslan, 2024]. These findings indicate that the incorporation of pumpkin flour may improve the mineral content of rice analogs and contribute to their nutritional value.

The fiber content of rice analogs increased significantly from 2.59 to 5.71 g/100 g as the proportion of pumpkin flour and mocaf increased in the formulation (**Table 2**). Pumpkin flour is a rich source of dietary fiber, with insoluble dietary fiber constituting its major fraction [Aktaş & Gerçekaslan, 2024]. In formulations, dietary fiber of pumpkin flour may compete with starch for available water, thereby limiting starch granule swelling and gelatinization and reducing the availability of enzymes to starch, which may contribute to lower starch digestibility and to a reduced glycemic response [Zhang *et al*., 2025; Zhang *et al*., 2022].

The carbohydrate content of rice analog increased as the proportion of pumpkin flour and mocaf in the flour blend increased and reached 80.88 g/100 g for the formulation with sorghum flour, mocaf, and pumpkin flour at 20:40:40 (*w/w/w*) (**Table 2**). The relatively high carbohydrate content of the rice analog formulations may be attributed to the carbohydrate-rich nature of mocaf, which contained 88.61 g/100 g carbohydrate (**Table 1**). The gelatinization properties of cassava starch are influenced by the amylose-to-amylopectin ratio, which affects the development of structure and texture during cooking [Li *et al*., 2022]. In addition, higher proportions of mocaf may contribute to increased water absorption and rehydration capacity. Similar functional characteristics have been reported for cassava-based rice analogs [Putri *et al*., 2022]. Although mocaf has a high carbohydrate content, its resistant starch fraction may reduce starch digestibility by limiting enzymatic hydrolysis, thereby contributing to a lower glycemic response [Rahmadani *et al*., 2025].

Color characteristics of rice analogs

The color of rice analogs exhibited a significant ($p<0.05$) decrease in *L** from 76.91 to 64.90 and increases in *a** from 3.27 to 9.52 and *b** from 8.72 to 21.02 with increasing pumpkin flour and mocaf proportion in the flour blend (**Table 3**). These values indicate a color shift from white-cream to a more intense yellow-orange. The simultaneous increase in *a** and *b** and a decrease in *L** values were probably caused by carotenoid pigments, especially β-carotene from pumpkin flour, which, as was previously reported, imparts a yellow-orange color to starch-based products [Alefew *et al*., 2024]. The reduction in *L** value may also be due to thermal browning reactions occurring during extrusion processing, particularly Maillard reactions, which can generate colored compounds and reduce product lightness [Chaturvedi & Manickavasagan, 2024; Sun *et al*., 2023].

Table 3. Color coordinates of instant rice analogs produced from sorghum flour, mocaf, and pumpkin flour blended in various proportions.

Sorghum flour to mocaf and pumpkin flour ratio	*L**	*a**	*b**
100:0:0 (*w/w/w*)	76.91±1.04^{a}	3.27±0.81^{d}	8.72±0.95^{d}
80:10:10 (*w/w/w*)	73.07±2.11^{b}	3.65±0.65^{d}	12.53±1.03^{c}
60:20:20 (*w/w/w*)	72.43±1.42^{b}	5.09±0.19^{c}	13.44±1.53^{c}
40:30:30 (*w/w/w*)	68.57±1.93^{c}	7.81±0.26^{b}	17.93±1.18^{b}
20:40:40 (*w/w/w*)	64.90±2.06^{d}	9.52±0.47^{a}	21.02±1.72^{a}

Data are reported as mean ± standard deviation. Different letters within a column indicate significant differences ($p<0.05$). *L**, lightness; *a**, redness/greenness; *b**, yellowness/blueness.

Physical and functional properties of rice analogs

Increasing the proportion of mocaf and pumpkin flour in the formulation led to an increase in hydration capacity and oil retention, a decrease in density, and stabilization of the a_w value of rice analogs (**Table 4**). The water absorption capacity (WAC) increased significantly from 2.13 g/g in the rice analog produced from sorghum flour (100:0:0 formulation) to 3.24 g/g in the product made from the 20:40:40 (*w/w/w*) blend of sorghum flour, mocaf, and pumpkin flour. WAC is the ability of insoluble compounds to absorb and retain water during rehydration and serves as an important quality parameter of instant products [Ren *et al*., 2024]. The increase observed in our study was likely associated with the higher starch and fiber contents in the composite formulation. The contribution of dietary fiber from pumpkin flour may support water retention through its structural properties and water-holding capacity. The more porous structure may facilitate water diffusion and retention, which could contribute to the rehydration capacity of the rice analogs [Shaikh *et al*., 2025]. The combination of starch and fiber in the composite formulations might have also influenced water absorption capacity of the rice analogs.

The oil absorption capacity (OAC) of the rice analogs increased from 1.35 g/g in the 100:0:0 formulation to 2.05 g/g in the formulation containing sorghum flour, mocaf, and pumpkin flour at 20:40:40 (*w/w/w*) (**Table 4**). This increase indicates an enhanced ability of the matrix to absorb and retain oil as the proportions of mocaf and pumpkin flour increased. OAC reflects material ability to bind oil *via* capillary forces and hydrophobic interactions and is strongly influenced by the composition of proteins and non-starch compounds [Kaushik *et al*., 2021]. The higher OAC observed in the formulations with greater proportions of mocaf and pumpkin flour may be due to their higher dietary fiber content and the formation of a more porous matrix, which can facilitate oil retention. Higher OAC can increase

Table 4. Physical and functional properties of instant rice analogs produced from sorghum flour, mocaf, and pumpkin flour blended in various proportions.

Sorghum flour to mocaf and pumpkin flour ratio	Water absorption capacity (g/g)	Oil absorption capacity (g/g)	Bulk density (g/mL)	Water activity	Swelling power (g/g)	Cooking loss (%)
100:0:0 (*w/w/w*)	2.13±0.04^{d}	1.35±0.01^{e}	0.83±0.00^{a}	0.37±0.04^{c}	5.82±0.98^{e}	5.74±0.65^{e}
80:10:10 (*w/w/w*)	2.37±0.01^{c}	1.59±0.09^{d}	0.61±0.00^{b}	0.33±0.01^{d}	6.34±0.15^{d}	6.48±0.84^{d}
60:20:20 (*w/w/w*)	2.52±0.07^{c}	1.64±0.05^{c}	0.56±0.03^{c}	0.42±0.00^{a}	7.18±0.83^{c}	7.83±0.91^{c}
40:30:30 (*w/w/w*)	2.86±0.01^{b}	1.82±0.00^{b}	0.53±0.01^{d}	0.39±0.00^{b}	7.96±0.17^{b}	9.21±0.74^{b}
20:40:40 (*w/w/w*)	3.24±0.05^{a}	2.05±0.02^{a}	0.46±0.00^{e}	0.32±0.02^{d}	8.63±0.70^{a}	10.67±0.08^{a}

Data are reported as mean ± standard deviation. Different letters within a column indicate significant differences (p<0.05).

Table 5. Starch fractions with different digestibility of instant rice analogs produced from sorghum flour, mocaf, and pumpkin flour blended in various proportions.

Sorghum flour to mocaf and pumpkin flour ratio	Total starch digestibility (%)	Rapidly digestible starch (%)	Slowly digestible starch (%)	Resistant starch (%)
100:0:0 (*w/w/w*)	88.7±3.4^{a}	62.7±2.2^{a}	26.0±1.2^{c}	3.32±0.19^{d}
80:10:10 (*w/w/w*)	86.2±2.9^{b}	59.4±3.1^{b}	26.7±2.2^{c}	3.68±0.93^{d}
60:20:20 (*w/w/w*)	85.0±3.7^{b}	56.6±3.9^{c}	28.4±1.7^{b}	4.04±0.77^{c}
40:30:30 (*w/w/w*)	81.7±2.0^{c}	52.2±3.1^{d}	29.5±2.0^{a}	5.37±0.42^{b}
20:40:40 (*w/w/w*)	77.8±3.0^{d}	48.6±2.3^{e}	29.3±1.2^{a}	6.84±0.33^{a}

Data are reported as mean ± standard deviation. Different letters within a column indicate significant differences (p<0.05).

flavor retention and palatability because oil acts as a carrier of volatile compounds in the food matrix [Zhang *et al*., 2021].

The bulk density of the rice analogs decreased significantly from 0.83 g/mL at 100:0:0 to 0.46 g/mL at 20:40:40 (*w/w/w*) ratio of sorghum flour, mocaf, and pumpkin flour (**Table 4**), indicating increased porosity and changes in the composite matrix structure. This parameter is influenced by particle geometry, material composition, and the extrusion and drying processes. The increase in pumpkin fiber content and the modification of mocaf starch during heating resulted in a more porous structure, thereby reducing the bulk density. Functionally, lower bulk density correlates with higher hydration capacity and lighter texture after cooking [Webb *et al*., 2023].

The water activity (a_w) of the composite rice analogs ranged from 0.32 to 0.42 (**Table 4**). All a_w values were below 0.60, a threshold below which microbial growth is generally not observed, indicating good microbiological stability during dry storage [Beuchat, 1981]. Microbial growth is limited at low water activity because the availability of free water required for metabolic activity is reduced [Tarlak, 2023]. In addition, at low a_w, the chemical reaction rates are reduced, which improves product stability during storage.

Increasing the proportion of mocaf and pumpkin flour increased the swelling power of the rice analogs from 5.82 to 8.63 g/g (**Table 4**). This behavior may be related to differences in starch composition and the resulting hydration characteristics. The increase in swelling power indicates that starch has a greater ability to absorb water and expand during cooking [Zhang *et al*., 2025]. The inclusion of easily hydrated mocaf might have enhanced the water absorption capacity of products, facilitating starch swelling. In addition, extrusion could modify starch structure and affect its hydration properties, thereby influencing swelling behavior [Shaikh *et al*., 2025].

Cooking loss increased significantly (p<0.05), from 5.74% to 10.67%, as the levels of mocaf and pumpkin flour increased in the rice analog formulations (**Table 4**), suggesting reduced starch matrix integrity during cooking. This increase was consistent with the increase in swelling power, reflecting more intense granule swelling and greater amylose release due to the disruption of the starch gel structure [Shaikh *et al*., 2025]. Moreover, this effect could also be due to the presence of fibers and non-starch components which are known to disrupt the continuity of the starch network and weaken structural cohesion [Zhao *et al*., 2026].

Starch digestibility of rice analogs

With the increase in the proportions of mocaf and pumpkin flour in the formulation of the rice analogs, a decrease was observed in their total starch digestibility, *i.e.*, from 87.42% to 76.05% (**Table 5**). This decrease may be associated with differences in starch composition of flours and the presence of dietary fiber. The accessibility of amylases to starch granules is reduced in the rice analogs with dietary fiber-rich material [Miao & Hamaker, 2021]. Dietary fiber forms a physical barrier that impairs enzyme diffusion. Moreover,

it enhances matrix complexity through interactions with starch, proteins, and non-starch components. Additionally, phenolic compounds may inhibit α-amylase activity, thereby reducing enzymatic starch hydrolysis and starch digestibility [Sun *et al*., 2020].

The rapidly digestible starch (RDS) fraction decreased significantly from 62.74% in the rice analog produced from sorghum flour (100:0:0 formula) to 48.58% in the product based on the 20:40:40 (*w/w/w*) formulation (**Table 5**). This result indicates that increasing the proportion of mocaf and pumpkin flour reduced the susceptibility of starch to enzymatic hydrolysis during the early stages of digestion. A lower RDS fraction suggests reduced rapid glucose release during digestion, which has been associated with glycemic response [Kim *et al*., 2024].

The slowly digestible starch (SDS) fraction increased from 26.03% in the rice analog from sorghum flour to 29.55% in the product made from the 40:30:30 (*w/w/w*) formulation and stabilized at 29.26% in the product from the 20:40:40 (*w/w/w*) formulation (**Table 5**). This increase may be related to compositional and structural changes in the matrix that influence the rate of starch hydrolysis. The increase in SDS content may be associated with interactions among starch, dietary fiber, and proteins, which can reduce enzyme accessibility to starch and thereby promote slower starch digestion, although these interactions were not directly measured. An increase in SDS is generally associated with a more gradual release of glucose during digestion [Kim *et al*., 2024].

Resistant starch (RS) fraction increased significantly from 3.32% to 6.84% (**Table 5**), indicating an enhanced proportion of starch that resists digestion in the small intestine and functions as a form of dietary fiber [Miao & Hamaker, 2021]. This increase may be due to starch retrogradation during extrusion and subsequent drying, coupled with interactions between starch and non-starch components. These thermal processes may facilitate the formation of resistant starch fractions in starch-based products [Rahmadani *et al*., 2025; Shaikh *et al*., 2025].

Bioactive compound content of rice analogs

A significant increase in β-carotene content of the rice analogs was observed from 4.60 µg/g for the 100:0:0 formulation to 32.66 µg/g for the 20:40:40 (*w/w/w*) formulation containing sorghum flour, mocaf, and pumpkin flour (**Table 6**). Higher inclusion levels of pumpkin flour and mocaf contributed to an increased β-carotene content, with pumpkin flour serving as the primary source of carotenoids [Ninčević Grassino *et al*., 2023]. The retention of carotenoids in the rice analog formulations may be influenced by the composition and structure of the food matrix during processing. Zhang *et al*. [2017] reported that changes in the pumpkin food matrix during drying altered carotenoid release and bioaccessibility, indicating that matrix characteristics play an important role in carotenoid stability.

The total phenolic content (TPC) increased significantly from 2.54 to 9.15 mg GAE/g with increasing levels of mocaf and pumpkin flour (**Table 6**), indicating the accumulation of phenolic compounds derived from these composite materials. The concurrent increase in β-carotene content and TPC among the formulations highlights the contribution of pumpkin flour as a source of bioactive compounds. This trend suggests that increasing the proportion of pumpkin flour increases contents of both lipophilic (β-carotene) and hydrophilic (phenolic compounds) bioactive fractions within the composite systems.

Table 6. β-Carotene content and total phenolic content of instant rice analogs produced from sorghum flour, mocaf, and pumpkin flour blended in various proportions.

Sorghum flour to mocaf and pumpkin flour ratio	β-Carotene content (µg/g)	Total phenolic content (mg GAE/g)
100:0:0 (*w/w/w*)	4.60±0.96^{e}	2.54±0.17^{e}
80:10:10 (*w/w/w*)	11.83±1.15^{d}	3.11±0.86^{d}
60:20:20 (*w/w/w*)	23.61±1.89^{c}	4.87±0.15^{c}
40:30:30 (*w/w/w*)	28.59±2.01^{b}	7.08±0.53^{b}
20:40:40 (*w/w/w*)	32.66±1.96^{a}	9.15±0.72^{a}

Data are reported as mean ± standard deviations. Different letters within a column indicate significant differences (p<0.05). GAE, gallic acid equivalent.

Texture profile analysis of cooked rice analogs

The hardness of rice analogs ranged from 36.9 to 18.4 N and decreased with increasing proportion of mocaf and pumpkin flour in the formulation (**Table 7**). Lower hardness values may reflect weakening of the continuous starch gel matrix, which reduced product resistance to compressive forces [Barbosa *et al*., 2023]. Increasing the proportion of mocaf and pumpkin flour increased the fiber content of the rice analogs. The high fiber content and changes in the starch ratio in the composite formulation likely interfere with the formation of the starch gel network. The incorporation of insoluble fiber creates discontinuities within the gel matrix, reducing its resistance to deformation and thereby lowering hardness values [Gu *et al*., 2026].

A decrease was found in the cohesiveness of rice analogs from 0.61 to 0.42 as sorghum flour substitution with mocaf and pumpkin flour increased (**Table 7**). This decrease reflects a reduced ability of the internal structure to withstand successive deformation cycles in TPA. This was due to two main reasons: first, the reduced content of sorghum starch, which forms a gel matrix, thereby reducing cohesiveness [Bahlawan *et al*., 2023], and second, the higher fiber content which may create structural discontinuities within the gel matrix, thereby weakening internal bonding [Shaikh *et al*., 2025].

The decrease in the springiness of the rice analogs from 0.82 to 0.54 with increasing substitution of sorghum flour with mocaf and pumpkin flour (**Table 7**) indicates a reduced ability of the sample to return to its original shape after deformation, reflecting diminished elastic recovery of the gel structure. The reduction in the dominance of the main starch and changes in the amylose-amylopectin ratio, particularly the relatively high

Table 7. Texture profile parameters of cooked instant rice analogs produced from sorghum flour, mocaf, and pumpkin flour blended in various proportions.

Sorghum flour to mocaf and pumpkin flour ratio	Hardness (N)	Cohesiveness	Springiness	Chewiness (N)
100:0:0 (*w/w/w*)	36.9±2.6[a]	0.61±0.01[a]	0.82±0.03[a]	14.95±1.06[a]
80:10:10 (*w/w/w*)	33.7±1.3[b]	0.54±0.03[b]	0.78±0.00[b]	13.71±0.95[a]
60:20:20 (*w/w/w*)	28.1±2.1[c]	0.49±0.00[c]	0.75±0.02[b]	10.03±0.89[b]
40:30:30 (*w/w/w*)	25.2±1.9[d]	0.46±0.02[c]	0.67±0.05[c]	7.51±0.73[c]
20:40:40 (*w/w/w*)	18.4±1.1[e]	0.42±0.01[d]	0.54±0.01[d]	5.43±0.08[d]

Data are reported as mean ± standard deviation. Different letters within a column indicate significant differences ($p<0.05$).

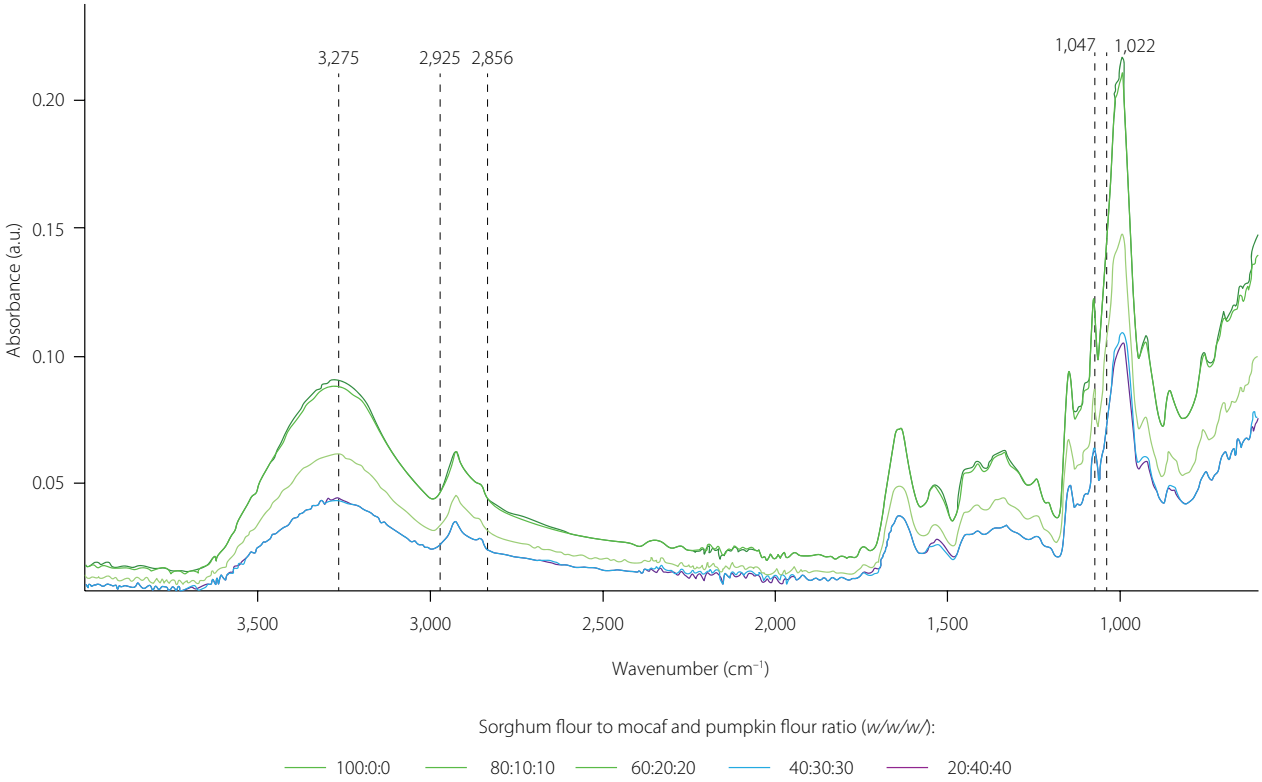

Figure 1. Fourier transform infrared (FTIR) spectra of instant rice analogs produced from sorghum flour, mocaf, and pumpkin flour blended in various proportions.

amylopectin content characteristic of mocaf starch, resulted in a less-organized, less-elastic gel network. Furthermore, the incorporation of higher levels of non-starch compounds, especially dietary fiber from pumpkin flour, induces structural irregularities within the starch matrix. These irregularities disrupt molecular interactions within the gel network, thereby reducing elasticity [Vandana *et al*., 2026]. Changes in composition may also affect the degree of gelatinization during extrusion, leading to a looser gel structure [Shaikh *et al*., 2025].

Chewiness of the rice analogs decreased from 14.95 N to 5.43 N with increasing proportions of mocaf and pumpkin flour in the formulation (**Table 7**). This decrease reflects the combined effect of reductions in hardness, cohesiveness, and springiness, as chewiness is a composite TPA parameter derived from these three attributes. Structurally, these changes are associated with modifications in the amylose-amylopectin ratio and with the disruption of the starch gel matrix by non-starch components, such as fiber and protein, during extrusion.

Structural characteristics of rice analogs

FTIR spectra of the rice analogs produced from sorghum flour, mocaf, and pumpkin flour blends at 100:0:0, 80:10:10, 60:20:20, 40:30:30, and 20:40:40 (*w/w/w*) ratios are shown in **Figure 1**. They exhibited the characteristic absorption pattern of starch without the formation of new functional groups, indicating that formulation variations primarily affected intermolecular interactions.

All rice analogs showed a broad band at approximately 3,275 cm^{-1} (**Figure 1**), corresponding to O–H stretching from starch hydroxyl groups and bound water. The intensity of this band was the highest for products from 100:0:0 and 80:10:10 (*w/w/w*) formulations, intermediate for the rice analog from the 40:30:30 (*w/w/w*) formulation, and lowest when the flour blends at

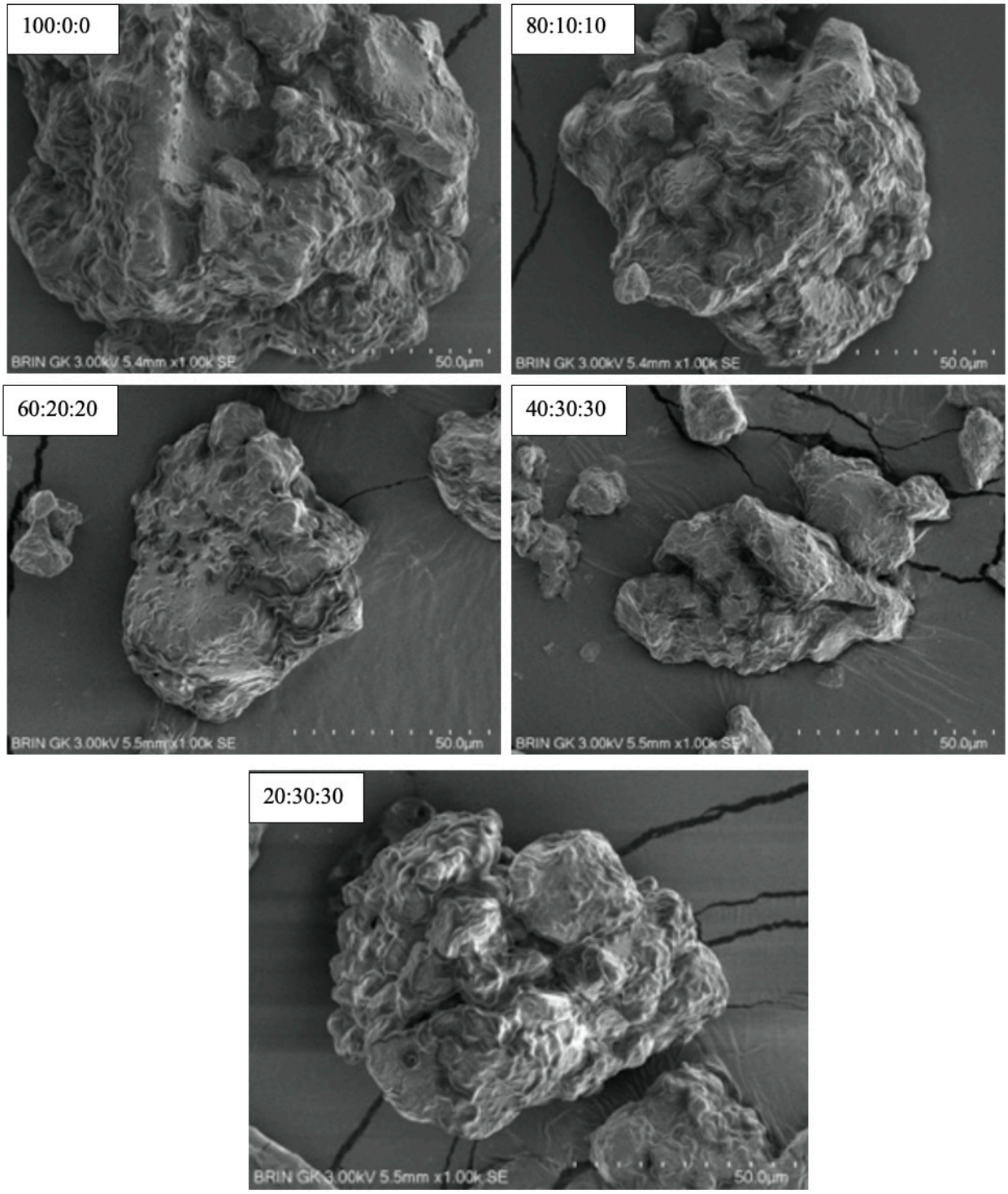

Figure 2. Microstructure of instant rice analogs produced from sorghum flour, mocaf, and pumpkin flour blended in various proportions.

the 60:20:20 and 20:40:40 (*w/w/w*) ratios were used, indicating differences in hydrogen-bonding interactions within the matrix. The bands at 2,925 and 2,856 cm^{-1} correspond to the asymmetric and symmetric C–H stretching vibrations of aliphatic groups [Kıymaz *et al*., 2025]. In the 1,200–900 cm^{-1} fingerprint region, all formulations exhibited bands at 1,047 and 1,022 cm^{-1}, which are commonly associated with the crystalline and amorphous regions of starch, respectively [van Soest *et al*., 1995].

Microstructure of rice analogs

SEM images show that increasing the substitution of sorghum flour with mocaf and pumpkin flour in the formulations from 100:0:0 to 20:40:40 (*w/w/w*) progressively modified the morphology of the rice analogs (**Figure 2**). The 100:0:0 formulation formed a compact and homogeneous matrix with minimal pores, indicating a continuous starch network and uniform gelatinization. In turn, the rice analogs produced from sorghum flour, mocaf

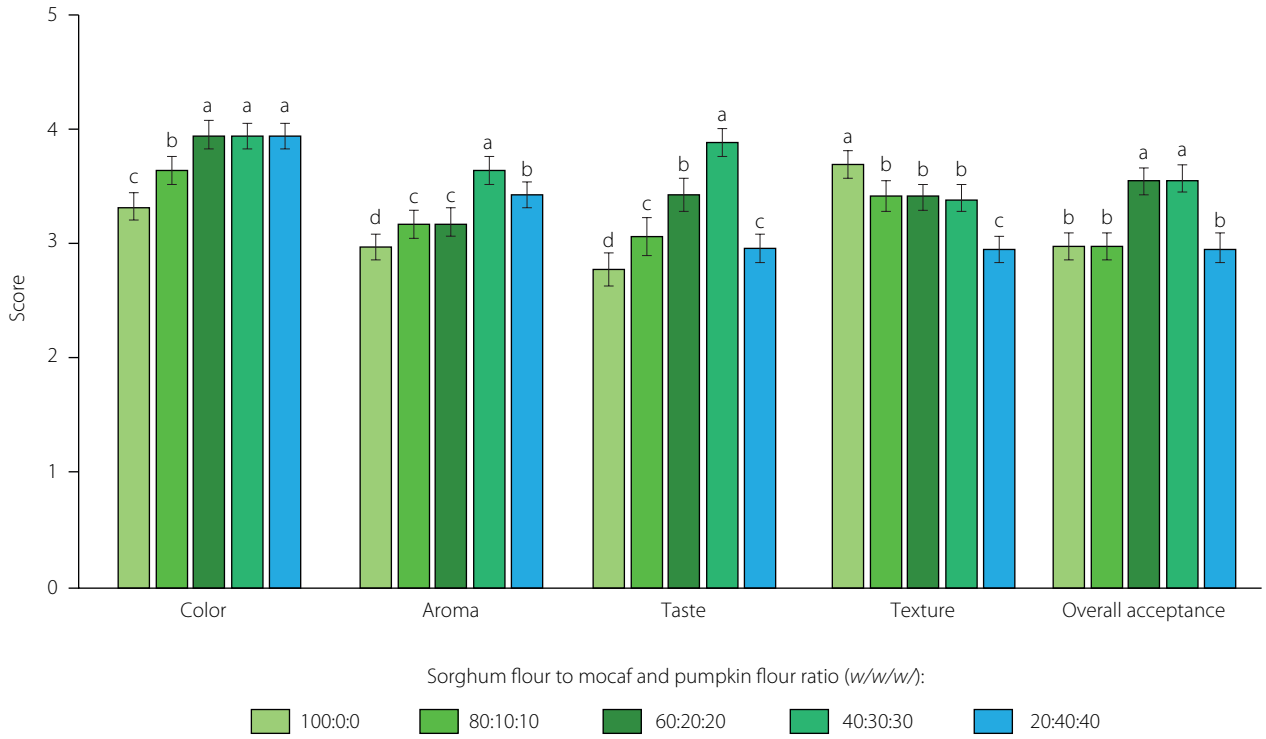

Figure 3. Sensory acceptance of cooked rice analogs produced from sorghum flour, mocaf, and pumpkin flour blended in various proportions. Results are shown as mean and standard deviation. Different letters (a–d) above the bars within the same sensory attribute indicate significant differences ($p<0.05$).

and pumpkin flour at 80:10:10 and 60:20:20 (*w/w/w)* ratios exhibited microcracks and small cavities, resulting from the disruption of matrix continuity by non-starch components. The rice analogs obtained from flour blends in the 40:30:30 and 20:40:40 (*w/w/w*) ratios showed more pronounced porosity and cracks, indicating weakening of the starch network and structural heterogeneity after processing. These structural changes are consistent with the observed increase in water absorption capacity and a decrease in bulk density, suggesting that greater porosity facilitates water penetration and reduces matrix compactness. The more open and discontinuous matrix structure explains the observed reduction in hardness and cohesiveness in the texture profile analysis. This indicates weaker internal bonding within the gel network. Such morphological changes may also be related to starch reorganization during processing and cooling, which can influence the development of heterogeneous regions within the matrix [Chang *et al*., 2021]. In this study, the presence of pores and discontinuities in high-substitution formulations suggests that structural rearrangement occurs alongside increased incorporation of non-starch components. This structural modification contributes to the observed variations in the physicochemical and textural properties of the rice analogs.

Sensory acceptance of cooked rice analogs

Based on the 5-point hedonic scale, all rice analogs received mean scores above 3.0 for color, aroma, taste, texture, and overall acceptance, indicating acceptable consumer responses (**Figure 3**). The rice analog produced from the sorghum flour, mocaf, and pumpkin flour blend at the ratio of 40:30:30 (*w/w/w*) received the highest mean scores for taste and aroma. Furthermore, its overall acceptance score was high, although did not differ significantly ($p\geq0.05$) from that of the product based on sorghum flour, mocaf, and pumpkin flour at the 60:20:20 (*w/w/w*) ratio. Rice analogs made from formulations containing higher proportions of pumpkin flour (60:20:20, 40:30:30, and 20:40:40, *w/w/w*) received the highest color scores (4.00), which may be attributed to the presence of β-carotene pigment in pumpkin flour [Ninčević Grassino *et al*., 2023]. Aroma and taste scores improved with increasing proportions of mocaf and pumpkin flour in the formulation up to the 40:30:30 (*w/w/w*) formulation, whereas the 20:40:40 (*w/w/w*) formulation did not show further improvement. This trend may be related to differences in the composition of the flour blends and flavor development during processing.

No significant differences ($p\geq0.05$) were observed in texture acceptance among the rice analogs from 80:10:10, 60:20:20, and 40:30:30 (*w/w/w*) formulations. The texture of the sorghum flour product was rated the highest, while the texture of rice analog made from a flour blend at the 20:40:40 (*w/w/w*) ratio received the lowest score. Comparison of these results with the instrumental texture measurements suggests that texture acceptance was not solely determined by hardness and chewiness values among the formulations.

CONCLUSIONS

Increasing the proportion of mocaf and pumpkin flour in sorghum-based instant rice analogs significantly affected their chemical composition, functional properties, structural characteristics, and starch digestibility. Substitution of sorghum flour with mocaf and pumpkin flour increased contents of crude fiber, β-carotene, and total phenolics, and the proportions of slowly digestible starch and resistant starch, while decreased rapidly digestible starch, total starch digestibility, bulk density, and texture hardness. FTIR analysis indicated no formation of new functional groups but suggested changes in starch organization associated with an increased amorphous fraction, whereas SEM observations revealed greater matrix porosity and structural heterogeneity. These structural modifications were consistent with the higher hydration capacity and softer texture observed after cooking. Among the formulations evaluated, the sorghum flour, mocaf, and pumpkin flour blend at 40:30:30 (*w/w/w*) ratio provided the most favorable balance between functional properties and sensory acceptance of rice analogs. Overall, the developed rice analogs demonstrate potential as a locally sourced functional food with increased contents of bioactive compounds and a modified starch digestibility profile.

RESEARCH FUNDING

This research was financially supported through a national collaborative research program involving Universitas Mercu Buana Yogyakarta, Universitas Khairun, and the National Research and Innovation Agency (BRIN) Gunungkidul, Indonesia, under Contract No. 003/C.01/H.05/MOU/I/2025.

CONFLICT OF INTERESTS

The authors declare no conflict of interest.

ADDITIONAL INFORMATION

Ethical approval for the sensory evaluation was obtained from the Research Ethics Committee of Universitas Alma Ata, Yogyakarta, Indonesia (Approval No. 142/EC/X/2025).

ORCID IDs

B. Kanetro **https://orcid.org/0000-0002-4522-5575**
H. Rasulu **https://orcid.org/0000-0001-7446-7939**
A. Slamet **https://orcid.org/0000-0001-6229-7004**

REFERENCES

1. Adebo, J.A., Kesa, H. (2023). Evaluation of nutritional and functional properties of anatomical parts of two sorghum (*Sorghum bicolor*) varieties. *Heliyon*, *9*(6), art. no. e17296. **https://doi.org/10.1016/j.heliyon.2023.e17296**
2. Aktaş, N., Gerçekaslan, K.E. (2024). Pumpkin (*Cucurbita pepo* L.) pulp flour as a source of dietary fiber: Chemical, physicochemical and technological properties. *Akademik Gıda*, *22*(1), 14–22. **https://doi.org/10.24323/akademik-gida.1460957**
3. Alamu, E.O., Maziya-Dixon, B., Dixon, A.G. (2017). Evaluation of proximate composition and pasting properties of high quality cassava flour (HQCF) from cassava genotypes (*Manihot esculenta* Crantz) of β-carotene-enriched roots. *LWT – Food Science and Technology*, *86*, 501–506. **https://doi.org/10.1016/j.lwt.2017.08.040**
4. Alefew, Y.D., Tiruneh, A.T., Yehuala, T.F. (2024). Optimization of extrusion conditions for development of high quality rice-lupin-pumpkin based extruded snack food. *Heliyon*, *10*(24), art. no. e40913. **https://doi.org/10.1016/j.heliyon.2024.e40913**
5. Alija, D., Olędzki, R., Nikolovska Nedelkoska, D., Wojciechowicz-Budzisz, A., Xhabiri, G., Pejcz, E., Alija, E., Harasym, J. (2025). The addition of pumpkin flour impacts the functional and bioactive properties of soft wheat composite flour blends. *Foods*, *14*(2), art. no. 243. **https://doi.org/10.3390/foods14020243**
6. AOAC (2005). *Official Methods of Analysis (16th ed.)*. The Association of Official Analytical Chemists International, Arlington, VA, USA.
7. AOAC (2016). *Official Methods of Analysis* (20th ed.). The Association of Official Analytical Chemists International, Arlington, VA, USA.
8. Bahlawan, Z.A.S., Kumoro, A.C., Megawati, M., Wahono, S.K. (2023). Physico-chemical characteristics of novel analog rice from fermented sorghum flour by *Rhizopus oligosporus* and soybean flour. *Current Research in Nutrition and Food Science Journal*, *11*(3), 1022–1038. **https://doi.org/10.12944/CRNFSJ.11.3.09**
9. Barbosa, M.C., Silva, G.L., Viana, E.B.M., Bonomo, R.C.F., Rodrigues, L.B., Veloso, C.M. (2023). Effect of protein addition in properties of gels produced with jackfruit (*Artocarpus integrifolia*) seed starch: rheological and texture properties. *Journal of Food Science and Technology*, *60*(12), 2916–2926. **https://doi.org/10.1007/s13197-023-05793-1**
10. Beuchat, L.R. (1977). Functional and electrophoretic characteristics of succinylated peanut flour protein. *Journal of Agricultural and Food Chemistry*, *25*(2), 258–261. **https://doi.org/10.1021/jf60210a044**
11. Beuchat, L.R. (1981). Microbial stability as affected by water activity. *Cereal Foods World*, *26*, 345–349.
12. Bieżanowska-Kopeć, R., Ambroszczyk, A.M., Piątkowska, E., Leszczyńska, T. (2022). Nutritional value and antioxidant activity of fresh pumpkin flowers (*Cucurbita* sp.) grown in Poland. *Applied Sciences*, *12*(13), art. no. 6673. **https://doi.org/10.3390/app12136673**
13. Chang, Q., Zheng, B., Zhang, Y., Zeng, H. (2021). A comprehensive review of the factors influencing the formation of retrograded starch. *International Journal of Biological Macromolecules*, *186*, 163–173. **https://doi.org/10.1016/j.ijbiomac.2021.07.050**
14. Chao, C., Liang, S., Zhang, Z., Gidley, M.J., Liu, Y., Wang, S. (2024). New insight into the effects of endogenous protein and lipids on the enzymatic digestion of starch in sorghum flour. *Foods*, *13*(5), art. no. 663. **https://doi.org/10.3390/foods13050663**
15. Chaturvedi, S., Manickavasagan, A. (2024). Rice analogues: Processing methods and product quality. *Trends in Food Science & Technology*, *148*, art. no. 104493. **https://doi.org/10.1016/j.tifs.2024.104493**
16. Chiodetti, M., Tuccio, M.G., Carini, E. (2024). Effect of water content on gelatinization functionality of flour from sprouted sorghum. *Current Research in Food Science*, *8*, art. no. 100780. **https://doi.org/10.1016/j.crfs.2024.100780**
17. Englyst, H.N., Kingman, S.M., Cummings, J.H. (1992). Classification and measurement of nutritionally important starch fractions. *European Journal of Clinical Nutrition*, *46*(Suppl 2), S33–S50.
18. Gu, Y., Xu, R., McClements, D.J., Liu, T., Zhao, X., Su, G., Zhao, M., Zhao, Q. (2026). Both gelation properties and digestibility of mung bean starch are differentially affected by soluble and insoluble dietary fiber. *Food Research International*, *225*, art. no. 118113. **https://doi.org/10.1016/j.foodres.2025.118113**
19. Jiali, L., Wu, Z., Liu, L., Yang, J., Wang, L., Li, Z., Liu, L. (2024). The research advance of resistant starch: structural characteristics, modification method, immunomodulatory function, and its delivery systems application. *Critical Reviews in Food Science and Nutrition*, *64*(29), 10885–10902. **https://doi.org/10.1080/10408398.2023.2230287**
20. Kaushik, N., Yadav, P., Khandal, R.K., Aggarwal, M. (2021). Review of ways to enhance the nutritional properties of millets for their value-addition. *Journal of Food Processing and Preservation*, *45*(6), art. no. 15550. **https://doi.org/10.1111/jfpp.15550**
21. Kim, M.K., Park, J., Kim, D. (2024). Resistant starch and type 2 diabetes mellitus: Clinical perspective. *Journal of Diabetes Investigation*, *15*(4), 395–401. **https://doi.org/10.1111/jdi.14139**
22. Kishore, S.G., Dwivedi, M., Dalbhagat, C.G., Thota, N., Singh, C.N., Saravanan, S., Nikitha, G., Kumar, N.V., Vignesh, V. (2024). Development of extruded millet analogue rice: A comparison of rheological, structural, physiochemical, and cooking properties with conventional rice. *ACS Food Science & Technology*, *4*(10), 2504–2516. **https://doi.org/10.1021/acsfoodscitech.4c00629**

23. Kıymaz, B.M., Ozmen, D., Moin, A., Çiçek, B., Toker, O.S., Arici, M. (2025). Modification of taro starch using ball milling process. *International Journal of Biological Macromolecules*, *321*(Pt1), art. no. 146300. **https://doi.org/10.1016/j.ijbiomac.2025.146300**
24. Leach, H.W., McCowen, L.D., Schoch, T.J. (1959). Structure of the starch granule. I. Swelling and solubility patterns of various starches. *Cereal Chemistry*, 534–544.
25. Li, E., Cao, P., Cao, W., Li, C. (2022). Relations between starch fine molecular structures with gelatinization property under different moisture content. *Carbohydrate Polymers*, *278*, art. no. 118955. **https://doi.org/10.1016/j.carbpol.2021.118955**
26. Li, H., McKee, L.S. (2023). Measuring enzyme kinetics of glycoside hydrolases using the 3,5-dinitrosalicylic acid assay. In D.W. Abbott, W.F. Zandberg (Eds.), *Carbohydrate-Protein Interactions, Methods in Molecular Biology*, vol 2657. Humana, New York, NY, USA, pp. 15–25. **https://doi.org/10.1007/978-1-0716-3151-5_2**
27. Martins, G.R., Monteiro, A.F., do Amaral, F.R.L., da Silva, A.S. (2021). A validated Folin-Ciocalteu method for total phenolics quantification of condensed tannin-rich açaí (*Euterpe oleracea* Mart.) seeds extract. *Journal of Food Science and Technology*, *58*(12), 4693–4702. **https://doi.org/10.1007/s13197-020-04959-5**
28. Miao, M., Hamaker, B.R. (2021). Food matrix effects for modulating starch bioavailability. *Annual Review of Food Science and Technology*, *12*(1), 169–191. **https://doi.org/10.1146/annurev-food-070620-013937**
29. Nikrad, N., Hosseini, B., Pakmehr, A., Tousi, A.Z., Ardekani, A.M., Farhangi, M.A., Akhavan-Sigari, R. (2023). Dietary carbohydrate quality index (CQI), cardio-metabolic risk factors and insulin resistance among adults with obesity. *BMC Endocrine Disorders*, *23*(1), art. no. 171. **https://doi.org/10.1186/s12902-023-01420-4**
30. Ninčević Grassino, A., Rimac Brnčić, S., Badanjak Sabolović, M., Šic Žlabur, J., Marović, R., Brnčić, M. (2023). Carotenoid content and profiles of pumpkin products and by-products. *Molecules*, *28*(2), art. no. 858. **https://doi.org/10.3390/molecules28020858**
31. Putri, R.D.A., Rohmah, K.A.N., Lestari, I.P., Bahlawan, Z.A.S., Astuti, W., Kusumaningrum, M., Yanuar, T.R., Nurzulcha, F., Purwanti, D. (2022). Physical characteristics and nutritional value of cassava analogue rice with fortified protein tempeh and the addition of xanthan gum for healthy dieters. *IOP Conference Series: Earth and Environmental Science*, *969*(1), art. no. 012036. **https://doi.org/10.1088/1755-1315/969/1/012036**
32. Rahmadani, M., Fidriyanto, R., Nahrowi, Khotijah, L., Jayanegara, A. (2025). Investigating the impact of modified cassava starch with tannic acid and heat moisture treatment on physicochemical and *in vitro* starch digestibility. *Journal of Agriculture and Food Research*, *19*, art. no. 101686. **https://doi.org/10.1016/j.jafr.2025.101686**
33. Ren, Y., Jia, F., Li, D. (2024). Ingredients, structure and reconstitution properties of instant powder foods and the potential for healthy product development: a comprehensive review. *Food & Function, 15*(1), 37–61. **https://doi.org/10.1039/D3FO04216B**
34. Shaikh, J.R., Pathare, A.M., Chakraborty, S., Annapure, U.S. (2025). Evaluating the effectiveness of extrusion in fortifying rice analogues with dietary fiber. *Journal of Food Science*, *90*(8), art. no. e70443. **https://doi.org/10.1111/1750-3841.70443**
35. Slamet, A., Kanetro, B., Purwaningsih, H. (2025). Physicochemical and sensory evaluation of pumpkin-based instant porridge with mocaf and cowpea flour. *Scifood*, *19*(1), 96–109. **https://doi.org/10.5219/scifood.8**
36. Slamet, A., Kanetro, B., Purwaningsih, H. (2026). Physicochemical properties, antioxidant activities, beta-carotene content, and sensory properties of gluten-free pumpkin-fortified egg roll. *Food Research*, *10*(1), 188–198. **https://doi.org/10.26656/fr.2017.10(1).047**
37. Sumardiono, S., Budiyono, Kusumayanti, H., Prakoso, N.I.A., Paundrianagari, F.P., Cahyono, H. (2021). Influence of composite flour constituents and extrusion temperature in the production of analog rice. *Food Science and Nutrition*, *9*(8), 4385–4393. **https://doi.org/10.1002/fsn3.2411**
38. Sun, D., Zhang, B., Zhou, C., Ren, W., Wu, M. (2023). Effect of high-moisture extrusion process on quality attribute and fibrous formation mechanism of pea protein: Insight into dynamic changes of textural protein. *Innovative Food Science & Emerging Technologies*, *89*, art. no. 103486. **https://doi.org/10.1016/j.ifset.2023.103486**
39. Sun, L., Wang, Y., Miao, M. (2020). Inhibition of α-amylase by polyphenolic compounds: Substrate digestion, binding interactions and nutritional intervention. *Trends in Food Science & Technology*, *104*, 190–207. **https://doi.org/10.1016/j.tifs.2020.08.003**
40. Sutrisno, A., Suloi, A.N.F., Murtini, E.S., Bahmid, N.A. (2024). The effect of corn starch and transglutaminase on quality improvement of soybean-based analog rice. *Future Foods*, *10*, art. no. 100407. **https://doi.org/10.1016/j.fufo.2024.100407**
41. Tarlak, F. (2023). The use of predictive microbiology for the prediction of the shelf life of food products. *Foods*, *12*(24), art. no. 4461. **https://doi.org/10.3390/foods12244461**
42. van Soest, J.J.G., Tournois, H., de Wit, D., Vliegenthart, J.F.G. (1995). Short-range structure in (partially) crystalline potato starch determined with attenuated total reflectance Fourier-transform IR spectroscopy. *Carbohydrate Research*, *279*, 201–214. **https://doi.org/10.1016/0008-6215(95)00270-7**
43. Vandana, M., Vishwakarma, S., Mandliya, S., Mishra, H.N., Bhosale, Y. (2026). Incorporation of microcrystalline cellulose into extruded rice analogue: effects on the physicochemical, technofunctional, textural, cooking and structural properties, *in vitro* digestibility and estimated glycaemic index. *Sustainable Food Technology*, *4*(2), 1509–1524. **https://doi.org/10.1039/D5FB00272A**
44. Webb, D., Dogan, H., Li, Y., Alavi, S. (2023). Use of legume flours and fiber for tailoring structure and texture of pea protein-based extruded meat alternatives. *Journal of Food Science*, *88*(1), 57–71. **https://doi.org/10.1111/1750-3841.16397**
45. Zhang, B., Li, X., Dong, J., Wang, Y., Jin, Z., Bai, Y. (2025). Deciphering the role of starch outer shell in the swelling behavior of waxy maize starch granules and mechanism analysis. *Food Hydrocolloids*, *166*, art. no. 111325. **https://doi.org/10.1016/j.foodhyd.2025.111325**
46. Zhang, H., Sun, S., Ai, L. (2022). Physical barrier effects of dietary fibers on lowering starch digestibility. *Current Opinion in Food Science*, *48*, art. no. 100940. **https://doi.org/10.1016/j.cofs.2022.100940**
47. Zhang, K., Zhao, D., Song, J., Guo, D., Xiao, Y., Shen, R. (2021). Effects of green wheat flour on textural properties, digestive and flavor characteristics of the noodles. *Journal of Food Processing and Preservation*, *45*(3), art. no. e15199. **https://doi.org/10.1111/jfpp.15199**
48. Zhang, Z., Wang, X., Li, Y., Wei, Q., Liu, C., Nie, M., Li, D., Xiao, Y., Liu, C., Xu, L., Zhang, M., Jiang, N. (2017). Evaluation of the impact of food matrix change on the *in vitro* bioaccessibility of carotenoids in pumpkin (*Cucurbita moschata*) slices during two drying processes. *Food & Function*, *8*(12), 4693–4702. **https://doi.org/10.1039/C7FO01382E**
49. Zhao, J., Shen, M., Wang, R., Gu, Z., Hong, Y., Li, Z., Li, C., Ban, X., Cheng, L. (2026). Effects of removing endogenous non-starch components on the structure, physicochemical properties, and in vitro digestibility of *Castanopsis sclerophylla* flour. *Food Research International*, *230*, art. no. 118567. **https://doi.org/10.1016/j.foodres.2026.118567**
50. Zheng, H., Ma, C., Bian, X., Wang, B., Xu, Y., Zhang, G., Liu, X., Wang, Y., Yang, Y., Zhang, N. (2026). Effects of rice starch esterified with citric acid and malic acid: Functional properties and structural characteristics. *Carbohydrate Polymers*, *374*, art. no. 124690. **https://doi.org/10.1016/j.carbpol.2025.124690**
51. Zulfa, F., Rochmah, A.N., Saputri, F.D., Suleman, D.P., Anandito, R.B.K. (2023). Macronutrient profile of analog rice based on cornstarch, modified cassava flour, and suweg flour. *BIO Web of Conferences*, *69*, art. no. 03009. **https://doi.org/10.1051/bioconf/20236903009**

ORIGINAL ARTICLE
http://journal.pan.olsztyn.pl

Polish Journal of Food and Nutrition Sciences
2026, Vol. 76, No. 3, 264–278
DOI: 10.31883/pjfns/225559
ISSN 1230-0322, e-ISSN 2083-6007

Improving the Quality of Composite Bread Using Amylolytic Hydrolyzed Orange Sweet Potato Flour and Hydroxypropyl Methylcellulose

Rike T.K. Dewi*, Fransisca, Dwining P. Elfriede, Kadek W. Arinata, Andre I. Samosir

Department of Food Technology, School of STEM, Prasetiya Mulya University, EduTown I.1, BSD Raya Utama Street, Pagedangan District, Tangerang Regency, Indonesia

The incorporation of non-wheat flours to a composite bread formula presents a significant challenge in its development. This study aimed to improve bread quality particularly in terms of loaf volume, crumb structure, moisture retention, and dough machinability by substituting wheat flour with orange sweet potato flour hydrolyzed using amylase produced by *Bacillus spizizenii* ATCC 6633 and adding hydrocolloid hydroxypropyl methylcellulose (HPMC). Fifteen bread formulations containing hydrolyzed orange sweet potato flour (HOSPF; 0–60 g/100 g flour blend) and HPMC (0–3 g/100 g flour blend) were evaluated. Amylolytic hydrolysis significantly modified the physicochemical properties of orange sweet potato flour, as indicated by enhanced hydration gel properties, altered pasting behavior, disrupted starch microstructure, as well as increased reducing sugar content, amylopectin-to-amylose ratio, and β-carotene retention. Incorporation of HOSPF increased crumb firmness and color intensity. The effect of HPMC on loaf volume, specific volume, and dough machinability depended on HOSPF level in the formula. Among all formulations, A1H0 (15 g HOSPF/100 g flour blend), A1H2 (15 g HOSPF/100 g flour blend + 3 g HPMC/100 g flour blend), and A2H0 (30 g HOSPF/100 g flour blend) exhibited the most balanced characteristics. These results demonstrate that the combined use of amylolytic hydrolysis and HPMC offers an effective strategy to enhance the composite bread quality.

Keywords: amylase, bakery product, flour blend, hydrocolloid, potato flour hydrolysis

INTRODUCTION

Composite bread is formulated through the incorporation of wheat and non-wheat flours, primarily to reduce dependence on wheat flour and promote the utilization of locally available raw materials. The development of composite bread is closely associated with food security strategies, as it supports the diversification of carbohydrate sources and mitigates reliance on imported wheat. In recent years, the consumption of composite bread has increased substantially, driven by growing consumer awareness of healthier and diverse dietary patterns. Nevertheless, wheat flour remains a critical component in breadmaking due to the functional role of gluten in imparting elasticity and gas-holding capacity to the dough. The formation of a continuous gluten network enables the retention of gases produced during fermentation, thereby resulting in a light and porous crumb structure [Ronie *et al*., 2021]. Based on available evidence, non-wheat flours have not been reported to fully mimic the functional properties of gluten in breadmaking. Several studies have indicated that acceptable mechanical characteristics are typically achieved only when wheat flour substitution levels are kept below 30 g/100 g, such as in formulations containing 20 g/100 g pedada flour [Irmawati

***Corresponding Author:**
Email: **rike.dewi@prasetiyamulya.ac.id** (R.T.K. Dewi)

Submitted: 12 February 2026
Accepted: 7 July 2026
Published on-line: 22 July 2026

et al., 2024], and red bean flour at 10 g/100 g [Espinosa-Ramírez *et al*., 2022].

Orange sweet potato flour represents a promising alternative to wheat flour due to its favorable starch composition and nutritional value. Content of amylose and amylopectin in its starch is approximately 18–24 g/100 g and 76–82 g/100 g, respectively [Wang *et al*., 2020], which is comparable to the profile of wheat starch (14–19 g/100 g and 81–86 g/100 g, respectively) [Valková *et al*., 2019]. However, similar starch composition does not always result in similar bread quality because starches from tuber crops behave differently from cereal starches. In addition, orange sweet potato is rich in β-carotene, a precursor of vitamin A, thereby providing enhanced nutritional benefits relative to wheat flour [Malavi *et al*., 2022]. Indonesia also reports a substantial production of orange sweet potato, reaching 1.4 million tons in 2024 [Ministry of Agriculture of the Republic of Indonesia, 2024]. Collectively, these factors highlight its potential as a raw material for breadmaking. The relative proportion of amylose and amylopectin is key determinant of bread structure and texture: amylose contributes to the formation of a stronger starch network, whereas amylopectin enhances starch granule swelling and water absorption during baking, thereby influencing bread volume and crumb characteristics [van Rooyen *et al*., 2023]. However, the leaching of amylose from starch granules during baking may accelerate starch retrogradation upon cooling, thereby contributing to crumb firming, while excessive amylopectin may result in sticky dough with inferior handling properties. These phenomena may ultimately shorten bread shelf-life [Chen *et al*., 2021].

The incorporation of non-wheat flours at substitution levels exceeding 30 g/100 g remains a technological challenge, particularly with respect to dough rheology and loaf volume. One potential approach to overcome these limitations is starch modification through enzymatic hydrolysis using amylase. Amylase catalyzes the hydrolysis of starch polymers into shorter chains, thereby influencing viscosity, water absorption, and dough rheology [Chen *et al*., 2021]. *Bacillus spizizenii* ATCC 6633 has been reported to produce amylase suitable for food industry applications, as the enzyme exhibits stability at elevated temperatures, indicating thermal stability under baking conditions [Maity *et al*., 2015]. In parallel, hydrocolloids have been reported to partially mimic the structural functionality of gluten, leading to improvements in loaf volume, crumb texture, and storage stability [Irondi *et al*., 2023]. Hydroxypropyl methylcellulose (HPMC) is one of the most widely used among the hydrocolloids commonly applied in composite breadmaking, as it has been shown to exert superior functionality by stabilizing gas cells and promoting a fine crumb structure [Sadat *et al*., 2023].

Previous studies have reported that various non-wheat flours hydrolyzed by amylase from different microbial sources have been successfully applied in composite breadmaking. For instance, amylase-hydrolyzed rice flour and purple sweet potato flour have been shown to increase specific volume of loaf and improve its texture compared to loaves made using untreated flours [Freire *et al*., 2025; Safari *et al*., 2013]. Furthermore, studies have also demonstrated that the addition of HPMC to composite breads based on rice, corn, and potato flours resulted in improved crumb softness and optimal loaf volume [Belorio & Gómez, 2020]. To date, there is limited information regarding the combined use of amylolytically-hydrolyzed orange sweet potato flour and hydrocolloids to enhance the quality of composite bread. Based on these considerations, the objective of this study was to evaluate the effect of substituting wheat flour with α-amylase-hydrolyzed orange sweet potato flour and adding HPMC on the physical quality characteristics of breads and to identify the most promising formulation.

MATERIALS AND METHODS

Materials

The materials used in this study included *B. spizizenii* ATCC 6633 (Bio-Microbiology Laboratory Collection, Food Technology Department, Prasetiya Mulya University, Tangerang, Indonesia); starch substrate, nutrient agar, and nutrient broth (Merck, Darmstadt, Germany) for microbial cultivation; pure amylose and amylopectin for amylose content determination (Merck); and distilled water (Evoqua, Pittsburgh, PA, USA). The main ingredients for breadmaking were wheat flour (Indofood, Jakarta, Indonesia), orange sweet potato flour (Selera Organik, Bantul, Indonesia), water, sugar powder (GMP, Central Lampung, Indonesia), salt (Susanti Megah, Tangerang, Indonesia), margarine (Upfield, Cikarang, Indonesia), yeast (Lesaffre, Wavrin, France), milk powder (Karya Pranata, Bekasi, Indonesia), and HPMC (Jaya Mulyo, Bantul, Indonesia).

Experimental design

The study employed a randomized block design with two factors and three replications. The experimental factors were the proportion of amylolytically-hydrolyzed orange sweet potato flour (HOSPF) in a blend with wheat flour (0, 15, 30, 45, and 60 g/100 g) and the addition level of HPMC to a flour blend (0, 1.5, and 3 g/100 g). Each treatment combination was coded as A*H*, where A represents the level of HOSPF (A0, A1, A2, A3, and A4, respectively) and H represents the addition level of HPMC (H0, H1, and H2, respectively). For example, A4H1 corresponds to substituting wheat flour with 60 g HOSPF *per* 100 g of the flour blend and adding 1.5 g HPMC to 100 g of the flour blend. In negative control, only non-hydrolyzed orange sweet potato flour (NHOSPF) was used, and positive control was prepared from wheat flour. The research was conducted in several stages. Initially, orange sweet potato flour was hydrolyzed using amylase produced by *B. spizizenii* ATCC 6633, followed by evaluation of its functional properties. Subsequently, composite bread was prepared using HOSPF with HPMC incorporation. The resulting breads were then evaluated for physical properties. Finally, the quality of the selected composite bread formula was compared with that of conventional wheat-based bread.

Obtaining crude amylase and amylolytic hydrolysis of orange sweet potato flour

Inoculum preparation and α-amylase production were performed following the method previously used by Abd-Elaziz *et al*. [2020], with some modifications. *B. spizizenii* ATCC 6633 was first activated on nutrient agar and incubated at 37°C for 24 h. A loopful of culture was subsequently transferred into nutrient broth and cultivated at 30°C with agitation at 2.3×*g* until an optical density (OD580) of 0.8 was reached, corresponding to the exponential growth phase. The resulting culture was used as inoculum at 10% (*v/v*) and introduced into a fermentation medium consisting of nutrient broth supplemented with 2% starch substrate. Fermentation was carried out at pH 7, 30°C, and 2.3×*g* for 48 h. Following fermentation, the culture medium was centrifuged at 3,260×*g* for 25 min (Thermo Fisher Scientific, Waltham, MA, USA) to separate the bacterial biomass from the liquid fraction. The recovered supernatant was collected and used as the crude α-amylase extract. Amylase activity was determined according to the procedure described by Punia *et al*. [2016], with some modifications. Briefly, 0.1 mL of a crude α-amylase extract diluted 100-fold with distilled water was mixed with 0.9 mL of phosphate-citrate buffer (pH 7) and incubated at 37°C for 5 min. Subsequently, 2 mL of 2% gelatinized starch was added and further incubated at 37°C for 30 min. The reaction was terminated by adding 3 mL of dinitrosalicylic acid (DNS) reagent, followed by boiling at 90°C for 5 min, then cooling and adjustment to ambient temperature. The absorbance was measured using a spectrophotometer (Shimadzu, Kyoto, Japan) at λ=540 nm, and glucose was used to construct a standard curve. One unit of amylase activity was defined as the amount of enzyme that releases 1 µmol of glucose *per* min under assay conditions.

Based on the measured enzyme activity, the required volume of enzyme solution was calculated to obtain a dosage of 50 U/g flour. The enzyme was then applied to hydrolyze a sweet potato flour suspension (20 g/100 mL of distilled water, pH 7) for 24 h at 25°C [Safari *et al*., 2013]. The amylase was subsequently inactivated, and the flour suspension was simultaneously concentrated by heating the hydrolysate at 80°C for 150 min. The hydrolyzed flour was then washed with distilled water, dried at 60°C for 16 h, and used for bread preparation.

Determination of physical properties of flours

Color

Color of hydrolyzed and unhydrolyzed orange sweet potato flours, as well as wheat flour was evaluated using the CIELab color system using the colorimeter (ColorFlex EZ HunterLAB instrument, Reston, VA, USA). It was calibrated using the manufacturer's standard white and black calibration tiles prior to analysis. Color parameters were measured under illuminant D65 and a 10° standard observer. The parameters L^* (lightness 100 – darkness 0), a^* (redness $+a^*$ – greenness $-a^*$), and b^* (yellowness $+b^*$ – blueness $-b^*$) were recorded.

Gel hydration properties and moisture content

The water absorption index (WAI) and water solubility index (WSI) of flours were measured by placing 1 g of the sample into a 15 mL centrifuge tube, followed by the addition of 10 mL of distilled water at 25°C for 30 min. The tube was centrifuged at 1,449×*g* for 10 min. The supernatant was removed and placed into an evaporating dish, while the resulting gel was weighed. The WAI was calculated as the ratio of the hydrated gel to the initial dry sample weight (g/g). The WSI was determined by drying the collected supernatant at 105°C for 4 h to obtain the dissolved solids. WSI was expressed as a percentage (%) and calculated as the ratio of the weight of the dissolved solids to the initial dry sample weight, multiplied by 100 [Yea *et al*., 2019]. The moisture content of the flours was determined by drying the samples in a forced-draft oven (BINDER, Tuttlingen, Germany) at 105°C for 3 h [AOAC, 2006].

Pasting properties

Pasting properties were measured using a Rapid Visco Analyzer (RVA 4500; Perten Instruments, Hägersten, Sweden) following the procedure described by Martínez *et al*. [2015], with some modifications. The flour slurry was prepared by mixing 3.5 g (±0.1) of flour with 25 g (±0.1) of distilled water. The slurry was stirred at 960 rpm for 10 s and subsequently at 160 rpm throughout the analysis. The temperature profile consisted of holding at 50°C, heating from 50 to 95°C at 12°C/min, holding at 95°C for 2.5 min, cooling to 50°C at 12°C/min, and holding at 50°C for 2 min. The RVA pasting profile was used to determine pasting temperature (°C), peak viscosity, final viscosity, breakdown viscosity, and setback viscosity. Breakdown viscosity was calculated as the difference between peak viscosity and trough viscosity, whereas setback viscosity was calculated as the difference between final viscosity and trough viscosity. All viscosity values were expressed in mPa×s.

Microstructure

Micrographs of flours were obtained using a Zeiss EVO MA10 scanning electron microscope (SEM; Zeiss, Oberkochen, Germany). The instrument was equipped with a tungsten filament, and operated at 9 mm working distance, as well as an accelerating voltage of 10 kV. The samples were sprayed and coated with gold, and then observed at a magnification of ×2,000.

Determination of the chemical composition of flours

Reducing sugar content

Reducing sugar content of hydrolyzed and unhydrolyzed orange sweet potato flours, as well as wheat flour was determined using DNS method [Miller, 1959]. Samples were 100-fold diluted with distilled water, and 2 mL of the resulting suspension were mixed with 3 mL of the DNS reagent. The mixture was boiled at 90°C for 5 min, then cooled and adjusted to ambient temperature. The absorbance was measured using a spectrophotometer (Shimadzu) at a wavelength of 540 nm. The amount of reducing sugars was

calculated using a glucose standard curve and corrected for the dilution factor. The results were expressed as g of glucose equivalent *per* 100 g of flour.

Content of total starch, amylose, and amylopectin

Amylose and amylopectin contents were determined using the spectrophotometric method by Reddappa *et al*. [2022], with some modifications. Approximately 100 mg of the sample were treated with 500 µL of aqueous ethanol (80 g/100 mL) to remove soluble non-starch compounds, and centrifuged at 16,099×*g* for 5 min. The process was repeated twice. The pellet was washed with 500 µL of a 0.1 M NaCl solution with toluene (10 g/100 mL) and re-washed with aqueous ethanol (80 g/100 mL), then dried at 80°C for 4 h to obtain a purified starch residue. A total of 25 mg of starch residue were solubilized in 2.5 mL of 1 M NaOH and heated in a boiling water bath for 15 min. After cooling, the volume was adjusted to 25 mL with distilled water. An aliquot of 1.25 mL was treated with 150 µL of 1 M acetic acid, 100 µL of 1 M NaOH, and 500 µL of a potassium iodide solution, then adjusted to 25 mL with distilled water. The mixture was incubated for 20 min at room temperature, and absorbance was measured at 620 nm using a spectrophotometer (Shimadzu). Amylose content was calculated from a standard curve for pure amylose and amylopectin (Merck) mixtures with ratios ranging from 100:0 to 0:100 (*w/w*) and expressed as g *per* 100 g flour on a dry weight basis. The total starch content was obtained from 25 mg of the purified starch residue. Amylopectin content was calculated by subtracting the amylose content from the total starch content.

β-Carotene content

β-Carotene content was determined using high-performance liquid chromatography (HPLC) on an Agilent 1200 series system (Agilent Technologies, Santa Clara, CA, USA). Chromatographic separation was performed on a reversed-phase C18 column following the method of Rathi *et al*. [2022]. The mobile phase consisted of methanol and ultrapure water, used under gradient elution from 95:5 (*v/v*) to 100:0 (*v/v*) in 15 min, 100:0 (*v/v*) in 27 min and back to 95:5 (*v/v*) in 3 min, giving a total run time of 45 min. The flow rate was maintained at 0.8 mL/min, the column temperature at 30°C, and the injection volume was 20 µL. Detection was carried out at 440 nm. β-Carotene was identified by comparing retention time and absorption spectra with those of authentic standards. Quantification was performed using the external standard calibration method. β-Carotene standard (≥93% purity) was obtained from Sigma-Aldrich (St. Louis, MO, USA). Results were expressed as mg/kg flour sample.

Bread preparation

Wheat bread was prepared using a formulation consisting of 100 g of total flour, 11.11 g of powdered sugar, 1.94 g of yeast, and 16.67 g of milk powder. In composite bread formulations, a portion of wheat flour was substituted with HOSPF in accordance with experimental design. A bread sample with complete wheat flour substitution with NHOSPF was prepared as well. All dry ingredients were mixed for 1 min, followed by the addition of 66.67 g of water, HPMC at the level specified by the experimental design (g/100 g of total flour blend), 0.17 g of salt, and 11.11 g of margarine. The dough was then kneaded until a smooth and elastic consistency was achieved. Subsequently, the dough was proofed at 25°C for 20 min, remixed, divided into two equal portions, placed into baking molds (17×8×7 cm), and allowed to undergo a second proofing at 25°C for 15 min. The dough was then baked at 180°C for 35 min using an electric oven (KAO-K30, Konka, China). After baking, the bread was cooled at ambient temperature for 2–4 h prior to analysis [Bakare *et al*., 2016].

Determination of physical characteristics of breads

Loaf volume and specific volume

Loaf volume was measured based on the rapeseed displacement technique, modified by replacing rapeseed with mung beans [Manyatsi *et al*., 2020]. The method is based on the principle that the volume of the bread corresponds to the volume of granular material displaced. The loaf volume was calculated as the difference between the volume of the measuring container and the volume occupied by the mung beans after bread insertion. Specific volume was calculated by dividing loaf volume by its weight (mL/g) [Guan *et al*., 2023].

Texture profile

Three bread slices, including the central slice and one from each side, were used for texture profile analysis (TPA) using a texture analyzer (TX-700, Lamy Rheology Instruments, Champagne-au-Mont-d'Or, France). Analysis was performed at room temperature under the following conditions: a 50-mm stainless cylinder (TX-PL50SS) as the probe, a 10 kg load, 1 mm/s of speed, 5 mm of distance, 1 N of sample detection, 1 mm/s speed for return, and 5 mm position for return. The testing method followed that of Wang *et al*. [2006], with parameters analyzed including cohesiveness, chewiness (N), resilience, and hardness (N). Texture parameters were determined from the force–time curves generated during analysis. Hardness was defined as the maximum force during the first compression cycle. Cohesiveness was calculated as the ratio of the area under the second compression curve to that under the first compression curve. Chewiness was calculated as the product of hardness, cohesiveness, and springiness, while resilience was determined as the ratio of the recovery area to the compression area during the first cycle.

Dough rheology

Three composite bread samples were selected based on their physical property scores (as presented in **Table S1** in Supplementary Materials), representing the best-performing formulations, for further dough rheology analysis. Dough machinability was assessed by TPA determination in a TX-700 texture analyzer (Lamy Rheology Instruments) by using a 5-cm diameter probe, 75 s waiting period, and 60 g/100 g compression as described previously by Angioloni *et al*. [2008]. The measured

Figure 1. Color of (**A**) wheat flour, (**B**) non-hydrolyzed orange sweet potato flour (NHOSPF), and (**C**) hydrolyzed orange sweet potato flour (HOSPF).

parameters included cohesiveness, chewiness (N), resilience, and hardness (N).

Statistical analysis

All experiments were conducted in triplicate. Results are expressed as mean and standard deviation (SD). Two-way analysis of variance (ANOVA) was used for physical characteristics of breads; one-way ANOVA for flour characteristics and dough rheology, followed by Tukey's multiple comparison test to determine significant differences among means at a significance level of $p<0.05$. Statistical analysis was carried out using XLSTAT 2025 Statistical Software (Lumivero, Denver, CO, USA).

RESULTS AND DISCUSSION

Use of the crude amylase preparation

Due to the lack of a purification step, crude bacterial enzymes are economically cheaper to produce than purified commercial enzymes and can be cost-effective in applications [Mahfudz *et al*., 2024]. Therefore, in our study, crude amylase from *B. spizizenii* ATCC 6633 was obtained and used for the hydrolysis of orange sweet potato flour. A fixed enzyme dosage of 50 U/g flour was applied following the method of Safari *et al*. [2013], who reported that this dosage was sufficient to achieve partial hydrolysis of purple sweet potato flour and to improve the swelling volume and firmness of wheat–purple sweet potato composite bread. In addition, previous studies have demonstrated that crude microbial enzyme preparations may contain multiple carbohydrases that are capable of synergistically improving dough rheology and bread quality [Hmad *et al*., 2024]. However, no additional enzymatic activities of the crude amylase preparation obtained in our study were determined. Therefore, the effects observed are discussed primarily in relation to the action of α-amylase.

Physical properties of flours

Color of flours

HOSPF exhibited a significantly darker color than NHOSPF and wheat flour (**Figure 1**). Considering color parameters, HOSPF had the lowest L^* value (68.29), followed by NHOSPF (77.47), while wheat flour showed the highest L^* value (93.28) (**Table 1**). In contrast, HOSPF exhibited the highest redness (a^* – 14.43) and yellowness (b^* – 24.44), followed by NHOSPF

Table 1. Physical and chemical properties of wheat flour, non-hydrolyzed orange sweet potato flour (NHOSPF), and hydrolyzed orange sweet potato flour (HOSPF).

Parameter	Wheat flour	NHOSPF	HOSPF
Color			
L^*	93.28±0.02^a	77.47±0.03^b	68.29±0.12^c
a^*	0.38±0.01^c	13.83±0.02^b	14.43±0.12^a
b^*	10.44±0.01^c	23.20±0.02^b	24.44±0.33^a
Hydration gel properties			
WAI (g/g)	1.85±0.03^c	2.72±0.18^b	3.20±0.04^a
WSI (%)	5.04±0.19^c	21.19±0.38^b	22.66±0.45^a
Moisture (g/100 g)	12.00±0.16^a	6.54±0.23^c	7.32±0.11^b
Pasting properties			
Peak viscosity (mPa×s)	2,493±24^a	513.3±3.1^c	986.0± 4.4^b
Trough viscosity (mPa×s)	1,073±13^a	121.0±3.6^c	966.7±4.5^b
Breakdown viscosity (mPa×s)	1,421±15^a	392.3±0.6^b	19.3±1.5^c
Final viscosity (mPa×s)	2,231±35^a	163.3±6.1^c	1,521±22^b
Setback viscosity (mPa×s)	1,158±23^a	42.3±3.2^c	555±20^b
Peak time (min)	9.47±0.00^b	6.27±0.00^c	11.27±0.12^a
Pasting temperature (°C)	85.02±0.24^b	77.57±0.03^c	87.48±0.40^a
Chemical composition			
Reducing sugars (g/100 g)	0.49±0.1^c	9.81±0.01^b	19.11±0.36^a
Amylose (g/100 g)	23.58±0.04^a	17.65±0.09^b	14.74±0.16^c
Amylopectin (g/100 g)	47.19±0.88^b	48.06±0.77^{ab}	51.02±0.62^a
Total starch (g/100 g)	70.77±0.91^a	65.70±0.86^b	65.76±0.79^b
Amylopectin-to-amylose ratio	2.00	2.72	3.46
β-Carotene (mg/kg)	0.02±0.0^c	1277±18^a	872.5±6.4^b

Values are expressed as mean ± standard deviation. Mean values within the same row followed by different letters are significantly different ($p<0.05$) according to Tukey's multiple comparison test. WAI, water absorption index; WSI, water solubility index; L^*, lightness; a^*, redness–greenness, b^*, yellowness–blueness.

(13.38 and 23.20, respectively), whereas wheat flour exhibited an *a** value close to zero (0.38), indicating almost no red or green hue, as well as the lowest *b** value (10.44). The reddish-yellow hue of HOSPF and NHOSPF may be due to the presence of carotenoids. In turn, the more intense reddish-yellow color of HOSPF was probably associated with the combined effects of enzymatic hydrolysis and subsequent heat treatment (enzyme inactivation at 80°C for 150 min and flour drying at 60°C for 16 h). Enzymatic hydrolysis increased the reducing sugar content, while orange sweet potato flour naturally contains proteins [Olugbuyi *et al*., 2024], which provide amino groups that participate in the Maillard reaction [Rebholz *et al*., 2021]. Therefore, interactions between reducing sugars and amino groups may have promoted non-enzymatic browning during these subsequent heat-treatment steps, resulting in the formation of brown-colored compounds and a darker flour color. Similar observations were reported by Pongpaiboon *et al*. [2016], who suggested that the darker color of α-amylase-treated rice flour might be related to Maillard reactions between reducing sugars and amino groups during processing. Moreover, previous studies have demonstrated that moderate heat treatment (60–70°C) can promote Maillard reactions in food matrices containing reducing sugars and amino groups, contributing to browning during drying [Chaipoot *et al*., 2026].

Gel hydration properties and moisture content

HOSPF exhibited the highest WAI and WSI (3.20 g/g and 22.66%, respectively) (**Table 1**). The hydrolysis process enhanced the ability of starch to bind water. Enzymatic hydrolysis altered the surface characteristics of starch granules and promoted a granule disruption. The enzymes preferentially hydrolyzed the amorphous fractions rather than the crystalline domains. Since water first enters the amorphous region before penetrating crystalline domains, these structural changes may facilitate water penetration into starch granules [Almeida *et al*., 2019]. Consequently, partially hydrolyzed starch in HOSPF demonstrated a higher water solubility level than both NHOSPF and wheat flour.

Moisture contents of all samples remained below the maximum limit for wheat flour (14.5 g/100 g) [Codex Alimentarius Commission, 2019], although significant ($p<0.05$) differences were observed between flours (**Table 1**). The lowest value was found for NHOSPF. The hydrolysis resulted in a significant increase in moisture content. However, wheat flour exhibited the highest moisture content, which may be attributed to differences in the processing conditions of the commercial wheat flour and commercial orange sweet potato flour used in this study, as well as the additional enzymatic hydrolysis applied to produce HOSPF.

Pasting properties

The viscosity of the starch slurry generally decreases after enzymatic hydrolysis due to starch depolymerization and reduction in its molecular weight [Sigüenza-Andrés *et al*., 2022]. After drying, the hydrolyzed flour exhibits increased pasting viscosity. However, in our study, HOSPF exhibited a higher peak viscosity (986.0 mPa×s) compared to NHOSPF (513.3 mPa×s). This behavior can be attributed to several mechanisms. Firstly, hydrolysis products, such as oligosaccharides and branched limit dextrins, can interact with leached amylose and long outer chains of amylopectin from starch granules during gelatinization, forming a molecular association that contributes to a more developed viscous system. Secondly, due to their relatively low molecular weight and high mobility, these hydrolysis products can readily diffuse into the starch network and interact with starch molecules during pasting. Thirdly, the hydroxyl (–OH) groups present in these hydrolysis products can interact with water molecules, reducing the amount of available water and restricting starch chain mobility, thereby contributing to increased viscosity [Wang *et al*., 2018]. Collectively, these mechanisms explain the higher viscosity of HOSPF compared to NHOSPF, which was however lower than that of wheat flour (2,493 mPa×s). In addition, HOSPF showed a significantly ($p<0.05$) higher trough viscosity (966.7 mPa×s) and a lower breakdown viscosity (19.3 mPa×s) compared to NHOSPF (121.0 and 392.3 mPa×s, respectively), indicating improved resistance to thermal and mechanical disintegration. This study, in line with previous findings by Shariffa *et al*. [2017], showed that the hydrolysis of sweet potato starch increased peak viscosity while decreased breakdown viscosity. Notably, the breakdown viscosity of HOSPF was even lower than that of wheat flour, suggesting superior viscosity stability of HOSPF under the tested conditions.

Interestingly, the final viscosity of HOSPF (1,521 mPa×s) was intermediate between wheat flour (2,231 mPa×s) and NHOSPF (163.3 mPa×s) (**Table 1**), indicating a more balanced structural re-association during cooling. This suggests a lower retrogradation tendency than in wheat flour, which may contribute to reduced staling in composite bread, while still providing a firmer structure than NHOSPF. However, HOSPF exhibited a longer peak time (11.27 min) compared to NHOSPF (6.27 min), and wheat flour (9.47 min), as well as a higher pasting temperature (87.48°C) than NHOSPF (77.57°C), and wheat flour (85.02°C). These values indicate that the modified starch system requires higher thermal energy for gelatinization, likely due to strengthened molecular interactions and reduced water mobility. In contrast to physical treatments, such as high hydrostatic pressure (HHP), which induce pre-gelatinization and structural disruption leading to reduced pasting viscosity [Gu *et al*., 2026], enzymatic hydrolysis in the present study resulted in an increase in peak viscosity. This finding suggests that enzymatic treatment does not excessively damage starch granules but instead promotes molecular interactions that enhance viscosity development. Overall, enzymatic hydrolysis improved the pasting properties of non-wheat flour, as reflected in HOSPF, highlighting its potential as a functional ingredient and partial substitute for wheat flour in composite bread formulation.

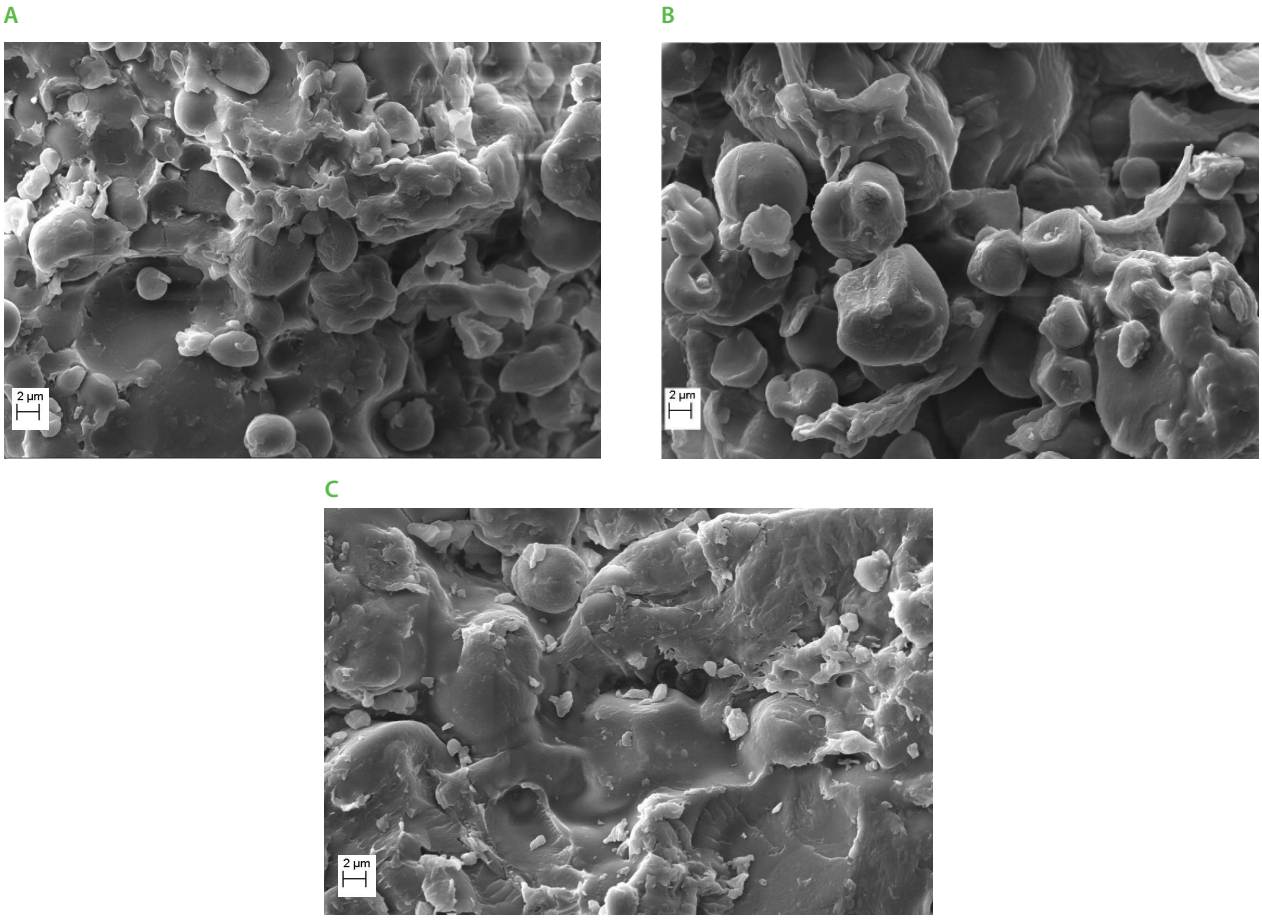

Figure 2. Scanning electron microscope (SEM) micrographs (×2,000) of (**A**) wheat flour, (**B**) non-hydrolyzed orange sweet potato flour (NHOSPF), and (**C**) hydrolyzed orange sweet potato flour (HOSPF).

Flour microstructure

Figure 2 shows that starch granules in wheat flour and NHOSPF appeared intact and compact, exhibiting minimal surface damage or fragmentation. The granules showed relatively smooth surfaces and fairly uniform, round-to-oval morphology. Starch granules generally exhibit round or oval shapes with smooth structural features. Such structural characteristics contribute to elastic dough properties and facilitate the formation of a strong gluten network. Starch granules occupy and fill the gluten matrix, thereby reducing gluten density and enhancing dough flexibility and gas expansion during fermentation [Gao *et al*., 2020]. The starch granules of NHOSPF were significantly larger than those of wheat flour (**Figure 2**), suggesting potentially inferior dough-forming performance in terms of elasticity, and consequently, potentially reduced dough stability and a lower loaf volume.

In contrast, starch granules of HOSPF were no longer clearly distinguishable (**Figure 2**), indicating extensive granule disruption induced by amylolytic hydrolysis. The granules exhibited irregular surfaces, porous structures, agglomeration, surface erosion, and reduction in granule size, similar to those reported in a previous study for cassava starch hydrolyzed with α-amylase and glucoamylase [Cornejo *et al*., 2022]. This structural degradation is due to enhanced starch solubility and water absorption capacity.

Chemical composition of flours

Reducing sugar content

The content of reducing sugars in HOSPF was significantly ($p<0.05$) higher compared to NHOSPF and wheat flour. This difference was expected, as the hydrolysis of starch by amylase produces reducing sugars including glucose, maltose, maltotriose, and other maltooligosaccharides [Rebholz *et al*., 2021].

Content of total starch, amylose, and amylopectin

During dough kneading, flour starch swells due to the penetration of water into amorphous regions of the granules, which may be followed by limited amylose leaching into the extra-granular space [van Rooyen *et al*., 2023]. Subsequently, starch granules undergo gelatinization during baking, allowing extensive granule swelling, which is strongly influenced by the amylopectin-to-amylose ratio. Starches with a higher amylopectin-to-amylose ratio generally exhibit greater swelling power because the highly branched structure of amylopectin is primarily responsible for granule swelling, particularly with the sufficient water content during gelatinization. In contrast, a higher amylose content has been associated with reduced granule swelling and swelling power [Chiodetti *et al*., 2024].

In the present study, the total starch content of wheat flour (70.77 g/100 g) was higher than that of NHOSPF (65.70 g/100 g) and HOSPF (65.76 g/100 g) (**Table 1**). However, the amylopectin-

-to-amylose ratio of wheat flour (2.00) was lower than those of NHOSPF (2.72) and HOSPF (3.46), indicating that the swelling power of wheat flour starch may be lower than that of orange sweet potato flours. Previous studies have reported that wheat flour does not usually exhibit the highest swelling power compared to non-wheat flours, *e.g.*, potato flour, which has larger granules, showed a higher swelling power than wheat flour at 70–90°C [Fan *et al*., 2024]. In addition to its effect on starch swelling power, the lower amylose content has been associated with the formation of softer starch gels [Teng *et al*., 2013]. As shown in **Table 1**, the amylose content of HOSPF (14.74 g/100 g) was significantly ($p<0.05$) lower than that of NHOSPF (17.65 g/100 g). Consequently, the lower amylose content of HOSPF could contribute to enhanced crumb softness compared with NHOSPF.

The starch, amylose, and amylopectin contents determined in this study differed from those previously reported in the literature. For example, de Souza *et al*. [2020] reported starch, amylose, and amylopectin contents within the ranges of 51.6–59.1, 9.7–15.1, and 84.9–90.3 g/100 g, respectively, for four Brazilian sweet potato genotypes. These differences were expected because starch composition is largely influenced by genotypes. This finding has been further supported by Wang *et al*. [2020], who demonstrated that different sweet potato genotypes exhibited various starch, amylose, and amylopectin contents even when grown under the same environmental conditions, indicating that genotype is a major determinant of starch composition. Similarly, the orange sweet potato used in the present study belonged to a different genotype compared to those used in previous studies, which may explain the differences in its starch composition.

β-Carotene content

A substantial variation was demonstrated in β-carotene content among wheat flour, NHOSPF, and HOSPF (**Table 1**). Wheat flour exhibited a negligible β-carotene content (0.02 mg/kg), confirming that conventional wheat-based products contribute minimally to provitamin A intake. In contrast, NHOSPF showed the highest β-carotene content (1,277 mg/kg), highlighting its potential as a functional ingredient rich in bioactive compounds. This value was substantially higher than those reported by Oloniyo *et al*. [2021] (36.3–188.3 mg/kg). The higher β-carotene content determined in the present study may be attributed to differences in sweet potato cultivars, as carotenoid content varies considerably among varieties. This explanation is supported by Islam *et al*. [2016], who reported significant variation in carotenoid content among orange-fleshed sweet potato cultivars. The HOSPF exhibited a significantly lower β-carotene content (872.5 mg/kg) compared to its non-hydrolyzed counterpart, indicating that the hydrolysis process may lead to partial degradation or loss of β-carotene. The reduction in β-carotene following hydrolysis can be attributed to oxidative degradation and *trans–cis* isomerization reactions induced by exposure to oxygen and enzymatic activity during processing [Mordi *et al*., 2020]. This may reduce the intensity of the yellow color in orange sweet potato flour. Nevertheless, HOSPF still retained a considerably higher β-carotene level than wheat flour, suggesting that it remains a valuable source of provitamin A.

Physical properties of breads

Bread appearance

The appearance of breads produced from wheat flour (positive control) and its blends with HOSPF, without or with HPMC addition, as well as from NHOSPF (negative control) is shown in **Figure 3**. Breads of various formulations revealed differences in the volume, texture, and color, the extent of which was found to depend on the wheat flour substitution with HOSPF (A0––A4) and the addition of HPMC (H0–H2). In the A0 treatment (0 g HOSPF/100 g flour blend) with different HPMC contents, the resulting breads exhibited the lightest color, like the positive control, with satisfactory volume, particularly in A0H1 and A0H2. This indicates that the addition of HPMC was able to maintain bread structure and expansion even in the absence of sweet potato flour. As the levels of wheat flour substitution with HOSPF increased (A1–A4), the bread color became progressively darker, shifting toward the characteristic orange-brown hue of sweet potato. Bread in treatment A1 (15 g/100 g flour blend) still exhibited good expansion with a golden-yellow color, whereas at higher incorporation levels, such as A3 (45 g/100 g flour blend) and A4 (60 g/100 g flour blend), the bread color turned darker brown, and loaf volume tended to decrease. This observation is consistent with the higher reducing sugar content of HOSPF (**Table 1**). During bread production, α-amylase hydrolyzes starch, releasing glucose, maltose, and other reducing sugars which serve as substrates for the Maillard reaction [Rebholz *et al*., 2021]. These reducing sugars readily react with amino groups from proteins in wheat and orange sweet potato flours *via* the Maillard reaction, producing brown melanoidin pigments responsible for crust darkening [Helou *et al*., 2016]. Accordingly, increasing HOSPF substitution intensified the Maillard reaction, resulting in a darker and more reddish appearance.

Loaf volume and specific volume of breads

The highest loaf volume and specific volume were determined for the bread produced from A0H2 formulation (0 g HOSPF/100 g flour blend and addition of 3 g HPMC/100 g flour blend), reaching 1,218.7 mL and 3.30 mL/g, respectively (**Figure 4**). In contrast, negative control (NHOSPF without HPMC) showed the lowest loaf volume and specific volume, at 318.0 mL and 0.90 mL/g, respectively. These results indicate that the addition of HPMC to wheat flour had the pronounced effect on improving the expansion of breads by stabilizing gas bubbles and partially replacing gluten functionality, thereby enhancing dough structure during fermentation and baking [Torres-Pérez *et al*., 2024]. However, the effect of HPMC on bread expansion depended on the presence of HOSPF (**Figure 4**). In the breads containing HOSPF, HPMC generally reduced loaf volume and specific volume. This result was further confirmed by two-way ANOVA analysis,

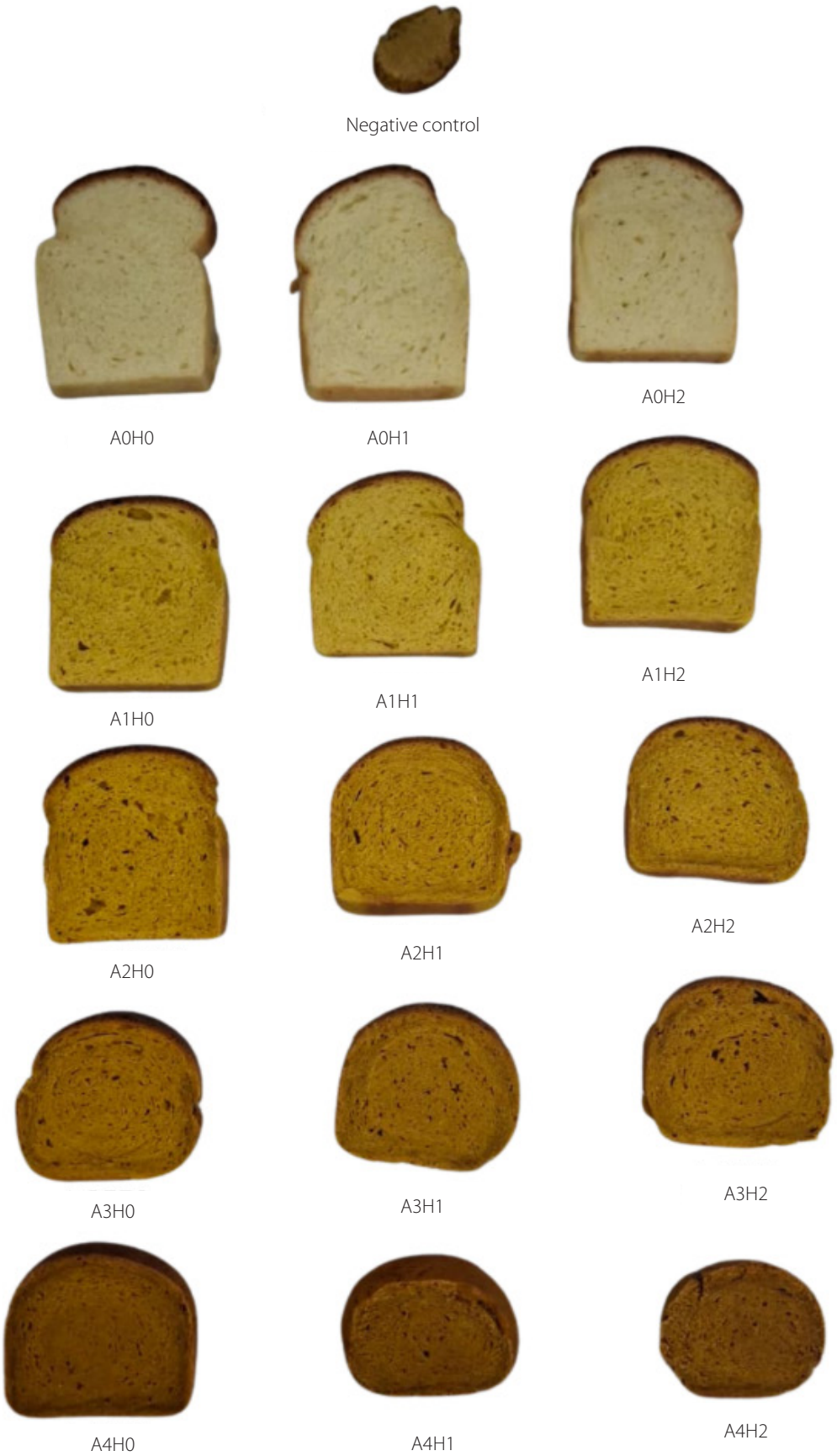

Figure 3. Cross-sectional appearance of breads produced from wheat flour and its blends with hydrolyzed orange sweet potato flour (HOSPF) with or without hydroxypropyl methylcellulose (HPMC) addition. Treatments were coded as A*H*, where A indicates HOSPF substitution level (A0=0, A1=15, A2=30, A3=45, A4=60 g/100 g flour blend) and H indicates HPMC addition level to flour blend (H0=0, H1=1.5, H2=3 g/100 g). Bread made from non-hydrolyzed orange sweet potato flour without HPMC was negative control.

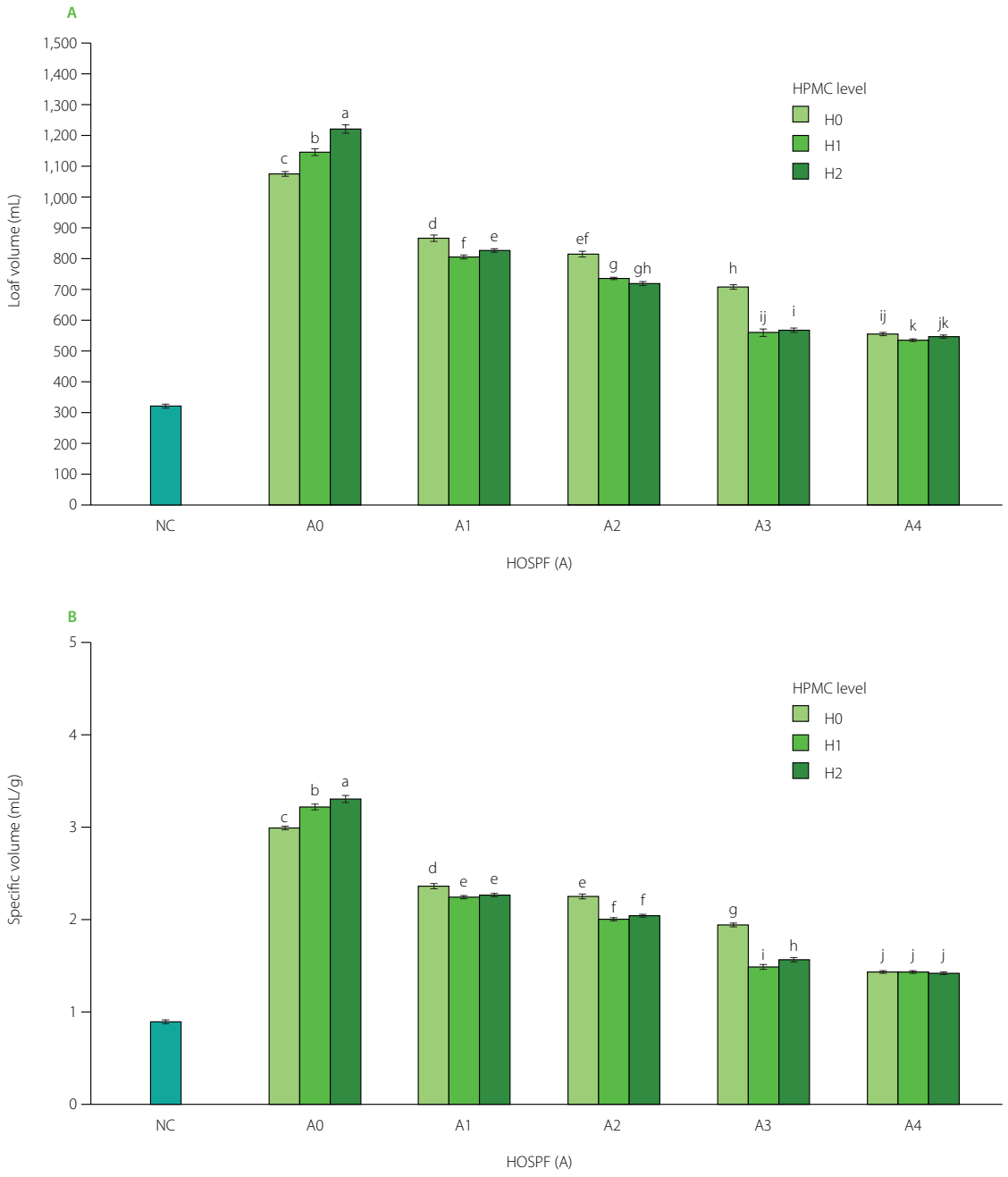

Figure 4. (**A**) Loaf volume, and (**B**) specific volume of breads produced from wheat flour and its blends with hydrolyzed orange sweet potato flour (HOSPF) with or without hydroxypropyl methylcellulose (HPMC) addition. Different letters above bars indicate significant differences between breads (p<0.05). Treatments were coded as A*H*, where A indicates HOSPF substitution level (A0=0, A1=15, A2=30, A3=45, A4=60 g/100 g flour blend) and H indicates HPMC addition level to flour blend (H0=0, H1=1.5, H2=3 g/100 g). NC, negative control (bread from non-hydrolyzed orange sweet potato flour without HPMC).

which showed that the interaction between main factors (HOSPF and HPMC) significantly influenced the volume and specific volume of composite breads (p<0.05) (**Table S2** in Supplementary Materials). The higher volume observed in the breads containing HOSPF compared to that produced from NHOSPF can be attributed to the amylolytic hydrolysis, which generates reducing sugars that accelerate yeast fermentation and increase CO_2 production, ultimately enhancing loaf expansion at certain incorporation levels [Struyf *et al.*, 2017]. However, with increasing HOSPF incorporation levels, loaf volume tended to decrease, likely due to excessive gluten dilution and weakening of the dough matrix, which impaired gas retention capacity. This effect sustained despite the addition of HPMC, as both HPMC and HOSPF strongly compete for water, thereby limiting gluten hydration and restricting dough expansion.

Texture profile parameters of breads

TPA results showed significant differences among samples in all parameters examined (**Figure 5**). Bread with higher HOSPF incorporation exhibited high hardness and chewiness, particularly at a substitution level of 45 g/100 g flour blend (A3). This effect is attributed to gluten dilution, as sweet potato flour lacks

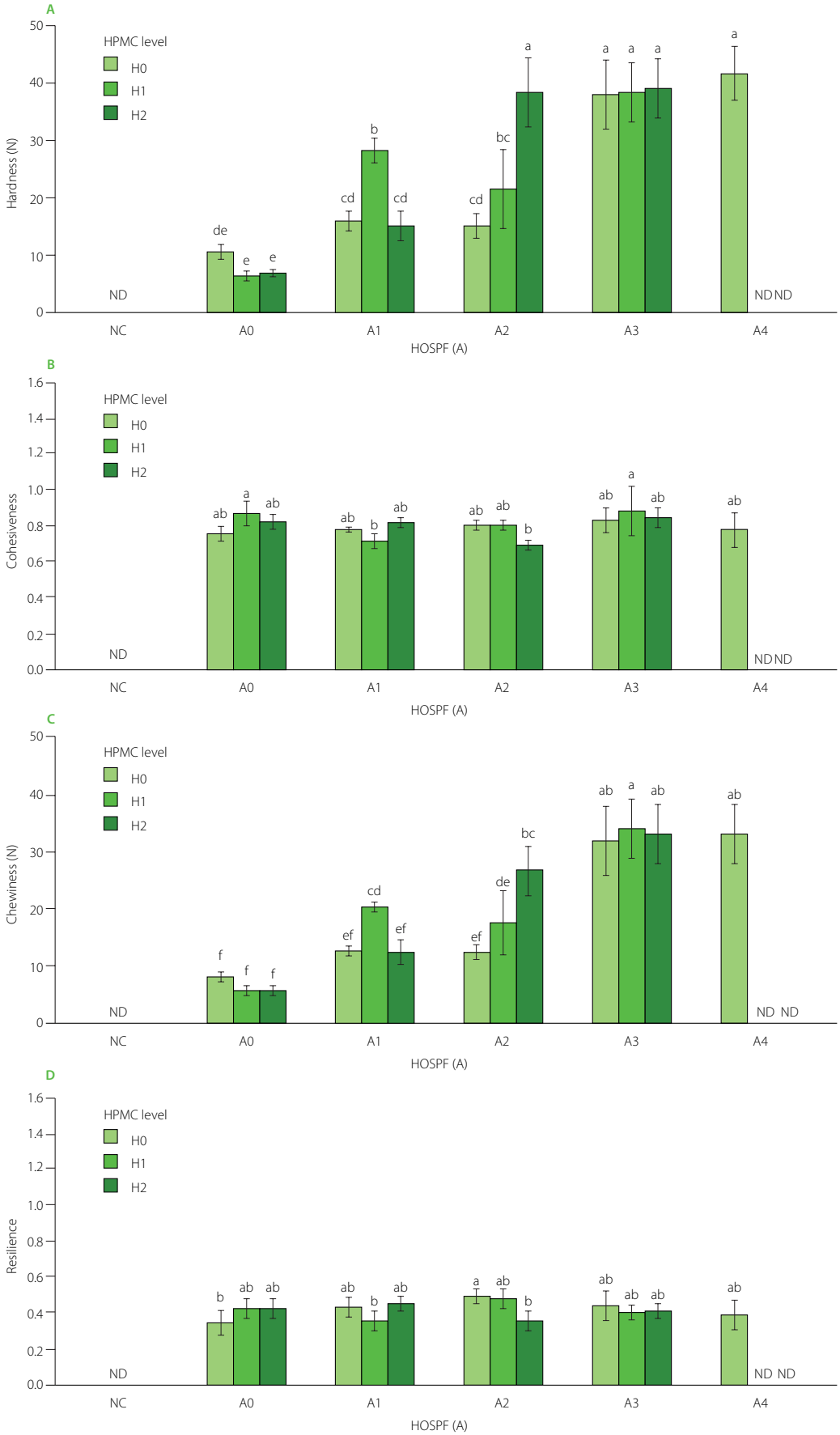

Figure 5. (**A**) Hardness, (**B**) cohesiveness, (**C**) chewiness, and (**D**) resilience of breads produced from wheat flour and its blends with hydrolyzed orange sweet potato flour (HOSPF) with or without hydroxypropyl methylcellulose (HPMC) addition. Different letters above bars indicate significant differences between breads ($p<0.05$). Treatments were coded as A*H*, where A indicates HOSPF substitution level (A0=0, A1=15, A2=30, A3=45, A4=60 g/100 g flour blend) and H indicates HPMC addition level to flour blend (H0=0, H1=1.5, H2=3 g/100 g); Negative control (NC), A4H1, and A4H2 could not be measured due to excessive hardness; ND, not detected.

Table 2. Rheological properties of wheat flour dough and doughs from blend of wheat flour and hydrolyzed orange sweet potato flour (HOSPF) with or without the addition of hydroxypropyl methylcellulose (HPMC).

Parameter	A0H0	A1H0	A1H2	A2H0
Cohesiveness	1.36±0.04^{a}	1.03±0.17^{b}	0.96±0.04^{bc}	0.85±0.04^{c}
Chewiness (N)	2.07±0.07^{bc}	1.94±0.12^{c}	2.35±0.14^{ab}	2.71±0.22^{a}
Resilience	0.73±0.02^{a}	0.64±0.04^{b}	0.50±0.04^{c}	0.51±0.03^{c}
Hardness (N)	1.66±0.03^{c}	2.09±0.05^{c}	2.67±0.07^{b}	3.47±0.32^{a}

Values are expressed as mean ± standard deviation. Mean values within the same row followed by different letters are significantly different (p<0.05) according to Tukey's multiple comparison test. Treatments were coded as A*H*, where A indicates HOSPF substitution level (A0=0, A1=15, A2=30 g/100 g flour blend) and H indicates HPMC addition level to flour blend (H0=0, H2=3 g/100 g flour blend).

gluten-forming proteins, thereby weakening the three-dimensional dough network responsible for gas retention. Reduced gas retention lowers specific volume and crumb porosity, resulting in a denser structure that requires greater force to deform [Gan *et al*., 1995]. Although HOSPF exhibited a lower amylose content (**Table 1**), characteristics generally associated with a softer crumb, these potential benefits were insufficient to counteract the adverse effect of gluten dilution at the higher substitution levels. These findings agree with observations made by Chikpah *et al*. [2023], who reported that higher incorporation levels of non-wheat flour (orange-fleshed sweet potato and pumpkin flour) increased hardness and chewiness in composite bread.

Generally, higher cohesiveness reflects a crumb structure that remains intact during mastication, whereas lower cohesiveness results in increased crumbling [Encina-Zelada *et al*., 2018]. In our study, cohesiveness ranged from 0.689 (A2H2) to 0.882 (A3H1), with positive control (A0H0) at 0.749 and did not exhibit a consistent trend with increasing HOSPF levels (**Figure 5**). In the absence of HPMC (H0), replacing wheat flour with HOSPF resulted in cohesiveness values comparable to those of the positive control. Similarly, HPMC supplementation resulted in fluctuating cohesiveness across HOSPF substitution levels, indicating that no consistent effect of HPMC on crumb cohesiveness could be established.

The two-way ANOVA revealed a significant interaction between HOSPF and HPMC for all TPA parameters (p<0.05) (**Table S2**). This interaction explains the inconsistent role of HPMC across treatments, as its functionality varied depending on the composite flour matrix. In wheat bread, HPMC reduced hardness by improving gas retention, and increasing specific volume as mentioned previously, resulting in a lighter crumb [Belorio & Gómez, 2020]. However, HPMC tended to increase hardness in the composite breads containing HOSPF. This shift in functionality reflects the interaction between both factors, where the presence of HOSPF alters the ability of HPMC to improve structure. This occurs due to water competition between HOSPF, HPMC, and gluten. Given the identical water levels were used in all formulations, the higher water-binding capacity of HOSPF and HPMC likely resulted in limited gluten hydration and matrix expansion, reducing gas retention, and producing a denser crumb [Culetu *et al*., 2021]. A comparable effect has been reported by Encina-Zelada *et al*. [2018], who observed that increasing xanthan gum content at a constant water level increased crumb hardness, whereas increasing the water content reduced hardness and improved specific volume. Although a different hydrocolloid was used, these findings underscore the importance of maintaining an appropriate hydrocolloid-to-water ratio for desirable bread texture.

Regarding the main effects, neither HOSPF nor HPMC showed a significant influence on resilience (p≥0.05) (**Table S2**), suggesting that the elastic recovery of the crumb was not substantially affected by these factors and mainly determined by the gluten network. In addition, the main effect of HPMC was not significant (p≥0.05) for cohesiveness, indicating that HPMC had a limited role in modifying the internal structural integrity of the crumb, which is more strongly influenced by starch composition and crumb density.

Negative control, A4H1, and A4H2 could not be analyzed due to excessive hardness, which prevented the instrument from detecting the texture parameters. This result implies that adding hydrocolloids along with high incorporation levels of HOSPF may result in an overly stiff and technologically unsuitable crumb structure. Excessive hydrocolloid-starch interactions have been reported to cause severe stiffness in composite and gluten-free bread systems [Culetu *et al*., 2021]. Overall, these results indicate that the level of HOSPF in bread formula plays a more dominant role in determining bread quality than the hydrolysis process itself, while hydrolysis mainly acts as a supporting factor by improving flour functionality.

Dough rheological properties

Dough rheology analysis was performed on selected samples based on their similarity in physical characteristic scores to A0H0 (positive control). The selection was based on a scoring approach derived from multiple physical parameters, and the complete scoring data are provided in **Table S1**. The top three samples were A1H0, A1H2, and A2H0, which, together with the positive control, were further analyzed for dough rheology.

The rheological properties of the composite dough were significantly influenced by the proportion of HOSPF in the flour blend and the addition of HPMC (**Table 2**). The positive control dough (A0H0) exhibited the highest cohesiveness and resilience, reflecting a strong and elastic gluten network typical of wheat-based dough. As the level of HOSPF increased, cohesiveness and resilience progressively decreased, indicating weakening of the dough structure due to partial dilution of gluten and modification of starch-protein interactions [Culetu *et al*., 2021]. The formulation containing 30 g HOSPF/100 g flour blend (A2H0) showed the highest hardness values, suggesting a denser and more rigid dough matrix. This result may be attributed to the altered starch structure resulting from hydrolysis, which can increase water absorption and limit dough extensibility, thereby producing a stiffer dough.

The addition of HPMC at 3 g/100 g flour blend (A1H2) partially mitigated the negative effects of flour substitution on dough structure. HPMC likely contributed to these effects by forming a hydrocolloid gel that interacts with starch and proteins, improving water retention, and reinforcing the dough matrix in the absence of sufficient gluten. Overall, increasing levels of HOSPF reduced dough elasticity and cohesiveness while increasing firmness. However, the incorporation of HPMC helped improve dough functionality by enhancing structural integrity and viscoelastic behavior [Torres-Pérez *et al*., 2024]. These results highlight the importance of hydrocolloid addition when formulating composite doughs with HOSPF to achieve rheological properties suitable for bread making.

CONCLUSIONS

This study demonstrates that the combination entailing substitution of wheat flour with orange sweet potato flour hydrolyzed using amylase from *B. spizizenii* ATCC 6633 and addition of hydroxypropyl methylcellulose influenced the physical characteristics of composite bread. Amylolytic hydrolysis enhanced the orange sweet potato flour functionality, such as gel hydration properties and pasting properties. The level of substitution was found to be a dominant factor affecting bread quality. Increasing hydrolyzed orange sweet potato flour levels beyond 30 g/100 g flour blend led to a reduced loaf volume and increased crumb firmness due to excessive gluten dilution and intensified competition for water, which limited dough expansion. The most favorable balance for physical properties was achieved in formulations A1H0 (15 g HOSPF/100 g flour blend), A1H2 (15 g HOSPF/100 g flour blend + 3 g HPMC/100 g flour blend), and A2H0 (30 g HOSPF/100 g flour blend), indicating its suitability for composite bread formulation. Although amylolytic hydrolysis improved flour functionality, it could not fully compensate for structural weakening at higher substitution levels. This study highlights the potential of HOSPF as a functional ingredient for partial wheat flour substitution. However, the absence of proximate nutritional analysis and sensory evaluation in this study is acknowledged as a limitation. Future studies are, thus, recommended to include these aspects to provide a more comprehensive evaluation of product quality.

ACKNOWLEDGEMENTS

The authors gratefully acknowledge the Directorate General of Higher Education, Ministry of Higher Education, Science, and Technology of the Republic of Indonesia for research funding; and Directorate of Research, Publication, and Community Development, Prasetiya Mulya University, for administrative facilitation and research support. The authors also thank the Collaborative STEM Laboratories, Prasetiya Mulya University, for providing research facilities, equipment, and materials essential to this study. Special appreciation is extended to Ms. Wulan Chairunisa for her technical assistance in microstructural analysis.

RESEARCH FUNDING

This study was supported by the Directorate of Research, Technology, and Community Service (DPPM), Directorate General of Higher Education, Ministry of Higher Education, Science, and Technology of the Republic of Indonesia, under the Fundamental Research scheme (Project No. 2/2/04.02/0491/06/2025, 2025), led by the corresponding author.

CONFLICT OF INTERESTS

Authors declare no conflict of interests.

GENERATIVE AI USE DECLARATION

The authors used generative artificial intelligence (AI) tools solely for language editing to improve the clarity and academic tone of the manuscript. All scientific content, data interpretation, and conclusions were developed by the authors. The authors take full responsibility for the accuracy and integrity of the manuscript.

SUPPLEMENTARY MATERIALS

The following are available online at **https://journal.pan.olsztyn.pl/Improving-the-Quality-of-Composite-Bread-Using-Amylolytic-Hydrolyzed-Orange-Sweet,225559,0,2.html**; **Table S1**. Result score of composite bread characteristics. **Table S2**. Bread physical characteristics.

ORCID IDs

K.W. Arinata **https://orcid.org/0009-0004-4055-9471**
R.T.K. Dewi **https://orcid.org/0000-0002-5505-8934**
D.P. Elfriede **https://orcid.org/0000-0003-1220-3780**
Fransisca **https://orcid.org/0000-0003-4902-9026**
A.I. Samosir **https://orcid.org/0009-0004-6247-8146**

REFERENCES

1. Abd-Elaziz, A.M., Karam, E.A., Ghanem, M.M., Moharam, M.E., Kansoh, A.L. (2020). Production of a novel α-amylase by *Bacillus atrophaeus* NRC1 isolated from honey: Purification and characterization. *International Journal of Biological Macromolecules*, *148*, 292–301. **https://doi.org/10.1016/J.IJBIOMAC.2020.01.120**
2. Almeida, R.L.J., dos Santos Pereira, T., de Andrade Freire, V., Santiago, Â.M., Oliveira, H.M.L., de Sousa Conrado, L., de Gusmão, R.P. (2019). Influence of enzymatic hydrolysis on the properties of red rice starch. *International Journal of Biological Macromolecules*, *141*, 1210–1219. **https://doi.org/10.1016/j.ijbiomac.2019.09.072**
3. Angioloni, A., Balestra, F., Pinnavaia, G.G., Rosa, M.D. (2008). Small and large deformation tests for the evaluation of frozen dough viscoelastic behaviour. *Journal of Food Engineering*, *87*(4), 527–531. **https://doi.org/10.1016/J.JFOODENG.2008.01.007**

4. AOAC (2006). *Official Methods of Analysis* (18th ed.). The Association of Official Analytical Chemists International, Gaithersburg, MD, USA.
5. Bakare, A.H., Osundahunsi, O.F., Olusanya, J.O. (2016). Rheological, baking, and sensory properties of composite bread dough with breadfruit (*Artocarpus communis* Forst) and wheat flours. *Food Science and Nutrition*, *4*(4), 573–587. **https://doi.org/10.1002/fsn3.321**
6. Belorio, M., Gómez, M. (2020). Effect of hydration on gluten-free breads made with hydroxypropyl methylcellulose in comparison with psyllium and xanthan gum. *Foods*, *9*(11), art. no. 1548. **https://doi.org/10.3390/foods9111548**
7. Chaipoot, S., Kulprachakarn, K., Wiriyacharee, P., Somjai, C., Chaimueng, K., Jaijoi, S., Khampakool, A., Wongwatcharayothin, W., Srinuanpan, S., Pathomrungsiyounggul, P., Phongphisutthinant, R. (2026). Temperature-driven Maillard conjugation and phenolic changes in dried lychee pulp: Implications for antioxidative enhancement. *Foods, 15*(3), art. no. 468. **https://doi.org/10.3390/foods15030468**
8. Chen, Y., Eder, S., Schubert, S., Gorgerat, S., Boschet, E., Baltensperger, L., Städeli, C., Kuster, S., Fischer, P., Windhab, E.J. (2021). Influence of amylase addition on bread quality and bread staling. *ACS Food Science Technology*, *1*(6), 1143–1150. **https://doi.org/10.3929/ethz-b-000502118**
9. Chikpah, S.K., Korese, J.K., Hensel, O., Sturm, B., Pawelzik, E. (2023). Influence of blend proportion and baking conditions on the quality attributes of wheat, orange-fleshed sweet potato and pumpkin composite flour dough and bread: optimization of processing factors. *Discover Food*, *3*(2), art. no. 2. **https://doi.org/10.1007/s44187-023-00041-z**
10. Chiodetti, M., Tuccio, M.G., Carini, E. (2024). Effect of water content on gelatinization functionality of flour from sprouted sorghum. *Current Research in Food Science*, *8*, art. no. 100780. **https://doi.org/10.1016/j.crfs.2024.100780**
11. Codex Alimentarius Commission (2019). *Standard for Wheat and Durum Wheat (CXS 199-1995)*. FAO/WHO.
12. Cornejo, F., Maldonado-Alvarado, P., Palacios-Ponce, S., Hugo, D., Rosell, C.M. (2022). Impact of cassava starch varieties on the physiochemical change during enzymatic hydrolysis. *Molecules*, *27*(18), art. no. 6098. **https://doi.org/10.3390/molecules27186098**
13. Culetu, A., Duta, D.E., Papageorgiou, M., Varzakas, T. (2021). The role of hydrocolloids in gluten-free bread and pasta; rheology, characteristics, staling and glycemic index. *Foods, 10*(12), art. no. 3121. **https://doi.org/10.3390/foods10123121**
14. de Souza, A.G., Viana, D.J.S., dos Santos, A.S., Andrade Júnior, V.C. de, Rosa, D. dos S. (2020). Structure and properties of starch and flour of four Brazilian sweet potatoes (*Ipomoea batatas*) cultivars. *Revista Materia*, *25*(3), 1–10. **https://doi.org/10.1590/s1517-707620200003.1128**
15. Encina-Zelada, C.R., Cadavez, V., Monteiro, F., Teixeira, J.A., Gonzales-Barron, U. (2018). Combined effect of xanthan gum and water content on physicochemical and textural properties of gluten-free batter and bread. *Food Research International*, *111*, 544–555. **https://doi.org/10.1016/J.FOODRES.2018.05.070**
16. Espinosa-Ramírez, J., Mariscal-Moreno, R.M., Chuck-Hernández, C., Serna-Saldivar, S.O., Espiricueta-Candelaria, R.S. (2022). Effects of the substitution of wheat flour with raw or germinated ayocote bean (*Phaseolus coccineus*) flour on the nutritional properties and quality of bread. *Journal of Food Science*, *87*(9), 3766–3780. **https://doi.org/10.1111/1750-3841.16263**
17. Fan, C., Cheng, L., Hong, Y., Li, Z., Li, C., Ban, X., Gu, Z. (2024). Study on the gelatinization and digestive characteristics of wheat starch and potato starch under low moisture conditions. *International Journal of Biological Macromolecules*, *269*(Pt2), art. no. 132192. **https://doi.org/10.1016/j.ijbiomac.2024.132192**
18. Freire, B., Prinyawiwatkul, W., Negrete, A.M., Golub, E., King, J.M. (2025). Development of gluten-free bread with high-protein rice flour and effects of alpha-amylase enzyme on bread properties. *Journal of Food Science*, *90*(12), art. no. e70733. **https://doi.org/10.1111/1750-3841.70733**
19. Gan, Z., Ellis, P.R., Schofield, J.D. (1995). Gas cell stabilisation and gas retention in wheat bread dough. *Journal of Cereal Science*, *21*(3), 215–230. **https://doi.org/10.1006/JCRS.1995.0025**
20. Gao, X., Tong, J., Guo, L., Yu, L., Li, S., Yang, B., Wang, L., Liu, Y., Li, F., Guo, J., Zhai, S., Liu, C., Rehman, A., Farahnaky, A., Wang, P., Wang, Z., Cao, X. (2020). Influence of gluten and starch granules interactions on dough mixing properties in wheat (*Triticum aestivum* L.). *Food Hydrocolloids*, *106*, art. no. 105885. **https://doi.org/10.1016/J.FOODHYD.2020.105885**
21. Gu, A., Wang, J., Ding, L., Wu, X., Han, J., Liu, X., Wang, L. (2026). Effect of high hydrostatic pressure on the structural, physicochemical, and functional properties of quinoa flour. *Food Chemistry*, *498*, art. no. 147175. **https://doi.org/10.1016/J.FOODCHEM.2025.147175**
22. Guan, Y., Yang, X., Pan, C., Kong, J., Wu, R., Liu, X., Wang, Y., Chen, M., Li, M., Wang, Q., He, G., Yang, G., Chang, J., Li, Y., Wang, Y. (2023). Comprehensive analyses of breads supplemented with tannic acids. *Foods*, *12*(20), art. no. 3756. **https://doi.org/10.3390/foods12203756**
23. Helou, C., Jacolot, P., Niquet-Léridon, C., Gadonna-Widehem, P., Tessier, F.J. (2016). Maillard reaction products in bread: A novel semi-quantitative method for evaluating melanoidins in bread. *Food Chemistry*, *190*, 904–911. **https://doi.org/10.1016/j.foodchem.2015.06.032**
24. Hmad, I.B., Ghribi, A.M., Bouassida, M., Ayadi, W., Besbes, S., Chaabouni, S.E., Gargouri, A. (2024). Combined effects of α-amylase, xylanase, and cellulase coproduced by *Stachybotrys microspora* on dough properties and bread quality as a bread improver. *International Journal of Biological Macromolecules*, *277*(Pt.3), art. no. 134391. **https://doi.org/10.1016/j.ijbiomac.2024.134391**
25. Irmawati, I., Jariyah, J., Sarofa, U. (2024). Effect of substitution of wheat flour and pedada flour (*Sonneratia caseolaris*) to characteristic of white bread. *AJARCDE (Asian Journal of Applied Research for Community Development and Empowerment)*, *8*(2), 254–260. **https://doi.org/10.29165/ajarcde.v8i2.435**
26. Irondi, E.A., Imam, Y.T., Ajani, E.O., Alamu, E.O. (2023). Natural and modified food hydrocolloids as gluten replacement in baked foods: Functional benefits. *Grain & Oil Science and Technology*, *6*(4), 163–171. **https://doi.org/10.1016/J.GAOST.2023.10.001**
27. Islam, S.N., Nusrat, T., Begum, P., Ahsan, M. (2016). Carotenoids and β-carotene in orange fleshed sweet potato: A possible solution to vitamin A deficiency. *Food Chemistry*, *199*, 628–631. **https://doi.org/10.1016/J.FOODCHEM.2015.12.057**
28. Mahfudz, M.K., Jaikhan, S., Phirom-on, K., Apiraksakorn, J. (2024). Cost-effective strategy and feasibility for amylase production from Okara by *Bacillus subtilis* J12. *Fermentation*, *10*(11), art. no. 561. **https://doi.org/10.3390/fermentation10110561**
29. Maity, S., Mallik, S., Basuthakur, R., Gupta, S. (2015). Optimization of solid state fermentation conditions and characterization of thermostable alpha amylase from *Bacillus subtilis* (ATCC 6633). *Journal of Bioprocessing & Biotechniques*, *5*(4), art. no. 218. **https://doi.org/10.4172/2155-9821.1000218**
30. Malavi, D., Mbogo, D., Moyo, M., Mwaura, L., Low, J., Muzhingi, T. (2022). Effect of orange-fleshed sweet potato purée and wheat flour blends on β-carotene, selected physicochemical and microbiological properties of bread. *Foods*, *11*(7), art. no. 1051. **https://doi.org/10.3390/foods11071051**
31. Manyatsi, N.T., Solomon, W.K., Shelembe, J.S. (2020). Optimization of blending ratios of wheat-maize-sprouted mungbean (*Vigna radiata* L.) composite flour bread using D-optimal mixture design. *Cogent Food and Agriculture*, *6*(1), art. no. 1824304. **https://doi.org/10.1080/23311932.2020.1824304**
32. Martínez, M.M., Pico, J., Gómez, M. (2015). Physicochemical modification of native and extruded wheat flours by enzymatic amylolysis. *Food Chemistry*, *167*, 447–453. **https://doi.org/10.1016/J.FOODCHEM.2014.07.031**
33. Miller, G.L. (1959). Use of dinitrosalicylic acid reagent for determination of reducing sugar. *ACS Analytical Chemistry*, *31*(3), 426-428. **https://doi.org/10.1021/ac60147a030**
34. Ministry of Agriculture of the Republic of Indonesia. (2024). *Production and Harvested Area of Sweet Potato* (Retrieved June 30, 2026, from **https://bdsp2.pertanian.go.id/bdsp/id/home.html#).**
35. Mordi, R.C., Ademosun, O.T., Ajanaku, C.O., Olanrewaju, I.O., Walton, J.C. (2020). Free radical mediated oxidative degradation of carotenes and xanthophylls. *Molecules*, *25*(5), art. no. 1038. **https://doi.org/10.3390/molecules25051038**
36. Oloniyo, R.O., Omoba, O.S., Awolu, O.O. (2021). Biochemical and antioxidant properties of cream and orange-fleshed sweet potato. *Heliyon*, *7*(3), art. no. e06533. **https://doi.org/10.1016/J.HELIYON.2021.E06533**
37. Olugbuyi, A., Oyinloye, A., Araoye, K., Ariseloye, O. (2024). Orange fleshed sweet potato-rice bran flour: Optimization, proximate and amino acid composition for dough meal production. *Journal of Agriculture and Food Research*, *15*, art. no. 100920. **https://doi.org/10.1016/j.jafr.2023.100920**
38. Pongpaiboon, W., Srichamnong, W., Srichamnong, S. (2016). Physical properties and resistant starch content of rice flour residues hydrolyzed by α-amylase. *International Journal of Nursing and Health Sciences*, *10*(11), 730–735.
39. Punia, P., Kaushik, S., Jyoti, A., Kalwar, K. (2016). Optimization of production conditions and partial characterization of extracellular amylase from *Bacillus subtilis* under submerged condition. *Journal of Scientific & Industrial Research*, *75*, 371–377.

40. Rathi, D.N.G., Rashed, A.A., Noh, M.F.M. (2022). Determination of retinol and carotenoids in selected Malaysian food products using high-performance liquid chromatography (HPLC). *SN Applied Sciences*, *4*(93). **https://doi.org/10.1007/s42452-022-04955-8**
41. Rebholz, G.F., Sebald, K., Dirndorfer, S., Dawid, C., Hofmann, T., Scherf, K.A. (2021). Impact of exogenous α-amylases on sugar formation in straight dough wheat bread. *European Food Research and Technology*, *247*(3), 695–706. **https://doi.org/10.1007/s00217-020-03657-y**
42. Reddappa, S.B., Chhabra, R., Talukder, Z.A., Muthusamy, V., Zunjare, R.U., Hossain, F. (2022). Development and validation of rapid and cost-effective protocol for estimation of amylose and amylopectin in maize kernels. *3 Biotech*, *12*(3), art. no. 62. **https://doi.org/10.1007/s13205-022-03128-z**
43. Ronie, M.E., Zainol, M.K., Mamat, H. (2021). A review on the recent applications of gluten-free flour, functional ingredients and novel technologies approach in the development of gluten-free bakery products. *Food Research, 5*(5), 43–54. **https://doi.org/10.26656/fr.2017.5(5).721**
44. Sadat, A., Cao, W., Sharma, M., Duizer, L., Joye, I.J. (2023). Enhancing zein-starch dough and bread properties by addition of hydrocolloids. *Food Hydrocolloids*, *143*, art. no. 108860. **https://doi.org/10.1016/j.foodhyd.2023.108860**
45. Safari, A., Kamara, D.S., Silalahi, F., Fadhlillah, M., Kardi, I., Ishmayana, S. (2013). Partial hydrolysis of purple sweet potato flour by amylase from *Saccharomycopsis fibuligera* and its application for composite breadmaking. *Journal of Microbiology, Biotechnology, and Food Sciences*, *5*(2), 2340–2343.
46. Shariffa, Y.N., Uthumporn, U., Karim, A.A., Zaibunnisa, A.H. (2017). Hydrolysis of native and annealed tapioca and sweet potato starches at sub-gelatinization temperature using a mixture of amylolytic enzymes. *International Food Research Journal*, *24*(5), 1925–1933.
47. Sigüenza-Andrés, T., Pando, V., Gómez, M., Rodríguez-Nogales, J.M. (2022). Optimization of a simultaneous enzymatic hydrolysis to obtain a high-glucose slurry from bread waste. *Foods*, *11*(12), art. no. 1793. **https://doi.org/10.3390/foods11121793**
48. Struyf, N., Verspreet, J., Verstrepen, K.J., Courtin, C.M. (2017). Investigating the impact of α-amylase, α-glucosidase and glucoamylase action on yeast-mediated bread dough fermentation and bread sugar levels. *Journal of Cereal Science*, *75*, 35–44. **https://doi.org/10.1016/J.JCS.2017.03.013**
49. Teng, L.Y., Chin, N.L., Yusof, Y.A. (2013). Rheological and textural studies of fresh and freeze-thawed native sago starch–sugar gels. II. Comparisons with other starch sources and reheating effects. *Food Hydrocolloids*, *31*(2), 156–165. **https://doi.org/10.1016/J.FOODHYD.2012.11.002**
50. Torres-Pérez, R., Martínez-García, E., Siguero-Tudela, M.M., García-Segovia, P., Martínez-Monzó, J., Igual, M. (2024). Enhancing gluten-free bread production: Impact of hydroxypropyl methylcellulose, psyllium husk fiber, and xanthan gum on dough characteristics and bread quality. *Foods*, *13*(11), art. no. 1691. **https://doi.org/10.3390/foods13111691**
51. Valková, V., Ïúranová, H., Bilčíková, J., Žofajová, A., Havrlentová, M. (2019). The content and quality of starch in different wheat varieties growing in experimental conditions. *Journal of Microbiology, Biotechnology and Food Sciences*, *9*(SpecialIssue13), 462-466. **https://doi.org/10.15414/JMBFS.2019.9.SPECIAL.462-466**
52. van Rooyen, J., Simsek, S., Oyeyinka, S.A., Manley, M. (2023). Wheat starch structure–function relationship in breadmaking: A review. *Comprehensive Reviews in Food Science and Food Safety*, *22*(3), 2292–2309. **https://doi.org/10.1111/1541-4337.13147**
53. Wang, H., Yang, Q., Ferdinand, U., Gong, X., Qu, Y., Gao, W., Ivanistau, A., Feng, B., Liu, M. (2020). Isolation and characterization of starch from light yellow, orange, and purple sweet potatoes. *International Journal of Biological Macromolecules*, *160*, 660–668. **https://doi.org/10.1016/J.IJBIOMAC.2020.05.259**
54. Wang, L., Xu, J., Fan, X., Wang, Q., Wang, P., Yuan, J., Yu, Y., Zhang, Y., Cui, L. (2018). Characterization of branched limit dextrin and impact on corn starch pasting properties. *Food Hydrocolloids*, *79*, 55–62. **https://doi.org/10.1016/j.foodhyd.2017.12.005**
55. Wang, R., Zhou, W., Yu, H.-H., Chow, W.-F. (2006). Effects of green tea extract on the quality of bread made from unfrozen and frozen dough processes. *Journal of the Science of Food and Agriculture*, *86*(6), 857–864. **https://doi.org/10.1002/jsfa.2423**
56. Yea, C.S., Nevara, G.A., Muhammad, K., Ghazali, H.M., Karim, R. (2019). Physical properties, resistant starch content and antioxidant profile of purple sweet potato powder after 12 months of storage. *International Journal of Food Properties*, *22*(1), 974–984. **https://doi.org/10.1080/10942912.2019.1620765**

ORIGINAL ARTICLE
http://journal.pan.olsztyn.pl

Polish Journal of Food and Nutrition Sciences
2026, Vol. 76, No. 3, 279–287
DOI: 10.31883/pjfns/226185
ISSN 1230-0322, e-ISSN 2083-6007

Prevalence of *Listeria* Pathogenicity Islands in *Listeria innocua* Isolates from Meat, Meat Products, and Meat-Processing Environments in Poland

Anna Zawiasa[1]*, Agnieszka Olejnik-Schmidt[1]

Department of Food Biotechnology and Microbiology, Poznan University of Life Sciences, Wojska Polskiego 48, 60-627 Poznan, Poland

Among the members of the genus *Listeria*, *Listeria innocua* is the species most commonly isolated from food products and food-processing environments. Although it is generally regarded as non-pathogenic, several reports have described cases of listeriosis caused by atypical *L. innocua* strains harboring virulence-associated genes. In this study, the presence of 28 virulence-associated genes was investigated by PCR in the genomes of 51 *L. innocua* isolates obtained from meat products and meat-processing environments in Poland. The hemolytic phenotype of the isolates was assessed as well. Among the *Listeria* pathogenicity island 1 (LIPI-1)-associated genes, *prfA* was detected in 10% of the isolates, while *plcA* and *hly* were each identified in 6% of the analyzed strains. The *actA1* gene was present in 4% of the isolates. Internalin genes were largely absent, as *inlA* and *inlB* were not detected, while *inlC* and *inlJ* were each identified in only 2% of the isolates. Among other genes, *sigB* was present in all isolates (100%), whereas *iap* and *flaA* were detected in 7 and 6 isolates, respectively. In contrast, genes associated with *Listeria* pathogenicity island 3 (LIPI-3) were considerably more prevalent. Genes located in the 5′ region of the island (*llsA, llsG, llsH,* and *llsX*) were detected in approximately 69–73% of the isolates and frequently co-occurred, whereas genes from the 3′ region were much less common (5–13%). A complete LIPI-3 island was identified in two isolates (4%), while partial LIPI-3 profiles were detected in 40 isolates (78%). Among *Listeria* pathogenicity island 4 (LIPI-4) genes, *licC* and *glvA* were detected in 100% and 94% of the isolates, respectively. In the hemolysis assay, no hemolytic activity was detected in any of the isolates. These findings underscore a heterogeneous distribution of pathogenicity island-associated genes in *L. innocua*.

Keywords: food safety, hemolysis *Listeria innocua,* pathogenicity, virulence

INTRODUCTION

Members of the genus *Listeria* are Gram-positive, bacteria that are ubiquitous in natural ecosystems as well as in agricultural and food-processing environments. Their ability to tolerate osmotic stress, grow at refrigeration temperatures, and form biofilms enables their persistence in food-processing facilities and along the production chain [Cebeci & Otlu, 2024]. Among the described species, *Listeria monocytogenes* is the main pathogen responsible for listeriosis in humans and animals [Kaszoni-Rückerl *et al*., 2020]. In contrast, *Listeria innocua* has long been considered non-pathogenic and is commonly used as a model organism due to its close genetic relatedness to *L. monocytogenes* [Matto *et al*., 2022]. It is frequently isolated from raw materials and food-processing environments, often co-occurring with *L. monocytogenes* and, in many cases, representing the predominant *Listeria* species detected [Arslan *et al*., 2020]. Despite its traditional classification as harmless, recent studies have suggested that certain atypical *L. innocua* strains may harbor virulence-associated determinants.

***Corresponding Author:**
E-mail: **anna.zawiasa@up.poznan.pl** (A. Zawiasa)

Submitted: 19 May 2026
Accepted: 21 July 2026
Published on-line: 28 July 2026

These strains may arise through horizontal gene transfer or due to evolutionary divergence from a virulent ancestor shared with *L. monocytogenes* [Ramadan *et al*., 2023; Zanolli Moreno *et al*., 2012]. Phylogenetic analyses support this view, indicating that both species originated from a common ancestor, with the attenuated phenotype of *L. innocua* likely resulting from the loss of key virulence genes [Clayton *et al.*, 2014; Gana *et al.*, 2023]. The presence of pathogenicity islands, such as *Listeria* pathogenicity island 1 (LIPI-1), (*Listeria* pathogenicity island 3 (LIPI-3), and *Listeria* pathogenicity island 4 (LIPI-4), in atypical *L. innocua* isolates further supports their evolutionary and genetic relatedness to *L. monocytogenes* [Clayton *et al.*, 2014; Li M. *et al.*, 2021; Zanolli Moreno *et al.*, 2012]. Although these strains generally exhibit lower virulence than *L. monocytogenes* [Moura *et al.*, 2019], some hemolytic variants have demonstrated the ability to cross the intestinal barrier and disseminate within host tissues [Gwida *et al.*, 2020]. Clinical reports have linked atypical *L. innocua* to severe infections in immunocompromised individuals, including bacteremia [Perrin *et al.*, 2003], meningitis [Favaro *et al.,* 2014], ventriculoperitoneal shunt infection [Karli *et al.*, 2014], neonatal listeriosis [Arumugam *et al.*, 2021], meningoencephalitis [Liao *et al.*, 2022], and joint infection [Gupta *et al.*, 2024]. Animal infections, such as cerebral listeriosis in cattle, have also been described [Matto *et al.*, 2022; Rocha *et al.*, 2013].

Virulence in pathogenic *Listeria* species is mediated by a coordinated set of adhesion, invasion, and intracellular survival factors enabling colonization of the gastrointestinal tract and translocation across the intestinal barrier [Wiktorczyk-Kapischke *et al.*, 2023]. The core virulence determinants are primarily located within LIPI-1, which comprises genes encoding two phospholipases (*plcA* and *plcB*), the pore-forming toxin (*hly*), a metalloprotease (*mpl*), and the actin-polymerization factor (*actA*) responsible for intracellular motility. Expression of LIPI-1 genes is regulated by the transcriptional activator PrfA (encoded by *prfA* gene) [Lee *et al*., 2023]. Among the genes located within LIPI-1, the most critical is *hly*, which encodes listeriolysin O (LLO), a toxin responsible for β-hemolytic activity. *L. innocua*, which typically lacks the *hly* gene, is therefore generally considered a non-hemolytic species. However, atypical *L. innocua* strains exhibiting hemolytic activity have also been described [Johnson *et al*., 2004]. Conversely, rare, atypical *L. monocytogenes* strains, in which spontaneous loss of virulence genes resulted in a nonhemolytic phenotype, have been reported by Olaimat *et al*. [2018]. These observations highlight the necessity for continuous monitoring of hemolytic properties and associated virulence determinants. Another important group of virulence-associated proteins are internalins, *i.e.*, surface proteins mediating adhesion and invasion of host cells. The best-characterized members include *inlA* and *inlB*, while additional internalins, such as *inlC*, *inlJ*, *inlH*, *inlK*, *inlL*, *inlF*, and *inlP*, have also been implicated in host interaction and dissemination [Liu *et al.,* 2007]. Other factors contributing to pathogenic potential include the invasion-associated protein (*iap*), flagellin (*flaA*), and the alternative sigma factor B (*sigB*), which regulates the general stress response and enhances bacterial survival under adverse environmental conditions [Osek & Wieczorek, 2022]. In addition to LIPI-1, hypervirulent *Listeria* strains may harbor LIPI-3 and LIPI-4. LIPI-3 consists of eight genes (*llsA*, *llsG*, *llsH*, *llsX*, *llsB*, *llsD*, *llsP*, and *llsY*) encoding listeriolysin S (LLS), *i.e.*, a second cytolytic peptide that exhibits properties of both a bacteriocin and a hemolytic cytotoxic factor. LLS contributes to the modulation of the intestinal microbiota and promotes gastrointestinal colonization [Clayton *et al.*, 2014; Cotter *et al.*, 2008; Lee *et al*., 2023]. Notably, the *llsX* gene is commonly regarded as a molecular marker for the presence of the LIPI-3 [Wiktorczyk-Kapischke *et al*., 2023]. LIPI-4, composed of six genes, encodes a cellobiose-family phosphotransferase system (PTS) and has been associated with enhanced neural and placental tropism, suggesting a role in central nervous system and maternal-neonatal infections [Lee *et al.*, 2023; Li M. *et al.*, 2021]. Although virulence factors have been extensively investigated in *L. monocytogenes*, knowledge regarding their distribution in other *Listeria* species remains limited.

Listeriosis remains a significant cause of mortality worldwide. Identifying and characterizing virulence factors is essential for both basic scientific research and ongoing medical challenges. Therefore, this study aimed to investigate the occurrence of selected virulence-associated genes and the hemolytic phenotype of *L. innocua* isolates recovered from meat products and meat-processing environments in Poland.

MATERIALS AND METHODS

Bacterial isolates and genetic material

A total of 51 *L. innocua* isolates were included in this investigation. Of these, 32 were recovered from raw poultry, pork, and beef, as well as from processed meat products, including bacon, ham, and sausages. The remaining 19 isolates originated from meat-processing environments and were recovered from swab samples collected from production lines, processing equipment, walls, and floors. The isolates were obtained through collaboration with an accredited microbiological diagnostic laboratory in Poland. Due to the confidential nature of the source information, detailed data regarding the exact origin of the isolates and the individual meat-processing facilities cannot be disclosed. All isolates were obtained in Poland during 2020–2021. Genomic DNA was extracted with the Genomic Mini kit (A&A Biotechnology, Gdańsk, Poland) following the supplier's protocol and served as the template for PCR analyses. Isolates stored at –80°C in brain heart infusion (BHI; Oxoid, Warsaw, Poland) supplemented with glycerol were used for the evaluation of hemolytic activity. Prior to the experiments, the taxonomic identity of all isolates had been verified as *L. innocua via* polymerase chain reaction–restriction fragment length polymorphism (PCR-RFLP) and multiplex polymerase chain reaction (multiplex PCR). Exact methodologies were reported previously [Li F. *et al.*, 2021; Paillard *et al*., 2003].

Detection of virulence-associated genes

Conventional PCR was performed to detect selected virulence-associated genes in *L. innocua* isolates. The analysis of the *actA*

gene was conducted using two primer pairs, designated *actA1* and *actA2*. Additionally, PCR assays targeting LIPI-4 genes were subjected to optimization; reproducible amplification was achieved for *licC* and *glvA*, whereas optimization attempts for the remaining genes did not yield reproducible results across all isolates. Therefore, these genes were excluded from further analysis. Each PCR reaction contained 0.2 U of RUN DNA polymerase (A&A Biotechnology) with the corresponding reaction buffer, 0.2 mM of each deoxynucleoside triphosphate (dNTP) (A&A Biotechnology), and the appropriate primer pair (**Table 1**), synthesized by Genomed S.A. (Warsaw, Poland). Approximately 10 ng of template DNA were added to each reaction, and the final reaction volume was adjusted to 10 µL. PCR amplification was carried out using a Biometra TOne thermal cycler (Biometra, Göttingen, Germany). Three *L. monocytogenes* isolates obtained from food samples were used as positive controls. Following amplification, PCR fragments were examined by agarose gel electrophoresis using Midori Green Advance (1×; NIPPON Genetics EUROPE, Düren, Germany). Gel images were acquired with the Gel Doc imaging system (Bio-Rad, Hercules, CA, USA). For each target gene, a representative fragment of the expected length was selected for purification with the Gel-Out Concentrator kit (A&A Biotechnology)

Table 1. Detailed information about PCR conditions.

Virulence genes	Primers name	Target	Primers' sequence	Annealing temperature (°C)	Amplicon length (bp)	Reference
Listeria pathogenicity island 1 (LIPI-1)	*prfA*	Listeriolysin-positive regulatory protein	F: 5′-GATACAGAAACATCGGTTGGC-3′ R: 5′-GTGTAATCTTGATGCCATCAGG-3′	49	274	D'Agostino *et al.* [2004]
	plcA	Phosphatidylinositol-specific phospholipase C	F: 5′-CTGCTTGAGCGTTCATGTCTCATCCCCC-3′ R: 5′-CATGGGTTTCACTCTCCTTCTAC-3′	60	1,484	Notermans *et al.* [1991]
	plcB	Phosphatidylicholin-specific phospholipase C	F: 5′-GCAAGTGTTCTAGTCTTTCCGG-3′ R: 5′-ACCTGCCAAAGTTTGCTGTGA-3′	55	795	Nishibori *et al.* [1995]
	mpl	Metalloprotease	F: 5′-GGCTCATTTCACTATGACGG-3′ R: 5′-GCTTCCCAAGCTTCAGCAACT-3′	55	1,473	
	hly	Listeriolysin O	F: 5′-GCAGTTGCAAGCGCTTGGAGTGAA-3′ R: 5′-GCAACGTATCCTCCAGAGTGATCG-3′	60	210	Park *et al.* [2006]
	actA1	Actin polymerization protein	F: 5′-CGCCGCGGAAATTAAAAAAAGA-3′ R: 5′-ACGAAGGAACCGGGCTGCTAG-3′	62	839 (or 950)	Jallewar *et al.* [2007]
	actA2	Actin polymerization protein	F: 5′-GACGAAAATCCCGAAGTGAA-3′ R: 5′-CTAGCGAAGGTGCTGTTTCC-3′	63	268 (or 385)	Jaradat *et al.* [2002]
Other virulence--associated genes	*sigB*	Sigma factor	F: 5′-TCATCGGTGTCACGGAAGAA-3′ R: 5′-TGACGTTGGATTCTAGACAC-3′	51	310	Bae *et al.* [2012]
	iap	Invasion associated protein	F: 5′-ACAAGCTGCACCTGTTGCAG-3′ R: 5′-TGACAGCGTGTGTAGTAGCA-3′	56	131	Furrer *et al.* [1991]
	flaA	Flagellin	F: 5′-TTACTAGATCAAACTGCTCC-3′ R: 5′-AAGAAAAGCCCCTCGTCC-3′	54	538	Borucki & Call [2003]
Internalins	*inlA*	Internalin A	F: 5′-ACGAGTAACGGGACAAATGC-3′ R: 5′-CCCGACAGTGGTGCTAGATT-3′	55	800	Liu *et al.* [2007]
	inlJ	Internalin J	F: 5′-TGTAACCCCGCTTACACAGTT-3′ R: 5′-AGCGGCTTGGCAGTCTAATA-3′	55	238	
	inlB	Internalin B	F: 5′-CATGGGAGAGTAACCCAACC-3′ R: 5′-GCGGTAACCCCTTTGTCATA-3′	57	500	Zhang & Knabel [2005]
	inlC	Internalin C	F: 5′-CCCACAATCAAATAAGTGACCTT-3′ R: 5′-CTGGGTCTTTGACAGTATTTGTT-3′	57	400	
Listeria pathogenicity island 3 (LIPI-3)	*llsX*	Listeriolysin L	F: 5′-TTATTGCATCAATTGTTC TAGGG -3′ R: 5′-CCCCTATAAACATCATGCTAGTG-3′	55.5	200	Vilchis-Rangel *et al.* [2019]
	llsA		F: 5′-CGATTTCACAATGTGATAGGATG-3′ R: 5′-GCACATGCACCTCATAAC-3′	52	280	Clayton *et al.* [2014]
	llsG		F: 5′-GAGACTGGGCTTACTTGC-3′ R: 5′-TACCTCCTGTTCACTGCTTG-3′	50	415	Zhang *et al.* [2019]
	llsH		F: 5′-ATGATGTTCGCTATGGTT-3′ R: 5′-ACATTCCTACTGGCATCA-3′	45	421	
	llsB		F: 5′-TTACAATCAACCACCAGG-3′ R: 5′-AGTGAACCGAATGACAGA-3′	45	334	

Table 1 cont. Detailed information about PCR conditions.

Virulence genes	Primers name	Target	Primers' sequence	Annealing temperature (°C)	Amplicon length (bp)	Reference
	llsD		F: 5'-TATGGTGGTATGGAGGGT-3' R: 5'-ATCACCCTGCTTATTTCA-3'	45	562	
	llsP		F: 5'-TTTCCAGGTATGCTTCTT-3' R: 5'-CAATTACGGTGGTTCTCA-3'	45	554	
	llsY		F: 5'-ATTAGAATAGGAACGCAGAC-3' R: 5'-TCATAGCACCCAGTTTCG-3'	50	581	
Listeria pathogenicity island 4 (LIPI-4)	*licA*	Phosphotransferase system (PTS) sugar transporter enzyme IIA (EIIA) subunit	F: 5'-GCCTCTTCCTCGTTTCTA-3' R: 5'-GACTTAACTAAATCGCAGTA-3'	45	227	Zhang *et al.* [2019]
	licB	Phosphotransferase system (PTS) sugar transporter enzyme IIB (EIIB) subunit	F: 5'-ATTGCGGCATCTGAGAAA-3' R: 5'-CAGCGATTAGAATTGGTACTGC-3'	55	232	
	licC	Phosphotransferase system (PTS) sugar transporter enzyme IIC (EIIC) subunit	F: 5'-GGGATTCCGAAACTACCT-3' R: 5'-CGAGTGCTCCTGTAACCC-3'	47	736	
	Lm900558-70012	Phosphotransferase system (PTS)-associated protein	F: 5'-TGGTAACAATGCCTGCTT-3' R: 5'-GCTGAAAGCCCACTGTAT-3'	50	369	
	Lm900558-70013	Transcriptional antiterminator	F: 5'-TATTCAGTGGTTACGAGGCT-3' R: 5'-CTCCGCCGAAATCTGGTA-3'	50	403	
	glvA	Maltose-6'-phosphate--glucosidase	F: 5'-TTACTATTGCTGGCGGAGGA-3' R: 5'-TGCTCACGACCATCCATT-3'	47	847	

and subsequently subjected to Sanger sequencing by Genomed S.A. (Warsaw, Poland). The resulting sequences were compared against reference entries in the NCBI BLAST database (version 2.15.0) to verify the identity of the amplified targets.

Hemolysis assay

Hemolytic activity was assessed using Columbia Agar supplemented with 5% sheep blood (Oxoid, Warsaw, Poland). Bacterial isolates stored as glycerol stocks were first streaked onto BHI agar and incubated at 35°C for 24 h. Subsequently, cultures were re-streaked onto blood agar plates and incubated at 35°C for 24 h and 48 h, with hemolysis evaluated after each incubation period. *Listeria ivanovii* ATCC 19119 was used as a positive control.

RESULTS AND DISCUSSION

Listeriosis is a significant foodborne disease transmitted primarily through contaminated food, including meat and meat products [Zanolli Moreno *et al*., 2014]. While the pathogenicity of *L. monocytogenes* is well characterized in terms of its virulence gene [Freitag *et al.*, 2009], the virulence potential of non-pathogenic *Listeria* species remains poorly understood. Therefore, this study analyzed the presence of 28 virulence-associated genes in 51 *L. innocua* isolates by PCR. Detailed results regarding the presence of individual virulence-associated genes in each isolate, together with the corresponding source of isolation, are presented in **Figure 1**.

Presence of LIPI-1 genes and internalin-associated genes

Genes associated with the LIPI-1 were detected sporadically among the analyzed isolates (**Figure 1**). The *prfA* gene was identified in 5 isolates (10%) from raw meat samples and food-processing environments, while *plcA* and *hly* were each detected in 3 isolates (6%). The *actA1* gene was present in 2 isolates (4%), whereas *plcB*, *actA2*, and *mpl* were not detected in any strain. In contrast, the stress-response regulator *sigB*, which is not part of LIPI-1, was present in all isolates (100%). Additionally, the *iap* gene was identified in 7 isolates (14%), and *flaA* in 6 isolates (12%). Notably, none of the analyzed isolates carried a complete LIPI-1.

The prevalence of LIPI-1 genes observed in the present study was generally lower than that reported in several previous investigations. For example, *plcA* was detected in 97.4% of *L. innocua* isolates recovered from beef, fish, raw milk, and traditional cheese samples in Turkey, followed by *iap* (35.8%) and *hlyA* (15.3%) [Cebeci *et al.*, 2024]. In the present study, *plcA* and *hly* were identified in only 6% of the isolates, while *iap* was detected in 15%, indicating a substantially lower prevalence of these virulence-associated determinants. The occurrence of the *iap* gene appears to vary considerably among studies. A markedly higher prevalence was reported, with *iap* identified in 36 isolates from the poultry production chain [Gwida *et al.*, 2020]. Similarly, the gene was detected in isolates originating from cattle and sheep [Matto *et al.*, 2022], raw milk and yogurt samples [Ramadan *et al.*, 2023] and grain samples [Yong *et al.*, 2024]. The prevalence of *plcA*

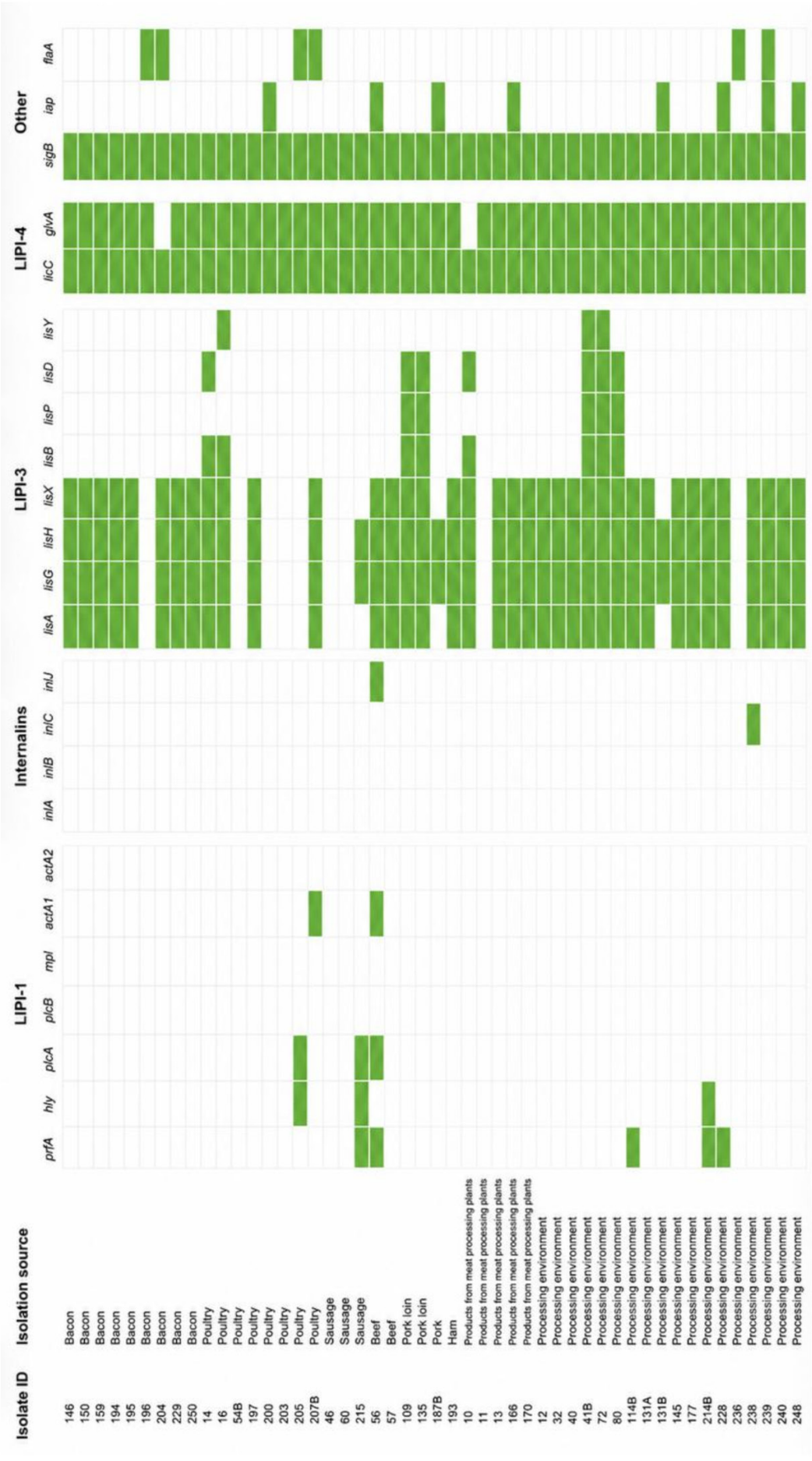

Figure 1. Presence of selected virulence-associated genes among *Listeria innocua* isolates from meat, meat products, and meat-processing environments analyzed in this study. Colored boxes indicate the presence (green) or absence (white) of each gene.

and *hly* has been reported to vary considerably among *L. innocua* isolates, with one study detecting both genes in all five isolates recovered from swine slaughterhouses and meat markets, whereas another identified them in only 9 of the 42 isolates collected from fecal samples of healthy birds in Finland [Moura *et al.*, 2019; Zanolli Moreno *et al.*, 2014]. In Polish research, *hly* was identified in 16.7% of isolates from fish and shrimp, while *plcA* and *iap* were absent [Zakrzewski *et al.*, 2020]. In contrast, no presence of *hly*, *plcA*, or *iap* was detected in *L. innocua* isolates from food and food-contact surfaces [Mafuna *et al.*, 2022; Rossi *et al.*, 2020]. The discrepancies between studies may reflect differences in isolate origin, genomic diversity, and the dynamic nature of virulence-associated gene acquisition or loss within *L. innocua* populations.

The present study demonstrated a very limited distribution of internalin-associated genes among the analyzed *L. innocua* isolates (**Figure 1**). Neither *inlA* nor *inlB* was detected in any of the examined strains. In contrast, *inlC* was identified in a single isolate recovered from a food-processing environment, while *inlJ* was detected in one isolate originating from a beef sample (2% each).

Similarly, low prevalence of internalin genes has been reported in other studies. In the study, five atypical *L. innocua* isolates were described, all of which harbored *inlA* and *inlJ*, suggesting that certain atypical strains may carry a broader repertoire of virulence-associated genes [Zanolli Moreno *et al.*, 2012]. The presence of *inlA* in only a single isolate obtained from food and food-manufacturing plants has also been reported [Rossi *et al.*, 2020]. Conversely, no *inlA, inlB, inlC, inlJ,* or *inlK* genes were detected among isolates from the poultry production chain [Gwida *et al.*, 2020]. Other studies have also reported the absence of major virulence determinants in *L. innocua*. Isolates from fresh and frozen soft fruits lacked LIPI-1 and internalin genes [Wartha *et al.*, 2023], while strains from slaughterhouses were found to be devoid of LIPI-1, internalins, and LIPI-3 elements [Qi *et al.*, 2024].

Although LIPI-1 and internalin-associated genes were generally detected sporadically and most often occurred individually, two isolates stood out due to their notably expanded virulence gene profiles. Isolate ID56, recovered from beef, harbored six virulence-associated genes (*prfA*, *sigB*, *iap*, *plcA*, *actA*, and *inlJ*), representing one of the most complex profiles identified in this study. Similarly, isolate ID 205, originating from poultry, carried four virulence-associated genes (*sigB*, *plcA*, *hly*, and *flaA*). The presence of multiple virulence determinants within single isolates is noteworthy and may indicate an increased adaptive or pathogenic potential, warranting further investigation to assess their functionality and possible contribution to virulence.

Presence of LIPI-3 genes

In contrast to the limited distribution of LIPI-1 and internalin-associated genes, LIPI-3 genes were considerably more prevalent among the analyzed *L. innocua* isolates. Genes located in the 5′ region of the LIPI-3 were detected at high frequencies. The *llsA* and *llsX* genes were each identified in 36 isolates (69%) and consistently co-occurred within the same strains. Similarly, *llsG* and *llsH* were detected in 37 isolates (73%) and were always present together. Notably, all isolates harboring *llsA* and *llsX* also carried *llsG* and *llsH*, indicating a strong tendency for co-occurrence of genes located in the 5′ region of the island. In contrast, genes located in the 3′ region of LIPI-3 were detected much less frequently. The *llsB* and *llsD* genes were each identified in 7 isolates (13%) and consistently co-occurred. The *llsP* gene was detected in 5 isolates (10%), whereas *llsY* was found in only 3 isolates (6%). A complete LIPI-3, defined as the presence of all eight analyzed LIPI-3 genes, was identified in 2 isolates (4%), both originating from distinct food-processing environment samples. Partial LIPI-3 profiles, characterized by the presence of at least one LIPI-3 gene, were detected in 40 isolates (78%), whereas 11 isolates (21%) did not harbor any of the analyzed LIPI-3 genes.

The predominance of LIPI-3 genes observed in the present study is consistent with previous findings demonstrating that these genes are more prevalent in *L. innocua* than other pathogenicity islands. Clayton *et al.* [2014] analyzed a total of 64 *L. innocua* isolates recovered from food products, of which 45 strains (70.3%) were positive for *llsA*. Eleven isolates carried a complete LIPI-3, whereas 25 exhibited a truncated LIPI-3 profile lacking *llsB*, *llsY*, *llsD*, and *llsP*, corresponding to the presence of *llsA*, *llsG*, *llsH*, and *llsX*. Nine isolates harbored only *llsA*, and 19 strains lacked all LIPI-3 genes. Notably, the LIPI-3-positive isolates described in that study were non-hemolytic, consistent with the findings of the present study [Clayton *et al.*, 2014]. In another investigation focusing on non-pathogenic *Listeria* spp. isolated from food and food-processing facilities, three *L. innocua* isolates harboring a complete LIPI-3 were identified among 36 analyzed strains [Mafuna *et al.*, 2022]. A larger survey conducted in South Africa examined 110 *L. innocua* isolates originating from cattle farms, beef abattoirs, and retail outlets. The *llsA* (66 isolates), *llsG* (66 isolates), *llsH* (65 isolates), and *llsX* (65 isolates) genes were frequently detected, whereas genes located in the 3′ region- *llsB* (7 isolates), *llsD* (8 isolates), *llsP* (6 isolates), and *llsY* (8 isolates), were considerably less prevalent [Gana *et al.*, 2023]. These findings corroborate the results of the present study, confirming the broader distribution of LIPI-3 compared with other pathogenicity islands in *L. innocua*. Hence, a consistent pattern emerges across studies, including the present one, demonstrating higher prevalence and frequent co-occurrence of genes located in the 5′ region of the island, accompanied by reduced detection of genes positioned toward the 3′ end. The structure of LIPI-3, therefore, appears to vary among *L. innocua* isolates, ranging from complete islands to partial remnants or total absence, reflecting ongoing genomic variability within the species. Notably, LIPI-3 has been reported to be considerably more widespread in *L. innocua* than in *L. monocytogenes*, where it is generally confined to selected hypervirulent lineages [Lee *et al.*, 2023; Zhang *et al.*, 2019].

Presence of selected LIPI-4 genes

Among the LIPI-4 genes, *licC* and *glvA* were successfully analyzed. The *licC* gene was detected in all examined isolates

(51/51; 100%), while *glvA* was identified in 48 isolates (94%). The remaining LIPI-4 genes were not included in the present analysis.

LIPI-4 is a relatively recently described pathogenicity island and remains the least extensively investigated among the known *Listeria* pathogenicity islands. In *L. monocytogenes*, its occurrence is largely restricted to the hypervirulent clonal complex CC4 [Lee *et al.*, 2023]. Data regarding its distribution in *L. innocua* remains limited compared with LIPI-1 and LIPI-3. Structurally, LIPI-4 encodes a PTS system: *licC*, encoding the enzyme IIC component (EIIC) of the phosphotransferase system (PTS) sugar transporter, responsible for substrate recognition and facilitates sugar transport into the cell, and *glvA*, encoding maltose-6'-phosphate glucosidase [Zhang *et al.*, 2019]. Both genes were highly prevalent among the examined isolates, with *licC* detected in all strains and *glvA* in the vast majority. Although genes associated with the LIPI-4 region were frequently detected, the limited number of target genes successfully amplified did not allow confirmation of the presence of a complete and functional LIPI-4 in the studied collection. Previous studies have reported the occurrence of intact LIPI-4 in *L. innocua*, including three food-derived isolates harboring the complete cluster [Li M. *et al.*, 2021], as well as a high prevalence of the full island among 36 analyzed strains [Mafuna *et al.*, 2022]. The frequent detection of *licC* and *glvA* suggests enhanced metabolic adaptability of the analyzed isolates, particularly in the utilization of specific carbohydrates. Such capabilities may support persistence in food environments, improve competitiveness against other microorganisms, and potentially facilitate host colonization. At the same time, the widespread presence of these genes cautiously indicates that LIPI-4 related elements may be common in *L. innocua*. However, further investigations are necessary to determine the presence of the remaining LIPI-4 genes and to clarify the functional significance of the detected determinants.

Hemolysis assay

No hemolytic activity was observed among the analyzed *L. innocua* isolates, despite the presence of the *hly* gene in three isolates (205, 214B, and 215), indicating a lack of functional expression of this virulence determinant under the tested conditions. The discordance between the presence of *hly* and the absence of a clear hemolytic phenotype represents a particularly intriguing finding. Several explanations may account for this observation, including mutations within the *hly* coding sequence impairing listeriolysin O functionality, nonsense mutations leading to truncated protein products, or alterations within the promoter region affecting gene transcription. Additionally, impaired activity or mutations in the transcriptional regulator *prfA* could disrupt proper activation of LIPI-1 genes. To clarify the molecular basis of this discrepancy, further investigations should include sequencing of the *hly* gene and its regulatory regions, as well as analyses of gene expression. Although *L. innocua* is generally regarded as a non-hemolytic species, hemolytic isolates have occasionally been reported. An atypical strain carrying a complete set of LIPI-1 genes exhibited hemolytic activity but failed to induce disease in murine models, suggesting that hemolysis alone does not necessarily confer full pathogenic potential [Johnson *et al.*, 2004]. In contrast, other studies demonstrated that hemolytic *L. innocua* isolates harboring LIPI-1 and *inlA* may exhibit virulence, including the ability to cross the intestinal epithelium and disseminate systemically, albeit to a lesser extent than *L. monocytogenes* EGDe [Moura *et al.*, 2019]. Weakly hemolytic *hly*-positive isolates and additional hemolytic LIPI-1 positive strains from pork, seafood, and poultry have also been described [Milillo *et al.*, 2012; Volokhov *et al.*, 2007; Zanolli Moreno *et al.*, 2014]. Although exposure to atypical hemolytic *L. innocua* strains appears to be rare, both the present findings and previous reports indicate that phenotypic assessment of hemolysis may not always provide reliable results. The emergence of atypical isolates, including strains exhibiting low-hemolytic activity, further complicates species identification when conventional methods are applied. The present findings highlight that the presence of the *hly* gene alone is not sufficient to infer hemolytic phenotype in *L. innocua*, emphasizing the importance of combining genotypic and phenotypic approaches in virulence assessment.

CONCLUSIONS

This study provides the first comprehensive characterization of 28 virulence-associated genes in *L. innocua* isolates recovered from raw and processed meat products as well as meat-processing environments in Poland. The findings indicate a sporadic occurrence of genes clustered within the LIPI-1 and internalin-associated genes. In contrast, LIPI-3 genes, present either as a complete island or in truncated forms, were more widespread, demonstrating a predominance compared with other pathogenicity islands. The universal presence of *sigB*, together with the frequent detection of *licC* and *glvA*, may suggest enhanced metabolic adaptability of the analyzed isolates and could support their persistence in food and food-processing environments. Although *L. innocua* is generally regarded as non-pathogenic, its occurrence in food matrices warrants attention, particularly due to its frequent coexistence with *L. monocytogenes* and its potential role as a reservoir of virulence-associated genes. Importantly, the detection of virulence-associated genes at the genomic level does not necessarily imply their functional expression or pathogenic potential. As the present study was limited to DNA-based identification of these determinants, further investigations focusing on transcriptional activity and functional analyses are required to more accurately assess their potential contribution to the pathogenicity of *L. innocua*. Furthermore, the implementation of whole-genome sequencing (WGS) in future studies could further strengthen this approach by providing comprehensive

information on the genetic background, virulence-associated genes, and evolutionary relationships among *L. innocua* isolates. These findings emphasize the importance of including *L. innocua* in food safety monitoring and risk assessment frameworks.

ACKNOWLEDGEMENTS

We sincerely thank Iwona Kawacka (Department of Food Biotechnology and Microbiology, Poznan University of Life Sciences, Poland) for establishing the collection of *L. innocua* isolates used in this study.

RESEARCH FUNDING

No external funding was received for this study. The author received a free publication invitation as an award for participation in a scientific conference, the XXIX Session of the Young Scientists Section of the Polish Society of Food Technologists (PTTŻ), *"Food through the Eyes of the Young Generation"*, held on 29-30 May 2025 in Kraków, Poland.

CONFLICT OF INTERESTS

The authors declare no conflict of interests.

ORCID IDs

A. Olejnik-Schmidt https://orcid.org/0000-0002-5418-5632
A. Zawiasa https://orcid.org/0009-0001-0374-9899

REFERENCES

1. Arslan, S., Özdemir, F. (2020). Prevalence and antimicrobial resistance of *Listeria* species and molecular characterization of *Listeria monocytogenes* isolated from retail ready-to-eat foods. *FEMS Microbiology Letters*, *367*(4), art. no. fnaa006. https://doi.org/10.1093/femsle/fnaa006
2. Arumugam, S., Govindharaj, K., Subramaniam, A., Rangasamy, R. (2021). Neonatal *Listeria innocua* sepsis. *International Journal of Contemporary Pediatrics*, *8*(5), 938–940. https://doi.org/10.18203/2349-3291.ijcp20211691
3. Bae, D., Liu, C., Zhang, T., Jones, M., Peterson, S.N., Wang, C. (2012). Global gene expression of *Listeria monocytogenes* to salt stress. *Journal of Food Protection*, *75*(5), 906–912. https://doi.org/10.4315/0362-028x.jfp-11-282
4. Borucki, M.K., Call, D.R. (2003). *Listeria monocytogenes* serotype identification by PCR. *Journal of Clinical Microbiology*, *41*(12), 5537–5540. https://doi.org/10.1128/JCM.41.12.5537-5540.2003
5. Cebeci, T., Otlu, B. (2024). Prevalence, virulence potential, antibiotic resistance profile, heavy metal resistance genes of *Listeria innocua*: A first study in consumed foods for assessment of human health risk in Northern Turkey. *Environmental Science and Pollution Research*, *31*(56), 65078–65091. https://doi.org/10.1007/s11356-024-35582-y
6. Clayton, E.M., Daly, K.M., Guinane, C.M., Hill, C., Cotter, P.D., Ross, P.R. (2014). Atypical *Listeria innocua* strains possess an intact LIPI-3. *BMC Microbiology*, *14*, art. no. 58. https://doi.org/10.1186/1471-2180-14-58
7. Cotter, P.D., Draper, L.A., Lawton, E.M., Daly, K.M., Groeger, D.S., Casey, P.G, Ross, R.P. (2008). Listeriolysin S, a novel peptide haemolysin associated with a subset of lineage I *Listeria monocytogenes*. *PLoS Pathogens*, *4*(9), art. no. e1000144. https://doi.org/10.1371/journal.ppat.1000144
8. D'Agostino, M., Wagner, M., Vazquez-Boland, J.A., Kuchta, T., Karpiskova, R., Hoorfar, J., Novella, S., Scortti, M., Ellison, J., Murray, A., Fernandes, I., Kuhn, M., Pazlarova, J., Heuvelink, A., Cook, N. (2004). A validated PCR-based method to detect *Listeria monocytogenes* using raw milk as a food model – towards an international standard. *Journal of Food Protection*, *67*(8), 1646–1655. https://doi.org/10.4315/0362-028X-67.8.1646
9. Favaro, M., Sarmati, L., Sancesario, G., Fontana, C. (2014). First case of *Listeria innocua* meningitis in a patient on steroids and etanercept. *Journal of Medical Case Reports*, *1*(2), art. no. 003103. https://doi.org/10.1099/jmmcr.0.003103
10. Freitag, N.E., Port, G.C., Miner, M.D. (2009). *Listeria monocytogenes* – from saprophyte to intracellular pathogen. *Nature Reviews Microbiology*, *7*(9), 623–628. https://doi.org/10.1038/nrmicro2171
11. Furrer, B., Candrian, U., Hoefelein, C., Luethy, J. (1991). Detection and identification of *Listeria monocytogenes* in cooked sausage products and in milk by *in vitro* amplification of haemolysin gene fragments. *Journal of Applied Bacteriology*, *70*(5), 372–379. https://doi.org/10.1111/j.1365-2672.1991.tb02951.x
12. Gana, J., Gcebe, N., Pierneef, R.E., Chen, Y., Moerane, R., Adesiyun, A.A. (2023). Genomic characterization of *Listeria innocua* isolates recovered from cattle farms, beef abattoirs, and retail outlets in Gauteng Province, South Africa. *Pathogens*, *12*(8), art. no. 1062. https://doi.org/10.3390/pathogens12081062
13. Gupta, M., Saha, U.S., Kumar, R., Laik, J., Mishra, M. (2024). *Listeria innocua* infection in an old case of total knee replacement – an unusual case report. *Access Microbiology*, *6*(1), art. no. 000524.v3. https://doi.org/10.1099/acmi.0.000524.v3
14. Gwida, M., Lüth, S., El-Ashker, M., Zakaria, A., El-Gohary, F., Elsayed, M., Kleta, S., Al Dahouk, S. (2020). Contamination pathways can be traced along the poultry processing chain by whole genome sequencing of *Listeria innocua*. *Microorganisms*, *8*(3), art. no. 414. https://doi.org/10.3390/microorganisms8030414
15. Jallewar, P.K., Kalorey, D.R., Kurkure, N.V., Pande, V.V., Barbuddhe, S.B. (2007). Genotypic characterization of *Listeria* spp. isolated from fresh water fish. *International Journal of Food Microbiology*, *114*(1), 120–123. https://doi.org/10.1016/j.ijfoodmicro.2006.09.034
16. Jaradat, Z.W., Schutze, G.E., Bhunia, A.K. (2002). Genetic homogeneity among *Listeria monocytogenes* strains from infected patients and meat products from two geographic locations determined by phenotyping, ribotyping and PCR analysis of virulence genes. *International Journal of Food Microbiology*, 76(1–2), 1–10. https://doi.org/10.1016/S0168-1605(02)00050-8
17. Johnson, J., Jinneman, K., Stelma, G., Smith, B.G., Lye, D., Messer, J., Ulaszek, J., Evsen, L., Gendel, S., Bennett, R.W., Swaminathan, B., Pruckler, J., Steigerwalt, A., Kathariou, S., Yildirim, S., Volokhov, D., Rasooly, A., Chichikov, V., Wiedmann, M., Fortes, E., Duvall, R.E., Hitchins, A.D. (2004). Natural atypical *Listeria innocua* strains with *Listeria monocytogenes* pathogenicity island 1 genes. *Applied and Environmental Microbiology*, *70*(7), 4256–4266. https://doi.org/10.1128/AEM.70.7.4256-4266.2004
18. Karli, A., Sensoy, G., Unal, N., Yanik, K., Cigdem, H., Belet, N., Sofuoglu, A. (2014). Ventriculoperitoneal shunt infection with *Listeria innocua*. *Pediatrics International*, *56*(4), 621–623. https://doi.org/10.1111/ped.12302
19. Kaszoni-Rückerl, I., Mustedanagic, A., Muri-Klinger, S., Brugger, K., Wagner, K.-H., Wagner, M., Stessl, B. (2020). Predominance of distinct *Listeria innocua* and *Listeria monocytogenes* in recurrent contamination events at dairy processing facilities. *Microorganisms*, *8*(2), art. no. 234. https://doi.org/10.3390/microorganisms8020234
20. Lee, S., Parsons, C., Chen, Y., Dungan, R.S., Kathariou, S. (2023). Contrasting genetic diversity of *Listeria* pathogenicity islands 3 and 4 harbored by nonpathogenic *Listeria* spp. *Applied and Environmental Microbiology*, *89*(2), art. no. e02097-22. https://doi.org/10.1128/aem.02097-22
21. Li F., Ye Q., Chen M., Zhang J., Xue L., Wang J., Wu S., Zeng H., Gu Q., Zhang Y., Wei X., Ding Y., Wu Q. (2021). Multiplex PCR for the identification of pathogenic *Listeria* in *Flammulina velutipes* based on novel specific targets revealed by pan-genome analysis. *Frontiers in Microbiology*, *11*, art. no. 634255. https://doi.org/10.3389/fmicb.2020.634255
22. Li, M., Yan, S., Fanning, S., Li, F., Xu, J. (2021). Whole genome analysis of three multi-drug resistant *Listeria innocua* and genomic insights into their relatedness with resistant *Listeria monocytogenes*. *Frontiers in Microbiology*, *12*, art. no. 694361. https://doi.org/10.3389/fmicb.2021.694361
23. Liao, Y., Liu, L., Zhou, H., Fang, F., Liu, X. (2022). Case report: Refractory *Listeria innocua* meningoencephalitis in a three-year-old boy. *Frontiers in Pediatrics*, *10*, art. no. 857900. https://doi.org/10.3389/fped.2022.857900
24. Liu, D., Lawrence, M.L., Austin, F.W., Ainsworth, A.J. (2007). A multiplex PCR for species- and virulence-specific determination of *Listeria monocytogenes*. *Journal of Microbiological Methods*, *71*(2), 133–140. https://doi.org/10.1016/j.mimet.2007.08.007
25. Mafuna, T., Matle, I., Magwedere, K., Pierneef, R.E., Reva, O.N. (2022). Comparative genomics of *Listeria* species recovered from meat and food processing facilities. *Microbiology Spectrum*, *10*(5), art. no. e0118922. https://doi.org/10.1128/spectrum.01189-22

26. Matto, C., D'Alessandro, B., Mota, M.I., Braga, V., Buschiazzo, A., Gianneechini, E., Varela, G., Rivero, R. (2022). *Listeria innocua* isolated from diseased ruminants harbour minor virulence genes of *L. monocytogenes*. *Veterinary Medicine and Science*, *8*(2), 735–740. **https://doi.org/10.1002/vms3.710**
27. Milillo, S.R., Stout, J.C., Hanning, I.B., Clement, A., Fortes, E.D., den Bakker, H.C., Wiedmann, M., Ricke, S.C. (2012). *Listeria monocytogenes* and hemolytic *Listeria innocua* in poultry. *Poultry Science, 91*(9), 2158–2163. **https://doi.org/10.3382/ps.2012-02292**
28. Moura, A., Disson, O., Lavina, M., Thouvenot, P., Huang, L., Leclercq, A., Fredriksson-Ahomaa, M., Eshwar, A.K., Stephan, R., Lecuit, M. (2019). Atypical hemolytic *Listeria innocua* isolates are virulent, albeit less than *Listeria monocytogenes*. *Infection and Immunity*, *87*(4), art. no. e00758-18. **https://doi.org/10.1128/IAI.00758-18**
29. Nishibori, T., Cooray, K., Xiong, H., Kawamura, I., Fujita, M., Mitsuyama, M. (1995). Correlation between the presence of virulence-associated genes as determined by PCR and actual virulence to mice in various strains of *Listeria* spp. *Microbiology and Immunology*, *39*(5), 343–349. **https://doi.org/10.1111/j.1348-0421.1995.tb02211.x**
30. Notermans, S.H., Dufrenne, J., Leimeister-Wächter, M., Domann, E., Chakraborty, T. (1991). Phosphatidylinositol-specific phospholipase C activity as a marker to distinguish between pathogenic and nonpathogenic *Listeria* species. *Applied and Environmental Microbiology*, *57*(9), 2666–2670. **https://doi.org/10.1128/aem.57.9.2666-2670.1991**
31. Olaimat, A.N., Al-Holy, M.A., Shahbaz, H.M., Al-Nabulsi, A.A., Abu Ghoush, M.H., Osaili, T.M., Ayyash, M.M., Holley, R.A. (2018). Emergence of antibiotic resistance in *Listeria monocytogenes* isolated from food products: A comprehensive review. *Comprehensive Reviews in Food Science and Food Safety*, *17*(5), 1277–1292. **https://doi.org/10.1111/1541-4337.12387**
32. Osek, J., Wieczorek, K. (2022). *Listeria monocytogenes* – how this pathogen uses its virulence mechanisms to infect the hosts. *Pathogens*, *11*(12), art. no. 1491. **https://doi.org/10.3390/pathogens11121491**
33. Paillard D., Dubois V., Duran R., Nathier F., Guittet C., Caumette P., Quentin C. (2003). Rapid identification of *Listeria* species by using restriction fragment length polymorphism of PCR-amplified 23S rRNA gene fragments. *Applied and Environmental Microbiology*, 69(11), 6386–6392. **https://doi.org/10.1128/AEM.69.11.6386-6392.2003**
34. Park, Y.S., Lee, S.R., Kim, Y.G. (2006). Detection of *Escherichia coli* O157:H7, *Salmonella* spp., *Staphylococcus aureus* and *Listeria monocytogenes* in kimchi by multiplex polymerase chain reaction (mPCR). *Journal of Microbiology*, *44*(1), 92–97. **PMID: 16554723**v
35. Perrin, M., Bemer, M., Delamare, C. (2003). Fatal case of *Listeria innocua* bacteremia. *Journal of Clinical Microbiology*, *41*(11), 5308–5309. **https://doi.org/10.1128/JCM.41.11.5308-5309.2003**
36. Qi, Y., Cao, Q., Zhao, X., Tian, C., Li, T., Shi, W., Wei, H., Song, C., Xue, H., Gou, H. (2024). Comparative genomic analysis of pathogenic factors of *Listeria* spp. using whole-genome sequencing. *BMC Genomics, 25*, art. no. 935. **https://doi.org/10.1186/s12864-024-10849-3**
37. Ramadan, H., Al-Ashmawy, M., Soliman, A.M., Elbediwi, M., Sabeq, I., Yousef, M., Algammal, A.M., Hiott, L.M., Berrang, M.E., Frye, J.G., Jackson, C.R. (2023). Whole-genome sequencing of *Listeria innocua* recovered from retail milk and dairy products in Egypt. *Frontiers in Microbiology*, *14*, art. no. 1160244. **https://doi.org/10.3389/fmicb.2023.1160244**
38. Rocha, P.R., Dalmasso, A., Grattarola, C., Casalone, C., Del Piero, F., Bottero, M.T., Capucchio, M.T. (2013). Atypical cerebral listeriosis associated with *Listeria innocua* in a beef bull. *Research in Veterinary Science, 94*(1), 111–114. **https://doi.org/10.1016/j.rvsc.2012.07.017**
39. Rossi, F., Amadoro, C., Conficoni, D., Giaccone, V., Colavita, G. (2020). Occurrence, diversity of *Listeria* spp. isolates from food and food-contact surfaces and the presence of virulence genes. *Microorganisms*, *8*(2), art. no. 294. **https://doi.org/10.3390/microorganisms8020294**
40. Vilchis-Rangel, R.E., Espinoza-Mellado, M.D.R., Salinas-Jaramillo, I.J., Martinez-Peña, M.D., Rodas-Suárez, O.R. (2019). Association of *Listeria monocytogenes* LIPI-1 and LIPI-3 marker llsX with invasiveness. *Current Microbiology*, *76*(5), 637–643. **https://doi.org/10.1007/s00284-019-01671-2**
41. Volokhov, D.V., Duperrier, S., Neverov, A.A., George, J., Buchrieser, C., Hitchins, A.D. (2007). The presence of the internalin gene in natural atypically hemolytic *Listeria innocua* strains suggests descent from *Listeria monocytogenes. Applied and Environmental Microbiology, 73*(6), 1928–1939. **https://doi.org/10.1128/AEM.01796-06**
42. Wartha, S., Bretschneider, N., Dangel, A., Hobmaier, B., Hörmansdorfer, S., Huber, I., Murr, L., Pavlovic, M., Sprenger, A., Wenning, M., Alter, T., Messelhäußer, U (2023). Genetic characterization of *Listeria* from food of non-animal origin products and from producing and processing companies in Bavaria, Germany. *Foods, 12*(6), art. no. 1120. **https://doi.org/10.3390/foods12061120**
43. Wiktorczyk-Kapischke, N., Skowron, K., Wałecka-Zacharska, E. (2023). Genomic and pathogenicity islands of *Listeria monocytogenes* – overview of selected aspects. *Frontiers in Molecular Biosciences*, *10*, art. no. 1161486. **https://doi.org/10.3389/fmolb.2023.1161486**
44. Yong, S.S., Lee, J.I., Kang, D.H. (2024). Identifying a novel *Listeria innocua* subgroup and enhancing *Listeria* detection in grain: A duplex real-time PCR approach informed by comparative genomic analysis. *LWT – Food Science and Technology*, *199*, art. no. 116108. **https://doi.org/10.1016/j.lwt.2024.116108**
45. Zakrzewski, A.J., Chajęcka-Wierzchowska, W., Zadernowska, A., Podlasz, P. (2020). Virulence characterization of *Listeria monocytogenes*, *Listeria innocua*, and *Listeria welshimeri* isolated from fish and shrimp using *in vivo* early zebrafish larvae models and molecular study. *Pathogens*, *9*(12), art. no. 1028. **https://doi.org/10.3390/pathogens9121028**
46. Zanolli Moreno, L., Paixão, R., de Gobbi, D.D., Raimundo, D.C., Porfida Ferreira, T.S., Micke Moreno, A., Hofer, E., dos Reis, C.M., Matté, G.R., Matté, M.H. (2014). Phenotypic and genotypic characterization of atypical *Listeria monocytogenes* and *Listeria innocua* isolated from swine slaughterhouses and meat markets. *BioMed Research International*, *2014*, art. no. 742032. **https://doi.org/10.1155/2014/742032**
47. Zanolli Moreno, L., Paixão, R., Gobbi, D.D., Raimundo, D.C., Porfida Ferreira, T., Hofer, E., Matte, M.H., Micke Moreno, A. (2012). Characterization of atypical *Listeria innocua* isolated from swine slaughterhouses and meat markets. *Research in Microbiology*, *163*(4), 268–271. **https://doi.org/10.1016/j.resmic.2012.02.004**
48. Zhang, Y., Dong, S., Chen, H., Chen, J., Zhang, J., Zhang, Z., Yang, Y., Xu, Z., Zhan, L., Mei, L. (2019). Prevalence, genotypic characteristics and antibiotic resistance of Listeria monocytogenes from retail foods in Bulk in Zhejiang Province, China. *Frontiers in Microbiology*, 10, art. no. 1710. **https://doi.org/10.3389/fmicb.2019.01710**
49. Zhang, W., Knabel, S.J. (2005). Multiplex PCR assay simplifies serotyping and sequence typing of *Listeria monocytogenes* associated with human outbreaks. *Journal of Food Protection*, *68*(9), 1907–1910. **https://doi.org/10.4315/0362-028X-68.9.1907**

ORIGINAL ARTICLE
http://journal.pan.olsztyn.pl

Polish Journal of Food and Nutrition Sciences
2026, Vol. 76, No. 3, 288–300
DOI: 10.31883/pjfns/226183
ISSN 1230-0322, e-ISSN 2083-6007

Prebiotic Potential of *Polygonatum sibiricum* Red. Leaf Polysaccharides in Regulating Gut Microbiota to Alleviate Antibiotic-Associated Diarrhea

Qifan Zhang[1,#], Huiling Deng[2,3#], Xiurong Guo[1], Min Su[4], Nannan Wu[1], Yunbo Song[3], Qiuyu Liu[1], Aimin Fu[1], Can Song[1*]

[1]School of Pharmacy, Southwest Medical University, Luzhou, Sichuan, China
[2]School of Clinical Medicine, The First Affiliated Hospital of Chongqing Medical and Pharmaceutical College, China
[3]Chongqing Key Laboratory of Prevention and Treatment for Occupational Diseases and Poisoning, The First Affiliated Hospital of Chongqing Medical and Pharmaceutical College, Chongqing, China
[4]Key Laboratory of Condiment Supervision Technology for State Market Regulation, Chongqing Institute for Food and Drug Administration, Chongqing, China

Antibiotic-associated diarrhea (AAD) is a common adverse reaction primarily caused by gut microbiota dysbiosis. The polysaccharides from the *Polygonatum sibiricum* Red. leaves (PsPs) have been shown to possess gut microbiota-regulating activity. However, the efficacy of PsPs in alleviating AAD remains unclear. The purpose of this study was to investigate the efficacy of PsPs in alleviating AAD. First, PsPs were obtained by water extraction and ethanol precipitation. Subsequently, *in vitro* digestion and fecal fermentation were performed to evaluate the gastrointestinal stability of PsPs and the production of short-chain fatty acids (SCFAs). Thereafter, the AAD mice model was induced by lincomycin hydrochloride. The probiotic effects of PsPs were comprehensively analyzed by changes in C57BL/6J mice body weights, colonic histopathology and gut microbiota composition. *In vitro* results revealed that PsPs were resistant to digestive degradation (93.08%–93.34%), effectively reached the intestines, and was utilized by the gut microbiota, thereby reducing the proportion of *Klebsiella*, increasing the relative abundance of *Bifidobacterium*, and significantly increasing the SCFA yields. Animal experiment results show that PsPs intervention alleviates diarrhea in AAD mice, restores the damaged intestinal barrier, and reshapes the gut microbiota community, increasing the abundance of *Blautia* and reducing the abundance of *Klebsiella*. Moreover, PsPs reduced the levels of inflammatory factors (MCP-1, LPS, IL-6, TNF-α) in mice. This study demonstrates that PsPs foster prebiotic potential and offer new insights for the development of AAD adjunctive intervention strategies based on polysaccharides derived from food and medicine homology.

Keywords: bioactive polysaccharides, digestive stability, dysbiosis, fecal fermentation, intestine

INTRODUCTION

Antibiotic-associated diarrhea (AAD) is a common gastrointestinal adverse reaction associated with the clinical use of broad-spectrum antibiotics, and it is particularly prevalent among patients receiving antibiotic therapy [Zhang *et al.*, 2022]. AAD not merely affects patients' quality of life and treatment adherence, but may lead to complications such as dehydration, electrolyte imbalances, and *Clostridioides difficile* infection [Abad & Safdar, 2021]. Existing research indicates that the core pathogenesis of AAD lies in the "indiscriminate attack" of antibiotics on the gut microbiota, leading to an imbalance in the intestinal microecology and metabolic dysfunction [Ramirez *et al.*, 2020]. Specifically,

***Corresponding Author:**
E-mail: **cansong@swmu.edu.cn** (Dr. C. Song)
#These authors contributed equally to this work.

Submitted: 2 April 2026
Accepted: 21 July 2026
Published on-line: 29 July 2026

the amount of short-chain fatty acids (SCFAs), such as acetic and propionic acids, generated by gut microbial fermentation of dietary fiber, decreases significantly. Therefore, identifying intervention strategies that can effectively modulate the gut microbiota and restore SCFA levels is crucial for the prevention and treatment of AAD.

The gut microbiota, regarded as the body's "forgotten organ", serves a key function in preserving the health of the host [Wei *et al.*, 2024]. A close metabolic relationship exists between the gut microbiota and SCFAs. On the one hand, the gut microbiota secretes various carbohydrate-active enzymes to break down dietary fiber and polysaccharides, which are difficult for the host to digest, into monosaccharides or oligosaccharides, and then converted into SCFAs through metabolic pathways such as glycolysis and the pentose phosphate pathway. On the other hand, SCFAs, as key metabolic products of the microbiota, reciprocally regulate the composition and function of the gut microbiota, forming an interactive regulatory network among the microbiota, metabolites, and host [Hays *et al.*, 2024]. SCFAs exert a wide range of physiological effects: acetic acid, the most abundant short-chain fatty acid, regulates fat metabolism and appetite; propionic acid contributes to immune regulation and alleviates intestinal inflammation; butyric acid serves as the primary energy source for intestinal epithelial cells, promotes the expression of tight junction proteins, enhances intestinal barrier function, and maintains intestinal immune homeostasis. Accordingly, maintaining the dynamic balance between the gut microbiota structure and SCFAs metabolism is vital for the prevention and treatment of intestinal diseases.

In recent years, polysaccharides derived from medicinal and edible plants have demonstrated significant potential in modulating the gut microbiota due to their favorable safety profiles and notable prebiotic activity [Huang *et al.*, 2023; Liu *et al.*, 2024; Xu *et al.*, 2023]. These polysaccharides are typically resistant to degradation by human digestive enzymes but can be selectively utilized by the gut microbiota. *Polygonatum sibiricum* Red., a traditional and valuable edible-medicinal herb in China, has been extensively studied; its rhizomes have been shown to possess immunomodulatory, anti-inflammatory, and gut microbiota-regulating properties, with its polysaccharides considered the primary source of these bioactivities [Kuang *et al.*, 2024; Lai *et al.*, 2024]. However, during the cultivation and processing of *Polygonatum*, its aerial parts (leaves) are routinely discarded as waste, resulting in a significant waste of resources. Phytochemical studies have shown that *Polygonatum* leaves are also rich in polysaccharides, and their polysaccharides composition differs from that of the rhizomes, suggesting they may possess unique biological activities [Li *et al.*, 2022]. One should note that *Polygonatum* leaves have a history of culinary use in certain folk traditions across China; nevertheless, modern pharmacological research on them remains insufficient, particularly regarding their potential for regulating the gut microbiota and preventing or treating intestinal diseases. Given that the gut microbiota serves as a key bridge between dietary components and host health, studies on its response characteristics and metabolic transformation patterns regarding the *P. sibiricum* leaf polysaccharides (PsPs) in intestinal diseases are lacking.

Our previous research has shown that PsPs can increase the proportion of Firmicutes and reduce the abundance of Bacteroidetes in the gut microbiota of healthy mice, while significantly increasing SCFAs production [Luo *et al.*, 2022]. These results indicate that PsPs are promising candidates for prebiotic formulation development. Building on this, this study further investigates the alleviating effects of PsPs on AAD. We first extracted PsPs *via* water extraction and ethanol precipitation, and then evaluated their stability in the gastrointestinal environment, as well as their effects on microbial community structure and SCFAs production, through *in vitro* simulated digestion and human fecal fermentation experiments. Thereafter, the PsPs were evaluated for their effects on diarrhea symptoms, colonic histopathology and intestinal microbiota profile in C57BL/6J mice with AAD induced by lincomycin hydrochloride. The purpose of this study was to elucidate the beneficial effects of PsPs on AAD, with the goal of providing scientific evidence to support the high-value utilization of *Polygonatum* leaves (a non-traditional medicinal part), and offering new insights and experimental support for the development of AAD adjunctive intervention strategies based on polysaccharides derived from food-medicine dual-use sources.

MATERIALS AND METHODS

Materials and chemicals

Healthy mature *P. sibiricum* leaves harvested in Chongqing, China. Standard SCFAs were purchased from Sigma-Aldrich (Shanghai, China). Dextran standards were purchased from Aladdin Biochemical Technology Co., Ltd. (Shanghai, China). The reducing sugar assay kit was purchased from Solarbio Technology Co., Ltd. (Beijing, China). The total antioxidant capacity assay kit was purchased from Beyotime Biotechnology Co., Ltd. (Shanghai, China). The inflammatory cytokine assay kits used to determine monocyte chemoattractant protein-1 (MCP-1), lipopolysaccharide (LPS), interleukin-6 (IL-6), and tumor necrosis falpha (TNF-α) were purchased from ZCIBIO Technology Co. Ltd. (Shanghai, China). Anti-zonula occludens-1 (ZO-1) antibody was purchased from Wuhan Servicebio Co., Ltd. (Wuhan, China). The anti-zoocadin-1 and anti-zoocadin-2 antibodies were supplied by Proteintech Group Co., Ltd. (Chicago, IL, USA). The AnaeroPack anaerobic culture bags were purchased from Mitsubishi Chemical Analytech Co. Ltd (Tokyo, Japan).

Separation of leaf polysaccharides and their characterization

PsPs were obtained by extracting *P. sibiricum* leaves with water and precipitating with ethanol according to the method described in our previous study [Luo *et al.*, 2022]. Crushed leaves (2.5 kg) were soaked in water at twice their volume and heated in a 90°C water bath for 3 h. The extraction was repeated

three times. Then anhydrous ethanol at 1.5 volumes of the extraction liquid was added. After 24 h room-temperature standing, the solution was filtered to obtain crude polysaccharides. Afterward, the crude polysaccharides were dissolved in distilled water and decolorized by the macroporous resin. The crude polysaccharides solution was further purified using diethylaminoethyl (DEAE) cellulose, and then dialyzed in a dialysis bag (0.5–1.0 kDa) for 72 h. After dialysis, the purified polysaccharides were concentrated and freeze-dried to yield the dry powder. The monosaccharide composition of PsPs was: rhamnose (15.4%), arabinose (24%), glucose (8.8%), xylose (40.7%), mannose (6.6%), and galacturonic acid (4.5%) [Luo *et al.*, 2022]. The average molecular weight of PsPs was determined by high-performance gel-permeation chromatography (HPGPC) using an LC-2010 HPLC system (Shimadzu Corporation, Kyoto, Japan) with refractive index (RI) detector, equipped with a TSK-Gel GMPWXL column (7.8×300 mm, particle diameter 13 µm; Thermo Fisher Scientific, Waltham, MA, USA). The mobile phase consisted of a 0.02 M KH_2PO_4 solution. PsPs solutions (5 mg/mL) were filtered through a 0.22 µm filter membrane. Next, 20 µL of the filtered sample were injected into the HPLC column. A standard curve was prepared using dextran standards (1, 2, 30, 40, 70, 100, and 200 kDa). The average molecular weight of PsPs was calculated based on the calibration curve plotted using these dextran standards. The surface features and microstructure of the PsPs were characterized in detail using a SIGMA 300 scanning electron microscope (SEM; ZEISS, Oberkochen, Germany). Before analysis, the samples were given a gold coating under reduced pressure to improve conductivity and imaging quality. SEM photographs were taken at ×100 magnification.

In vitro models assessing leaf polysaccharides stability and microbial utilization

The *in vitro* models assessing PsPs stability and microbial utilization were conducted using modified versions of previously reported methods [Ma *et al.*, 2025; Zhao *et al.*, 2023]. PsPs (10 mg/mL) was dissolved in simulated saliva (primarily including NaCl, $NaHCO_3$, K_2CO_3; pH 6.8). Then equal volumes of simulated gastric (primarily including HCl, NaCl, pepsin; pH 1.5) and intestinal fluids (primarily including KH_2PO_4, K_2HPO_4, NaOH; pH 7.8) were added, and the mixture was incubated with shaking at 37°C to simulate the digestive process. At predetermined time points (0, 2 and 5 min) of salivary digestion, as well as 0.5, 1, 2 and 4 h of oral-gastric and oral-gastrointestinal digestion respectively, samples were collected for testing. The reaction mixture was heated in boiling water for 6 min. Heat treatment inactivated the digestive enzymes, thereby terminating the digestion. Subsequently, the total antioxidant capacity and reducing sugar content of the digested samples were determined employing commercial kits (Beyotime Biotechnology Co., Ltd. and Solarbio Technology Co., Ltd., respectively) and the microplate reader, and the total sugar content was measured using the phenol-sulfuric acid method with spectrophotometry [Dubois *et al.*, 1956]. The results of total antioxidant capacity were expressed as the amount of the antioxidant Trolox equivalent contained in each liter of solution. The results of reducing sugar content were expressed as the amount of mass of reducing sugars *per* milliliter of digesta solution. The results of total sugar content were expressed as the percentage by PsPs weight (%, *w/w*).

Fresh fecal samples were collected from three healthy male volunteers (aged 20–25 years) who had not taken antibiotics in the past three months, and the samples were mixed in equal volumes. Phosphate-buffered saline (PBS) was used to prepare a 10% (*w/v*) fecal suspension, which was then centrifuged (4°C, 908×*g*, 5 min). The resulting supernatant was blended with Luria-Bertani medium (without sugar source) containing PsPs (10 mg/mL) at a 1:9 (*v/v*) ratio to form the PsPs group. The blank control group (CN) was prepared in the same proportion without the addition of PsPs. The preparations were placed in AnaeroPack anaerobic culture bags. Anaerobic fermentation was conducted at 37°C for 24 h under conditions where oxygen concentration was below 0.1% and carbon dioxide concentration was maintained at approximately 10%. Finally, fermentation broths at 0, 6, 12, and 24 h were collected and centrifuged (4°C, 12,880×*g*, 3 min) to separate bacterial pellets from the fermentation supernatant for further microbial community and SCFAs analysis.

Animal experiments

Five-week-old male C57BL/6J mice were housed for 7 days in a standard facility (12 h light-dark cycle, 23±0.5°C, relative humidity 50±5%) to allow adaptation before the start of gavage administration. Thirty-two mice were randomly divided into four groups (*n*=8): AAD group, blank control group (CN), PsPs group, and natural recovery group (NR). The experiment involved continuous gavage for 10 days [Lai *et al.*, 2025]. CN group received twice-daily gavage of normal saline for 10 days. Remaining three groups were gavaged with 3 g/kg lincomycin hydrochloride daily twice for three days to induce AAD. Afterward, the PsPs group was gavaged with 300 mg/kg PsPs daily twice a day, and the NR group was gavaged daily with normal saline twice a day, for 7 days. Finally, the cecum, blood, and feces of four groups mice were collected for subsequent experimental analysis. All experiments were approved by the Ethics Committee of Southwest Medical University (SWMU, Luzhou, China), approval number swmu20250266.

16S ribosomal RNA sequencing and bioinformatics analysis

DNA extraction was performed on specimens derived from microbial fermentation and on mouse fecal matter with the QIAamp fast DNA stool mini kit (Qiagen, Hilden, NRW, DEU). Genomic DNA served as the template for PCR amplification of the 16S rRNA V3-V4 region, using the primers 338-F (5′-ACTCCTACGGGAGGCAGCAG-3′) and 806-R (5′-GGACTACHVGGGTWTCTAAT-3′) [Xu *et al.*, 2016]. And then, the PCR products were subjected to high-throughput sequencing at MajorBio Bio-Pharm Technology

Co., Ltd. (Shanghai, China). We utilized the MajorBio cloud platform (**https://cloud.majorbio.com**) to analyze the sequencing data. Quality control was performed on the sequencing reads, and they were assigned to amplicon sequence variant (ASV) clusters using a 100% similarity threshold. The identified ASVs were mapped to the Silva (SSU123) 16S rRNA database using the RDP classification algorithm (**http://rdp.cme.msu.edu**) to analyze their taxonomic characteristics. Alpha diversity was calculated using the MOTHUR software (version v.1.30.2; Patrick Schloss, Ann Arbor, MI, USA). Higher values of abundance-based coverage estimator (ACE) indicate greater species diversity, higher Shannon indices indicate higher species evenness, and higher Simpson indices indicate higher species concentration. A hierarchical clustering tree was constructed using the Bray-Curtis index *via* the Qiime2 software (Rob Knight, San Diego, CA, USA), followed by principal co-ordinates analysis (PCoA). The raw sequencing data and alignment information for the experimental samples are stored in the NCBI Sequence Read Archive (accession number: PRJNA1419527).

Short-chain fatty acid determination

The SCFA content in the supernatant of the fermentation broth was quantified using liquid chromatography–mass spectrometry (LC–MS/MS). Sample analysis was performed using an Exion-LC AD liquid chromatography system coupled with a QTRAP® 6500+ mass spectrometer (AB Sciex, Framingham, MA, USA). The procedure involved injecting 2 µL of the sample onto a BEH C18 (150×2.1 mm, 1.7 µm; Waters, Milford, MA, USA) column for chromatographic separation, followed by mass spectrometric detection. The mobile phase was composed of two solvents: A (water with 0.1% formic acid, *v/v*) and B (acetonitrile with 0.1% formic acid, *v/v*). Separation was achieved within 16 min at 40°C and a flow rate of 0.35 mL/min. The SCFAs were identified based on standards and literature references, and their content was quantified using a standard curve. The results were expressed as the mass of SCFA *per* milliliter of fermentation broth.

Tissue staining and immunofluorescence analysis

After formaldehyde fixation and paraffin embedding, cecal tissue sections were deparaffinized in xylene and rehydrated in ethanol. To examine histopathological changes, cecal sections were stained with hematoxylin and eosin (HE).

Cecal tissue sections were first fixed with formaldehyde and then washed with 100% ethanol. After incubation in a repair buffer and blocking with bovine serum albumin, the sections were incubated overnight at 4°C with ZO-1 antibody and anti-occludin-1 antibody. After incubation with Cy3-labeled ZO-1 antibody and FITC-labeled occludin-1 antibody, the sections were analyzed using an immunofluorescence microscope (Nikon, Tokyo, Japan).

Inflammatory factor measurement

The enzyme-linked immunosorbent assay (ELISA) kit (ZCIBIO Technology Co. Ltd.) was performed to determine the inflammatory cytokines profiles including MCP-1, LPS, IL-6, and TNF-α in mouse serum. After blood collection from the mice's eyes, the samples were kept stationary and then centrifuged to separate the supernatant serum, and the inflammatory factor concentrations were measured using the assay kit on the microplate reader (450 nm). The results of inflammatory factor concentrations were expressed as the amount of inflammatory cytokine *per* milliliter of serum.

Statistical analysis

Results from *in vitro* experiments were presented as the mean and standard deviation (SD) from three independent experiments. Results from animal experiments were expressed as the mean and SD from independent experiments of 8 mice per group. GraphPad Prism (v. 10.1.2; GraphPad Software, San Diego, CA, USA) and SPSS (v. 26; IBM, Armonk, New York, USA) were employed for statistical evaluation. Multigroup comparisons of body weight, colon length, and cytokine levels in animal experiments were performed using one-way analysis of variance (ANOVA). The *t*-test was used to analyze the results from the *in vitro* fermentation or to compare specific abundances between two groups. The α-diversity indices ACE, Shannon index and Simpson index were used the Kruskal–Wallis rank-sum test.

RESULTS AND DISCUSSION

Characterization of leaf polysaccharides

The average molecular weight of PsPs was $1.403\pm0.056\times10^5$ Da. SEM disclosed the microstructure of PsPs (**Figure S1** in Supplementary Materials). PsPs exhibits a flat, smooth, and porous lamellar morphology, which may allow it to be more effectively decomposed and utilized by the gut microbiota.

In vitro simulated digestion of leaf polysaccharides

As displayed in **Table 1**, the total sugar content of PsPs did not undergo significant changes ($p\geq0.05$) during the simulated digestion period, indicating that PsPs remained largely stable and was not extensively degraded under the simulated digestive conditions. The reducing sugar content of PsPs increased sharply upon initial contact with gastric digestive fluid and then gradually decreased (**Table 1**). The increase was likely due to the highly acidic environment of gastric fluid breaking some of the glycosidic bonds in PsPs, thus exposing more reducing ends on the sugar chains. This result is consistent with findings in the literature indicating that gastric stimulation affects reducing sugar content [Wu *et al.*, 2021]. In **Table 1**, the total antioxidant capacity of PsPs gradually decreases during digestion until it tends to stabilize.

In vitro simulated fermentation of leaf polysaccharides

The changes in total antioxidant capacity during the PsPs fermentation period are shown in **Table 2**. No significant ($p\geq0.05$) changes were observed during the first 6 h, followed by a continuous, significant ($p<0.05$) decrease. Results in **Table 2** show that the reducing sugar content in PsPs did not change significantly ($p\geq0.05$) during the first 6 h of fermentation but began to decrease markedly at 12 h. This could be attributed to the ongoing fermentation,

Table 1. Total sugar content, reducing sugar content, and total antioxidant capacity during *in vitro* digestion of *Polygonatum sibiricum* Red. leaf polysaccharides (PsPs).

Digestion stage	Total sugar content (%, *w/w*)	Reducing sugar content (mg/mL digesta solution)	Total antioxidant capacity (mmol TE/L digesta solution)
Undigested	93.08±0.98^{a}		
Oral digestion	92.82±1.10^{a}		
0 min		0.30±0.01^{f}	0.66±0.02^{a}
2 min		0.30±0.02^{f}	0.58±0.01^{b}
5 min		0.33±0.03^{f}	0.56±0.02^{b}
Oral-gastric digestion	94.81±0.92^{a}		
0.5 h		1.19±0.09^{e}	0.48±0.02^{c}
1 h		1.83±0.07^{a}	0.34±0.02^{d}
2 h		1.53±0.04^{ab}	0.31±0.02^{de}
4 h		1.49±0.03^{abc}	0.26±0.00^{ef}
Oral-gastrointestinal digestion	93.34±0.70^{a}		
0.5 h		1.44±0.08^{abc}	0.25±0.01^{fg}
1 h		1.39±0.01^{bc}	0.24±0.00^{fg}
2 h		1.34±0.02^{c}	0.26±0.02^{fg}
4 h		1.29±0.01^{d}	0.20±0.01^{g}

Data are mean ± standard deviation (n=3). Letter symbols: when the superscript letters are completely different in each column, a significant difference is indicated (p<0.05). TE, Trolox equivalent.

during which the sugar chains were further degraded for microbial consumption, leading to a decrease of reducing sugar content in the later fermentation phases. The above results indicate that PsPs may be utilized by microbial communities during the middle to late stages of *in vitro* fermentation.

The pH of the fermentation broth was recorded at specific time points (**Figure 1A**). In the unfermented state, no significant (p≥0.05) difference was observed between the PsPs and the CN group. During fermentation, the pH of the PsPs decreased at faster rates than the CN group.

As metabolic byproducts of bacterial fermentation, SCFAs play an essential role in maintaining gut homeostasis and enhancing intestinal barrier function. After 24 h fermentation, the total SCFA level in the PsPs group (131±3 μg/mL) was significantly (p<0.05) higher than in the CN group (86.4±2.1 μg/mL). In addition, the content of both main compounds in the SCFA profile, *i.e.*, acetic acid and propionic acid ,was substantially higher in the PsPs than in the CN group (**Figure 1B**). The elevated levels of acetic acid and propionic acid in the PsPs group were in line with our previous research findings in healthy mice [Luo *et al.*, 2022].

Microbial dynamics in the gut play pivotal roles in regulating host immunity and metabolic health. **Figure S2** in Supplementary Materials illustrate changes in the α-diversity of microbial communities in mixed fecal fermentation broth following 24 h fermentation, compared to broth supplemented with PsPs. After PsPs addition, the ACE showed no significant (p≥0.05) change, while the Shannon index increased, and the Simpson index decreased significantly (p<0.05). This indicates that sufficient sample data has been obtained for subsequent analysis. The sample-level hierarchical clustering tree constructed based on ASV levels (**Figure S3A** in Supplementary Materials) reveals significant intragroup similarities and intergroup differences in microbial community composition between the PsPs and CN groups. The microbial community composition of PsPs and CN at the phylum and genus levels are represented in **Figures S3B** and **C** in Supplementary Materials. Comparative analysis of fermentation results between the two sample groups at the phylum level (**Figure 1C**) demonstrates that PsPs significantly suppressed the Pseudomonadota proportion while significantly increasing the abundance of Bacillota, implying that PsPs have the potency to regulate gut microbiota dysbiosis [Voermans *et al.*, 2025]. PsPs also significantly enhanced the relative abundance of Bacteroidota, and the increase in both Bacteroidota and SCFAs suggests that PsPs may be beneficial for treating dysbiosis [Yu *et al.*, 2023]. At the genus level (**Figure 1D**), PsPs reduced the abundance of *Klebsiella* and *Escherichia-Shigella*, implying its potential to relieve AAD [Li *et al.*, 2023]. It is worth noting that PsPs have a significant promoting effect on *Bifidobacterium*, which may make them particularly effective in maintaining gut health and mitigating diarrhea symptoms [Hempel *et al.*, 2012]. Overall, PsPs possess prebiotic properties and may provide relief for AAD.

Interestingly, previous studies have shown that PsPs may contain β-glycosidic bonds and branched structures, which protect against degradation by host digestive enzymes while still allowing microbial carbohydrate-active enzymes (CAZymes) to break

Table 2. Total antioxidant capacity and reducing sugar content of broths during *in vitro* fermentation of *Polygonatum sibiricum* Red. leaf polysaccharides (PsPs).

Parameter	0 h	6 h	12 h	24 h
Total antioxidant capacity (mmol TE/L)	0.78±0.04^{a}	0.76±0.02^{a}	0.67±0.02^{b}	0.60±0.01^{c}
Reducing sugar content (mg/mL)	0.70±0.04^{a}	0.88±0.10^{a}	0.43±0.07^{b}	0.30±0.02^{b}

Data are mean ± standard deviation (n=3). Letter symbols: when the superscript letters are completely different in each row, a significant difference is indicated (p<0.05). TE, Trolox equivalent.

Figure 1. *In vitro* fermentation of PsPs. (**A**) Changes in pH during fermentation. (**B**) Profile of short-chain fatty acids (SCFAs) after fermentation. (**C**) and (**D**) The proportions in the abundance of bacteria at the phylum and genus level, respectively. CN, blank control group; PsPs, *Polygonatum sibiricum* Red. leaf polysaccharides group. *, **, ***, and ****indicate statistical significance at $p<0.05$, $p<0.01$, $p<0.001$, and $p<0.0001$, respectively.

down [Guan *et al.*, 2026; Subhash *et al.*, 2026]. The interactions among polysaccharide structure, gut microbiota metabolism, and host health are increasingly recognized as the fundamental mechanisms underlying the regulatory effects of polysaccharide prebiotics. Moreover, differences in monosaccharide composition and glycosidic bond configuration determine the selective fermentation patterns and subsequent metabolic outcomes [Zhang *et al.*, 2026]. The selective promotion of specific bacterial groups by PsPs may be related to the action of CAZymes, which are the primary enzymatic systems responsible for polysaccharide degradation in the gut microbiota. Glycosidase hydrolases (GHs) and polysaccharide lyases are organized into

polysaccharide utilization loci, enabling gut bacteria to recognize, bind, uptake, and degrade complex polysaccharides [Qu *et al.*, 2025]. The *Bifidobacterium* enrichment observed during PsPs fermentation is consistent with the characteristic of this genus, possessing multiple CAZymes specialized for the degradation of plant-derived polysaccharides [Pokusaeva *et al.*, 2011]. In detail, the *Bifidobacterium* possesses numerous glycoside hydrolase (GH) families targeting arabinoxylans and xylans, enabling it to efficiently ferment arabinoxylans and xylans commonly found in plants. Therefore, the significant proliferation effect of *Bifidobacterium* in PsPs likely reflects the metabolic specialization of *Bifidobacterium* in utilizing the structure of these polysaccharides, which are rich in arabinose and xylose. The monosaccharide composition of PsPs may partially explain these fermentation changes. Previous research indicates that the monosaccharide composition of dietary fiber influences gut microbiota composition and fermentation products, and that arabinose oligosaccharide structures selectively stimulate beneficial bacteria such as *Bifidobacterium* [Jensen *et al.*, 2024; Leschonski *et al.*, 2024]. Therefore, the increase in *Bifidobacterium* and SCFAs may be related to the high levels of xylose and arabinose in PsPs. Furthermore, the presence of minute amounts of galacturonic acid and rhamnose residues may imply the presence of pectin domains, as fermentation of these domains by intestinal pectin-degrading bacteria would yield acetate and propionate [Yüksel *et al.*, 2025].

Effects of leaf polysaccharides on mice

After successfully inducing the AAD model in mice, the mice were gavaged with PsPs or a normal saline solution for 7 days. During the gavage period, weights of mice in the AAD and NR groups decreased significantly, whereas in the PsPs group, weights gradually recovered nearing those of the CN group (**Figure S4A** in Supplementary Materials). Mice in the CN group showed positive behavioral responses, while the mice from the AAD and NR groups experienced evident diarrhea; in contrast, diarrhea symptoms were distinctly alleviated in the PsPs group. This demonstrates that PsPs has an ameliorative effect on AAD in mice. The colon lengths of the four groups of mice were compared (**Figure S4B** in Supplementary Materials). In AAD and NR groups, the colons were statistically shorter than in both the CN and PsPs groups, while no significant difference was detected between the CN and PsPs groups. This confirms successful modeling of AAD. These recovery patterns are similar to findings from natural polysaccharide studies, which suggest that they may alleviate AAD by restoring microbial fermentation, improving epithelial repair, and limiting inflammatory damage [Lai *et al.*, 2025; Xu *et al.*, 2023]. From a mechanistic perspective, the improvement in body weight, diarrhea symptoms, and colon length demonstrates that PsPs likely accelerate symptom recovery and may also promote the restoration of mucosal homeostasis following antibiotic-induced ecological disruption.

The arrow in the HE–stained images of cecal tissues of the AAD mice (**Figure 2A**) shows substantial inflammatory cell infiltration, verifying successful model development. In addition, the NR group exhibited more mucus accumulation compared to the PsPs and CN groups, implying that PsPs may possess certain restorative activity against intestinal pathology. The histological differences between the PsPs group and the NR group have potential biological significance, as natural recovery following antibiotic suspension may be insufficient to rapidly rehabilitate mucosal metabolism. Given that intestinal barrier dysfunction and LPS derived from the microbiota can exacerbate systemic inflammation [Di Vincenzo *et al.*, 2024], the attenuated inflammatory infiltration observed in the PsPs group supports a mechanism involving the microbiota-barrier-inflammation axis, not simply a cessation of diarrhea.

Tight junction proteins are vital for maintaining the integrity of the intestinal barrier. The impact of PsPs on tight junction proteins was investigated through immunofluorescence analysis (**Figure 2B**). Images with higher brightness indicate relatively stronger expression levels of the relevant indexes. Compared with the AAD and NR groups, PsPs could upregulate the expression of ZO-1 in the intestine, rendering the expression profile closer to the CN group. This demonstrates that PsPs have the capacity to strengthen intestinal barrier functions. It is possible that this is related to the microbial fermentation driven by PsPs.

Effects of leaf polysaccharides on the gut microbiota of mice

The relative abundance and diversity of species in the experimental groups were analyzed with α-diversity statistics. As evidenced in **Figure S5** in Supplementary Materials, there were statistical differences in the ACE, Shannon, and Simpson indexes across the four groups, reflecting alterations in the richness and evenness of the gut microbiota in mice following PsPs gavage. PCoA based on ASV levels demonstrated tight clustering of individuals within each group, with significant differences observed in the CN and AAD groups compared to the PsPs or NR groups (**Figure 3A**), as well as distinct separations between the PsPs and NR groups (**Figure 3B**). These results suggest that the microbial community composition in the PsPs and NR groups has undergone considerable modification compared to the CN and AAD groups, and furthermore, the microbial structure of the PsPs group differed significantly from the NR group. Moreover, compared with the AAD group, the PsPs group showed significant improvements in microbial richness and evenness.

Figure S6 in Supplementary Materials showcase the compositional differences in the gut microbiota across the four groups at the phylum and genus levels. As shown in **Figure 4A–C**, PsPs notably suppressed *Klebsiella* abundance compared to the NR; this is likely the primary factor contributing to AAD alleviation. However, in contrast to the outcomes of *in vitro* fermentation experiments, PsPs did not display an inhibitory effect on the proportion of *Escherichia-Shigella* in AAD animal experiments. It is particularly noteworthy that the *Blautia* content

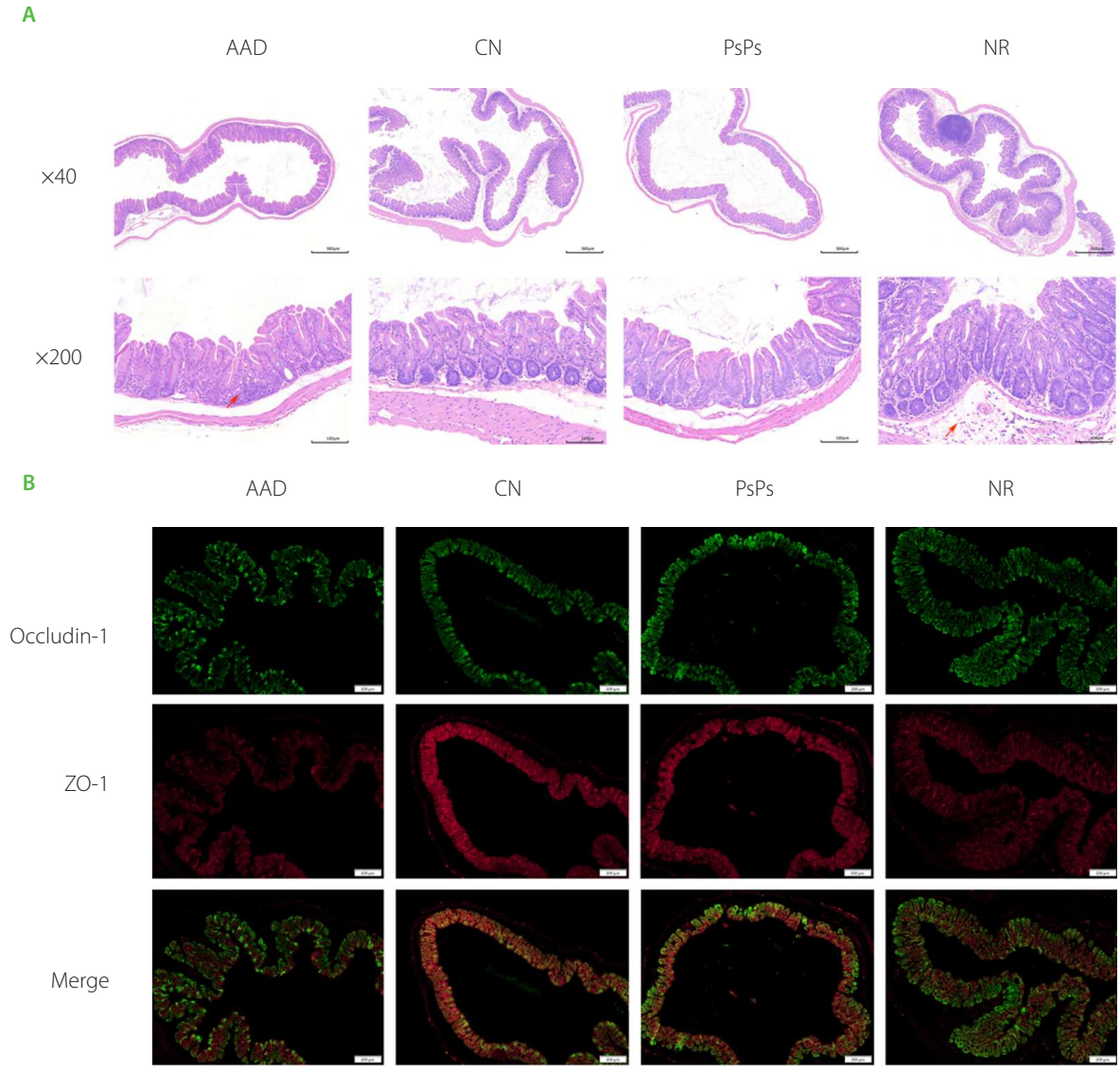

Figure 2. (**A**) Images of hematoxylin and eosin (HE) stained mice cecum (×40 and ×200). (**B**) Immunofluorescence microscope images of the mice cecum, with brighter fluorescence indicating higher expression levels. AAD, antibiotic-associated diarrhea group; CN, blank control group; PsPs, *Polygonatum sibiricum* Red. leaf polysaccharides group; NR, natural recovery group.

was significantly higher in the PsPs group than in the CN group, which may be the major factor facilitating the recovery of cecal tissue in the PsPs group. *Blautia* is a probiotic that helps balance host health [Liu *et al.*, 2021]. *Blautia* stimulates immune regulation, and increased concentrations are often accompanied with higher acetate production, which is supported by findings from *in vitro* fermentation experiments on augmented SCFA yields [Ye *et al.*, 2023]. And compared to the CN group, the richness of *Akkermansia* was also substantially higher in the PsPs group, which may be another important way PsPs supports gut wellness. These results all demonstrate that PsPs can alleviate AAD and confer prebiotic benefits. In the context of AAD, the selective inhibition of *Klebsiella* is particularly important, as antibiotic pressure often promotes the proliferation of facultative anaerobes and Enterobacteriaceae. This increases the endotoxin burden and exacerbates epithelial inflammation. Therefore, the diminished *Klebsiella* levels in the PsPs group suggest that PsPs may have attenuated the inflammation-driving response triggered by pathogen-associated microbiota. The enrichment of *Blautia* may promote epithelial repair through acetic acid production and mucus maintenance, which aligns with reports that SCFAs sourced from *Blautia* support colonic mucus function [Holmberg *et al.*, 2024]. The increase in *Akkermansia* is also noteworthy, as this mucus-associated bacterium is involved in mucus layer renewal as well as host metabolic and immune homeostasis [Ioannou *et al.*, 2025]. Remarkably, because the initial microbial communities in the feces of healthy humans differ from those in mouse feces, this complex ecosystem has prevented the inhibitory effect of PsPs on microbial communities observed through *in vitro* fermentation, which was not fully reproduced in the disease mouse model. Similar observation has also been made in our previous research [Ma *et al.*, 2025]. Although some microbial changes in the PsPs group tended toward the NR group, they also exhibited distinct differences in overall microbiota composition

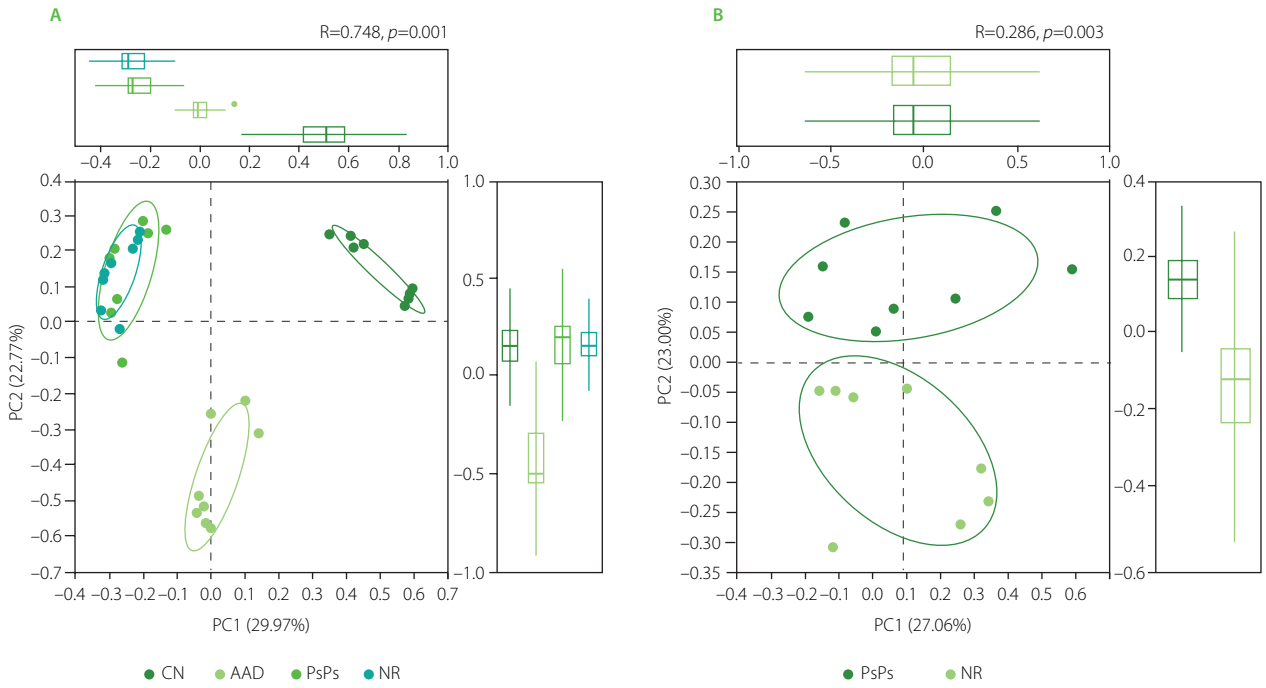

Figure 3. The effect of PsPs on mice gut microbiota. (**A**) Plot of principal co-ordinates analysis (PCoA) of gut microbiota in four groups on amplicon sequence variant (ASV) level. (**B**) Plot of PCoA of gut microbiota in PsPs and NR groups on ASV level. AAD, antibiotic-associated diarrhea group; CN, blank control group; PsPs, *Polygonatum sibiricum* Red. leaf polysaccharides group; NR, natural recovery group.

in the PCoA, suggesting that PsPs administration in mice might not only promote recovery but also increase the proportion of certain beneficial bacteria compared to natural recovery. Taken together, the *in vivo* microbial profile suggests PsPs may shift the post-antibiotic ecosystem from a state dominated by pathogenic commensals to a microbiota that supports metabolism and barrier function.

Effects of leaf polysaccharides on serum cytokine levels

Inflammatory cytokine levels are closely associated with disease development. Changes in serum cytokine levels in AAD mice after PsPs gavage intervention are shown in **Table 3**. The concentrations of MCP-1, LPS, IL-6, and TNF-α in the PsPs group were significantly lower than in the AAD and NR group, and there was no obvious difference in the levels of MCP-1, IL-6, and TNF-α between the PsPs and CN group. MCP-1 is intimately connected with numerous inflammatory diseases [Singh *et al.*, 2021]. Raised MCP-1 expression in the AAD group signifies successful model induction, while MCP-1 in PsPs declines to near the CN group level, reflecting an effective attenuation of the inflammatory response triggered by AAD. The elevation of LPS is related to gut microbiota dysbiosis and intestinal barrier dysfunction [Di Vincenzo *et al.*, 2024]. Compared to the AAD and NR group, the LPS contents in the PsPs group were considerably lower, which may be attributed to the fact that PsPs could modulate the microbiota composition and enhance the ZO-1 expression of the intestinal barrier. Overall, the reduction in cytokine levels demonstrates that PsPs possess pronounced anti-inflammatory activity *in vivo* and can mitigate the inflammatory reaction elicited by AAD. Notably, these responses may be linked to previously observed modifications in gut flora, hinting that PsPs may exercise its immunomodulatory function *via* the gut-immune axis [Dinakis *et al.*, 2024]. Decreases in MCP-1 levels indicate reduced chemotactic recruitment of monocytes and macrophages, while decreased levels of IL-6 and TNF-α suggest that pro-inflammatory cascades are restrained. Considering the reduced LPS levels and the restoration of ZO-1 staining, these data suggest that PsPs may alleviate systemic inflammation by limiting the transport of endotoxins through the diseased intestinal barrier.

These findings also support the potential of PsPs for application in animal nutrition. In poultry, the addition of *P. sibiricum* polysaccharides to feed enhances growth performance, antioxidant capacity, intestinal structure, and the gut microbiota [Yang *et al.*, 2024]. Therefore, PsPs also hold promise as a low-cost prebiotic feed ingredient; however, their dosage, safety, palatability, and cost-effectiveness for different species require further validation. Nevertheless, this study has certain limitations, such as the use of only 16S rRNA sequencing and the absence of experiments with positive controls. In addition to the perspective of feed composition, future research should transition from static endpoint observations to dynamic intestinal physiological models. "Gut-on-a-chip" platforms can replicate luminal flow, shear stress, mucus secretion, the epithelium-endothelium compartment, immune cell interactions, and peristaltic-like mechanical signals, thereby establishing a controllable bridge between anaerobic fermentation and animal models [Taavitsainen *et al.*, 2024]. A recent platform integrating human fecal microbiota and peristaltic-like movements reveals that multi-omics readouts can be used to replicate and monitor

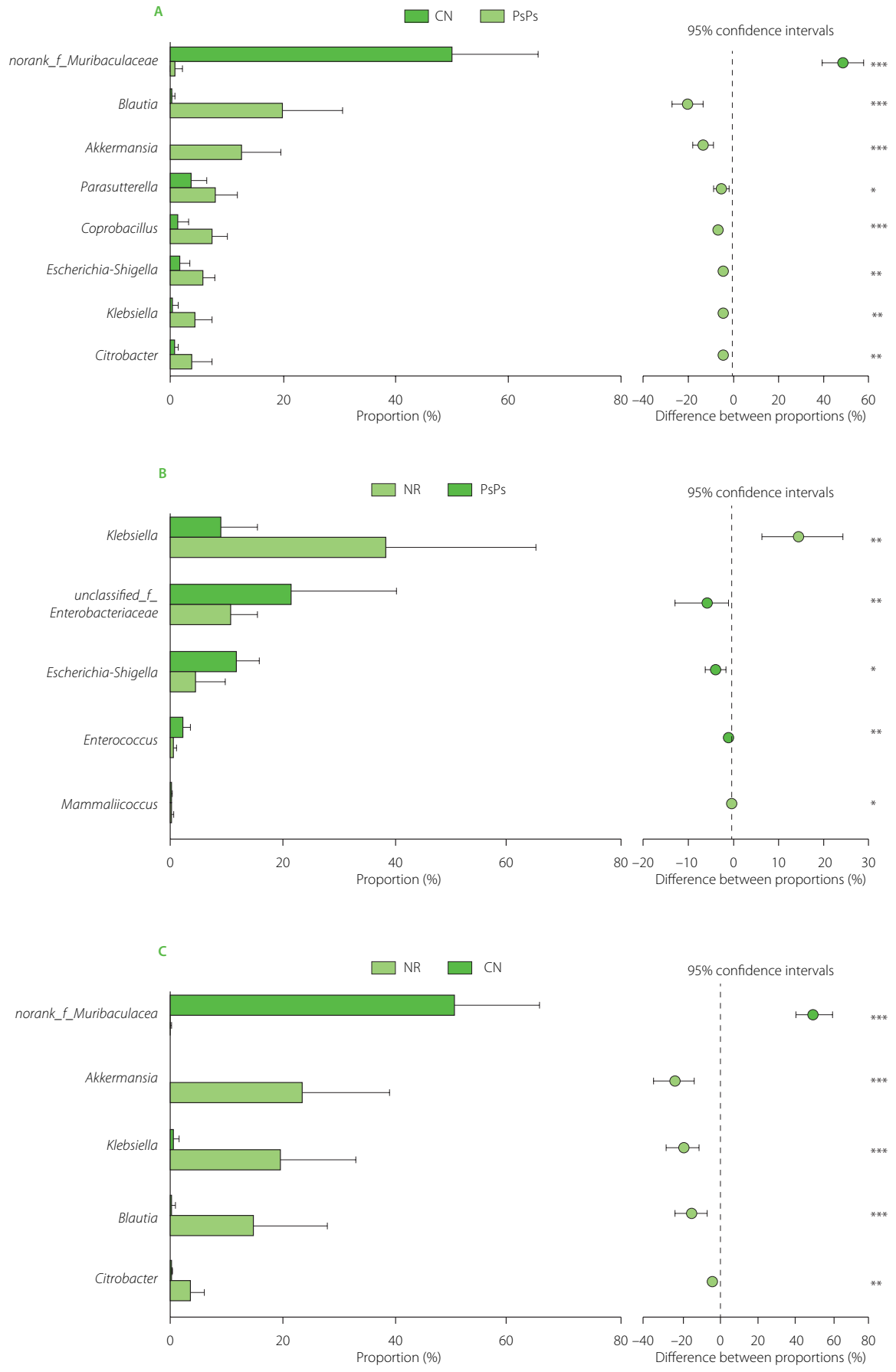

Figure 4. Comparison of the mice gut microbiota: (**A**) CN and PsPs groups, (**B**) PsPs and NR groups, and (**C**) CN and NR groups. CN, blank control group; PsPs, *Polygonatum sibiricum* Red. leaf polysaccharides group; NR, natural recovery group. *, **, and *** indicate statistical significance at $p<0.05$, $p<0.01$, and $p<0.001$, respectively.

Table 3. Serum cytokine levels in mice from experimental groups.

Cytokine	AAD	CN	PsPs	NR
MCP-1 (pg/mL)	39.6±5.9^{a}	25.4±2.8^{b}	28.6±1.2^{b}	37.6±5.2^{a}
LPS (EU/L)	37.8±3.0^{a}	20.3±1.5^{d}	25.2±2.0^{c}	32.1±2.5^{b}
IL-6 (pg/mL)	257.6±22.9^{a}	200.1±16.0^{c}	201.0±13.7^{c}	230.7±17.7^{b}
TNF-α (pg/mL)	689.5±63.4^{a}	500.4±36.9^{c}	527.7±35.1^{c}	619.6±42.8^{b}

Data are mean ± standard deviation (n=8). Letter symbols: when the superscript letters in each column are completely different, a significant difference is indicated (p<0.05). MCP-1, monocyte chemoattractant protein-1; LPS, lipopolysaccharide; IL-6, interleukin-6; TNF-α, tumor necrosis factor-alpha; AAD, antibiotic-associated diarrhea group; CN, blank control group; PsPs, *Polygonatum sibiricum* Red. leaf polysaccharides group; NR, natural recovery group.

host-microbiome interactions and barrier responses [Ballerini *et al.*, 2025]. For PsPs, such systems will enable real-time assessment of changes in mucus kinetics, cytokine release, and microbial metabolites under antibiotic interference and PsPs intervention. In parallel, complementary multi-omics analyses will provide further insight into the mechanisms underlying the detected 16S rRNA changes. Broad-range metagenomics will determine whether the increase in *Blautia* and *Akkermansia* is accompanied by enrichment of CAZymes and SCFAs synthesis pathways, or depletion of the pathogenic bacterium *Klebsiella*. Targeted and untargeted metabolomics can link microbiome changes to SCFAs and inflammatory lipid mediators, while metabolome-transcriptomics or metabolic modeling can reveal whether these pathways are transcriptionally active [Dell'Olio *et al.*, 2024; Go *et al.*, 2024]. This strategy helps distinguish taxa solely associated with recovery from microbial functions that may mediate barrier repair and anti-inflammatory effects.

CONCLUSIONS

This study investigated the alleviating effects of PsPs on AAD mice model and its potential mechanisms. PsPs exhibits gastrointestinal stability *in vitro*, enables utilization by gut microbiota, promotes the generation of SCFAs through fermentation, and reshapes the microbial community by reducing conditionally pathogenic and disease-causing bacterial genera (such as *Klebsiella* and *Escherichia-Shigella*) *in vitro*, while increasing beneficial or barrier-associated taxa (including *Blautia* and *Akkermansia*) *in vivo*. In mouse models, PsPs alleviated diarrhea-related phenotypes, improved colonic length and cecal histological structure, enhanced ZO-1 expression, and reduced serum levels of MCP-1, LPS, IL-6, and TNF-α. Conclusively, we hypothesize that PsPs may alleviate AAD by modulating the gut microbiota – SCFAs – barrier – inflammation axis, wherein the restoration of microbial fermentation function and the suppression of pathogen-associated endotoxin stress jointly promote epithelial repair and immune rebalancing. This work provides scientific evidence for the high-value utilization of the non-traditional application part of *Polygonatum* leaves, and offers new insights toward developing applications of polysaccharides derived from food and medicine homology in the fields of functional foods and pharmaceuticals.

RESEARCH FUNDING

This work supported by Horizontal scientific research project of the First Affiliated Hospital of Chongqing Medical and Pharmaceutical College (Chongqing Medical and Pharmaceutical College, Grant No. 2025YGZKY11).

CONFLICT OF INTERESTS

The authors declare no competing financial interests.

ADDITIONAL INFORMATION

The animal study was approved by the Ethics Committee of the Animal Experimentation Center of Southwest Medical University (approval number swmu20250266). The study was conducted in accordance with the local legislation and institutional requirements.

SUPPLEMENTARY MATERIALS

The following are available online at **https://journal.pan.olsztyn.pl/Prebiotic-Potential-of-Polygonatum-sibiricum-Red-Leaf-Polysaccharides-in-Regulating,226183,0,2.html**; **Figure S1**. Scanning electron microscope (SEM) images of *Polygonatum sibiricum* Red. leaf polysaccharides (×100). **Figure S2**. *In vitro* fermentation of PsPs. (A) Abundance-based coverage estimator (ACE). (B) Shannon index. (C) Simpson index. ASV, amplicon sequence variant; CN, blank control group; PsPs, *Polygonatum sibiricum* Red. Leaf polysaccharides group. * indicates statistical significance at p<0.05. **Figure S3**. *In vitro* fermentation of PsPs. (A) Hierarchical clustering tree of CN and PsPs. (B) and (C) Composition of gut microbiota at the phylum and genus level, respectively. CN, blank control group; PsPs, *Polygonatum sibiricum* Red. leaf polysaccharides group. **Figure S4**. The effect PsPs on (A) body weight and (B) colon length in mice. AAD, antibiotic-associated diarrhea group; CN, blank control group; PsPs, *Polygonatum sibiricum* Red. leaf polysaccharides group; NR, natural recovery group. *, ***, and **** indicate statistical significance at p<0.05, p<0.001, and p<0.0001, respectively. **Figure S5**. The effect of PsPs on mice gut microbiota. (A) Abundance-based coverage estimator. (B) Shannon index. (C) Simpson index. AAD, antibiotic-associated diarrhea group; CN, blank control group; PsPs, *Polygonatum sibiricum* Red. leaf polysaccharides group;

NR, natural recovery group. *** indicate statistical significance at $p<0.001$. **Figure S6**. The effect of PsPs on mice gut microbiota. (A) and (B) Composition of gut microbiota at the phylum and genus level, respectively. AAD, antibiotic-associated diarrhea group; CN, blank control group; PsPs, *Polygonatum sibiricum* Red. leaf polysaccharides group; NR, natural recovery group.

ORCID IDs

H. Deng https://orcid.org/0009-0002-5020-1292
A. Fu https://orcid.org/0000-0002-8837-5784
X. Guo https://orcid.org/0009-0002-2353-0605
Q. Liu https://orcid.org/0009-0008-7253-5342
C. Song https://orcid.org/0000-0001-8518-1549
Y. Song https://orcid.org/0009-0005-8630-7584
M. Su https://orcid.org/0009-0003-7941-3296
N. Wu https://orcid.org/0009-0004-9053-7182
Q. Zhang https://orcid.org/0009-0006-2444-7087

REFERENCES

1. Abad, C.L.R., Safdar, N. (2021). A review of *Clostridioides difficile* infection and antibiotic-associated diarrhea. *Gastroenterology Clinics of North America*, *50*(2), 323-340. https://doi.org/10.1016/j.gtc.2021.02.010
2. Ballerini, M., Galiè, S., Tyagi, P., Catozzi, C., Raji, H., Nabinejad, A., Macandog, A.D.G., Cordiale, A., Slivinschi, B.I., Kugiejko, K.K., Freisa, M., Occhetta, P., Wargo, J.A., Ferrucci, P.F., Cocorocchio, E., Segata, N., Vignati, A., Morgun, A., Deleidi, M., Manzo, T., Rasponi, M., Nezi, L. (2025). A gut-on-a-chip incorporating human faecal samples and peristalsis predicts responses to immune checkpoint inhibitors for melanoma. *Nature Biomedical Engineering*, *9*(6), 967-984. https://doi.org/10.1038/s41551-024-01318-z
3. Dell'Olio, A., Scott, W.T., Jr., Taroncher-Ferrer, S., San Onofre, N., Soriano, J.M., Rubert, J. (2024). Tailored impact of dietary fibers on gut microbiota: a multi-omics comparison on the lean and obese microbial communities. *Microbiome*, *12*(1), art. no. 250. https://doi.org/10.1186/s40168-024-01975-x
4. Di Vincenzo, F., Del Gaudio, A., Petito, V., Lopetuso, L.R., Scaldaferri, F. (2024). Gut microbiota, intestinal permeability, and systemic inflammation: a narrative review. *Internal and Emergency Medicine*, *19*(2), 275-293. https://doi.org/10.1007/s11739-023-03374-w
5. Dinakis, E., O'Donnell, J.A., Marques, F.Z. (2024). The gut-immune axis during hypertension and cardiovascular diseases. *Acta Physiologica*, *240*(8), art. no. e14193. https://doi.org/10.1111/apha.14193
6. Dubois, M., Gilles, K.A., Hamilton, J.K., Rebers, P.A., Smith, F.J.A.C. (1956). Colorimetric method for determination of sugars and related substances. *Analytical Chemistry, 28*(3), 350-356. https://doi.org/10.1021/ac60111a017
7. Go, D., Yeon, G.H., Park, S.J., Lee, Y., Koh, H.G., Koo, H., Kim, K.H., Jin, Y.S., Sung, B.H., Kim, J. (2024). Integration of metabolomics and other omics: from microbes to microbiome. *Applied Microbiology and Biotechnology*, *108*(1), art. no. 538. https://doi.org/10.1007/s00253-024-13384-z
8. Guan, Y., Li, R., Lv, Z., Bo, N., Wang, T., Guo, Y., Liang, Z., Zhang, J., Fan, Q., Dang, L., Zhao, M., Chen, J. (2026). The change in structure and improvement of anti-aging effects of polysaccharides in Polygonati Rhizoma after the traditional "Nine Steaming-Nine Sun-Drying". *Carbohydrate Polymers*, *373*, art. no. 124597. https://doi.org/10.1016/j.carbpol.2025.124597
9. Hays, K.E., Pfaffinger, J.M., Ryznar, R. (2024). The interplay between gut microbiota, short-chain fatty acids, and implications for host health and disease. *Gut Microbes*, *16*(1), art. no. 2393270. https://doi.org/10.1080/19490976.2024.2393270
10. Hempel, S., Newberry, S.J., Maher, A.R., Wang, Z., Miles, J.N., Shanman, R., Johnsen, B., Shekelle, P.G. (2012). Probiotics for the prevention and treatment of antibiotic-associated diarrhea: a systematic review and meta-analysis. *JAMA*, *307*(18), 1959-1969. https://doi.org/10.1001/jama.2012.3507
11. Holmberg, S.M., Feeney, R.H., Prasoodanan, P.K.V., Puértolas-Balint, F., Singh, D.K., Wongkuna, S., Zandbergen, L., Hauner, H., Brandl, B., Nieminen, A.I., Skurk, T., Schroeder, B.O. (2024). The gut commensal *Blautia* maintains colonic mucus function under low-fiber consumption through secretion of short-chain fatty acids. *Nature Communications*, *15*(1), art. no. 3502. https://doi.org/10.1038/s41467-024-47594-w
12. Huang, S., Zou, Y., Tang, H., Zhuang, J., Ye, Z., Wei, T., Lin, J., Zheng, Q. (2023). *Cordyceps militaris* polysaccharides modulate gut microbiota and improve metabolic disorders in mice with diet-induced obesity. *Journal of the Science of Food and Agriculture*, *103*(4), 1885-1894. https://doi.org/10.1002/jsfa.12409
13. Ioannou, A., Berkhout, M.D., Geerlings, S.Y., Belzer, C. (2025). *Akkermansia muciniphila*: biology, microbial ecology, host interactions and therapeutic potential. *Nature Reviews Microbiology*, *23*(3), 162-177. https://doi.org/10.1038/s41579-024-01106-1
14. Jensen, N., Maldonado-Gomez, M., Krishnakumar, N., Weng, C.Y., Castillo, J., Razi, D., Kalanetra, K., German, J.B., Lebrilla, C.B., Mills, D.A., Taft, D.H. (2024). Dietary fiber monosaccharide content alters gut microbiome composition and fermentation. *Applied and Environmental Microbiology*, *90*(8), art. no. e0096424. https://doi.org/10.1128/aem.00964-24
15. Kuang, S., Liu, Z., Liu, L., Fu, X., Sheng, W., Hu, Z., Lin, C., He, Q., Chen, J., Gao, S. (2024). *Polygonatum sibiricum* polysaccharides protect against knee osteoarthritis by inhibiting the TLR2/NF-κB signaling pathway *in vivo* and *in vitro*. *International Journal of Biological Macromolecules*, *274*(Pt 1), art. no. 133137. https://doi.org/10.1016/j.ijbiomac.2024.133137
16. Lai, W., Ning, Q., Wang, G., Gao, Y., Liao, S., Tang, S. (2024). Antitumor activity of *Polygonatum sibiricum* polysaccharides. *Archives of Pharmacal Research*, *47*(8-9), 696-708. https://doi.org/10.1007/s12272-024-01511-3
17. Lai, Y., Zhang, Q., Xu, M., Guo, X., Zhou, Q., Liu, Q., Deng, H., Song, C. (2025). Restoration of antibiotic associated diarrhea induced gut microbiota disorder by using *Dictyophora indusiata* water-insoluble polysaccharides in C57BL/6J mice. *Frontiers in Nutrition*, *12*, art. no. 1607365. https://doi.org/10.3389/fnut.2025.1607365
18. Leschonski, K.P., Mortensen, M.S., Hansen, L.B.S., Krogh, K., Kabel, M.A., Laursen, M.F. (2024). Structure-dependent stimulation of gut bacteria by arabinoxylo-oligosaccharides (AXOS): a review. *Gut Microbes*, *16*(1), art. no. 2430419. https://doi.org/10.1080/19490976.2024.2430419
19. Li, J., Hsiung, S.Y., Kao, M.R., Xing, X., Chang, S.C., Wang, D., Hsieh, P.Y., Liang, P.H., Zhu, Z., Cheng, T.R., Shie, J.J., Liou, J.P., Abbott, D.W., Kwon, S.W., Hsieh, Y.S.Y. (2022). Structural compositions and biological activities of cell wall polysaccharides in the rhizome, stem, and leaf of *Polygonatum odoratum* (Mill.) Druce. *Carbohydrate Research*, *521*, art. no. 108662. https://doi.org/10.1016/j.carres.2022.108662
20. Li, W., Zhang, S., Wang, Y., Bian, H., Yu, S., Huang, L., Ma, W. (2023). Complex probiotics alleviate ampicillin-induced antibiotic-associated diarrhea in mice. *Frontiers in Microbiology*, *14*, art. no. 1156058. https://doi.org/10.3389/fmicb.2023.1156058
21. Liu, W., Zhang, Y., Zheng, M., Ye, Y., Shi, M., Wang, X., Cao, L., Wang, L. (2024). Polysaccharides in medicinal and food homologous plants regulate intestinal flora to improve type 2 diabetes: Systematic review. *Phytomedicine*, *134*, art. no. 156027. https://doi.org/10.1016/j.phymed.2024.156027
22. Liu, X., Mao, B., Gu, J., Wu, J., Cui, S., Wang, G., Zhao, J., Zhang, H., Chen, W. (2021). *Blautia* – a new functional genus with potential probiotic properties? *Gut Microbes*, *13*(1), art. no. 1875796. https://doi.org/10.1080/19490976.2021.1875796
23. Luo, Y., Fang, Q., Lai, Y., Lei, H., Zhang, D., Niu, H., Wang, R., Song, C. (2022). Polysaccharides from the leaves of *Polygonatum sibiricum* Red. regulate the gut microbiota and affect the production of short-chain fatty acids in mice. *AMB Express*, *12*(1), art. no. 35. https://doi.org/10.1186/s13568-022-01376-z
24. Ma, L., Zhang, Q., Lai, Y., Long, X., Wang, F., Feng, B., Guo, X., Liu, Q., Song, C. (2025). The sulfated modification of polysaccharide from *Poria cocos* and its prebiotic effects on gut microbiota. *Journal of the Science of Food and Agriculture*, *105*(14), 7853-7867. https://doi.org/10.1002/jsfa.70037
25. Pokusaeva, K., Fitzgerald, G.F., van Sinderen, D. (2011). Carbohydrate metabolism in *Bifidobacteria*. *Genes & Nutrition*, *6*(3), 285-306. https://doi.org/10.1007/s12263-010-0206-6
26. Qu, Z., Liu, H., Yang, J., Zheng, L., Huang, J., Wang, Z., Xie, C., Zuo, W., Xia, X., Sun, L., Zhou, Y., Xie, Y., Lu, J., Zhu, Y., Yu, L., Liu, L., Zhou, H., Dai, L., Leung, E.L. (2025). Selective utilization of medicinal polysaccharides by human gut *Bacteroides* and *Parabacteroides* species. *Nature Communications*, *16*(1), art. no. 638. https://doi.org/10.1038/s41467-025-55845-7
27. Ramirez, J., Guarner, F., Bustos Fernandez, L., Maruy, A., Sdepanian, V.L., Cohen, H. (2020). Antibiotics as major disruptors of gut microbiota. *Frontiers in Cellular and Infection Microbiology*, *10*, art. no. 572912. https://doi.org/10.3389/fcimb.2020.572912
28. Singh, S., Anshita, D., Ravichandiran, V. (2021). MCP-1: Function, regulation, and involvement in disease. *International Immunopharmacology*, *101*(Pt B), art. no. 107598. https://doi.org/10.1016/j.intimp.2021.107598

29. Subhash, A.J., Abdin, M., Bamigbade, G.B., Arachchi, M.P., Ullah, N., Ayyash, M. (2026). A comprehensive review on structural, chemical, and functional perspectives of dietary polysaccharide-driven gut microbiota modulation: Mechanisms and challenges. *Biochemistry and Biophysics Reports*, *46*, art. no. 102575.
https://doi.org/10.1016/j.bbrep.2026.102575
30. Taavitsainen, S., Juuti-Uusitalo, K., Kurppa, K., Lindfors, K., Kallio, P., Kellomäki, M. (2024). Gut-on-chip devices as intestinal inflammation models and their future for studying multifactorial diseases. *Frontiers in Lab on a Chip Technologies, 2*, art. no. 1337945.
https://doi.org/10.3389/frlct.2023.1337945
31. Voermans, B., Gerdes, V., Nieuwdorp, M. (2025). Gut microbiota alterations and their role in the pathophysiology of obesity following bariatric surgery. *Expert Review of Endocrinology & Metabolism*, *20*(4), 291-305.
https://doi.org/10.1080/17446651.2025.2512551
32. Wei, X., Wang, F., Tan, P., Huang, H., Wang, Z., Xie, J., Wang, L., Liu, D., Hu, Z. (2024). The interactions between traditional Chinese medicine and gut microbiota in cancers: Current status and future perspectives. *Pharmacological Research*, *203*, art. no. 107148.
https://doi.org/10.1016/j.phrs.2024.107148
33. Wu, D.-T., Nie, X.-R., Gan, R.-Y., Guo, H., Fu, Y., Yuan, Q., Zhang, Q., Qin, W. (2021). *In vitro* digestion and fecal fermentation behaviors of a pectic polysaccharide from okra (*Abelmoschus esculentus*) and its impacts on human gut microbiota. *Food Hydrocolloids*, *114*, art. no. 106577.
https://doi.org/10.1016/j.foodhyd.2020.106577
34. Xu, H., Wang, S., Jiang, Y., Wu, J., Chen, L., Ding, Y., Zhou, Y., Deng, L., Chen, X. (2023). *Poria cocos* polysaccharide ameliorated antibiotic-associated diarrhea in mice *via* regulating the homeostasis of the gut microbiota and intestinal mucosal barrier. *International Journal of Molecular Sciences*, *24*(2), art. no. 1423.
https://doi.org/10.3390/ijms24021423
35. Xu, N., Tan, G., Wang, H., Gai, X.J.E.J.o.S.B. (2016). Effect of biochar additions to soil on nitrogen leaching, microbial biomass and bacterial community structure. *European Journal of Soil Biology, 74*, 1-8.
https://doi.org/10.1016/j.ejsobi.2016.02.004
36. Yang, B., Li, X., Mesalam, N.M., Elsadek, M.F., Abdel-Moneim, A.E. (2024). The impact of dietary supplementation of polysaccharide derived from *Polygonatum sibiricum* on growth, antioxidant capacity, meat quality, digestive physiology, and gut microbiota in broiler chickens. *Poultry Science*, *103*(6), art. no. 103675.
https://doi.org/10.1016/j.psj.2024.103675
37. Ye, L., Hou, Y., Hu, W., Wang, H., Yang, R., Zhang, Q., Feng, Q., Zheng, X., Yao, G., Hao, H. (2023). Repressed *Blautia*-acetate immunological axis underlies breast cancer progression promoted by chronic stress. *Nature Communications*, *14*(1), art. no. 6160.
https://doi.org/10.1038/s41467-023-41817-2
38. Yu, Z., Li, D., Sun, H. (2023). Herba Origani alleviated DSS-induced ulcerative colitis in mice through remolding gut microbiota to regulate bile acid and short-chain fatty acid metabolisms. *Biomedicine & Pharmacotherapy*, *161*, art. no. 114409.
https://doi.org/10.1016/j.biopha.2023.114409
39. Yüksel, E., Voragen, A.G.J., Kort, R. (2025). The pectin metabolizing capacity of the human gut microbiota. *Critical Reviews in Food Science and Nutrition*, *65*(25), 4823-4845.
https://doi.org/10.1080/10408398.2024.2400235
40. Zhang, J., Ma, Y., Chang, R., Wang, R., Zhang, J. (2026). The interplay of plant polysaccharide structure, gut microbiota metabolism, and host health: Mechanisms and perspectives. *Life Sciences*, *395*, art. no. 124383.
https://doi.org/10.1016/j.lfs.2026.124383
41. Zhang, L., Zeng, X., Guo, D., Zou, Y., Gan, H., Huang, X. (2022). Early use of probiotics might prevent antibiotic-associated diarrhea in elderly (>65 years): a systematic review and meta-analysis. *BMC Geriatrics*, *22*(1), art. no. 562.
https://doi.org/10.1186/s12877-022-03257-3
42. Zhao, Y.X., Huang, L., Wu, D.T., Li, J., Lei, J., Fu, M.X., Zhang, Q., Qin, W. (2023). Catabolism of *Dictyophora indusiata* polysaccharide and its impacts on gut microbial composition during *in vitro* digestion and microbial fermentation. *Foods*, *12*(9), art. no. 1909.
https://doi.org/10.3390/foods12091909

ORIGINAL ARTICLE
http://journal.pan.olsztyn.pl

Polish Journal of Food and Nutrition Sciences
2026, Vol. 76, No. 3, 301–311
DOI: 10.31883/pjfns/226452
ISSN 1230-0322, e-ISSN 2083-6007

Influence of Germination Time and Ultraviolet Light Treatment on γ-Aminobutyric Acid Content and Microbial Dynamics of Germinated Red Rice in a Partially Circulated System

Hadi Munarko[1]*, Nadia I. Arifah[1], Muhammad A. Kurnianto[1], Ajeng A. Brahmanti[1], Jariyah[1], Yusuf Andriana[2], Reka M. Sari[2], Ahmad K. Faizin[3], Fawwaz A. Akbar[4]

[1]Food Technology Study Program, Faculty of Engineering and Science, Universitas Pembangunan Nasional Veteran Jawa Timur, Surabaya 60294, Indonesia
[2]Research Center for Food Technology and Processing, National Research and Innovation Agency (PRTPP-BRIN), Gunungkidul 55861, Indonesia
[3]Department of Mechanical Engineering, Faculty of Engineering and Science, Universitas Pembangunan Nasional Veteran Jawa Timur, Surabaya 60294, Indonesia
[4]Department of Informatics, Faculty of Computer Science, Universitas Pembangunan Nasional Veteran Jawa Timur, Surabaya 60294, Indonesia

Germination is a promising strategy to enhance bioactive compound content, particularly γ-aminobutyric acid (GABA) in red rice. However, conventional soaking germination methods are associated with high water consumption and microbial proliferation. This study evaluated the use of a partially circulated germinator with integrated microfiltration and ultraviolet (UV) treatment to process red rice for GABA accumulation while monitoring microbial dynamics. Red rice was germinated for 24, 48, and 72 h under UV and non-UV conditions, with water circulation applied at 90 min intervals for 5 min, and subsequently evaluated for pH, germination performance parameters, GABA content, and microbial quality. Microbial community diversity was characterized in one selected sample using next-generation sequencing (NGS). The results showed that the germinator effectively maintained water pH, mitigated drastic acidification commonly observed in static soaking systems. GABA content increased significantly with germination time, reaching maximum values at 48 h in both systems. Moreover, UV treatment resulted in higher GABA levels at 24 h. Total plate counts in circulation water exceeded 4 log CFU/mL, while reached 9.44 log CFU/g in dried germinated rice. UV treatment of the circulating water successfully reduced microbial load at 24 h germination time. Metagenomic profiling of freshly germinated red rice under non-UV treatment at 48 h revealed dominance of *Phytobacter* and *Enterobacter*, linked to seedling growth promotion, followed by *Cronobacter* spp., which presence suggested potential safety considerations. The findings demonstrate that partial circulation effectively enhances the functional value of red rice with reduced water consumption, offering a more environmentally sustainable alternative to conventional soaking methods.

Keywords: GABA, microbial diversity, partially circulated germinator, red rice sprouts, UV treatment

INTRODUCTION

Red rice is recognized as a nutrient-rich cereal with bioactive compounds including phenolic acids, flavonoids, and proanthocyanidins [Rodrigues *et al*., 2024]. These compounds are associated with antioxidant activity, metabolic regulation, and cancer prevention, making red rice a promising ingredient of functional foods [Baptista *et al*., 2024; Chen *et al*., 2025]. Similar to other unpolished rice, red rice is generally less preferred by consumers due to its relatively firm texture and the presence of hay-like notes, which are often regarded as undesirable sensory

***Corresponding Author:**
Tel.: +62 31 8706369; fax: +62 31 8722432; e-mail: **hadi.munarko.tp@upnjatim.ac.id** (H. Munarko)

Submitted: 8 March 2026
Accepted: 27 July 2026
Published on-line: 28 August 2026

characteristics [Munarko *et al*., 2025]. Germination has been widely applied as an effective strategy to enhance both the eating quality and bioactive profile of rice [Jiamyangyuen & Ooraikul, 2007; Wang *et al*., 2016]. Among these bioactive compounds, γ-aminobutyric acid (GABA) has attracted particular attention due to its physiological roles in blood pressure regulations, stress modulation, and potential gut-brain axis interactions [Liwinski *et al*., 2023]. However, native GABA levels in ungerminated rice are relatively low, limiting its functional potential.

Germination has been widely applied as a bioprocessing strategy to enhance GABA accumulation in rice. Conventional germination methods generally involve full soaking of rice until coleoptile emergence or partial soaking followed by incubation under humid conditions [Munarko *et al*., 2021]. Although these approaches effectively enhance GABA content, they have drawbacks due to the need for frequent water replacement every 3–6 h to prevent microbial spoilage, resulting in high water consumption and wastewater generation. Membrane bioreactor systems have been proposed as an alternative, allowing water recirculation through microfiltration membranes during germination without replacement. This approach maintains soaking water quality and yields germinated rice with higher GABA content and antioxidant activity compared to manual soaking [Sitanggang *et al*., 2021]. However, continuous immersion may promote leaching of soluble bioactive compounds and does not fully eliminate microbial growth, particularly when microorganisms can pass through membrane pores or persist on seed surfaces [Gaveau *et al*., 2017]. Previous studies have also indicated that partial soaking combined with incubation under atmospheric conditions resulted in higher GABA accumulation than full immersion, suggesting that prolonged water contact may negatively affect bioactive retention [Munarko *et al*., 2021]. Therefore, alternative germination configurations that balance hydration, bioactive retention, and microbial control are required.

A partially circulated germination system represents a modification of conventional soaking, combining periodic water spraying with recirculation through a filtration unit [Chungcharoen *et al*., 2024]. This configuration aims to maintain seed imbibition under controlled moisture conditions while reducing prolonged water contact and minimizing bioactive loss. Nevertheless, microbial proliferation during germination remains a critical issue, as the warm and humid environment favors rapid bacterial growth [Chen *et al*., 2024]. Ultraviolet (UV) irradiation has been widely applied in water treatment systems due to its chemical-free microbial inactivation capability [Kumar *et al*., 2025]. Integrating UV treatment within a recirculated germination system may provide an additional hurdle for microbial growth, although, its effectiveness in the system containing an organic load and suspended particles remains uncertain [Nooshabadi & Hashemi, 2024].

In addition to microbial enumeration, understanding the composition of microbial communities during germination is increasingly important. Seed-associated endophytes and environmental bacterial can influence both seedling development and product safety [Chen *et al*., 2024]. High-throughput sequencing approaches provide an opportunity to characterize microbial dynamics beyond conventional culture-dependent methods, enabling more comprehensive microbiological food safety risk assessment [Nanfack *et al*., 2024].

Despite advances in germination technology, limited information is available regarding the integration of partial water circulation and UV-assisted recirculation, as well as their effects on GABA content and microbial community composition during red rice germination. Therefore, the present study aimed to evaluate the effects of germination time and UV treatment within a partially circulated germination system on GABA accumulation, microbial load, and bacterial community composition in red rice. The findings are expected to provide insight into sustainable germination design and microbial risk consideration for functional rice production.

MATERIALS AND METHODS

Materials

Commercial organic red rice (var. A3) was purchased from PT. Sirtanio Organik Indonesia (Banyuwangi, East Java, Indonesia). Sodium hypochlorite (NaOCl) was obtained from Onemed (Sidoarjo, Indonesia). Sodium chloride (NaCl), plate count agar (PCA), and de Man, Rogosa and Sharpe agar (MRSA) were purchased from HiMedia (Thane, India), while calcium carbonate ($CaCO_3$), hydrogen peroxide (H_2O_2), trichloroacetic acid (TCA, 10%), and α-aminobutyric acid (AABA) standard were from Merck (Darmstadt, Germany). Additional reagents included AccQ•Tag reagent kit (Waters Corporation, Milford, MA, USA), Quick-DNA Magbead Plus Kit (Zymo Research Corporation, Irvine, CA, USA), and KOD Multi & Epi (Toyobo, Osaka, Japan).

Design of germinator

The schematic design of the partially circulated germinator is shown in **Figure 1**. The system consisted of two poly(methyl methacrylate) containers: container 1 (bottom) (4) serving as the spent water reservoir equipped with a pH sensor (2), and container 2 (top) (10) for germination, with a temperature sensor (3) and water sprayer (9). Water from container 1 was circulated by a direct current (DC) pump (HIU, China) (5) through a polypropylene microfiltration membrane (Nanotec, Cikarang, Indonesia) (6) with or without using a UV-C lamp (MILE, Indonesia) (7) and sprayed onto rice samples in container 2 *via* a ¼-inch (0.635 cm) hose (8). The UV-C lamp used had a length of 35 cm, a power of 16 W, and operated at a flow capacity of 15 L/min. The sprayed water then returned by gravity through a valve to container 1 for recirculation. Circulation intervals and durations were regulated using an automatic timer switch (Vetto, Tangerang, Indonesia). Real-time monitoring of pH and temperature was carried out using an Adafruit IoT system (Adafruit Industries, LLC, New York, NY, USA).

Germination procedure

Red rice grains were surface-sterilized with 0.1% (*v/v*) sodium hypochlorite for 30 min, rinsed thoroughly with tap water,

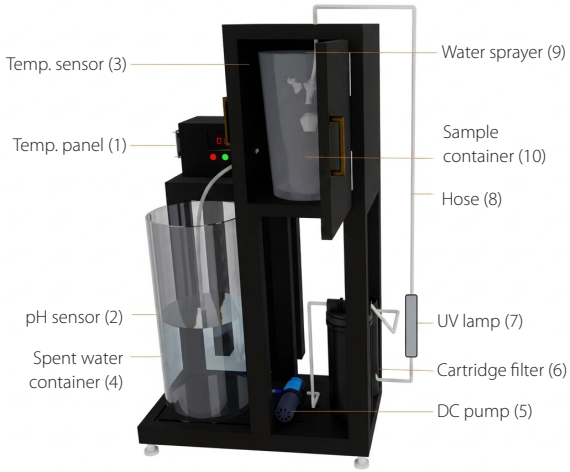

Figure 1. Design illustration of a partially circulated germinator.

and placed in the germinator. Germination was performed at room temperature (±30°C) with water circulation every 90 min for 5 min. For UV treatments, a UV lamp was installed after the filtration unit, while in the non-UV condition, the lamp was removed and replaced by a hose. pH values and temperatures were continuously recorded in real time during germination. Data were logged at 5-min intervals. Germination was carried out for 24, 48, and 72 h. At each time point, samples of circulation water were collected for analysis of total lactic acid bacteria (LAB) count and total plate count (TPC), while fresh germinated rice samples were tested for germination percentage, sprout length, and LAB count. After germination, rice samples were dried in a dehydrator at 45°C for 2 h, ground to 80 mesh, and analyzed for GABA content and TPC. The treatment yielding the highest GABA content was further subjected to microbial diversity analysis.

Analysis of germination performance parameters

Germination rate was determined by counting the number of germinated grains among ~50 randomly selected seeds *per* treatment, expressed as a percentage of the total seeds. Sprout length (shoot and radicle) was measured from 25 randomly selected germinated seeds *per* treatment using a digital caliper (Ningbo Deli Tools Co., Ltd, Hangzhou, Zhejiang, China).

Determination of γ-aminobutyric acid content

GABA content was determined following the method described by Rohman & Gandjar [2007] with modifications. Briefly, 0.1 g of rice flour was hydrolyzed with 5 mL of 6 M HCl at 110°C for 22 h, diluted to 50 mL with distilled water, and filtered (0.45 µm membrane). Filtrates (500 µL) were mixed with 40 µL of α-aminobutyric acid (AABA, internal standard) and 460 µL of ultrapure water. Derivatization was carried out by mixing 10 µL of the sample with 70 µL of AccQ•Tag fluor borate buffer and 20 µL of AccQ•Tag reagent, followed by incubation at 50°C for 10 min. The derivatized samples were injected (1 µL) into an ultra-performance liquid chromatography (UPLC) system equipped with a C18 ODS column and a photodiode array detector set at 260 nm. Gradient elution was performed using eluent A (AccQ•Tag Ultra Eluent A, 100%) and eluent B (AccQ•Tag Ultra Eluent B and water, 10:90, *v/v*). The GABA concentration in the samples was quantified based on the peak area ratio of the analyte to the internal standard. Results were expressed in g *per* 100 g of dried rice.

Total microbial count analysis

The total microbial load was determined following the United States Food and Drug Administration (FDA) Bacteriological Analytical Manual (BAM) method [Maturin & Peeler, 2001]. One gram of rice flour or one mL of circulation water was suspended in 9 mL of a sterile NaCl solution and serially diluted up to 10^{-5}. Aliquots (1 mL) of each dilution were plated on the plate count agar in triplicate and incubated at 37°C for 24 h. Plates with 25–250 colonies were selected for enumeration, and results were expressed as log CFU/g for rice samples and log CFU/mL for water samples using the standard BAM formula.

Total lactic acid bacteria count analysis

Total LAB count analysis was conducted following BAM protocol with modification [Kurnianto *et al*., 2025; Maturin & Peeler, 2001]. One gram of fresh germinated rice or one mL of circulation water was diluted in 9 mL of a sterile NaCl solution, serially diluted to 10^{-5}, and plated on MRSA. Plates were incubated at 37°C for 48 h, and colonies were counted on plates containing 25–250 colonies. Results were expressed as log CFU/g for rice samples and log CFU/mL for water samples.

Microbial diversity analysis

Microbial community diversity analysis was conducted on freshly germinated red rice from a selected sample based on the highest GABA content. The analysis was performed based on the method described by Yang *et al*. [2023] with adjustments. DNA was extracted using the Quick-DNA MagBead Plus Kit. DNA concentration and purity were assessed using a Nanodrop spectrophotometer (Thermo Scientific, Waltham, MA, USA) and a Qubit fluorometer (Thermo Scientific). The V3–V4 region of the 16S rRNA gene was amplified using primers 341F and 805R. Polymerase chain reaction (PCR) products were verified by 1% agarose gel electrophoresis, purified with Agencourt AMPure XP beads, and quantified using a Qubit 2.0 fluorometer and a Bioanalyzer (Agilent, Santa Clara, CA, USA). Libraries were quantified by qPCR and sequenced on the Illumina MiSeq platform (Illumina, San Diego, CA, USA).

Statistical analysis

Data were expressed as means and standard deviations (SD). Statistical analysis was performed using SPSS version 22.0 (Statistical Graphics Corp., Princeton, NJ, USA). Two-way analysis of variance (ANOVA) was used to evaluate the importance of the significant factors (UV treatment, germination time, and their interaction). Duncan's multiple range test was applied to assess the significant

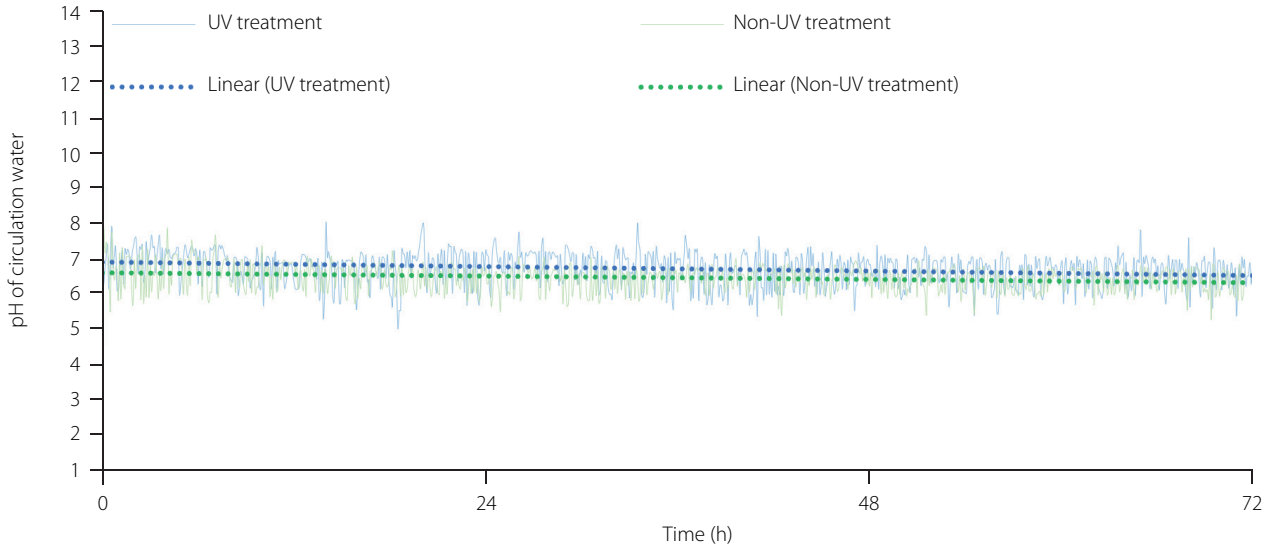

Figure 2. pH profiles of circulation water during the germination of red rice produced in a partially circulated germinator with and without UV treatment.

differences between samples. Microbial diversity data were interpreted descriptively based on relative abundance.

RESULTS AND DISCUSSION

pH stability during germination

The circulated water maintained relatively stable pH values close to neutrality throughout the germination period in both the UV and the non-UV system (**Figure 2**). This finding indicates that the partially circulated germinator effectively preserved the pH of the germination medium during the entire germination period. Similar observations were reported in our previous study [Munarko *et al*., 2021], which demonstrated that a microfiltration-based membrane reactor could maintain stable pH levels more efficiently than conventional soaking methods with periodic water replacement. Moreover, Sitanggang *et al*. [2021] observed a decline in water pH of up to 1.5-fold during rice soaking without water exchange, whereas membrane-based reactors kept the pH relatively stable, suggesting that the buffering effect of continuous recirculation likely contributed to maintaining stable environment condition preventing microbial proliferation.

Germination performance parameters

The germination rate and the sprout length of red rice treated in the partially circulated germinator are shown in **Figure 3**. A two-way ANOVA showed significant effect of the interaction ($p<0.05$) between germination time and UV treatment on germination percentage and root length. Moreover, germination rate increased significantly ($p<0.05$) with prolonged germination time. The highest percentage was 64.3%–70.3% at 72 h, while the lowest values (49.5%–52.6%) were recorded at 24 h. In terms of seedling development, shoot length reached 3.00 mm (process without UV irradiation) and 5.12 mm (upon UV treatment), while root length ranged from 0.40 mm to 4.15 mm after 72 h. Shoots became visible after 24 h of germination, whereas radicle emergence was only observed after 48 h, indicating different developmental dynamics between the two organs. This pattern aligns with earlier reports indicating that shoot growth rates often exceed those of roots during germination [Ramírez-Olvera *et al*., 2018].

UV treatment significantly ($p<0.05$) enhanced all germination performance parameters, particularly shoot and root lengths (**Figure 3**). This enhancement may be attributed to improved water quality under UV treatment. The findings of this study are consistent with previous research on okra seeds, which reported that although different water sources did not significantly affect the overall germination percentage, higher quality water contributed to a faster rate of sprout elongation [Nana *et al*., 2019].

γ-Aminobutyric acid production during germination

The content of GABA in red rice germinated in the partially circulated germinator with and without UV treatment is shown in **Figure 4**. Germination with this system effectively enhanced GABA content over time. After 24 h, GABA levels reached 17.03 mg/100 g in the UV-treated group compared to 13.16 mg/100 g in the non-UV group. Contents increased significantly ($p<0.05$) at 48 h, reaching 35.38 and 36.73 mg/100 g, respectively. However, no significant ($p\geq0.05$) increase was observed between 24 and 72 h, with levels of 40.99 mg/100 g for UV and 34.39 mg/100 g for non-UV treatments at 72 h. No significant ($p\geq0.05$) interaction between UV treatment and germination time was detected, indicating that GABA accumulation was predominantly governed by germination time. The effect of UV treatment was limited to the early stage of germination and became negligible at later stages.

The increase in GABA levels with prolonged germination is consistent with previous studies on various rice cultivars under different germination methods [Munarko *et al*., 2022; Wang *et al*., 2016]. In cereal grains, GABA is mainly synthesized *via* the GABA

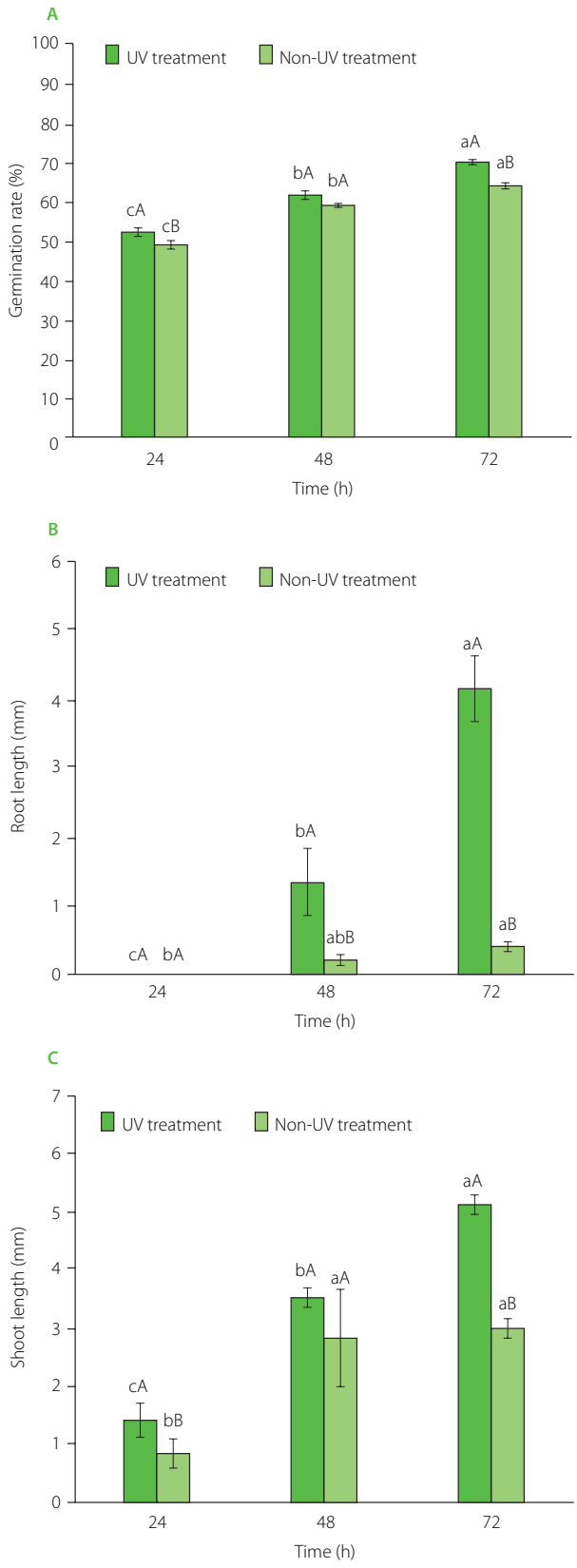

Figure 3. Germination rate (**A**), root length (**B**), and shoot length (**C**) of germinated red rice produced in a partially circulated germinator with and without UV treatment. Different lowercase letters indicate significant differences among germination times within the same treatment ($p<0.05$). Different uppercase letters indicate significant differences between the UV and non-UV treatments at the same germination time ($p<0.05$).

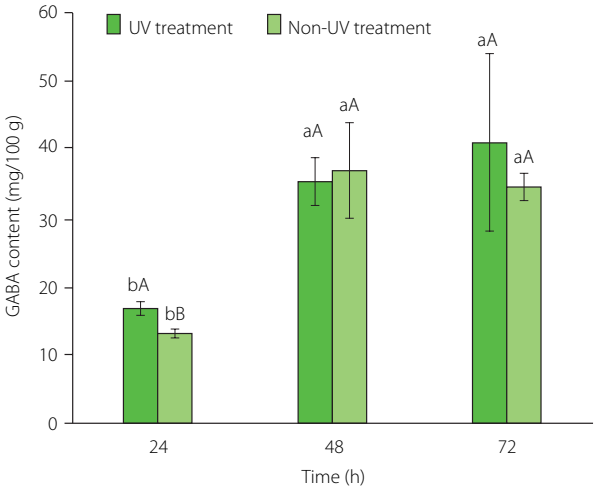

Figure 4. γ-Aminobutyric acid (GABA) content in red rice germinated in a partially circulated germinator with and without UV treatment. Different lowercase letters indicate significant differences among germination times within the same treatment ($p<0.05$). Different uppercase letters indicate significant differences between the UV and non-UV treatments at the same germination time ($p<0.05$).

shunt pathway, where glutamate undergoes decarboxylation by glutamate decarboxylase (GAD) activity, with minor contributions from the polyamine degradation pathway [Ansari *et al*., 2021; Shelp *et al*., 2012; Zhu *et al*., 2022]. The efficiency of GABA accumulation is strongly influenced by the germination method. Sitanggang *et al*. [2021] demonstrated that the use of membrane bioreactors significantly improved GABA levels compared to conventional soaking [Sitanggang *et al*., 2021]. Similarly, our previous study [Munarko *et al*., 2021] showed that partial soaking combined with incubation under humid conditions resulted in a higher GABA content in germinated rice than either full soaking or conventional partial soaking. The partially circulated germinator used in this study represents a further refinement of the membrane-based partial method by integrating periodic water spraying with membrane filtration and recirculation. The results showed that in this system GABA was also efficiently produced during rice germination.

UV irradiation applied to the circulating water as a decontamination step in our system, was expected to support germination efficiency and GABA accumulation. It was proved at 24 h (**Figure 3**). However, the lack of significant differences ($p\geq0.05$) for 48- and 72-h samples, suggests that UV treatment may contribute to early-stage of germination. As germination progressed, the influence of UV treatment on metabolic responses became less pronounced, possibly because metabolic changes associated with prolonged germination played a more dominant role. The position of the UV light appears to be a critical factor as well. Zhu *et al*. [2023] demonstrated that placing UV-C irradiation directly in the germination chamber (180 μW/cm^2 for 8 h *per* day) significantly enhanced GABA accumulation. Likewise, Yan *et al*. [2021] reported that UV-C treatment at the dose

of 4 kJ/m^2 increased GABA content in tomato fruits during storage by regulating the genes involved in GABA metabolism. These findings suggest that further research should investigate the direct application of UV irradiation within the germination chamber to optimize GABA synthesis in germinated rice.

Microbial proliferation

Total plate counts in circulation water under both UV and non-UV treatments ranged from 4 to 6 log CFU/mL (**Figure 5A**). At 24 h of germination, the microbial load was numerically lower in the UV-treated samples than in the non-UV-treated samples for both the circulated water and dried germinated rice; however, these differences were not statistically significant ($p \geq 0.05$) (**Figure 5B**). Similarly, no significant differences in the TPC of the circulation water were observed between UV and non-UV treatments after 48 and 72 h of germination ($p \geq 0.05$). The TPC of dried rice ranged from 7.76 to 9.44 log CFU/g after 24–72 h of germination and was not significantly affected by germination time, UV treatment, or their interaction ($p \geq 0.05$). These results align with the study by Zhang *et al*. [2018], who observed microbial counts exceeding 9 log CFU/g after 24 h of soaking of brown rice, with sustained proliferation during germination. Cereal grains inherently harbour diverse microbial populations originating from field environments, harvesting, and post-harvest handling process. Several investigations have demonstrated that microbial populations in rice and other sprouted grains increase significantly during germination due to favourable moisture and nutrient availability [Cotter & Hill, 2003]. The germinated rice was dried in our study at 45°C. Although drying at this temperature reduced seed moisture, it was insufficient for microbial inactivation. Vegetative bacterial cells generally require 60°C for thermal inactivation, and even higher temperatures under moist conditions are necessary to inactivate spores [Cebrián *et al*., 2017]. Consequently, many microorganisms likely survived or entered dormancy, leading to relatively high microbial counts *per* gram of dry material despite water removal.

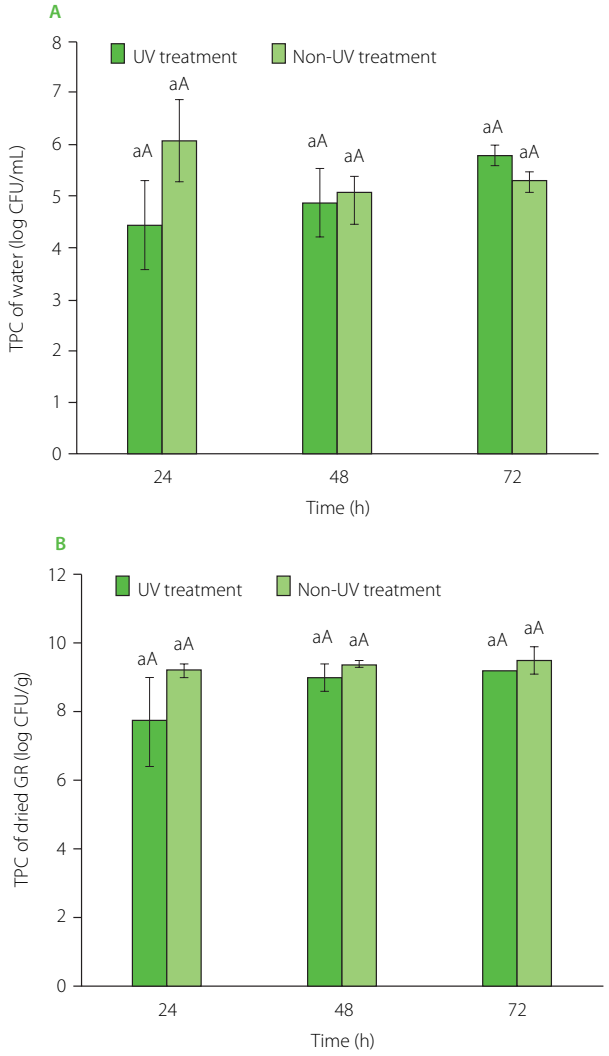

Figure 5. Total plate count (TPC) of circulated water (**A**) and dried germinated rice (GR) (**B**). Production was performed in a partially circulated germinator with and without UV treatment. Different lowercase letters indicate significant differences among germination times within the same treatment ($p<0.05$). Different uppercase letters indicate significant differences between the UV and non-UV treatments at the same germination time ($p<0.05$).

The total LAB counts in the circulated water and freshly germinated red rice are shown in **Figure 6**. At 24 h of germination, total LAB count in water did not differ significantly between the UV and non-UV treatments ($p \geq 0.05$). A significant difference was observed at 48 h, with the LAB population reaching 5.05 log CFU/mL in the non-UV treatment, whereas the UV treatment maintained a lower population of 3.65 log CFU/mL ($p<0.05$). However, by 72 h of germination, LAB populations had increased to approximately 5 log CFU/mL in both treatments, with no significant difference between them ($p \geq 0.05$).

UV-C irradiation at wavelengths between 200 and 280 nm is known to exert germicidal effects by inducing DNA damage and impairing microbial replication [Kowalski, 2009]. Previous studies by Moore *et al*. [2025] and Scarlett *et al*. [2016] demonstrated significant microbial inactivation by UV-C in water-based systems. The limited long-term effectiveness of UV treatment observed in our study may be associated with several factors. First, organic compounds released from germinating seeds can accumulate in the circulating water, increasing turbidity and reducing UV transmittance. Dissolved organic matter may absorb or scatter UV radiation, thereby shielding microorganisms from direct exposure [Scarlett *et al*., 2016]. Second, microorganisms attached to the surface of germinating grains continuously detach and re-enter the circulating water during spraying cycles, resulting in repeated microbial inoculation within the system. These mechanisms have also been reported in water treatment system where UV efficiency decreases in the presence of organic load or suspended solids [Kováříková *et al*., 2024].

Microbial community composition based on metagenomic analysis

Metagenomic analysis provided deeper insight into the microbial communities associated with germinated rice beyond what can be obtained from culture-based enumeration. It was performed on freshly germinated red rice sample under non-UV treatment

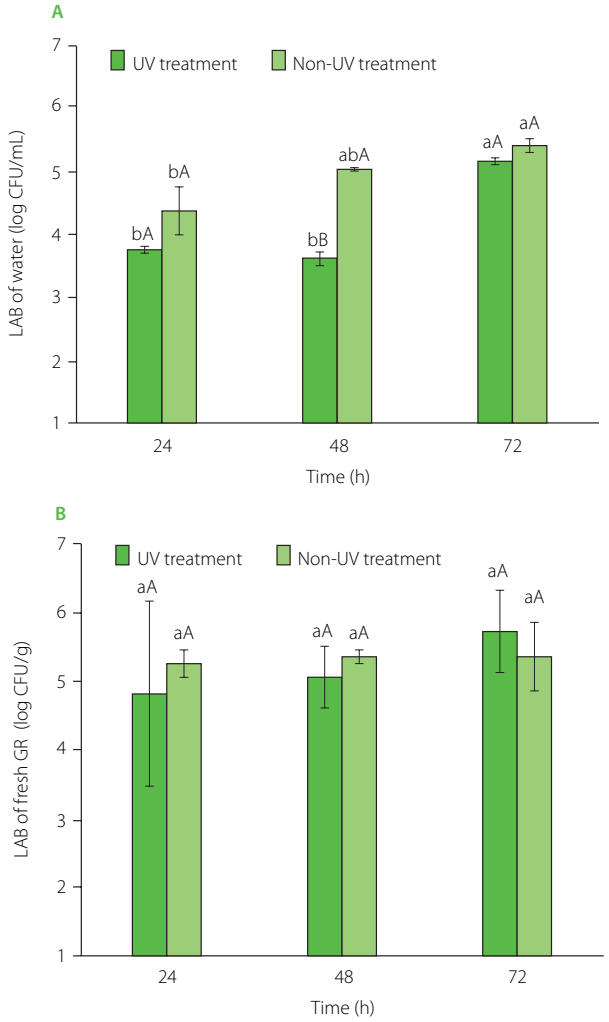

Figure 6. Total lactic acid bacteria (LAB) count of circulation water (**A**) and freshly germinated rice (GR) (**B**). Production was performed in a partially circulated germinator with and without UV treatment. Different lowercase letters indicate significant differences among germination times within the same treatment ($p<0.05$). Different uppercase letters indicate significant differences between the UV and non-UV treatments at the same germination time ($p<0.05$).

at 48 h. This treatment was selected due to its high GABA content, which was not significantly different from that observed under UV treatment or longer germination durations, making it a suitable representative model for microbial diversity analysis. In addition, this sample was chosen considering the potential for higher microbial loads, particularly bacteria, due to the absence of selective pressure from ultraviolet treatment. The sequencing results (**Figure 7**) revealed that the microbial community in germinated rice was dominated by several bacterial genera commonly associated with plant environments, including *Phytobacter* (31.17%), followed by *Enterobacter* (11.26%) and *Cronobacter* (10.47%). The high moisture content and release of nutrients during germination may provide favorable ecological conditions that support the proliferation of diverse bacterial groups [Cotter & Hill, 2003]. These microorganisms are frequently detected in cereal grains and plant tissues and are considered part of the natural microbiota associated with seeds [Eid *et al*., 2021].

Phytobacter is recognized as a seed-associated endophyte with nitrogen-fixing capacity and functions as a plant growth-promoting bacterium (PGPB) [Jana *et al*., 2025]. Its dominance is likely attributable to its persistence within seed tissues, where endophytic localization confers resistance to disinfection treatments [Kaga *et al*., 2009; Kubota *et al*., 2023]. Similarly, *Enterobacter* contributes to plant growth through phytohormone synthesis and antimicrobial metabolite production [Ngalimat *et al*., 2021]. Co-occurrence with *Enterobacter* may reflect a symbiotic interaction that enhances seedling development [Ng *et al*., 2012].

An important finding of this study was the detection of *Cronobacter* spp. within the microbial community. *Cronobacter* is recognized as an opportunistic pathogen that has been associated with contamination of various plant-derived food from the cultivation, post-harvest handling, or processing environments [Cechin *et al*., 2023]. This genus is particularly known for its ability to survive in low-moisture environments and persist in dry food matrices. Moreover, *Cronobacter* species have been associated with severe infections, including meningitis and sepsis, especially in neonates and other vulnerable populations [Koutsoumanis *et al*., 2014]. Although the relative abundance of *Cronobacter* detected in this study was low, its presence highlights potential food safety concern in germinated cereal products. The germination process provides a warm and high-moisture environment that can promote microbial proliferation [Yang *et al*., 2023]. However, relative abundance alone is insufficient to determine food safety risk. A comprehensive hazard assessment should instead be based on absolute microbial counts, strain-specific virulence characteristics, and the intended mode of consumption, particularly whether the product is consumed raw or subjected to a validated kill step [Billington *et al*., 2022].

Cronobacter spp. are heat sensitive vegetative bacteria. Osaili *et al*. [2009] reported that temperatures ≥ 70°C resulted in substantial microbial reductions by >4 log units. During high-temperature short-time (HTST) process (67.5°C for 15 s), the most heat- resistant *Cronobacter* strain was reduced by more than 6.7 log units [Pearce *et al*., 2012]. These findings indicate that conventional heat treatments, such as pasteurization, boiling, blanching, steaming, and baking, are generally effective in inactivating *Cronobacter*, although thermal resistance may vary depending on the food matrix.

Beyond these dominant genera, other bacteria such as *Pseudomonas*, *Aeromonas*, *Brevundimonas*, *Sphingobium*, and *Paenibacillus* were also detected, shaping the microbial dynamics of germinated rice. While some strains are beneficial, contributing to plant growth promotion and pathogen suppression [Devi & Kalaiselvi, 2020; Quibod *et al*., 2015; Tariq *et al*., 2025], others (*e.g., Brevundimonas* spp.) are opportunistic pathogens in humans [Ryan & Pembroke, 2018]. The microbial community composition observed in this study also reflects the dynamic nature of microbial ecosystems during germination [Dutta *et al*., 2022]. Germination alters the physicochemical environment surrounding seeds by increasing moisture content, oxygen availability,

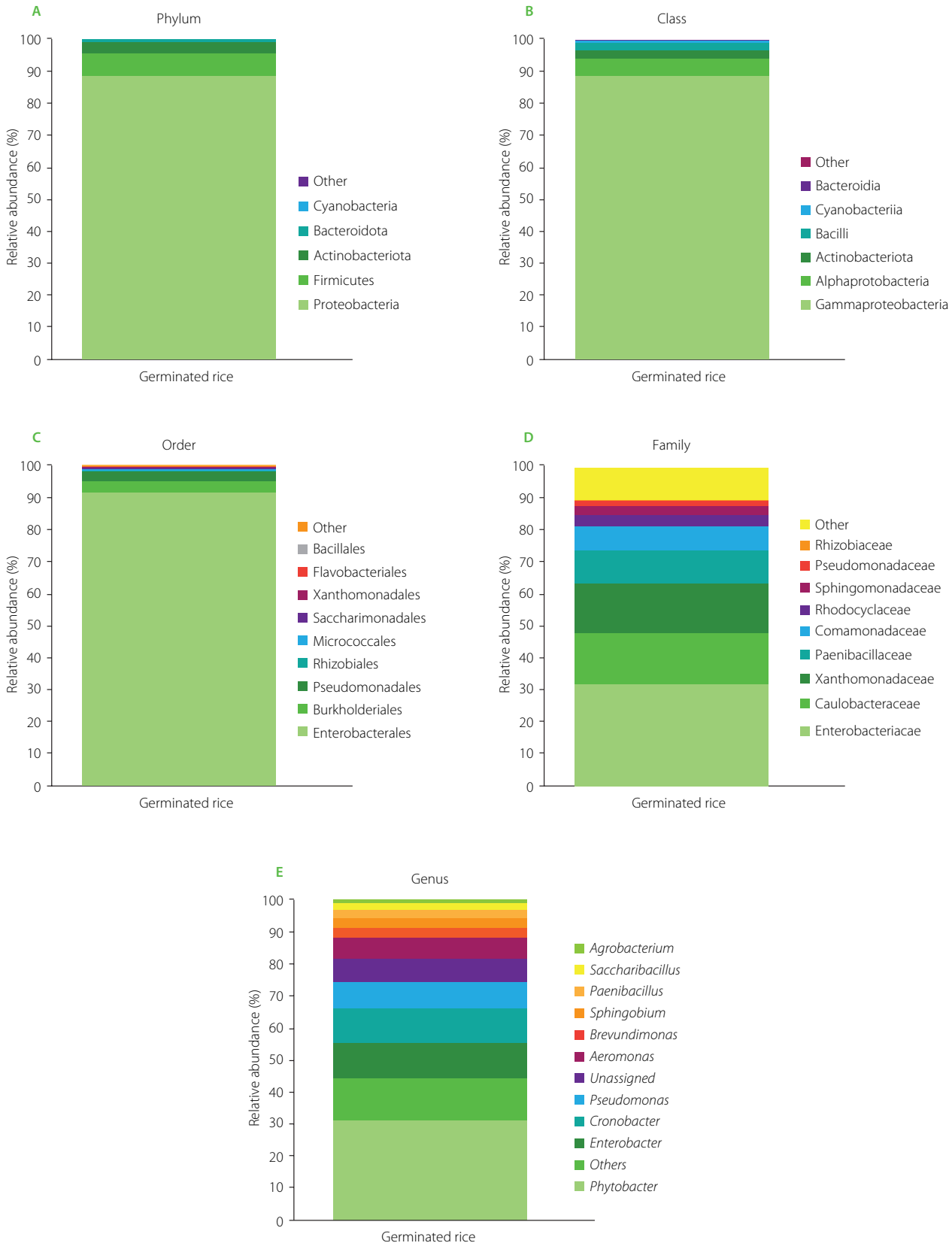

Figure 7. Relative abundance of bacteria at different taxonomy level: phylum (**A**), class (**B**), order (**C**), family (**D**), and genus (**E**) of freshly germinated red rice after 48 h of germination under non-UV treatment.

and nutrient release. These changes create ecological niches that enhance the growth of specific microorganisms capable of utilizing the available nutrients. As a result, microbial diversity and relative abundance can shift significantly during the germination process [Abdelfattah *et al*., 2021].

Overall, metagenomic analysis provides valuable insights into the microbial ecology of germinated rice and highlights the complexity of microbial communities associated with sprouting systems. While some detected microorganisms may contribute to natural microbial succession during germination, the presence of opportunistic pathogens emphasizes the importance of implementing effective sanitation strategies to ensure microbial safety in germinated grain production.

CONCLUSIONS

The present study demonstrated that a partially circulated germination system can be effectively used to germinate red rice and obtain a product with an increased functional value through GABA accumulation. Although microbial proliferation occurred during germination, the integration of UV treatment provided partial microbial control in the circulating water during the early stages of germination. Metagenomic analysis further revealed that the microbial community was largely dominated by seed-associated bacteria, highlighting the important role of intrinsic seed microbiota in shaping microbial dynamics during germination. Importantly, the partial circulation approach represents a promising strategy for developing more resource-efficient germination systems capable of improving the functional quality of cereal grains while minimizing environmental impact. Future optimization of sanitation strategies combined with water-efficient processing technologies may further improve microbial safety and support sustainable production of germinated functional foods.

ACKNOWLEDGEMENTS

The authors would like to acknowledge by the Ministry of Higher Education, Science, and Technology of Indonesia; Faculty of Engineering and Science, Universitas Pembangunan Nasional "Veteran" Jawa Timur; and the Research Center for Food Technology and Processing, BRIN for supporting this research.

RESEARCH FUNDING

This research was funded by the Ministry of Higher Education, Science, and Technology of Indonesia through the *"Penelitian Fundamental Reguler/*Regular Fundamental Research Grant Scheme" (Contract No. 098/C3/DT.05.00/PL/2025). This work also supported by Perjanjian Kerja Sama (PKS) / Cooperation Agreement between the Faculty of Engineering and Science, Universitas Pembangunan Nasional "Veteran" Jawa Timur, and the Research Center for Food Technology and Processing, BRIN, titled "*Pengembangan Pangan Fungsional Berbasis Komoditas Lokal dan Kemasan Cerdas*… / Development of Functional Foods from Local Commodities and Smart Packaging…", under PKS Numbers 465/V/KS/10/2025 and 77/UN63.3/PKS/TU/2025.

CONFLICT OF INTERESTS

The authors state no conflict of interests

ADDITIONAL INFORMATION

The authors declare they have not used Artificial Intelligence (AI) tools in the creation of this article. The AI, specifically ChatGPT (version GPT-4, OpenAI), was used to improve the readability and language of the article. The whole content has been reviewed and verified by the authors to ensure accuracy and integrity.

ORCID IDs

F.A. Akbar **https://orcid.org/0009-0003-8545-4852**
Y. Andriana **https://orcid.org/0000-0002-6052-301X**
N.I. Arifah **https://orcid.org/0009-0002-4289-9758**
A.A. Brahmanti **https://orcid.org/0009-0003-5820-6140**
A.K. Faizin **https://orcid.org/0000-0003-3613-0328**
Jariyah **https://orcid.org/0000-0003-4659-5516**
M.A. Kurnianto **https://orcid.org/0000-0002-7654-9548**
H. Munarko **https://orcid.org/0000-0002-6000-034X**
R.M. Sari **https://orcid.org/0000-0002-8995-4788**

REFERENCES

1. Abdelfattah, A., Wisniewski, M., Schena, L., Tack, A.J.M. (2021). Experimental evidence of microbial inheritance in plants and transmission routes from seed to phyllosphere and root. *Environmental Microbiology*, *23*(4), 2199–2214. **https://doi.org/10.1111/1462-2920.15392**
2. Ansari, M.I., Jalil, S.U., Ansari, S.A., Hasanuzzaman, M. (2021). GABA shunt: a key-player in mitigation of ROS during stress. *Plant Growth Regulation*, *94*(2), 131–149. **https://doi.org/10.1007/s10725-021-00710-y**
3. Baptista, E., Liberal, Â., Cardoso, R.V.C., Fernandes, Â., Dias, M.I., Pires, T.C.S.P., Calhelha, R.C., García, P.A., Ferreira, I.C.F.R., Barreira, J.C.M. (2024). Chemical and bioactive properties of red rice with potential pharmaceutical use. *Molecules*, *29*(10), art. no. 2265. **https://doi.org/10.3390/molecules29102265**
4. Billington, C., Kingsbury, J.M., Rivas, L. (2022). Metagenomics approaches for improving food safety: A review. *Journal of Food Protection*, *85*(3), 448–464. **https://doi.org/10.4315/JFP-21-301**
5. Cebrián, G., Condón, S., Mañas, P. (2017). Physiology of the inactivation of vegetative bacteria by thermal treatments: mode of action, influence of environmental factors and inactivation kinetics. *Foods*, *6*(12), art. no. 107. **https://doi.org/10.3390/foods6120107**
6. Cechin, C. da F., Carvalho, G.G., Bastos, C.P., Kabuki, D.Y. (2023). *Cronobacter* spp. in foods of plant origin: occurrence, contamination routes, and pathogenic potential. *Critical Reviews in Food Science and Nutrition*, *63*(33), 12398–12412. **https://doi.org/10.1080/10408398.2022.2101426**
7. Chen, L., Bao, H., Yang, J., Huo, Y., Zhang, J., Fang, R., Zhang, L. (2024). Dynamics of rice seed-borne bacteria from acquisition to seedling colonization. *Microbiome*, *12*(1), art. no. 253. **https://doi.org/10.1186/s40168-024-01978-8**
8. Chen, Z., Theppawong, A., Sangsawad, P., Fang, J., Ye, H., Deng, S., Yang, M., Gao, J., Kraithong, S. (2025). Bioactive compounds in colored rice: Exploring natural agents for cancer prevention *in vitro* and rodent model studies. *Journal of Functional Foods*, *129*, art. no. 106875. **https://doi.org/10.1016/j.jff.2025.106875**
9. Chungcharoen, T., Sansiribhan, S., Munsin, R., Phetpan, K., Fonghiransiri, S., Limmun, W. (2024). The improvement of germination method for producing the germinated brown rice using a water spraying system with a revolved sieve. *Engineering and Applied Science Research*, *51*(6), 739–746. **https://doi.org/10.14456/easr.2024.69**
10. Cotter, P.D., Hill, C. (2003). Surviving the acid test: Responses of Gram-positive bacteria to low pH. *Microbiology and Molecular Biology Reviews*, *67*(3), 429–453. **https://doi.org/10.1128/MMBR.67.3.429-453.2003**
11. Devi, P.A., Kalaiselvi, T. (2020). Evaluating the effect of *Sphingobium yanoikuyae* MH394206 and mixed consortia on growth of rice CO 51 in moisture deficit condition. *Journal of Pharmacognosy and Phytochemistry*, *9*(6), 2016–2021. **https://doi.org/10.22271/phyto.2020.v9.i6ac.13261**
12. Dutta, S., Choi, S.Y., Lee, Y.H. (2022). Temporal dynamics of endogenous bacterial composition in rice seeds during maturation and storage, and spatial dynamics of the bacteria during seedling growth. *Frontiers in Microbiology*, *13*, art. no. 877781. **https://doi.org/10.3389/fmicb.2022.877781**

13. Eid, A.M., Fouda, A., Abdel-Rahman, M.A., Salem, S.S., Elsaied, A., Oelmüller, R., Hijri, M., Bhowmik, A., Elkelish, A., El-Din Hassan, S. (2021). Harnessing bacterial endophytes for promotion of plant growth and biotechnological applications: An overview. *Plants*, *10*(5), art. no. 935. **https://doi.org/10.3390/plants10050935**
14. Gaveau, A., Coetsier, C., Roques, C., Bacchin, P., Dague, E., Causserand, C. (2017). Bacteria transfer by deformation through microfiltration membrane. *Journal of Membrane Science*, *523*, 446–455. **https://doi.org/10.1016/j.memsci.2016.10.023**
15. Jana, S.K., Bhattacharya, R., Mukherjee, S., Gupta, S., Hui, S.P., Chattopadhyay, A., Biswas, S.R., Mandal, S. (2025). *Phytobacter* sp. RSE02 is a rice seed endophytic plant probiotic bacterium with human probiotic features and cholesterol--lowering ability. *Scientific Reports*, *15*(1), art. no. 27865. **https://doi.org/10.1038/s41598-025-11212-6**
16. Jiamyangyuen, S., Ooraikul, B. (2007). The physico-chemical, eating and sensorial properties of germinated brown rice. *Journal of Food Agriculture & Environment*, *6*(2), 119–124.
17. Kaga, H., Mano, H., Tanaka, F., Watanabe, A., Kaneko, S., Morisaki, H. (2009). Rice seeds as sources of endophytic bacteria. *Microbes and Environments*, *24*(2), 154–162. **https://doi.org/10.1264/jsme2.ME09113**
18. Kim, K.-S., Kim, B.-H., Kim, M.-J., Han, J.-K., Kum, J.-S., Lee, H.-Y. (2012). Quantitative microbiological profiles of brown rice and germinated brown rice. *Food Science and Biotechnology*, *21*(6), 1785–1788. **https://doi.org/10.1007/s10068-012-0239-2**
19. Koutsoumanis, K.P., Lianou, A., Sofos, J.N. (2014). Food safety: Emerging pathogens. In N.K. Van Alfen (Ed.). *Encyclopedia of Agriculture and Food Systems* (Vol. 3), Academic Press, pp. 250–272. **https://doi.org/10.1016/B978-0-444-52512-3.00049-8**
20. Kováříková, E., Ny, V., Šulc, M., Rysová, J., Pečenková, N., Houška, M. (2024). Promotional effects on naturally occurring lactic acid bacteria without impairing chickpea germination. *Czech Journal of Food Sciences*, *42*(2), 85–92. **https://doi.org/10.17221/12/2024-CJFS**
21. Kowalski, W. (2009). Chapter 2: UVGI Disinfection theory. In *Ultraviolet Germicidal Irradiation Handbook*. Springer Berlin Heidelberg, pp. 17-50. **https://doi.org/10.1007/978-3-642-01999-9**
22. Kubota, H., Nakayama, T., Ariyoshi, T., Uehara, S., Uchitani, Y., Tsuchida, S., Nishiyama, H., Morioka, I., Koshinaga, T., Kusabuka, A., Nakatsubo, N., Yamagishi, T., Tabuchi, Y., Okuno, R., Kobayashi, K., Mitobe, M., Yokoyama, K., Shinkai, T., Suzuki, J., Sadamasu, K. (2023). Emergence of *Phytobacter diazotrophicus* carrying an IncA/C_2 plasmid harboring *bla* $_{NDM-1}$ in Tokyo, Japan. *mSphere*, *8*(4), art. no. e00147-23. **https://doi.org/10.1128/msphere.00147-23**
23. Kumar, N., Tripathi, K., Srivastava, Y. (2025). Effects of ultraviolet (UV) radiation on microbial growth: Mechanisms, responses, and applications. In K. Tripathi, Y. Srivastava, N. Kumar (Eds.), *Biotechnology Lab Techniques: Culture Media, Microscopy, and Microbial Analysis*, Deep Science Publishing, pp. 57–59. **https://doi.org/10.70593/978-93-49307-52-0_7**
24. Kurnianto, M.A., Adirama, S.I., Xu, W., Winarti, S., Rini, D.M. (2025). Enhancing the quality of traditional indonesian shrimp paste (terasi) through *Tetragenococcus halophilus* 54M106-3 inoculation: Physicochemical, sensory, and bioactivity insights. *Foods*, *14*(14), art. no. 2419. **https://doi.org/10.3390/foods14142419**
25. Liwinski, T., Lang, U.E., Brühl, A.B., Schneider, E. (2023). Exploring the therapeutic potential of gamma-aminobutyric acid in stress and depressive disorders through the gut–brain axis. *Biomedicines*, *11*(12), art. no. 3128. **https://doi.org/10.3390/biomedicines11123128**
26. Maturin, L., Peeler, J.T. (2001). Chapter 3: Aerobic Plate Count. In *Bacteriological Analytical Manual*. U.S. Food & Drug Administration. **https://www.fda.gov/food/laboratory-methods-food/bam-chapter--3-aerobic-plate-count**
27. Moore, M., Yang, T., Douraki, M.J., Rivard, C., Pliakoni, E., Nwadike, L., Bhullar, M. (2025). Effect of ultraviolet water treatment on survival and growth of *Escherichia coli* in recirculating hydroponic systems. *Journal of Food Protection*, *88*(9), art. no. 100575. **https://doi.org/10.1016/j.jfp.2025.100575**
28. Munarko, H., Kurnianto, M.A., Jariyah, J., Arwani, A., Sari, R.M. (2025). Physicochemical properties, sensory profile, and emotional perception of unpolished organic rice. *Polish Journal of Food and Nutrition Sciences*, *75*(2), 144–158. **https://doi.org/10.31883/pjfns/203936**
29. Munarko, H., Sitanggang, A.B., Kusnandar, F., Budijanto, S. (2021). Effect of different soaking and germination methods on bioactive compounds of germinated brown rice. *International Journal of Food Science & Technology*, *56*(9), 4540–4548. **https://doi.org/10.1111/ijfs.15194**
30. Munarko, H., Sitanggang, A.B., Kusnandar, F., Budijanto, S. (2022). Germination of five Indonesian brown rice: evaluation of antioxidant, bioactive compounds, fatty acids and pasting properties. *Food Science and Technology*, *42*, art. no. e19721. **https://doi.org/10.1590/fst.19721**
31. Nana, R., Maïga, Y., Ouédraogo, R.F., Kaboré, W.G.B., Badiel, B., Tamini, Z. (2019). Effect of water quality on the germination of okra (*Abelmoschus esculentus*) seeds. *International Journal of Agronomy*, *2019*, art. no. 4938349. **https://doi.org/10.1155/2019/4938349**
32. Nanfack, A.D., Nguefack, J., Musonerimana, S., La China, S., Giovanardi, D., Stefani, E. (2024). Exploiting the microbiome associated with normal and abnormal sprouting rice (*Oryza sativa* L.) seed phenotypes through a metabarcoding approach. *Microbiological Research*, *279*, art. no. 127546. **https://doi.org/10.1016/j.micres.2023.127546**
33. Ng, L.C., Sariah, M., Sariam, O., Radziah, O., Abidin, M.A.Z. (2012). Rice seed bacterization for promoting germination and seedling growth under aerobic cultivation system. *Australian Journal of Crops Science*, *6*(1), 170-175.
34. Ngalimat, M.S., Mohd Hata, E., Zulperi, D., Ismail, S.I., Ismail, M.R., Mohd Zainudin, N.A.I., Saidi, N.B., Yusof, M.T. (2021). Plant growth-promoting bacteria as an emerging tool to manage bacterial rice pathogens. *Microorganisms*, *9*(4), art. no. 682. **https://doi.org/10.3390/microorganisms9040682**
35. Nooshabadi, R., Hashemi, S.M. (2024). The effect of ultraviolet radiation on pathogenic microorganisms in milk, traditional fruit juice, and drinking water. *Food Hygiene*, *14*(54), fa21-fa33. **https://doi.org/10.71876/jfh.2024.1126133**
36. Osaili, T.M., Shaker, R.R., Al-Haddaq, M.S., Al-Nabulsi, A.A., Holley, R.A. (2009). Heat resistance of *Cronobacter* species (*Enterobacter sakazakii*) in milk and special feeding formula. *Journal of Applied Microbiology*, *107*(3), 928–935. **https://doi.org/10.1111/j.1365-2672.2009.04271.x**
37. Pearce, L.E., Smythe, B.W., Crawford, R.A., Oakley, E., Hathaway, S.C., Shepherd, J.M. (2012). Pasteurization of milk: The heat inactivation kinetics of milk-borne dairy pathogens under commercial-type conditions of turbulent flow. *Journal of Dairy Science*, *95*(1), 20–35. **https://doi.org/10.3168/jds.2011-4556**
38. Quibod, I.L., Grande, G., Oreiro, E.G., Borja, F.N., Dossa, G.S., Mauleon, R., Cruz, C.V., Oliva, R. (2015). Rice-infecting pseudomonas genomes are highly accessorized and harbor multiple putative virulence mechanisms to cause sheath brown rot. *PLoS One*, *10*(9), art. no. e0139256. **https://doi.org/10.1371/journal.pone.0139256**
39. Ramírez-Olvera, S.M., Trejo-Téllez, L.I., García-Morales, S., Pérez-Sato, J.A., Gómez-Merino, F.C. (2018). Cerium enhances germination and shoot growth, and alters mineral nutrient concentration in rice. *PLoS One*, *13*(3), art. no. e0194691. **https://doi.org/10.1371/journal.pone.0194691**
40. Rodrigues, L.A., Cañizares, L. da C.C., Meza, S.L.R., Peres, B.B., Jappe, S.N., Timm, N. da S., Oliveira, M. de, Coradi, P.C. (2024). A review of the influence of genotype, environment, and food processing on the bioactive compound profile of red rice (*Oryza sativa* L.). *Agronomy*, *14*(3), art. no. 616. **https://doi.org/10.3390/agronomy14030616**
41. Rohman, A., Gandjar, I.G. (2007). *Chromatography Methods for Food Analysis*. Pustaka Pelajar, Yogyakarta, pp. 48-54.
42. Ryan, M.P., Pembroke, J.T. (2018). *Brevundimonas* spp: Emerging global opportunistic pathogens. *Virulence*, *9*(1), 480–493. **https://doi.org/10.1080/21505594.2017.1419116**
43. Scarlett, K., Collins, D., Tesoriero, L., Jewell, L., van Ogtrop, F., Daniel, R. (2016). Efficacy of chlorine, chlorine dioxide and ultraviolet radiation as disinfectants against plant pathogens in irrigation water. *European Journal of Plant Pathology*, *145*(1), 27–38. **https://doi.org/10.1007/s10658-015-0811-8**
44. Shelp, B.J., Bozzo, G.G., Trobacher, C.P., Zarei, A., Deyman, K.L., Brikis, C.J. (2012). Hypothesis/review: Contribution of putrescine to 4-aminobutyrate (GABA) production in response to abiotic stress. *Plant Science*, *193–194*, 130–135. **https://doi.org/10.1016/j.plantsci.2012.06.001**
45. Sitanggang, A.B., Joshua, M., Munarko, H., Kusnandar, F., Budijanto, S. (2021). Increased γ-aminobutyric acid content of germinated brown rice produced in membrane reactor. *Food Technology and Biotechnology*, *59*(3), 295–305. **https://doi.org/10.17113/ftb.59.03.21.6846**
46. Tariq, H., Subramanian, S., Geitmann, A., Smith, D.L. (2025). *Bacillus* and *Paenibacillus* as plant growth-promoting bacteria in soybean and cannabis. *Frontiers in Plant Science*, *16*, art. no. 1529859. **https://doi.org/10.3389/fpls.2025.1529859**
47. Wang, Y., Li, M., Xu, F., Chai, L., Bao, J., Shen, S. (2016). Variation in polyphenols, tocols, γ-aminobutyric acid, and antioxidant properties in whole grain rice (*Oryza sativa* L.) as affected by different germination time. *Cereal Chemistry*, *93*(3), 268–274. **https://doi.org/10.1094/CCHEM-08-15-0171-R**

48. Yan, L., Zheng, H., Liu, W., Liu, C., Jin, T., Liu, S., Zheng, L. (2021). UV-C treatment enhances organic acids and GABA accumulation in tomato fruits during storage. *Food Chemistry*, *338*, art. no. 128126. **https://doi.org/10.1016/j.foodchem.2020.128126**
49. Yang, G., Xu, J., Xu, Y., Li, R., Wang, S. (2023). Analysis of dynamics and diversity of microbial community during production of germinated brown rice. *Foods*, *12*(4), art. no. 755. **https://doi.org/10.3390/foods12040755**
50. Zhang, C., Xia, X., Li, B., Hung, Y.-C. (2018). Disinfection efficacy of electrolyzed oxidizing water on brown rice soaking and germination. *Food Control*, *89*, 38–45. **https://doi.org/10.1016/j.foodcont.2018.01.007**
51. Zhu, J., Li, C., Sun, L., Cheng, Y., Hou, J., Fan, Y., Ge, Y. (2022). Application of γ-aminobutyric acid induces disease resistance in apples through regulation of polyamine metabolism, GABA shunt and reactive oxygen species metabolism. *Scientia Horticulturae*, *291*, art. no. 110588. **https://doi.org/10.1016/j.scienta.2021.110588**
52. Zhu, T., Ruan, S., Zhang, J., Zhou, B., Fang, L., Song, K., Tu, S., Tu, K. (2023). γ-Aminobutyric acid (GABA) mediated stilbene biosynthesis and alleviated oxidative stress induced by UV-C radiation during peanuts (*Arachis hypogaea* L.) germination. *Acta Physiologiae Plantarum*, *45*(8), art. no. 102. **https://doi.org/10.1007/s11738-023-03580-1**

ORIGINAL ARTICLE
http://journal.pan.olsztyn.pl

Polish Journal of Food and Nutrition Sciences
2026, Vol. 76, No. 3, 312–330
DOI: 10.31883/pjfns/231178
ISSN 1230-0322, e-ISSN 2083-6007

Comparative Characterization of Polysaccharides from *Rosa roxburghii* Tratt. Fruits Collected from Eight Major Producing Areas of Guizhou: Structure, Physicochemical Properties, and *In Vitro* Bioactivity

Guangjing Chen*, Xuemei Chen, Xianghui Yang, Meiwen Sun, Qingshan Yang

College of Food Science and Engineering, Guiyang University, Guiyang, Guizhou 550005, PR China

Polysaccharides from *Rosa roxburghii* Tratt. (RRTP) are predominantly pectic and are considered core bioactive compounds of the fruit. In this study, RRTPs were extracted from fruit of the cultivar 'Guinong 5' collected from eight major production areas in Guizhou, China, to evaluate source-associated differences in pectic structural features, physicochemical properties, antioxidant capacity, and inhibitory activity against α-amylase and α-glucosidase. Extraction yields ranged from 3.29% to 4.64%. All RRTPs exhibited typical pectic characteristics, but significant differences were observed in uronic acid content, monosaccharide composition, the distribution of homogalacturonan (HG) and rhamnogalacturonan-I (RG-I) domains, molecular weight, particle behavior, and thermal properties. Among the tested samples, RRTP from Congjiang County (RRTP-CJ) showed the highest galacturonic acid content (49.72 mol%) and one of the lowest molecular weights (80.6 kDa). It also exhibited the strongest DPPH$^{\bullet}$, ABTS$^{\bullet+}$, and $O_2^{\bullet-}$ scavenging activities with half-maximal inhibitory concentration (IC_{50}) values of 0.394, 0.300, and 0.452 mg/mL, respectively. RRTP-CJ also showed the strongest Fe^{2+}-chelating activity, with a half-maximal effective concentration (EC_{50}) of 0.671 mg/mL, and the strongest α-amylase and α-glucosidase inhibition, with IC_{50} values of 2.425 and 0.747 mg/mL, respectively. Correlation analyses indicated that uronic acid content and HG abundance were positively associated with antioxidant capacity and carbohydrase inhibitory activity, whereas higher molecular weight and extensive RG-I branching were negatively associated with these effects. Principal component analysis further distinguished highly bioactive samples characterized by lower molecular weight and a higher content of galacturonic acid. Overall, substantial source-associated heterogeneity was revealed among RRTPs, and RRTP-CJ was identified as a promising raw material for functional food ingredient development. These findings should be interpreted within the scope of a single cultivar and harvest year, providing a basis for raw-material selection, standardization, and subsequent multi-year validation.

Keywords: digestive-enzyme inhibition, homogalacturonan, molecular-weight distribution, pectic polysaccharides, rhamnogalacturonan-I, source-associated variation

ABBREVIATIONS

ABTS, 2,2′-azino-bis(3-ethylbenzothiazoline-6-sulfonic acid); BSA, bovine serum albumin; DPPH radical, 2,2-diphenyl-1-picrylhydrazyl radical; FTIR, Fourier transform infrared; HG, homogalacturonan; HPGPC, high-performance gel permeation chromatography; PCA, principal component analysis; *p*NPG, *p*-nitrophenyl-α-D-glucopyranoside; RG-I, rhamnogalacturonan-I; RG-II, rhamnogalacturonan-II; RRTPs, *Rosa roxburghii* Tratt.

***Corresponding Author:**
E-mail: **gyugjchen@gyu.edu.cn, gjchen1989@126.com** (G. Chen)

Submitted: 18 January 2026
Accepted: 17 August 2026
Published on-line: 4 September 2026

polysaccharides; TGA, thermogravimetric analysis; XRD, X-ray diffraction.

INTRODUCTION

Rosa roxburghii Tratt., commonly known as Cili because of its thorny fruits, is an edible fruit species mainly cultivated in the mountainous regions of southwestern China. Guizhou Province is the core area of commercial production, where large differences in altitude, climate, and cultivation conditions may contribute to variation in fruit quality and bioactive composition [Jain *et al.*, 2024]. The fruit is valued as a functional food resource because it is rich in ascorbic acid, phenolic compounds, organic acids, triterpenoids, superoxide dismutase, and polysaccharides [Wang *et al.*, 2021; Wang *et al.*, 2022a]. Several cultivars or types, including 'Guinong 1', 'Guinong 5', 'Guinong 7', and 'Seedless Cili', are currently used in production. Among them, 'Guinong 5' is widely cultivated in Guizhou because of its strong adaptability, disease resistance, stable yield, and good processing suitability [Li *et al.*, 2022]. Therefore, using this cultivar as a unified material can reduce cultivar-related interference and allow a more focused comparison of source-associated variation among producing areas.

Within this compositional background, *R. roxburghii* Tratt. polysaccharides (RRTPs) deserve particular attention because they represent one of the major macromolecular bioactive compounds of the fruit. Previous studies have shown that RRTPs can exhibit antioxidant activity, prebiotic potential, and hypoglycemic and hypolipidemic effects in experimental models [Wang *et al.*, 2020; Wang *et al.*, 2023]. These activities are closely related to structural features, such as monosaccharide composition, uronic acid content, molecular weight, glycosidic linkages, and chain conformation. Many RRTPs are acidic pectic polysaccharides. Pectin generally contains homogalacturonan (HG), rhamnogalacturonan-I (RG-I), and rhamnogalacturonan-II (RG-II) domains; HG is mainly formed by linear α-(1→4)-linked D-galacturonic acid residues, whereas RG-I contains alternating rhamnose and galacturonic acid residues with arabinose- and galactose-rich side chains [Voragen *et al.*, 2009]. Therefore, differences in HG/RG-I domain distribution may strongly influence the physicochemical behavior and bioactivity of RRTPs.

The antioxidant capacity and carbohydrate-hydrolyzing enzyme inhibitory activity of plant polysaccharides are especially relevant for functional food development. Polysaccharides may prevent oxidative damage by donating hydrogen or electrons and by chelating pro-oxidant metal ions; these effects are often affected by uronic acid content, molecular weight, charge density, and chain exposure [Fernandes & Coimbra, 2023]. In addition, inhibition of α-amylase and α-glucosidase can slow starch digestion and glucose release, thereby helping to attenuate postprandial hyperglycemia [Gong *et al.*, 2020; Zheng *et al.*, 2019]. For *R. roxburghii*, purified acidic polysaccharides and crude polysaccharide fractions have shown α-glucosidase inhibitory activity and glucose-modulating effects, indicating that RRTPs may be useful as food-derived ingredients for glycemic management [Wang *et al.*, 2018a; Wang *et al.*, 2019].

Source-associated variation is an important issue for plant polysaccharides because raw material origin can affect the extraction yield, structural characteristics, physicochemical properties, and bioactivity of the resulting polysaccharides. Such effects have been reported for pectins and polysaccharides from mango peel, jujube fruit, and *Gracilaria chouae*, where cultivar, growth region, or producing area influenced chemical composition, molecular characteristics, rheological behavior, and bioactivity of the resulting pectin or polysaccharide preparations [Deng *et al.*, 2020; Feng *et al.*, 2025; Li *et al.*, 2024]. However, most studies on RRTPs have used materials from a single location or have focused on extraction methods and processing conditions. Systematic comparison of RRTPs from major commercial sources under a unified cultivar background remains limited. It is therefore unclear whether RRTPs from different producing areas differ in pectic domain composition, molecular weight distribution, physicochemical properties, antioxidant capacity, and digestive enzyme inhibitory activity. Accordingly, this study compared RRTPs extracted from 'Guinong 5' fruits collected from eight major producing areas in Guizhou Province. The polysaccharides were evaluated for extraction yield, chemical composition, monosaccharide profile, pectic domain distribution, molecular weight, Fourier transform infrared spectra, crystallinity, particle behavior, thermal stability, antioxidant capacity, and inhibition of α-amylase and α-glucosidase. Correlation analysis and principal component analysis were further used to explore structure-activity relationships. This study aimed to identify source-associated differences among RRTPs and to provide a scientific basis for raw-material selection, quality standardization, and targeted development of *R. roxburghii* polysaccharides as functional food ingredients.

MATERIALS AND METHODS

Materials and chemicals

All *Rosa roxburghii* Tratt. fruits (RRT) used in this study were collected from the same cultivar ('Guinong 5') within a single harvest year from eight major producing areas in Guizhou Province, China: Panzhou, Shuicheng, Longli, Hezhang, Qixingguan, Sinan, Congjiang, and Zheng'an. To improve representativeness and reduce individual-plant bias, fruits from multiple healthy plants within each region were pooled to prepare a composite regional sample. This sampling strategy was adopted to better reflect source-associated characteristics at the regional level under a controlled cultivar background. The sampling sites, geographic coordinates, and altitudes are presented in **Table 1**. Because the present work was designed as a comparative study of source-associated variation rather than a direct environmental causality analysis, site-specific soil and meteorological parameters were not monitored. All fruit batches were transported under refrigerated conditions (4–8°C) before drying and extraction.

Monosaccharide standards, including galactose (Gal), mannose (Man), rhamnose (Rha), xylose (Xyl), glucose (Glc), arabinose (Ara), fucose (Fuc), glucuronic acid (GlcA), galacturonic acid (GalA), ribose (Rib), fructose (Fru), glucosamine (GlcN), galactosamine (GalN), guluronic acid (GulA), mannuronic acid

Table 1. Collection sites of *Rosa roxburghii* Tratt. (RRT) fruits and corresponding polysaccharide sample codes.

Code	Collection site	Altitude (m)	Geographic coordinates
RRTP-CJ	Congjiang, Qiandongnan	560	25°28′30.95″N, 108°32′47.54″E
RRTP-HZ	Hezhang, Bijie	1,448	27°13′51.99″N, 104°52′32.80″E
RRTP-LL	Longli, Qiannan	1,380	26°33′19.20″N, 106°55′12.24″E
RRTP-PZ	Panzhou, Liupanshui	1,905	25°54′5.62″N, 104°32′45.70″E
RRTP-QXG	Qixingguan, Bijie	1,669	27°26′32.83″N, 105°23′25.15″E
RRTP-SC	Shuicheng, Liupanshui	1,738	26°11′28.91″N, 104°41′27.03″E
RRTP-SN	Sinan, Tongren	586	27°43′9.30″N, 107°57′35.56″E
RRTP-ZA	Zheng'an, Zunyi	909	28°37′15.40″N, 107°30′31.50″E

(ManA), and *N*-acetyl-D-glucosamine (GlcNAc), were obtained from Tokyo Chemical Industry Co., Ltd. (Tokyo, Japan). α-Amylase, α-glucosidase, *p*-nitrophenyl-α-D-glucopyranoside (*p*NPG), and bovine serum albumin (BSA) were purchased from Yuanye Biotechnology Co., Ltd. (Shanghai, China). All remaining reagents were of analytical or chromatographic grade and were procured from local suppliers.

Isolation of polysaccharides from *Rosa roxburghii* Tratt. fruits

Polysaccharides were isolated by ultrasonic-assisted hot-water extraction under our previously optimized conditions [Chen & Kan, 2018]. Fresh fruits from the eight regions were rinsed to remove surface debris, the calyx and stem ends were trimmed, and tissues were cut into small pieces. Material was dried in a hot-air oven (DHG-9240, Shanghai Jinghong Instrument Equipment Co., LTD, Shanghai, China) at 50°C, milled, and sieved (60 mesh). Defatting and decolorization were performed by soaking the powder in petroleum ether at a solid to liquid ratio of 1:4 (*w/v*) at room temperature for 24 h with continuous stirring. Solvent was refreshed every 8 h. The mixture was vacuum-filtered, and the residue was soaked in 95% ethanol under identical conditions, followed by vacuum filtration and drying. Pretreated powder (10 g) was suspended in distilled water (400 mL) and subjected to ultrasonication (40 kHz, 150 W) at 80°C for 33 min using an SC25-12 DTD bath sonicator (Ningbo Scientz Biotechnology Co., Ltd., Ningbo, China). The extract was concentrated to one-quarter of the initial volume using a rotary evaporator (R-215, Buchi, Flawil, Switzerland) at 54°C under reduced pressure. Proteins were removed by the Sevag method: Sevag reagent (chloroform : *n*-butanol, 4:1, *v/v*) was added, the mixture was agitated at 180 rpm for 10 min, and phases were allowed to separate; the lower organic phase and interfacial protein layer were discarded, and the upper aqueous phase was retained. This step was repeated until no protein emulsion remained. The aqueous phase was transferred into regenerated cellulose dialysis tubing with a molecular weight cutoff of 8,000–14,000 Da (Yuanye Bio-technology Co., Ltd., Shanghai, China) and dialyzed against distilled water for 48 h. Polysaccharides were precipitated by adding four volumes of ethanol, collected, and freeze-dried to yield the final products. Samples of *Rosa roxburghii* Tratt. polysaccharides (RRTP) obtained from fruits collected in different areas of Guizhou were designated as RRTP-CJ (Congjiang), RRTP-HZ (Hezhang), RRTP-LL (Longli), RRTP-PZ (Panzhou), RRTP-QXG (Qixingguan), RRTP-SC (Shuicheng), RRTP-SN (Sinan), and RRTP-ZA (Zhen'an). The extraction yield (%, *w/w*) was calculated as according to Equation (1):

$$\text{RRTP yield (\%)} = \frac{\text{Weight of dried RRTPs (g)}}{\text{Initial weight of pretreated RRT (g)}} \quad (1)$$

Analysis of chemical composition of polysaccharides from *Rosa roxburghii* Tratt. fruits

Neutral sugar, uronic acid, and protein contents

Neutral sugar, uronic acid, and protein contents were determined colorimetrically. For neutral sugar determination, an RRTP solution was mixed with a phenol solution and concentrated sulfuric acid, incubated for color development, and measured at 490 nm using Glc as the standard [DuBois *et al.*, 1956]. Uronic acid content was determined by the *m*-hydroxydiphenyl method; briefly, an RRTP solution was reacted with a sulfuric acid–borate reagent, followed by the addition of the *m*-hydroxydiphenyl reagent, and absorbance was recorded at 525 nm using GalA as the standard [Blumenkrantz & Asboe-Hansen, 1973]. Protein content was measured using the Coomassie Brilliant Blue G-250 method (Bradford protein assay), with absorbance recorded at 595 nm and BSA used as the standard [Zor & Selinger, 1996]. Results were calculated from the corresponding calibration curves and expressed as g of standard equivalent *per* 100 g of dried RRTP sample: g glucose equivalent/100 g for neutral sugars, g galacturonic acid equivalent/100 g for uronic acids, and g BSA equivalent/100 g for proteins. Results were calculated based on calibration curves using Glc for neutral sugars, yielding $y = 0.0054\,x + 0.0711$ ($R^2 = 0.9987$, $n = 6$); BSA for protein, yielding $y = 0.0039\,x +$

+ 0.4173 (R^2 = 0.9985, n = 6); and GalA for uronic acids, yielding y = 0.0285 x + 0.0311 (R^2 = 0.997, n = 6).

Monosaccharide composition

Monosaccharide profiles were determined by high-performance anion-exchange chromatography (HPAEC) on a Thermo Dionex ICS-6000 system (Thermo Scientific, Waltham, MA, USA) following a validated procedure [Shi *et al*., 2025]. Each RRTPs sample (6 mg) was hydrolyzed in 2 M trifluoroacetic acid (4 mL) at 121°C for 3 h. Following acid removal, hydrolysates were diluted to 50 mL with distilled water, filtered (0.22 μm), and injected (25 μL) onto a Dionex CarboPac PA20 analytical column (3×150 mm; Thermo Scientific) equipped with a guard cartridge. Separation was performed at 30°C, 0.5 mL/min, using ultrapure water (A), 40 mM NaOH (B), 500 mM sodium acetate (C), and 250 mM NaOH (D) under the following gradient program: 0–20.05 min, 90% A and 10% B; 20.05–53.05 min, 70% A, 20% B and 10% C; 53.05–60.00 min, 50% A and 50% D. Peak identification and compound quantification were carried out using sixteen monosaccharide standards (Tokyo Chemical Industry Co., Ltd., Tokyo, Japan) analyzed under identical conditions. The amount of each monosaccharide was calculated from its corresponding external calibration curve and converted to molar amount. Results were expressed as relative molar fractions (mol%), calculated as ni/Σni, where ni represents the molar amount of an individual monosaccharide and Σni represents the total molar amount of all identified monosaccharides in the same sample. For each RRTP sample, the sum of the identified monosaccharide fractions was normalized to 100. Pectic structural parameters were estimated from the relative molar fractions; HG and RG-I were calculated according to Equations (2) and (3), respectively:

$$HG = GalA - Rha \quad (2)$$

$$RG\text{-}I = 2Rha + Ara + Gal \quad (3)$$

Rha/GalA was used to indicate the relative contribution of the RG-I backbone; and (Ara + Gal)/Rha was used to indicate the relative degree of RG-I side-chain branching.

Determination of physicochemical properties of polysaccharides from *Rosa roxburghii* Tratt. fruits

Molecular weight distribution

Molecular-weight distributions were assessed by high-performance gel permeation chromatography (HPGPC) using Agilent 1260 system with a refractive-index detector (Agilent Technologies, Santa Clara, CA, USA) [Shi *et al.*, 2025]. RRTPs were dissolved in a 0.1 M $NaNO_3$ solution at 5 mg/mL and filtered through 0.45 μm membranes. Samples were separated on a TSK-Gel GMPWXL column (7.8 × 300 mm; Tosoh Bioscience, Tokyo, Japan) at 30°C. A 0.1 M $NaNO_3$ solution was used as the mobile phase at a flow rate of 0.5 mL/min, and the injection volume was 25 μL. A calibration curve relating retention time to the logarithm of molecular weight (log Mw) was generated using dextran standards (6.3–739 kDa; Agilent Technologies).

Fourier transform infrared spectroscopy

Fourier transform infrared (FT-IR) spectra of RRTPs were acquired by the KBr-pellet method on a Spectrum Two FT-IR spectrometer (PerkinElmer, Waltham, MA, USA) as described by Shi *et al.* [2025]. For each run, RRTP samples (2 mg) were mixed with dry KBr (200 mg), finely ground in an agate mortar, and pressed into translucent disks. A blank KBr pellet was recorded as the background. Spectra were collected from 4,000 to 400 cm^{-1} at 4 cm^{-1} resolution to assign functional groups and backbone features.

Thermal stability

Thermal stability of RRTPs was evaluated by thermogravimetric analysis (TGA) on a DTG-60A instrument (Shimadzu, Kyoto, Japan) [Chen *et al.*, 2025]. Approximately 5 mg of the sample was sealed in a high-purity aluminum crucible, with an empty crucible used as the reference. Heating was performed from 25°C to 800°C at 10°C/min under nitrogen (50 mL/min). The thermogravimetric (TG) curve and the derivative thermogravimetric (DTG) curve were calculated separately to resolve mass-loss stages and peak decomposition temperatures.

Structural characterization by X-ray diffraction analysis

X-ray diffraction (XRD) analysis of RRTPs was performed using a D8 Advance diffractometer (Bruker, Leipzig, Germany) equipped with a copper anode producing Cu Kα radiation (λ=1.5406 Å) and operated at 40 kV and 40 mA. Diffraction patterns were collected over 2θ = 5°–60° at a scan speed of 10°/min. Peak deconvolution analysis was performed to resolve the crystalline (A_b) and amorphous (A_a) regions within the polysaccharide samples. The crystallinity index (CrI, %) was calculated according to Equation (4) [Wang *et al.*, 2022b]:

$$CrI\ (\%) = \frac{A_b}{A_b + A_a} \times 100 \quad (4)$$

Zeta potential and particle size distribution

Surface charge and hydrodynamic size of RRTPs (2 mg/mL in Milli-Q water) were determined at 25°C by dynamic light scattering on a Nano ZS90 analyzer (Malvern Instruments, Worcestershire, UK), following Shi *et al*. [2025]. Zeta potential was reported in mV, and particle size was expressed as the intensity-weighted Z-average diameter (nm). To ensure reproducibility, polydispersity indices (PDI) were maintained below 0.40 for all preparations. Measurement parameters were as follows: refractive indices of 1.414 (dispersed phase) and 1.330 (continuous phase), solvent viscosity of 0.8872 cP, and a target signal intensity of 80 counts/s.

Antioxidant capacity analysis of polysaccharides from *Rosa roxburghii* Tratt. fruits

The antioxidant capacity of RRTPs was evaluated by $DPPH^{\bullet}$-, $ABTS^{\bullet+}$-, and $O_2^{\bullet-}$-scavenging assays and by Fe^{2+}-chelating assay. RRTP solutions were prepared in distilled water at 0.25, 0.50, 1.00,

1.50, 2.00, and 2.50 mg/mL. Ascorbic acid was used as the positive control for radical-scavenging assays, and ethylenediaminetetraacetic acid (EDTA) was used as the positive control for the Fe^{2+}-chelating assay.

The DPPH$^{\bullet}$-scavenging assay was performed according to Brand-Williams *et al.* [1995], with appropriate modifications. An RRTP solution was mixed with a DPPH$^{\bullet}$ ethanol solution and incubated in the dark at room temperature, after which the absorbance was measured at 517 nm. A reaction mixture in which the RRTP solution was replaced with distilled water served as the control, and a sample blank without DPPH$^{\bullet}$ was used to correct the background absorbance of each RRTP solution. DPPH$^{\bullet}$ scavenging activity was calculated as follows (Equation (5)):

$$\text{Radical scavenging activity (\%)} = \left(1 - \frac{A_s - A_b}{A_0}\right) \times 100 \quad (5)$$

where A_s is the absorbance of the sample reaction mixture, A_b is the absorbance of the sample blank, and A_0 is the absorbance of the control.

The ABTS$^{\bullet+}$-scavenging assay was performed according to Re *et al.* [1999], with appropriate modifications. The ABTS$^{\bullet+}$ working solution was prepared by reacting ABTS with potassium persulfate in the dark and subsequently diluting the mixture to an absorbance of 0.70 ± 0.02 at 734 nm. The RRTP solution was mixed with the ABTS$^{\bullet+}$ working solution and incubated at room temperature, after which the absorbance was measured at 734 nm. ABTS$^{\bullet+}$ scavenging activity was calculated using Equation (5).

The $O_2^{\bullet-}$-scavenging assay was performed using the phenazine methosulfate (PMS) – reduced nicotinamide adenine dinucleotide (NADH) – nitroblue tetrazolium (NBT) system described by Nishikimi *et al.* [1972], with appropriate modifications. The reaction mixture contained the RRTP solution, NBT, NADH, and PMS in phosphate buffer. The reaction was initiated by adding PMS. Following incubation at room temperature, the absorbance was measured at 560 nm. A reaction mixture without RRTPs served as the control, and a sample blank without PMS was prepared to correct the background absorbance. $O_2^{\bullet-}$ scavenging activity was calculated using Equation (5).

The Fe^{2+} chelating assay was performed according to Dinis *et al.* [1994], with appropriate modifications, based on competition between RRTPs and ferrozine for Fe^{2+}. Formation of the Fe^{2+}–ferrozine complex was monitored at 562 nm, as originally described by Stookey [1970]. Briefly, the RRTP solution was mixed with the $FeCl_2$ solution, and the reaction was initiated by adding the ferrozine solution. Following incubation at room temperature, the absorbance of the Fe^{2+}–ferrozine complex was measured at 562 nm. A reaction mixture containing Fe^{2+} and ferrozine without RRTPs served as the control and represented 0% chelating activity. A sample blank without Fe^{2+} was used to correct the background absorbance of each RRTP solution. Fe^{2+}-chelating activity was calculated according to Equation (6):

$$Fe^{2+}\text{ chelating activity (\%)} = \left(1 - \frac{A_s - A_b}{A_0}\right) \times 100 \quad (6)$$

where A_s is the absorbance of the sample reaction mixture, A_b is the absorbance of the sample blank, and A_0 is the absorbance of the control. In this assay, 100% chelating activity represents complete prevention of Fe^{2+}–ferrozine complex formation after background correction.

Dose–response curves were constructed using the activity values obtained at different RRTP concentrations. The concentration required to achieve 50% radical-scavenging activity was expressed as the half-maximal inhibitory concentration (IC_{50}), whereas the concentration required to achieve 50% Fe^{2+}-chelating activity was expressed as the half-maximal effective concentration (EC_{50}).

Determination of *in vitro* hypoglycemic activity of polysaccharides from *Rosa roxburghii* Tratt. fruits

α-Glucosidase inhibitory activity

The α-glucosidase inhibitory activity of RRTPs was evaluated using a *p*NPG-based assay according to Tadera *et al.* [2006], with appropriate modifications. RRTP solutions were prepared in phosphate-buffered saline (PBS; 100 mM, pH 6.9) at concentrations of 0.5–7.0 mg/mL. α-Glucosidase solution (0.5 U/mL) and *p*NPG solution (6 mM) were also prepared in the same buffer. For each assay, 100 µL of the RRTP solution was combined with 100 µL of α-glucosidase solution and incubated at 37°C for 10 min. Subsequently, 100 µL of *p*NPG solution was added, and incubation was continued for 20 min at 37°C. Parallel controls were run in the absence of RRTPs and in the absence of enzyme; acarbose served as the positive control. Reactions were terminated with 1 mL of 1 M Na_2CO_3. Formation of *p*-nitrophenol was quantified at 405 nm using a microplate reader (Model 1500, Thermo Multiskan SkyHigh, Waltham, USA). Percentage inhibition was calculated according to Equation (7):

$$\text{Inhibition (\%)} = \left(1 - \frac{A_{\text{sample}} - A_{\text{control-1}}}{A_{\text{control-2}}}\right) \times 100 \quad (7)$$

where A_{sample} denotes the absorbance of the complete system (RRTP + enzyme + substrate), $A_{\text{control-1}}$ denotes the absorbance of the mixture in which α-glucosidase was replaced with the buffer, and $A_{\text{control-2}}$ denotes the absorbance of the mixture in which RRTP was replaced with the buffer. The IC_{50} value was defined as the RRTP concentration required to inhibit 50% of α-glucosidase activity. IC_{50} values were calculated from dose–response curves by plotting inhibition (%) against RRTP concentration and fitting the data by nonlinear regression.

Inhibitory kinetics toward α-glucosidase

The inhibition kinetics of RRTPs against α-glucosidase (0.5 U/mL) were evaluated by measuring enzyme activity at different *p*NPG concentrations (1–4 mM) in the absence or presence of RRTPs (0, 3, and 5 mg/mL). The inhibition mode and mechanism were analyzed using Lineweaver–Burk double-reciprocal plots

within the Michaelis–Menten framework [Lineweaver & Burk, 1934]. The data were analyzed according to the mixed-inhibition equation (Equation (8)), from which the Michaelis constant (K_m) and maximal velocity (V_{max}) were obtained. The slope and y-intercept of the Lineweaver–Burk plot were determined for each RRTP concentration. The dissociation constant for inhibitor binding to the free enzyme (K_i) was obtained from the absolute value of the x-intercept of the secondary plot of the Lineweaver–Burk slope *versus* inhibitor concentration (Equation (9)). The dissociation constant for inhibitor binding to the enzyme–substrate complex (K_{is}) was obtained from the absolute value of the x-intercept of the secondary plot of the Lineweaver–Burk y-intercept *versus* inhibitor concentration (Equation (10)) [Cornish-Bowden, 1974]. In Equations (8)–(10), v denotes the initial reaction rate, [S] stands for the substrate concentration, and [I] indicates the inhibitor concentration.

$$\frac{1}{v} = \frac{K_m}{V_{max}}\left(1 + \frac{[I]}{K_i}\right)\frac{1}{[S]} + \frac{1}{V_{max}}\left(1 + \frac{[I]}{K_{is}}\right) \quad (8)$$

$$\text{Slope} = \frac{K_m}{V_{max}} + \frac{K_m[I]}{V_{max}K_i} \quad (9)$$

$$\text{Y-intercept} = \frac{1}{V_{max}} + \frac{[I]}{K_{is}V_{max}} \quad (10)$$

α-Amylase inhibitory activity

The α-amylase inhibitory activity of RRTPs was determined using the 3,5-dinitrosalicylic acid (DNS)-based amylase assay described by Bernfeld [1955], with appropriate modifications. Sample solutions were prepared in 0.02 M phosphate buffer (pH 6.9). Equal volumes of the RRTP solution (500 µL) and α-amylase (10 U/mL) were combined and incubated at 37°C for 10 min. Soluble starch (1%, 500 µL) was then added as a substrate, and incubation was continued for 10 min at 37°C. Reactions were terminated by adding the DNS reagent (1 mL) and heating in a boiling water bath for 5 min. After dilution with distilled water (10 mL) and cooling to ambient temperature, absorbance was recorded at 540 nm. Percent inhibition was calculated according to Equation (7). Acarbose was used as the positive control. The IC_{50} value was defined as the RRTP concentration required to inhibit 50% of α-amylase activity. IC_{50} values were calculated from dose–response curves by plotting inhibition (%) against RRTP concentration and fitting the data by nonlinear regression.

Statistical analysis

Data were presented as mean and standard deviation (SD). Before analysis, the normality of the residuals and homogeneity of variances were assessed using the Shapiro-Wilk and Levene tests, respectively. When these assumptions were satisfied, differences among the RRTP samples were evaluated by one-way analysis of variance (ANOVA). Duncan's multiple range test was used for multiple comparisons among samples, whereas the least significant difference (LSD) test was used only for predefined pairwise comparisons. Differences were considered statistically significant at $p<0.05$, and all statistical tests were two-sided. Pearson correlation analysis was performed to examine the relationships among chemical composition, structural parameters, physicochemical properties, antioxidant capacity, and digestive-enzyme inhibitory activity of RRTPs. Correlations were expressed as Pearson's correlation coefficients (r), with significance determined at $p<0.05$ or $p<0.01$. Principal component analysis (PCA) was performed on standardized variables using the correlation matrix to visualize the overall relationships and differences among the RRTP samples. Statistical analyses were conducted using IBM SPSS Statistics 23.0 (IBM Corp., Armonk, NY, USA), and figures were prepared using OriginPro 2021 (OriginLab Corp., Northampton, MA, USA).

RESULTS AND DISCUSSION

Yield and chemical composition of polysaccharides from *Rosa roxburghii* Tratt. fruits

Substantial differences in extraction yield (3.29% to 4.64%, *w/w*) were observed among RRTPs from different production areas (**Table 2**). The highest yield was obtained for RRTP-LL, followed by RRTP-SN, RRTP-CJ, and RRTP-ZA, whereas the lowest yields were recorded for RRTP-HZ and RRTP-QXG. Under the present sampling framework, these findings indicate marked source-associated heterogeneity among RRTPs from commercially-relevant producing areas. Because site-level environmental variables were not directly monitored, and all samples were collected from the same cultivar ('Guinong 5') within one harvest year, the observed differences are interpreted here as comparative production-source variation rather than evidence of specific climatic or edaphic effects. The results highlight production-source-associated variability of practical relevance to raw-material selection and quality standardization.

Neutral sugar contents varied significantly among the RRTP samples, ranging from 57.32 to 66.59 g/ 100 g (**Table 2**). RRTP-LL and RRTP-SC contained the highest levels and did not differ significantly ($p\geq0.05$) from each other, whereas RRTP-QXG and RRTP-SN constituted the lowest-content group. RRTP-ZA, RRTP-PZ, RRTP-CJ, and RRTP-HZ showed intermediate values with partially overlapping significance groups. The observed range is comparable to the carbohydrate content reported for a hot-water-extracted RRT polysaccharide fraction (63.79 g/100 g) [Wang *et al.*, 2018b] and to the range of 57.47–68.56 g/100 g observed in RRTPs obtained from fruits subjected to different drying treatments [Zhang *et al.*, 2024]. These comparisons indicate that the present samples fall within the compositional range previously reported for water-extractable RRT polysaccharides, although direct quantitative comparisons should be made cautiously because raw-material pretreatment, extraction, purification, and analytical procedures differ among studies. Protein contents were uniformly low, ranging from 2.92 to 3.19 g/100 g, with no significant ($p\geq0.05$) differences among the eight RRTP samples (**Table 2**). This result indicates a relatively small and consistent amount of co-extracted or

Table 2. Extraction yields, chemical composition, monosaccharide profile, pectic structural parameters, average molecular weight, particle size, and zeta potential of polysaccharides from *Rosa roxburghii* Tratt. fruits (RRTP) collected in different producing areas of Guizhou Province in China.

Parameter	RRTP-CJ	RRTP-HZ	RRTP-LL	RRTP-PZ	RRTP-QXG	RRTP-SC	RRTP-SN	RRTP-ZA
Yield (%, *w/w*)	4.36±0.34^{ab}	3.66±0.11^{cd}	4.64±0.13^{a}	4.04±0.22^{bc}	3.29±0.35^{d}	3.93±0.29^{c}	4.40±0.38^{ab}	4.28±0.16^{ab}
Neutral sugar (g/100 g)	60.10±1.97^{b}	59.35±0.43^{bc}	66.59±2.11^{a}	60.95±0.72^{b}	57.32±0.67^{c}	66.04±0.65^{a}	57.74±0.42^{c}	61.86±0.90^{b}
Protein (g/100 g)	2.92±0.57^{a}	3.19±0.14^{cd}	3.01±0.27^{a}	3.17±0.17^{bc}	3.14±0.38^{d}	3.09±0.30^{c}	2.95±0.46^{ab}	3.09±0.41^{ab}
Uronic acid (g/100 g)	30.14±1.26^{a}	19.03±0.56^{c}	24.04±0.50^{b}	23.51±1.17^{b}	13.16±0.42^{d}	23.83±0.76^{b}	13.70±1.06^{d}	23.48±0.95^{b}
Monosaccharide composition (mol%)								
Fuc	0.71±0.02^{ab}	0.75±0.06^{a}	0.74±0.02^{a}	0.52±0.03^{d}	0.63±0.03^{bc}	0.71±0.06^{ab}	0.79±0.08^{a}	0.62±0.04^{c}
Rha	4.65±0.10^{e}	4.64±0.16^{e}	5.12±0.17^{cd}	5.13±0.13^{cd}	5.47±0.09^{b}	5.90±0.21^{a}	4.88±0.19^{de}	5.31±0.08^{bc}
Ara	10.72±0.26^{e}	17.81±0.70^{c}	16.14±0.33^{d}	16.80±0.63^{cd}	23.64±0.97^{a}	16.27±0.45^{d}	20.81±0.55^{b}	16.39±0.68^{d}
Gal	26.22±0.64^{e}	33.67±1.30^{c}	30.45±0.62^{d}	31.30±1.17^{d}	41.59±1.71^{a}	31.13±0.86^{d}	37.33±0.99^{b}	30.40±1.26^{d}
Glc	4.63±0.11^{e}	7.58±0.28^{b}	6.43±0.17^{d}	4.77±0.13^{e}	2.51±0.07^{f}	6.29±0.20^{d}	8.32±0.27^{a}	7.05±0.22^{c}
Xyl	2.54±0.06^{d}	3.24±0.12^{b}	3.11±0.08^{b}	2.81±0.09^{c}	3.23±0.06^{b}	3.14±0.17^{b}	3.65±0.12^{a}	2.51±0.07^{d}
Man	0.81±0.02^{d}	1.12±0.09^{b}	1.02±0.03^{bc}	0.92±0.07^{cd}	1.01±0.05^{bc}	1.32±0.11^{a}	1.46±0.14^{a}	1.42±0.04^{a}
GalA	49.72±1.21^{a}	31.19±1.48^{d}	36.99±0.76^{bc}	37.75±1.45^{b}	21.92±0.90^{e}	35.24±0.97^{c}	22.76±0.63^{e}	36.30±1.52^{bc}
HG (mol%)	45.07±1.78^{a}	26.55±1.24^{d}	31.87±0.78^{b}	32.62±1.42^{b}	16.45±0.94^{e}	29.34±1.01^{c}	17.88±0.63^{e}	30.99±1.39^{bc}
RG-I (mol%)	46.24±0.72^{f}	60.76±1.53^{c}	56.83±0.78^{e}	58.36±1.36^{de}	76.17±1.97^{a}	59.20±1.06^{cd}	67.90±1.19^{b}	57.41±1.44^{de}
Rha/GalA	0.09±0.00^{e}	0.15±0.01^{d}	0.14±0.01^{d}	0.14±0.01^{d}	0.25±0.02^{a}	0.17±0.01^{c}	0.21±0.02^{b}	0.15±0.00^{d}
(Gal+Ara)/Rha	7.94±0.23^{d}	11.09±0.50^{b}	9.10±0.33^{c}	9.38±0.35^{c}	11.93±0.41^{a}	8.03±0.28^{d}	11.91±0.52^{a}	8.81±0.30^{c}
Molecular weight (kDa)	80.6±1.0^{e}	135.0±3.5^{b}	109.8±4.1^{c}	97.3±1.9^{d}	179.4±3.7^{a}	97.0±1.7^{d}	181.1±4.2^{a}	77.8±1.3^{e}
Particle size (nm)	613±15^{b}	362±8^{e}	507±14^{d}	501±13^{d}	492±13^{d}	498±9^{d}	554±4^{c}	705±15^{a}
Polydispersity index	0.204±0.013^{b}	0.210 ±0.022^{b}	0.209±0.010^{b}	0.183±0.017^{c}	0.255±0.011^{a}	0.165±0.017^{c}	0.225±0.018^{a}	0.256±0.020^{a}
Zeta potential (mV)	−20.8±0.2^{e}	−14.5±0.8^{b}	−18.7±0.4^{d}	−18.6±0.2^{d}	−12.5±0.7^{a}	−17.2±0.7^{c}	−12.8±0.1^{a}	−17.9±0.2^{cd}

Values are presented as mean ± standard deviation (SD) (n=3). Different letters within the same row indicate significant differences among samples (p<0.05). Fuc, fucose; Rha, rhamnose; Ara, arabinose; Man, mannose; Gal, galactose; Glc, glucose; Xyl, xylose; GalA, galacturonic acid; HG, homogalacturonan; RG-I, rhamnogalacturonan-I. Sample codes are listed in **Table 1**.

retained protein. Uronic acid content displayed a broader range of 13.16–30.14 g/100 g and provided clearer compositional differentiation among the RRTP samples. RRTP-CJ contained significantly (p<0.05) more uronic acid than all the other samples. RRTP-LL, RRTP-PZ, RRTP-SC, and RRTP-ZA formed a statistically comparable intermediate group, followed by RRTP-HZ, whereas RRTP-QXG and RRTP-SN contained the lowest levels. Previous studies have reported a uronic acid content of 14.78 g/100 g in a hot-water-extracted RRT polysaccharide fraction [Wang *et al.*, 2018a] and values of 15.46–22.16 g/100 g for RRTPs prepared from differently dried fruits [Zhang *et al.*, 2024]. Thus, most of the present samples were within or close to the previously reported range, while the comparatively high value of RRTP-CJ suggests a greater abundance of acidic carbohydrate components. Given that uronic acid-rich pectic polysaccharides have been positively associated with antioxidant activities [Fernandes & Coimbra, 2023], the present data suggest that RRTPs from specific regions may possess enhanced functional properties and greater therapeutic potential.

Structural features of polysaccharides from *Rosa roxburghii* Tratt. fruits

Monosaccharide composition

The monosaccharide profile of RRTPs was analyzed using HPAEC. Representative chromatograms are presented in **Figure S1** (Supplementary Materials), and the relative contents of identified

monosaccharides are shown in **Table 2**. All eight RRTP samples contained the same eight monosaccharides, namely Rha, Fuc, Glc, Man, Xyl, Ara, Gal, and GalA. Despite this qualitative similarity, significant differences in their molar proportions were observed among the samples from different production sites, particularly for Ara, Gal, and GalA (**Table 2**). RRTP-CJ exhibited the highest GalA content (49.72 mol%), whereas RRTP-QXG and RRTP-SN had the lowest (21.92 and 22.76 mol%, respectively). These trends paralleled the uronic acid content, thereby reinforcing the regional structural heterogeneity of RRTPs. The predominance of GalA, Gal, and Ara – monosaccharides characteristic of pectic polysaccharides – indicated that RRTPs were primarily composed of pectin-type structures. Generally, three main domains are distinguished in the pectin structure: homogalacturonan (HG), rhamnogalacturonan-I (RG-I), and rhamnogalacturonan-II (RG-II). HG consists mainly of linear chains of α-(1→4)-linked GalA residues that may be partially methyl-esterified or acetylated, whereas RG-I contains an alternating Rha–GalA backbone bearing Ara- and Gal-rich side chains [Voragen *et al.*, 2009]. Quantitative analysis revealed that RG-I constituted a substantial portion of the RRTPs, ranging from 46.24 to 76.17 mol% (**Table 2**). The highest RG-I contents were found in RRTP-QXG (76.17 mol%) and RRTP-SN (67.90 mol%), whereas RRTP-CJ exhibited the lowest value (46.24 mol%).

The Rha/GalA and (Ara + Gal)/Rha ratios were further calculated as compositional indicators of the relative contribution of RG-I backbone residues and the abundance of Ara- and Gal--containing side chains, respectively [Dimopoulou *et al.*, 2019]. The Rha/GalA ratios of all RRTPs ranged from 0.09 to 0.25, consistent with the range of 0.05–1.00 commonly reported for RG-I-containing pectins [Schols & Voragen, 1996]. RRTP-QXG had the highest Rha/GalA ratio, whereas RRTP-QXG and RRTP-SN had the highest (Ara+Gal)/Rha ratios. In contrast, RRTP-CJ showed the lowest values for both indices and the highest estimated HG proportion (45.07 mol%), indicating a comparatively greater contribution of GalA-rich, less-branched regions. Together, these results demonstrate clear source-associated differences in monosaccharide composition and pectic domain distribution among RRTPs. RRTP-CJ had an elevated HG content and a relatively linear conformation, while RRTP-QXG exhibited the most extensive RG-I branching. Despite these architectural distinctions, all samples maintained high pectin purity. Such structural heterogeneity is expected to influence the physicochemical and functional properties of the polysaccharides and is therefore relevant to their targeted utilization in food and nutraceutical applications.

Molecular weight distribution

To evaluate source-associated variation, the molecular-weight characteristics of RRTPs from eight producing areas were analyzed by HPGPC. Calibration was performed using a dextran--based standard curve (**Figure S2** in Supplementary Materials). Each chromatogram of RRTP separations showed a single dominant, near-Gaussian peak (**Figure 1A**), suggesting a relatively narrow apparent molecular weight distribution within each RRTP preparation. However, shifts in the retention time of the main peak were observed among samples, indicating significant differences in average molecular weight, which ranged from 77.8 to 181.1 kDa (**Table 2**). For comparison, the average molecular weights of *R. roxburghii* fruit polysaccharides obtained by hot-water, saline, alkaline, and citric-acid extraction were previously reported to range from 80.53 to 97.22 kDa [Chen *et al.*, 2025]. The lower molecular weights observed in the present study were comparable to this range, whereas RRTP-LL, RRTP-HZ, RRTP-QXG, and RRTP-SN exhibited higher values. In turn, the average molecular weights observed here were lower than the value of 513.02 kDa reported for water-soluble polysaccharides from *R. roxburghii* by Wang *et al.* [2018b]. Therefore, the difference may be attributable to the variation in fruit material, extraction and post-extraction processing, which can influence the molecular-weight distribution of the recovered polysaccharides. Among the analyzed samples, RRTP-ZA and RRTP-CJ displayed the lowest average molecular weights (77.8 kDa and 80.6 kDa, respectively), whereas RRTP-QXG and RRTP-SN exhibited the highest values (179.4 kDa and 181.1 kDa, respectively). The higher average molecular weights of RRTP-QXG and RRTP-SN coincided with their higher Ara and Gal proportions and higher (Gal+Ara)/Rha ratios. This association is structurally plausible because the controlled enzymatic removal of specific pectic domains, including arabinan and galactan side chains, has been shown to progressively decrease the molecular weight of RG-I-rich citrus pectin [Wu *et al.*, 2020]. Overall, these findings demonstrate clear source--associated differences in molecular-weight profiles among RRTPs, further supporting substantial supramolecular heterogeneity among samples from different producing areas.

Fourier transform infrared spectroscopic characterization

Fourier-transform infrared spectroscopy was employed to identify the functional groups and backbone features of the RRTPs. The spectra of all eight samples showed a high degree of overlap (**Figure 1B**), indicating broadly similar functional-group profiles among the production sources. A broad, intense absorption band at 3,273 cm^{-1} was attributed to O–H stretching vibrations, while a peak at 2,922 cm^{-1} corresponded to aliphatic C–H stretching, confirming the polysaccharidic nature of the samples [Chen *et al.*, 2025]. Signals at 1,734 cm^{-1} and 1,603 cm^{-1} were assigned to ester carbonyl stretching and asymmetric stretching of ionized carboxylate groups, respectively [Synytsya *et al.*, 2003], which is the evidence for the presence of galacturonic acid residues. Weaker bands near 1,418 cm^{-1} and 1,370 cm^{-1} were consistent with C–H bending vibrations. In the range of 1,300–800 cm^{-1}, multiple diagnostic peaks were identified: 1,234 cm^{-1} and 1,067 cm^{-1} were attributed to C–O and C–O–C stretching vibrations; 1,012 cm^{-1} reflected C–O–H bending of pyranose rings [Kačuráková *et al.*, 2000]. A distinctive band at 824 cm^{-1} indicated α-glycosidic linkages [Barker *et al.*, 1954]. Overall, the similar spectra support the presence of a common pectic-polysaccharide framework in all RRTPs.

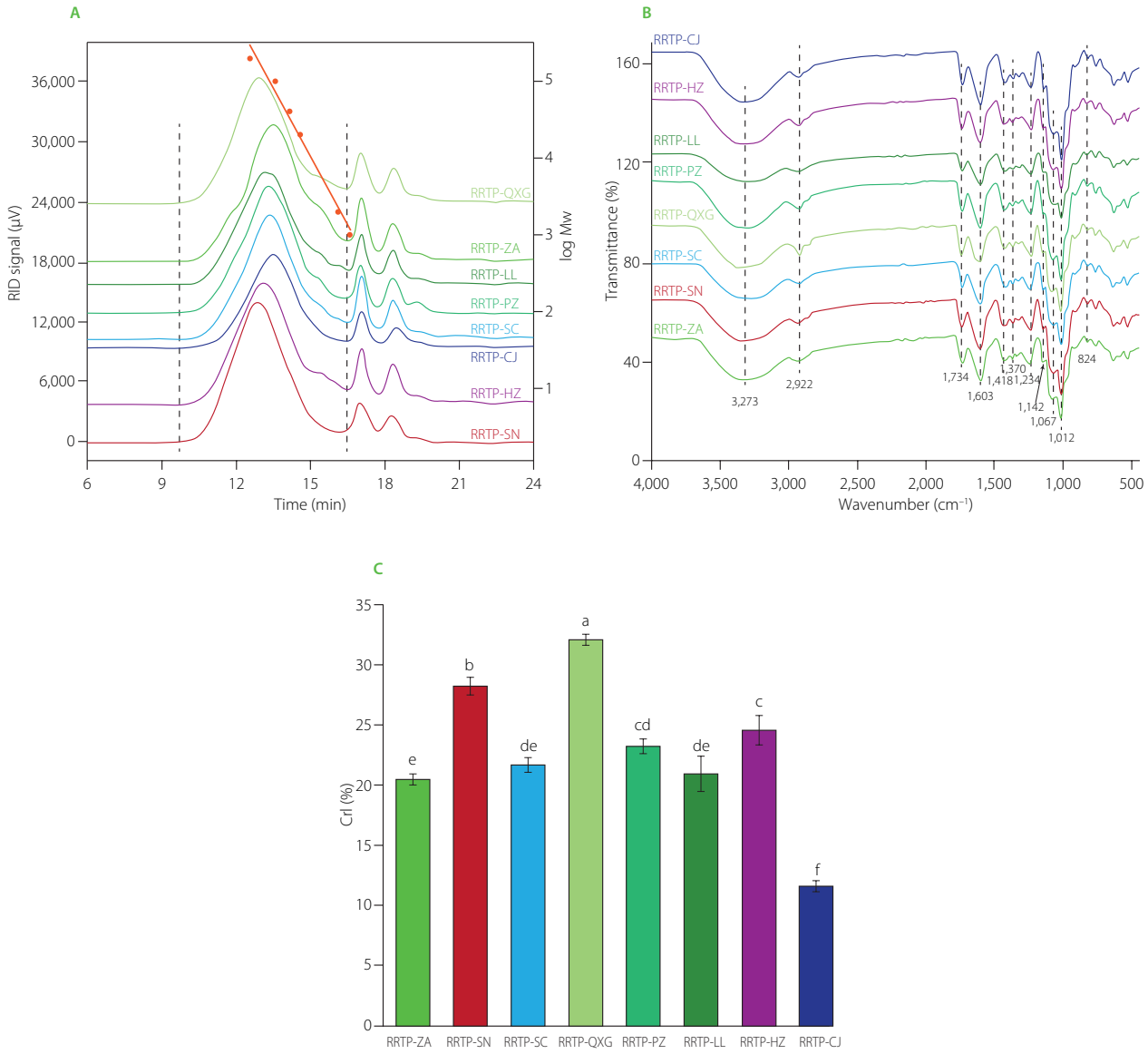

Figure 1. High-performance gel permeation chromatography (HPGPC) separations of polysaccharides from *Rosa roxburghii* Tratt. fruits (RRTP) collected in different producing areas of Guizhou Province in China and the corresponding molecular-weight calibration curve (**A**), Fourier-transform infrared (FT-IR) spectra of RRTPs (**B**), and crystallinity index (CrI) obtained by X-ray diffraction (XRD) analysis. CrI values not sharing a common letter differ significantly ($p<0.05$). Mw, molecular weight; RID, refractive-index detector. Sample codes are listed in **Table 1**.

Structural characterization

XRD analysis was conducted to qualitatively and semi-quantitatively evaluate the solid-state organization of RRTPs across amorphous, semicrystalline, and crystalline regions. The diffraction profiles of the eight RRTP samples are shown in **Figure S3** in Supplementary Materials. All samples exhibited broad halos centered around ~22° (2θ), without sharp Bragg reflections, indicating a predominantly amorphous microstructure. A minor exception was observed for RRTP-QXG, which displayed weak and broadened features near ~12° and ~22° (2θ), suggestive of localized short-range ordering within an otherwise disordered matrix. Although the positions of these diffuse features, and hence the associated d-spacings, were largely conserved in all samples, variations in peak widths and intensities caused crystallinity indices (CrI) to vary from 11.7% to 32.1% (**Figure 1C**). The highest CrI was recorded for RRTP-QXG. This relatively high CrI may reflect more regular packing of some polysaccharide chains, resulting in localized short-range ordered domains within the predominantly amorphous matrix. Similar broad XRD profiles, characterized by diffuse diffraction features at approximately 20–23° and the absence of prominent sharp reflections, have previously been reported for polysaccharides extracted from *R. roxburghii* fruit [Chen *et al.*, 2025; Zhang *et al.*, 2024].

Particle size and zeta-potential

Particle size and zeta-potential distributions of the RRTP samples were shown in **Figure S4** in Supplementary Materials, while average values are summarized in **Table 2**. All samples exhibited unimodal yet relatively broad particle size distributions, indicating compositional homogeneity within each preparation while also suggesting a general tendency toward aggregation. RRTP-ZA exhibited the largest particle diameter (705 nm),

followed by RRTP-CJ (613 nm) and RRTP-SN (554 nm). RRTP-LL, RRTP-PZ, RRTP-SC, and RRTP-QXG showed statistically comparable particle sizes, whereas RRTP-HZ had the smallest diameter (362 nm). Notably, RRTP-ZA and RRTP-CJ displayed relatively large hydrodynamic diameters despite their low average molecular weights (77.8 and 80.6 kDa, respectively). This pattern may be associated with differences in the organization of their pectic domains. Both samples had comparatively low RG-I contents (57.41 and 46.24 mol%, respectively) and low (Gal+Ara)/Rha ratios (8.81 and 7.94, respectively), indicating a relatively limited contribution of Ara- and Gal-rich neutral side chains. The composition and length of RG-I side chains have been shown to influence pectin hydration, while enzymatic removal of arabinose residues can enhance intermolecular association and aggregation [Kaczmarska *et al.*, 2024; Larsen *et al.*, 2011]. Therefore, the less extensive neutral side chains of RRTP-ZA and RRTP-CJ may provide weaker hydration and steric shielding, allowing closer intermolecular contacts and the formation of larger hydrodynamic assemblies. In contrast, RRTP-HZ, RRTP-QXG, and RRTP-SN exhibited higher estimated RG-I contents and/or (Gal+Ara)/Rha ratios, suggesting more extensive neutral side-chain structures that may enhance hydration and steric separation between polysaccharide chains. This structural feature may partly account for their smaller particle dimensions relative to their apparent molecular weights.

Zeta-potential measurements showed net negative surface charges across all RRTPs, ranging from −12.5 mV (RRTP-QXG) to −20.8 mV (RRTP-CJ) (**Table 2** and **Figure S4B** in Supplementary Material). RRTP-CJ exhibited the most negative zeta potential, whereas RRTP-QXG and RRTP-SN showed the lowest absolute values and did not differ significantly ($p \geq 0.05$) from each other. The negative charge of these polysaccharides was mainly attributable to the dissociation of carboxyl groups in GalA-containing pectic domains. Consistent with its relatively high uronic acid content, RRTP-CJ possessed a greater negative surface charge, indicating stronger electrostatic repulsion between dispersed polysaccharide particles [Lutz *et al.*, 2009]. In addition to uronic acid content, differences in the accessibility and ionization of carboxyl groups, as well as the molecular conformation of the polysaccharides, may also contribute to the variation in zeta potential among the RRTP samples. An absolute zeta potential of approximately 30 mV is commonly regarded as an empirical boundary for dispersions stabilized predominantly by electrostatic repulsion [Uskoković, 2012]. The absolute zeta-potential values of all RRTP samples were below this level, indicating relatively limited electrostatic stabilization and a tendency toward intermolecular association in aqueous solution. Among the samples, the more negative zeta potential of RRTP-CJ may nevertheless provide comparatively stronger electrostatic repulsion and better dispersion stability.

Thermal properties

Thermogravimetric analysis reflects the thermal stability of RRTPs, which is an important parameter for evaluating their suitability as functional food ingredients. The TG and DTG curves are presented in **Figure 2**. Heating from 25 to 800°C revealed three distinct stages of thermal degradation. Stage I corresponded to the evaporation of free and bound water and accounted for 11.9% to 15.6% of mass loss. The highest moisture losses were observed for RRTP-SN (15.6%), RRTP-PZ (15.2%), and RRTP-HZ (15.1%), while RRTP-CJ (11.9%) and RRTP-QXG (12.0%) exhibited the lowest losses, reflecting differences in water-binding capacity. Stage II represented the principal decomposition phase, characterized by cleavage of glycosidic linkages and degradation of polysaccharide side chains [Aburto *et al.*, 2015]. RRTP-SC, RRTP-PZ, and RRTP-QXG showed the lowest peak decomposition rates (−6.12%, −5.62%, and −5.55%/min, respectively), indicating greater thermal resilience than the other samples. Stage III involved the breakdown of more recalcitrant structures, including C–O bond cleavage and terminal disruption of the glycosidic backbone [Aburto *et al.*, 2015]. RRTP-ZA and RRTP-CJ exhibited the greatest mass losses during this phase, consistent with lower structural resistance under high thermal stress. Among all samples, RRTP-CJ demonstrated the lowest overall thermal stability. Despite exhibiting the highest onset temperature for stage II degradation (188.2°C), it incurred the largest stage II mass loss (67.3%), the greatest cumulative loss (84.1%), and retained the lowest residual mass (15.9%) at 800°C. In contrast, RRTP-QXG exhibited superior thermal resistance, with a relatively lower peak decomposition rate, the smallest total mass loss (73.5%), and the highest residual mass at terminal temperature. These thermal behaviors were closely associated with structural characteristics. A higher molecular weight, a high RG-I content, and greater side-chain complexity, reflected by elevated (Gal+Ara)/Rha ratios, have been reported to enhance thermal stability in pectic polysaccharides [Deng *et al.*, 2020]. RRTP-QXG, which exhibited the highest values of these parameters, showed the greatest thermal stability, whereas RRTP-CJ, with comparatively lower values, was the least stable. Collectively, these findings indicate that the thermal performance of RRTPs is governed primarily by molecular architecture, especially molecular weight distribution and branching complexity. Understanding these structure–property relationships is important for evaluating RRTPs from different production areas and for guiding their targeted utilization in food systems requiring specific thermal tolerance.

Antioxidant capacity of polysaccharides from *Rosa roxburghii* Tratt. fruits

Plant polysaccharides have been repeatedly shown to act as antioxidants [Fernandes & Coimbra, 2023]. To evaluate the antioxidant capacity of RRTPs obtained from fruits collected in eight geographically distinct regions, they were subjected to four *in vitro* antioxidant assays, in which scavenging activity against DPPH$^{\bullet}$, ABTS$^{\bullet+}$ and $O_2^{\bullet-}$, and ability to chelate ferrous-ions were determined. All RRTP samples exhibited a concentration-dependent increase in DPPH radical scavenging activity (**Figure 3A**). The IC_{50} values revealed the following order of antioxidant capacity: RRTP-CJ > RRTP-SC = RRTP-PZ > RRTP-LL ≥ RRTP-ZA ≥ RRTP-HZ > RRTP-QXG > RRTP-SN. Notably, RRTP-CJ achieved

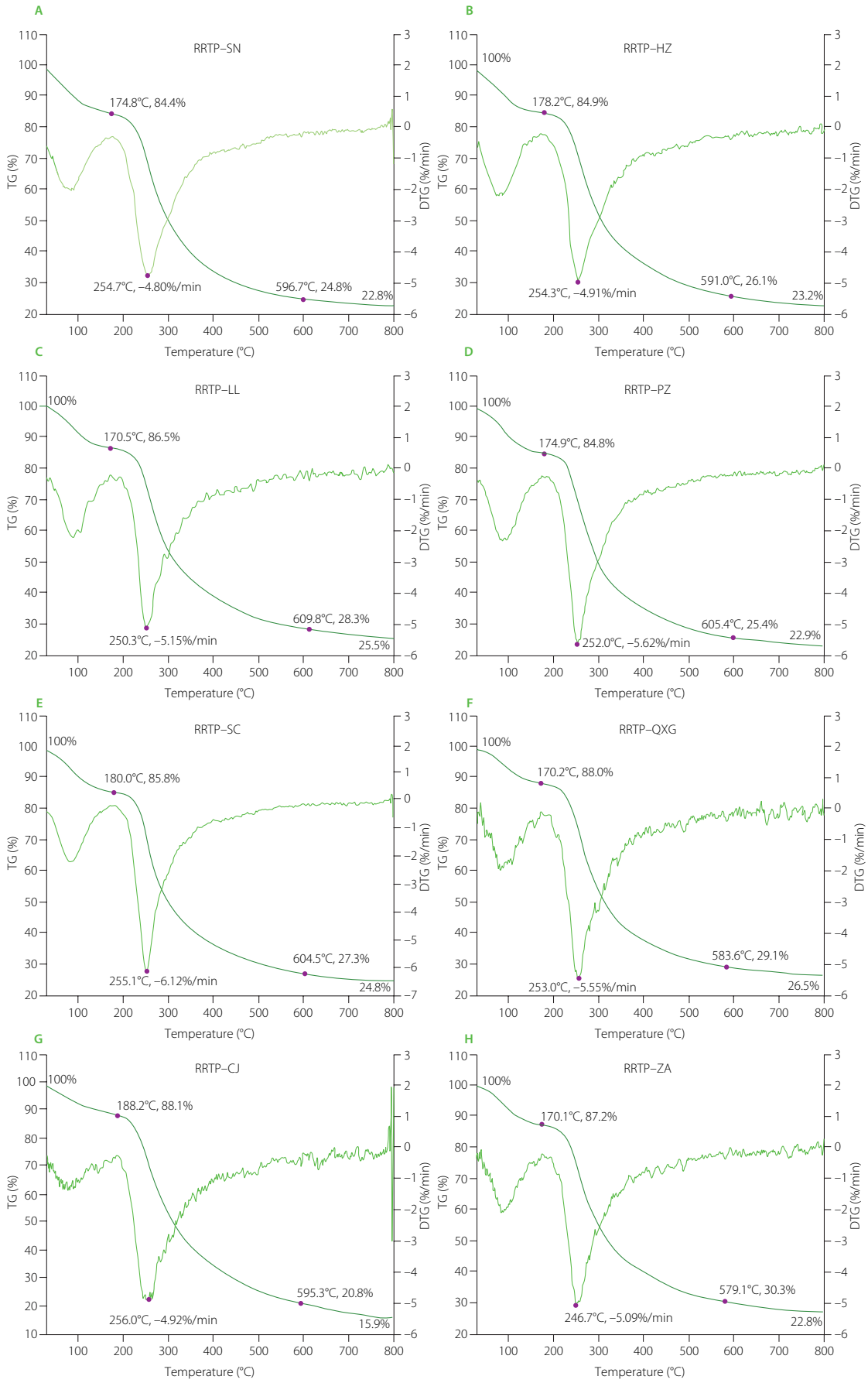

Figure 2. Thermogravimetric (TG) and derivative thermogravimetric (DTG) curves of polysaccharides from *Rosa. roxburghii* Tratt. fruits (RRTP) collected in different producing areas of Guizhou Province in China including Sinan, RRTP-SN (**A**); Hezhang, RRTP-HZ (**B**); Longli, RRTP-LL (**C**); Panzhou, RRTP-PZ (**D**); Shuicheng, RRTP-SC (**E**); Qixingguan, RRTP-QXG (**F**); Congjiang, RRTP-CJ (**G**), and Zheng'an, RRTP-ZA (**H**).

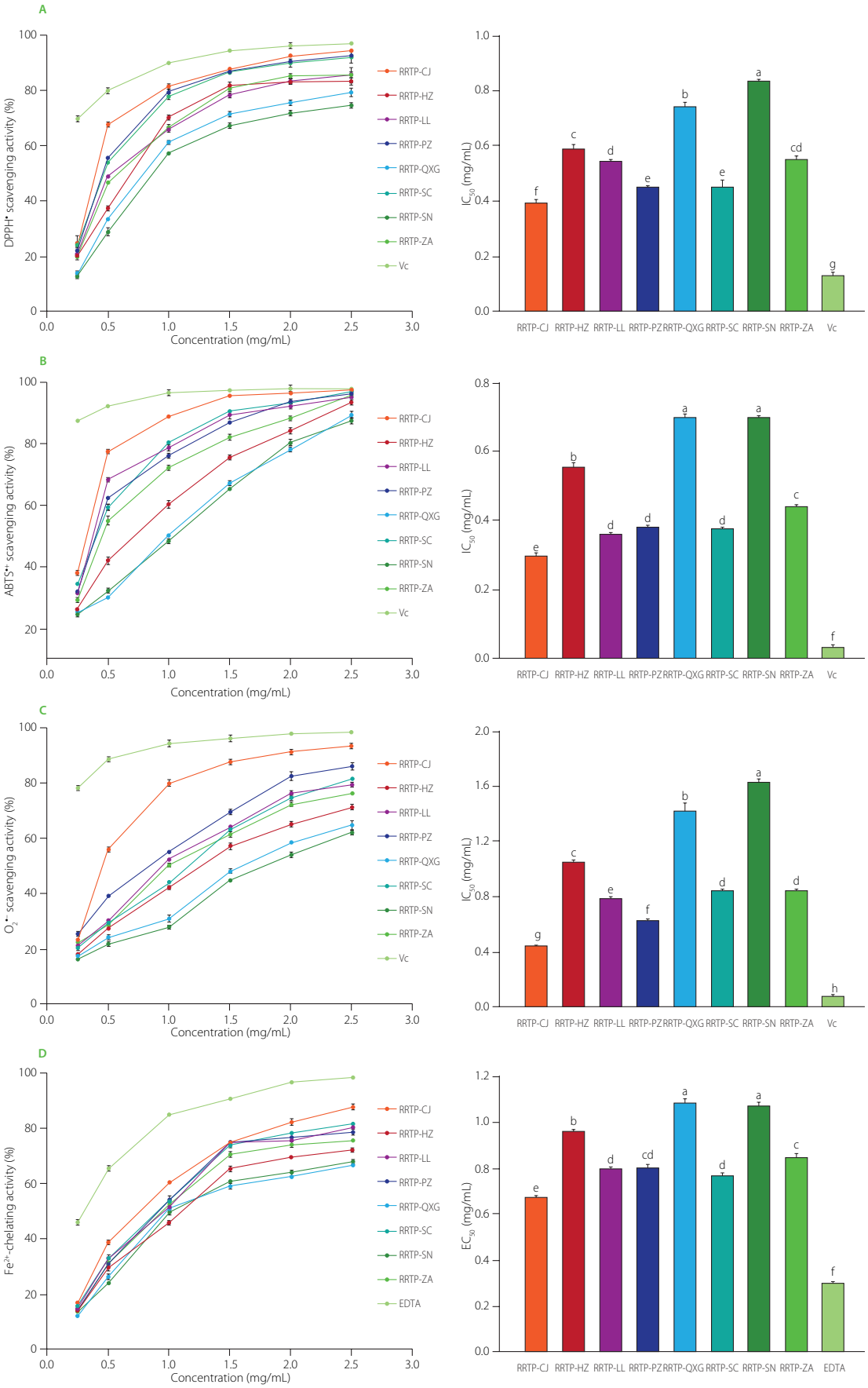

Figure 3. Antioxidant capacity of polysaccharides from *Rosa roxburghii* Tratt. fruits (RRTP) collected in different producing areas of Guizhou Province in China, determined as DPPH• scavenging activity (**A**), $ABTS^{\bullet+}$ scavenging activity (**B**), $O_2^{\bullet-}$ scavenging activity (**C**), and Fe^{2+}-chelating activity (**D**). Left graphs show RRTP concentration-dependent curves, and the right graphs show the half-maximal inhibitory concentration (IC_{50}) for the radical-scavenging assays (**A–C**) and the half-maximal effective concentration (EC_{50}) for the Fe^{2+}-chelating assay (**D**). IC_{50} or EC_{50} values not sharing a common letter differ significantly ($p<0.05$). DPPH•, 2,2-diphenyl-1-picrylhydrazyl radical; $ABTS^{\bullet+}$, 2,2′-azinobis(3-ethylbenzothiazoline-6-sulfonic acid) radical cation. Sample codes are listed in **Table 1**.

94.22% inhibition at 2.5 mg/mL. However, its IC_{50} (0.394 mg/mL) remained significantly ($p<0.05$) higher than that of ascorbic acid (0.131 mg/mL), indicating its lower antioxidant capacity compared to a standard antioxidant. No statistically significant differences ($p\geq0.05$) were detected between several sample pairs, including RRTP-PZ and RRTP-SC (IC_{50} of 0.451 *vs*. 0.449 mg/mL, respectively), RRTP-LL and RRTP-ZA (0.544 *vs*. 0.550 mg/mL, respectively), and RRTP-HZ and RRTP-ZA (0.586 *vs*. 0.550 mg/mL, respectively). RRTP-LL yielded 85.70% DPPH radical scavenging at 2.5 mg/mL, comparable to the 84.4% scavenging activity reported at 2.0 mg/mL for a polysaccharide preparation obtained from dried *R. roxburghii* fruit by ultrasound-assisted enzymatic extraction [Jiao *et al.*, 2025]. Similarly, the 79.01% scavenging activity observed for RRTP-QXG at 2.5 mg/mL was within the range reported for *R. roxburghii* fruit polysaccharide samples obtained by hot-water, saline, citric-acid, and alkaline extraction (73.77––82.22% at 4.0 mg/mL) [Chen *et al.*, 2025]

The ABTS assay revealed a clear dose-dependent scavenging effect across all RRTPs (**Figure 3B**). At 2.5 mg/mL, inhibition ranged from 87.27% to 97.56%, with RRTP-CJ exhibiting the highest activity. The order of RRTP samples with decreasing antioxidant capacity was as follows: RRTP-CJ = RRTP-LL = RRTP-SC = = RRTP-PZ > RRTP-ZA > RRTP-HZ > RRTP-QXG = RRTP-SN. Although RRTP-CJ exhibited the highest $ABTS^{\bullet+}$ scavenging activity among the RRTPs, its IC_{50} remained higher than that of ascorbic acid (0.0331 mg/mL, $p<0.05$). RRTP-LL, RRTP-SC, and RRTP-PZ exhibited IC_{50} values of 0.359, 0.375, and 0.382 mg/mL, respectively, with no significant differences among them ($p\geq0.05$).

All RRTP samples exhibited superoxide scavenging activity in a concentration-dependent manner (**Figure 3C**). Based on IC_{50} values, their scavenging efficiency ranked as follows: RRTP-CJ > > RRTP-PZ > RRTP-LL > RRTP-SC = RRTP-ZA > RRTP-HZ > > RRTP-QXG > RRTP-SN. While RRTP-CJ consistently demonstrated superior activity relative to other RRTPs, its IC_{50} remained higher than that of ascorbic acid (0.0807 mg/mL, $p<0.05$), consistent with results from the DPPH and ABTS assays.

Because transition metals catalyze hydroxyl radical production, the ability of RRTPs to chelate ferrous ion was also examined, and respective results are shown in **Figure 3D**. Chelating activity increased with increasing polysaccharide concentration (0.25–2.5 mg/mL). RRTP-CJ exhibited the highest chelating activity, achieving significant efficacy even at 1.0 mg/mL. In contrast, RRTP-QXG and RRTP-SN required concentrations exceeding 2.0 mg/mL to attain comparable activity. Consistent with these concentration–response profiles, RRTP-CJ had the lowest EC_{50} among the RRTP samples (0.671 mg/mL), indicating the strongest Fe^{2+}-chelating capacity, although it was less effective than EDTA (EC_{50} = 0.298 mg/mL; $p<0.05$). RRTP-SC and RRTP-LL showed comparable activities, with EC_{50} values of 0.766 and 0.794 mg/mL, respectively. RRTP-PZ exhibited an intermediate EC_{50} of 0.799 mg/mL and did not differ significantly ($p\geq0.05$) from RRTP-SC, RRTP-LL, or RRTP-ZA (0.847 mg/mL). RRTP-HZ showed weaker activity, with an EC_{50} of 0.961 mg/mL, while RRTP-SN and RRTP-QXG had the highest EC_{50} values (1.069 and 1.084 mg/mL, respectively) and did not differ significantly ($p\geq0.05$) from each other. Collectively, antioxidant capacity of RRTPs varied significantly with fruit geographic origin, and RRTP-CJ consistently exhibited the greatest efficacy across all assays.

In vitro inhibitory effect of polysaccharides from *Rosa roxburghii* Tratt. fruits on glycemic-related digestive enzymes

Inhibition of digestive carbohydrase activity

In this study, RRTPs collected from eight major production areas in Guizho were evaluated for their inhibitory effects on α-amylase and α-glucosidase, with acarbose serving as a pharmaceutical benchmark. All RRTP samples demonstrated concentration-dependent inhibition of α-amylase, with activities at 7.0 mg/mL ranging from 52.45% (RRTP-SN) to 79.64% (RRTP-CJ) (**Figure 4A**). Based on the IC_{50} values, the analyzed samples were ranked as follows: RRTP-CJ (2.425 mg/mL) < RRTP-ZA (3.175 mg/mL) < RRTP-LL (4.189 mg/mL) <RRTP-PZ (4.497 mg/mL) <RRTP-SC (5.068 mg/mL) < RRTP-HZ (5.441 mg/mL) < RRTP-QXG (5.817 mg/mL) = RRTP-SN (5.971 mg/mL). All RRTP samples had higher IC_{50} values than acarbose, indicating weaker α-amylase inhibition under the assay conditions. In contrast, the RRTPs showed stronger inhibition of α-glucosidase, yielding 67.73––92.46% inhibition at 7.0 mg/mL compared with 66.49% determined for acarbose (**Figure 4B**). Based on the IC_{50} values, they were ranked as follows: RRTP-CJ (0.747 mg/mL) < RRTP-ZA (0.826 mg/mL) < RRTP-LL (1.022 mg/mL) < RRTP-PZ (1.101 mg/mL) < RRTP-SC (1.434 mg/mL) < RRTP-SN (1.655 mg/mL) < RRTP-HZ (1.787 mg/mL) < RRTP-QXG (2.035 mg/mL) < acarbose (2.873 mg mL). The stronger inhibition of α-glucosidase than α-amylase observed for the RRTPs was consistent with previous findings for *R. roxburghii* fruit polysaccharides obtained using different extraction solvents, which showed IC_{50} values of 0.494––1.234 mg/mL against α-glucosidase and 0.758–2.003 mg/mL against α-amylase [Chen *et al.*, 2025]. The excellent inhibitory activity of RRTP-CJ and RRTP-ZA may be due to their relatively small molecular weight, a higher galacturonic acid content, and longer chains, which enhance their interaction with enzyme active sites [Zhang *et al.*, 2025b].

Kinetics of α-glucosidase inhibition

Lineweaver-Burk plots of α-glucosidase inhibition by RRTPs are shown in **Figure S5** in Supplementary Materials. For each RRTP, three inhibitor concentrations generated straight lines intersecting in the third quadrant, indicating a mixed-type mode of inhibition. Increasing polysaccharide concentrations reduced both V_{max} and K_m (**Table 3**), consistent with simultaneous binding to both the free enzyme (E) and the enzyme-substrate complex (ES). Secondary replots yielded apparent dissociation constants, K_i (E-I) and K_{is} (ES-I) (**Figure S6** in Supplementary Materials). For all RRTPs, $K_{is}<K_i$ (ratios 0.19–0.60), indicating preferential binding to the ES complex and a predominant non-competitive inhibition component [Zhang *et al.*, 2025a]. Among all preparations, RRTP-CJ displayed the strongest association (K_{is} = 0.336 mg/mL; K_{is}/K_i = 0.190) and the lowest IC_{50}, substantiating its position as the most potent inhibitor in this series. While all RRTPs moderated

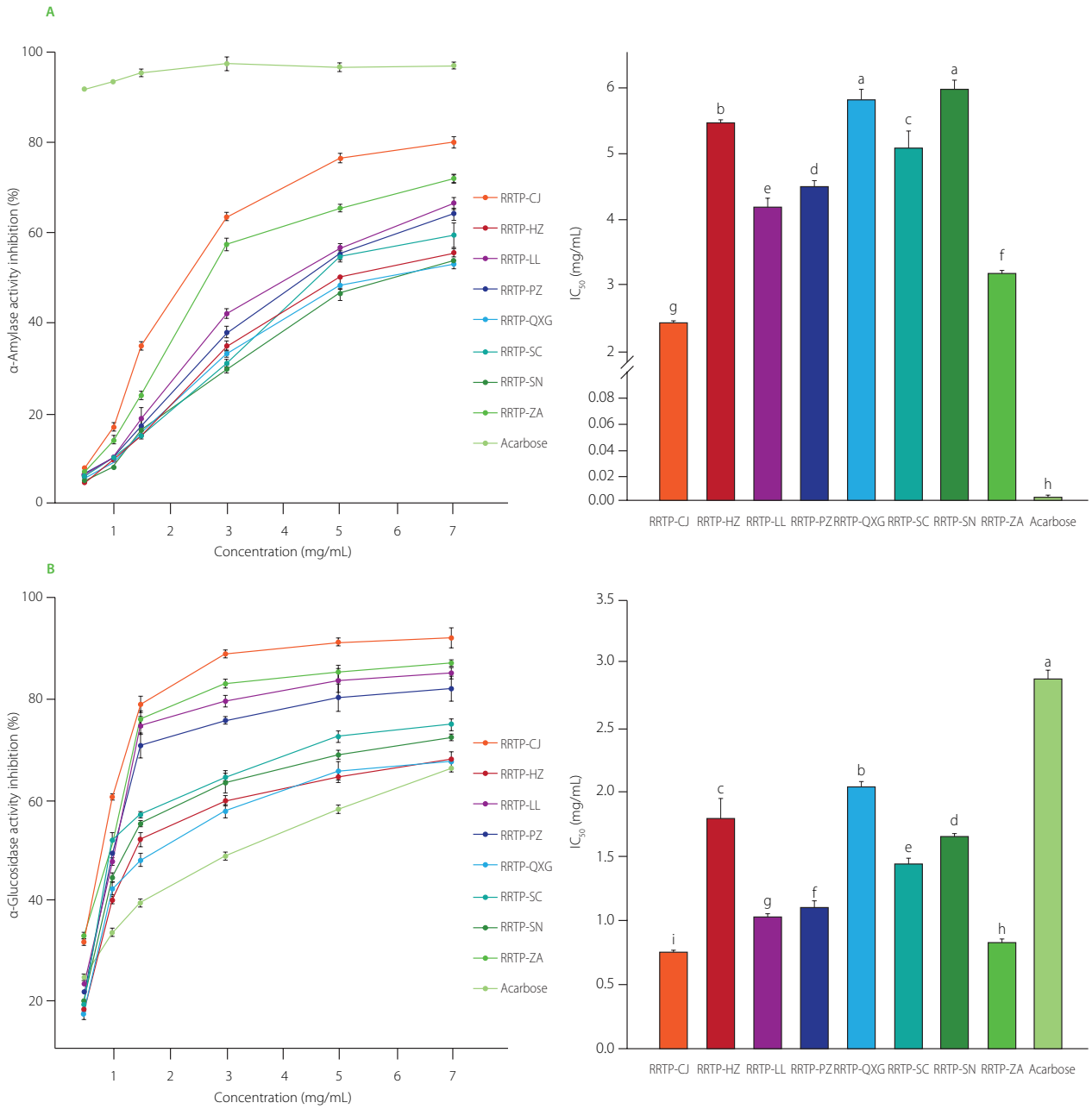

Figure 4. Inhibitory effects of polysaccharides from *Rosa roxburghii* Tratt. fruits (RRTP) collected in different producing areas of Guizhou Province in China on α-amylase activity (**A**) and α-glucosidase activity (**B**). Left graphs show RRTP concentration-dependent curves, and the right graphs show half-maximal inhibitory concentration (IC_{50}). IC_{50} values not sharing a common letter differ significantly ($p<0.05$). Sample codes are listed in **Table 1**.

digestive carbohydrase activity, the preparation from Congjiang (RRTP-CJ) consistently outperformed others, exhibiting potent α-glucosidase inhibition through a predominantly non-competitive, mixed-type mechanism. Given their additional antioxidant activity, RRTP-CJ, and to a lesser extent RRTP-ZA and RRTP-LL, emerge as promising functional ingredients for the dietary management of type 2 diabetes.

■ Interplay between structural attributes and bioactivity

Pearson correlations were employed to elucidate the physicochemical determinants underlying the antioxidant capacity and digestive carbohydrase activity inhibition of the eight RRTP preparations (**Figure 5A**). Uronic acid content emerged as the most potent positive predictor, exhibiting strong and significant correlations ($p<0.01$) with antioxidant capacity (all assays) and enzyme-inhibitory activity. Average molecular weight was significantly negatively correlated with the IC_{50} or EC_{50} values obtained from the antioxidant and enzyme-inhibition assays ($p<0.01$), indicating that the RRTPs with higher average molecular weights generally exhibited stronger bioactivities. The architecture of pectic domains further modulated bioactivity: HG content correlated positively with antioxidant capacity and inhibitory activity ($p<0.05$), while RG-I, Rha/GalA, and Gal+Ara)/Rha ratios correlated negatively with these activities ($p<0.05$). Significant associations were also observed for the molar fractions of arabinose, galactose, xylose, and galacturonic acid ($p<0.01$),

Table 3. Kinetic parameters of α-glucosidase inhibition by polysaccharides from *Rosa roxburghii* Tratt. fruits (RRTP) collected in different producing areas of Guizhou Province in China.

Sample	RRTP (mg/mL)	Inhibition type	K_m (mM)	V_{max} (ΔA405/min)	K_i (mg/mL)	K_{is} (mg/mL)	K_{is}/K_i
RRTP-CJ	0	Mixed-type	3.515	0.143	1.765	0.336	0.190
	3		1.618	0.0392			
	5		1.191	0.0141			
RRTP-HZ	0	Mixed-type	3.528	0.148	10.712	5.879	0.549
	3		2.987	0.104			
	5		2.788	0.0841			
RRTP-LL	0	Mixed-type	3.572	0.140	4.054	1.125	0.278
	3		2.138	0.0603			
	5		1.652	0.0328			
RRTP-PZ	0	Mixed-type	3.553	0.144	5.604	1.634	0.291
	3		2.279	0.0718			
	5		1.783	0.0419			
RRTP-QXG	0	Mixed-type	3.583	0.147	11.087	6.658	0.600
	3		3.224	0.117			
	5		3.022	0.092			
RRTP-SC	0	Mixed-type	3.493	0.151	7.254	2.434	0.336
	3		2.558	0.0857			
	5		2.062	0.0541			
RRTP-SN	0	Mixed-type	3.522	0.144	9.940	4.023	0.405
	3		2.951	0.104			
	5		2.460	0.0724			
RRTP-ZA	0	Mixed-type	3.571	0.146	2.738	0.604	0.221
	3		1.770	0.0450			
	5		1.354	0.0206			

K_m, Michaelis constant; V_{max}, maximum reaction velocity; K_i, dissociation constant for the enzyme-inhibitor complex; K_{is}, dissociation constant for the enzyme-inhibitor-substrate complex. Sample codes are listed in **Table 1**.

highlighting the multifactorial nature of structure-activity relationships within this polysaccharide series.

The antioxidant and enzyme-inhibitory activities of polysaccharides are jointly influenced by uronic acid content, molecular weight, and monosaccharide composition. Radical scavenging by bioactive polysaccharides generally occurs through electron transfer or hydrogen-atom donation. In uronic acid-rich polysaccharides, carboxyl groups may contribute to radical scavenging and metal-ion chelation [Chen *et al.*, 2019], consistent with the close association between uronic acid content and antioxidant activity observed in the present study. Molecular weight can also affect antioxidant activity by altering the accessibility of reactive groups. In some polysaccharide systems, controlled depolymerization generates additional reducing ends and consequently enhances radical-scavenging activity [Qi *et al.*, 2005; Zhang *et al.*, 2019]. However, the effect of molecular weight is dependent on the overall molecular architecture and should therefore be considered together with monosaccharide composition and pectic-domain structure. Digestive enzyme inhibition may involve direct association between polysaccharide chains

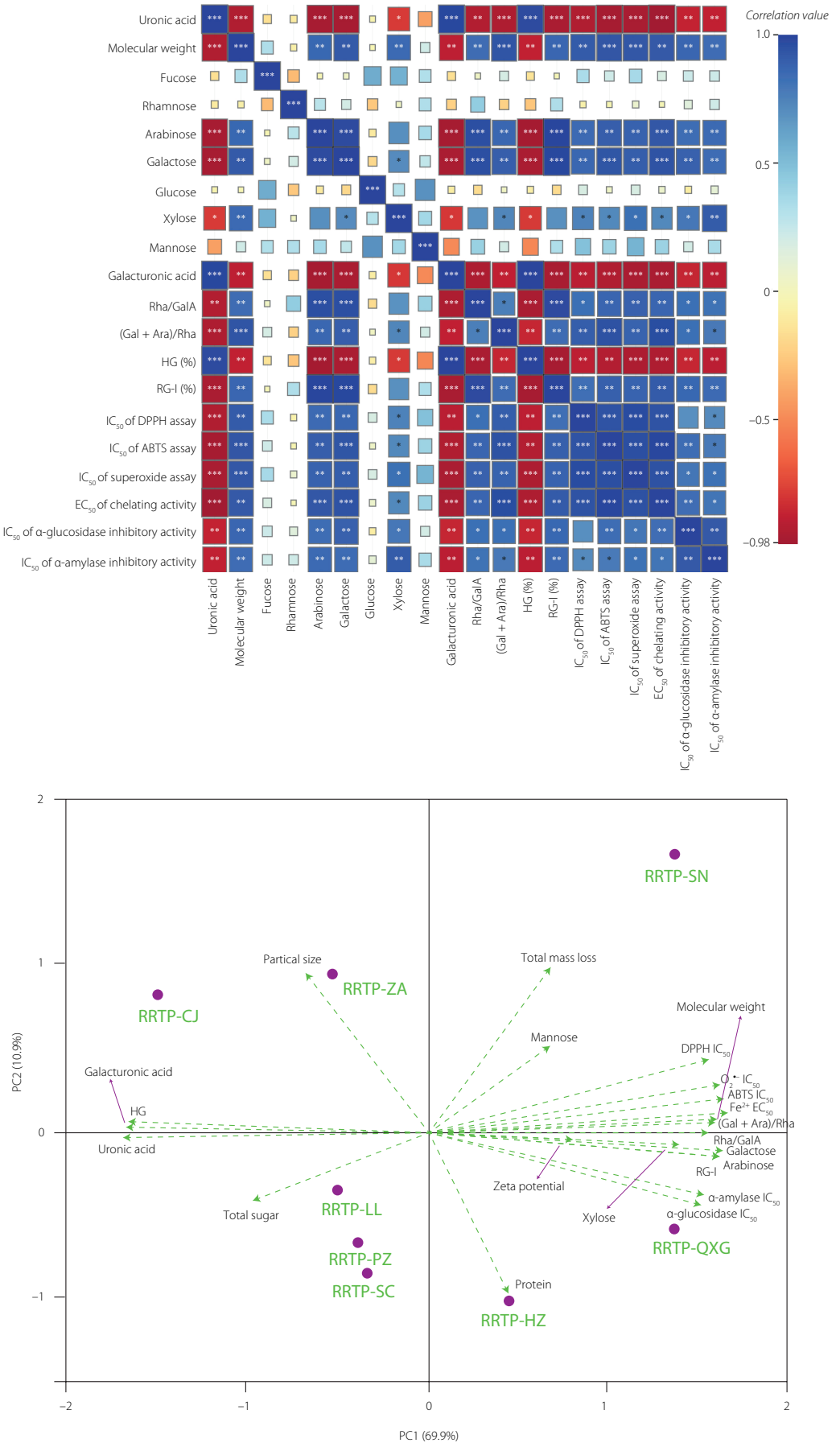

Figure 5. Multivariate analysis of structure-activity relationships among polysaccharides from *Rosa roxburghii* Tratt. fruits (RRTP) collected in different producing areas of Guizhou Province in China: Pearson correlation heatmap (**A**) and principal component analysis (PCA) loading plot (**B**).

and the enzyme proteins. A purified acidic polysaccharide from *R. roxburghii* fruit was previously shown to bind α-glucosidase and induce conformational changes in the enzyme [Wang *et al.*, 2018a]. The hydroxyl and carboxyl groups of acidic polysaccharides may contribute to these interactions through hydrogen bonding and electrostatic forces. Among the eight samples, RRTP-CJ was distinguished by its high uronic acid content and HG proportion. These compositional characteristics, together with its molecular-weight distribution, may jointly account for its strong radical-scavenging and carbohydrase-inhibitory activities. Accordingly, RRTP-CJ represents a promising candidate for further evaluation as an antioxidant and glucose-modulating functional food ingredient.

PCA was applied to the comprehensive structural and functional dataset for polysaccharides isolated from RRTs from eight cultivation areas in Guizhou. Two orthogonal components accounted for 80.8% of the cumulative variance (PC1 = 69.9%; PC2 = 10.9%) (**Figure 5B**). PC1 mainly reflected the association between pectic structural characteristics and bioactivity. Average molecular weight, the RG-I-related indices (Rha/GalA and (Gal+Ara)/Rha), the IC_{50} values for DPPH$^{\bullet}$, ABTS$^{\bullet+}$, $O_2^{\bullet-}$ scavenging activities and α-amylase and α-glucosidase inhibition, and the EC_{50} value for Fe^{2+}-chelating activity were located on the positive side of PC1. In contrast, total uronic acid, galacturonic acid, and HG content were located on its negative side. Because lower IC_{50} or EC_{50} values indicate stronger activity, this distribution suggests that RRTP samples rich in uronic acid and HG generally exhibited stronger antioxidant and digestive-enzyme inhibitory activities, whereas higher molecular weight and more pronounced RG-I-related characteristics were associated with weaker activities. PC2 captured secondary variation in particle and thermal properties. Particle diameter, total mass loss, and mannose content loaded positively on PC2, whereas zeta potential and protein content loaded negatively. PC2 therefore differentiated the RRTP samples primarily according to their particle size, thermal behavior, surface charge, and protein content.

PCA distinguished the RRTP samples mainly along a structure-bioactivity axis. Samples such as RRTP-CJ and RRTP-ZA were associated with lower molecular weight, higher galacturonic-acid-related characteristics, and lower IC_{50} values in antioxidant and enzyme-inhibition assays, whereas RRTP-QXG and RRTP-SN were associated with higher molecular weight, more pronounced RG-I branching features, and weaker *in vitro* activities. These results support the conclusion that pectic domain distribution and molecular size were the major contributors to the observed functional differences among RRTPs. Importantly, the PCA results describe associations within the present comparative dataset and should not be interpreted as direct evidence for specific environmental drivers. From an application perspective, the superior profile of RRTP-CJ suggests that this source may be more suitable for the development of functional ingredients with antioxidant and digestive enzyme inhibitory potential, whereas samples with weaker activity may require further processing or structural modification before targeted utilization.

CONCLUSIONS

This study comparatively characterized polysaccharides extracted from *R. roxburghii* fruits collected from eight major production areas in Guizhou Province, China, under a shared cultivar background. Marked differences were observed in uronic acid content, pectic domain composition, molecular weight, physicochemical properties, antioxidant capacity, and inhibitory activity against α-amylase and α-glucosidase. RRTP-CJ showed the most favorable overall profile, combining lower molecular weight and higher galacturonic-acid-related characteristics with stronger *in vitro* antioxidant capacity and lower IC_{50} values for α-amylase and α-glucosidase inhibition. Kinetics analysis further demonstrated that all RRTPs inhibited α-glucosidase through a mixed-type mode with a predominant non-competitive component, as evidenced by their preferential binding to the enzyme-substrate complex ($K_{is}<K_i$), with RRTP-CJ showing the strongest inhibitory interaction. Correlation and multivariate analyses further indicated that lower molecular weight, higher homogalacturonan-related features, and higher uronic acid content were associated with improved bioactivity, whereas more extensive RG-I branching was generally associated with weaker effects. These findings provide comparative evidence of source-associated heterogeneity among commercially relevant *R. roxburghii* materials from Guizhou and offer a practical basis for raw-material selection, standardization, and targeted utilization in functional food and nutraceutical applications. Because the present study was conducted within one cultivar and one harvest year and did not include direct site-level environmental measurements, the observed differences should be interpreted as comparative production-source variation rather than direct environmental causation. To improve the broader applicability of these findings, future studies should incorporate cross-provincial and multi-year sampling, direct monitoring of site-level environmental variables, and *in vivo* functional validation to further clarify the factors contributing to source-associated variation and to support more robust raw-material evaluation and industrial standardization.

RESEARCH FUNDING

This work was supported by Guizhou Province High Level Innovative Talent Training Program - "1000" talents (No. ZKHT--GCC-[2023]001), Graduate Student Scientific Research Innovation project of Guiyang University (GYU-YJS-[2025]08), and College Students' Innovation and Entrepreneurship Training Program of Guizhou Province (S202010976024).

CONFLICT OF INTERESTS

The authors declare that they have no known competing financial interests or personal relationships that could have appeared to influence the work reported in this paper.

SUPPLEMENTARY MATERIALS

The following are available online at **https://journal.pan.olsztyn.pl/Comparative-Characterization-of-Polysaccharides-from-Rosa-roxburghii-Tratt-Fruits,231178,0,2.html**;

Figure S1. High-performance anion-exchange chromatography (HPAEC) separations showing the monosaccharide composition of polysaccharides from *Rosa roxburghii* Tratt. fruits (RRTP) collected in different producing areas of Guizhou Province in China. **Figure S2**. High-performance gel permeation chromatography (HPGPC) separations of molecular-weight standards and corresponding molecular-weight calibration curve. **Figure S3**. X-ray diffraction (XRD) patterns of polysaccharides from *Rosa roxburghii* Tratt. fruits (RRTP) collected in different producing areas of Guizhou Province in China. **Figure S4**. Colloidal properties of polysaccharides from *Rosa roxburghii* Tratt. fruits (RRTP) collected in different producing areas of Guizhou Province in China: Particle-size distribution (A) and zeta-potential distribution (B). **Figure S5**. Lineweaver–Burk plots for α-glucosidase inhibition by polysaccharides from *Rosa roxburghii* Tratt. fruits (RRTP) collected in different producing areas of Guizhou Province in China including Congjiang, RRTP-CJ (A); Hezhang, RRTP-HZ (B); Longli, RRTP-LL (C); Panzhou, RRTP-PZ (D); Qixingguan, RRTP-QXG (E); Shuicheng, RRTP-SC (F); Sinan, RRTP-SN (G); and Zheng'an, RRTP-ZA (H). **Figure S6**. Secondary replots for the determination of inhibition constants: Slope *versus* inhibitor concentration for K_i determination (A) and intercept *versus* inhibitor concentration for K_{is} determination (B). K_i, dissociation constant for the enzyme-inhibitor complex; K_{is}, dissociation constant for the enzyme-inhibitor-substrate complex.

ORCID IDs

G. Chen https://orcid.org/0000-0002-6968-0169
X. Chen https://orcid.org/0009-0007-5272-0383
M. Sun https://orcid.org/0009-0006-6462-9854
Q. Yang https://orcid.org/0009-0004-1428-9201
X. Yang https://orcid.org/0009-0008-2271-6671

REFERENCES

1. Aburto, J., Moran, M., Galano, A., Torres-García, E. (2015). Non-isothermal pyrolysis of pectin: A thermochemical and kinetic approach. *Journal of Analytical and Applied Pyrolysis*, *112*, 94-104. https://doi.org/10.1016/j.jaap.2015.02.012
2. Barker, S.A., Bourne, E.J., Stephens, R., Whiffen, D.H. (1954). Infra-red spectra of carbohydrates. Part II. Anomeric configuration of some hexo- and pento--pyranoses. *Journal of the Chemical Society (Resumed)*, *157*, 3468-3473. https://doi.org/10.1039/JR9540003468
3. Bernfeld, P. (1955). [17] Amylases, α and β. *Methods in Enzymology*, *1*, 149-158. https://doi.org/10.1016/0076-6879(55)01021-5
4. Blumenkrantz, N., Asboe-Hansen, G. (1973). New method for quantitative determination of uronic acids. *Analytical Biochemistry*, *54*(2), 484-489. https://doi.org/10.1016/0003-2697(73)90377-1
5. Brand-Williams, W., Cuvelier, M.E., Berset, C. (1995). Use of a free radical method to evaluate antioxidant activity. *LWT – Food Science and Technology*, *28*(1), 25-30. https://doi.org/10.1016/S0023-6438(95)80008-5
6. Chen, G., Li, C., Wang, S., Mei, X., Zhang, H., Kan, J. (2019). Characterization of physicochemical properties and antioxidant activity of polysaccharides from shoot residues of bamboo (*Chimonobambusa quadrangularis*): Effect of drying procedures. *Food Chemistry*, *292*, 281-293. https://doi.org/10.1016/j.foodchem.2019.04.060
7. Chen, G., Wan, X., Zhang, X., Chen, X., Deng, H. (2025). Polysaccharides from *Rosa roxburghii* Tratt fruit: The effect of extraction solvent on their chemical structure, bioactivities, *in vitro* simulated digestion and fecal fermentation characteristics. *Food Chemistry: X*, *32*, art. no. 103233. https://doi.org/10.1016/j.fochx.2025.103233
8. Chen, G.J., Kan, J.Q. (2018). Ultrasound-assisted extraction, characterization, and antioxidant activity *in vitro* and *in vivo* of polysaccharides from Chestnut rose (*Rosa roxburghii* tratt) fruit. *Journal of Food Science and Technolog*, 55(3), 1083-1092. https://doi.org/10.1007/s13197-017-3023-8
9. Cornish-Bowden, A. (1974). A simple graphical method for determining the inhibition constants of mixed, uncompetitive and non-competitive inhibitors. *Biochemical Journal: Molecular Aspects*, *137*(1), 143-144. https://doi.org/10.1042/bj1370143
10. Deng, Z., Pan, Y., Chen, W., Chen, W., Yun, Y., Zhong, Q., Zhang, W., Chen, H. (2020). Effects of cultivar and growth region on the structural, emulsifying and rheological characteristic of mango peel pectin. *Food Hydrocolloids*, *103*, art. no. 105707. https://doi.org/10.1016/j.foodhyd.2020.105707
11. Dimopoulou, M., Alba, K., Campbell, G., Kontogiorgos, V. (2019). Pectin recovery and characterization from lemon juice waste streams. *Journal of the Science of Food and Agriculture*, *99*(14), 6191-6198. https://doi.org/10.1002/jsfa.9891
12. Dinis, T., Maderia, V., Almeida, L. (1994). Action of phenolic derivatives (acetaminophen, salicylate, and 5-aminosalicylate) as inhibitors of membrane lipid peroxidation and as peroxyl radical scavengers. *Archives of Biochemistry and Biophysics*, *315*(1), 161-169. https://doi.org/10.1006/abbi.1994.1485
13. DuBois, M., Gilles, K.A., Hamilton, J.K., Rebers, P.A., Smith, F. (1956). Colorimetric method for determination of sugars and related substances. *Analytical Chemistry*, *28*(3), 350-356. https://doi.org/10.1021/ac60111a017
14. Feng, J., Luo, X., Li, B., Yang, X.-Y., Zhang, L., Huang, J.-W., Hu, Y.-C., Zou, L., Wu, D.-T. (2025). Chemical structures, antioxidant capacities, and immunostimulatory activities of pectic polysaccharides from jujube fruits collected from different producing areas. *Food Bioscience*, *68*, art. no. 106485. https://doi.org/10.1016/j.fbio.2025.106485
15. Fernandes, P.A.R., Coimbra, M.A. (2023). The antioxidant activity of polysaccharides: A structure-function relationship overview. *Carbohydrate Polymers*, *314*, art. no. 120965. https://doi.org/10.1016/j.carbpol.2023.120965
16. Gong, L., Feng, D., Wang, T., Ren, Y., Liu, Y., Wang, J. (2020). Inhibitors of α-amylase and α-glucosidase: Potential linkage for whole cereal foods on prevention of hyperglycemia. *Food Science & Nutrition*, *8*(12), 6320-6337. https://doi.org/10.1002/fsn3.1987
17. Jain, A., Sarsaiya, S., Gong, Q., Wu, Q., Shi, J. (2024). Chemical diversity, traditional uses, and bioactivities of *Rosa roxburghii* Tratt: A comprehensive review. *Pharmacology & Therapeutics*, *259*, art. no. 108657. https://doi.org/10.1016/j.pharmthera.2024.108657
18. Jiao, X., Zhang, M., Xu, B., Wu, C. (2025). Structural characterization and bioactivity of polysaccharides extracted from dried fruits of *Rosa roxburghii* Tratt fruit. *Science and Technology of Food Industry*, *46*(21), 104-111 (in Chinese, English abstract). https://doi.org/10.13386/j.issn1002-0306.2024110077
19. Kačuráková, M., Capek, P., Sasinková, V., Wellner, N., Ebringerová, A. (2000). FT-IR study of plant cell wall model compounds: pectic polysaccharides and hemicelluloses. *Carbohydrate Polymers*, *43*(2), 195-203. https://doi.org/10.1016/S0144-8617(00)00151-X
20. Kaczmarska, A., Pieczywek, P.M., Cybulska, J., Zdunek, A. (2024). Effect of enzymatic modification on the structure and rheological properties of diluted alkali-soluble pectin fraction rich in RG-I. *Scientific Reports*, *14*(1), art. no. 11454. https://doi.org/10.1038/s41598-024-62180-2
21. Larsen, F.H., Byg, I., Damager, I., Diaz, J., Engelsen, S.B., Ulvskov, P. (2011). Residue specific hydration of primary cell wall potato pectin identified by solid-state 13c single-pulse MAS and CP/MAS NMR spectroscopy. *Biomacromolecules*, *12*(5), 1844-1850. https://doi.org/10.1021/bm2001928
22. Li, H., Fang, W., Wang, Z., Chen, Y. (2022). Physicochemical, biological properties, and flavour profile of *Rosa roxburghii* Tratt, *Pyracantha fortuneana*, and *Rosa laevigata* Michx fruits: A comprehensive review. *Food Chemistry*, *366*, art. no. 130509. https://doi.org/10.1016/j.foodchem.2021.130509
23. Li, X., Yao, W., Hu, C., Lin, C., You, L., Mao, J. (2024). Comparative analysis of *Gracilaria chouae* polysaccharides derived from different geographical regions: Focusing on their chemical composition, rheological properties, and gel characteristics. *Gels*, *10*(7), art. no. 454. https://doi.org/10.3390/gels10070454
24. Lineweaver, H., Burk, D. (1934). The determination of enzyme dissociation constants. *Journal of the American Chemical Society*, *56*(3), 658-666. https://doi.org/10.1021/ja01318a036
25. Lutz, R., Aserin, A., Wicker, L., Garti, N. (2009). Structure and physical properties of pectins with block-wise distribution of carboxylic acid groups. *Food Hydrocolloids*, *23*(3), 786-794. https://doi.org/10.1016/j.foodhyd.2008.04.009
26. Nishikimi, M., Rao, N.A., Yagi, K. (1972). The occurrence of superoxide anion in the reaction of reduced phenazine methosulfate and molecular oxygen. *Biochemical and Biophysical Research Communications*, *46*(2), 849-854. https://doi.org/10.1016/S0006-291X(72)80218-3

27. Qi, H., Zhao, T., Zhang, Q., Li, Z., Zhao, Z., Xing, R. (2005). Antioxidant activity of different molecular weight sulfated polysaccharides from *Ulva pertusa* Kjellm (Chlorophyta). *Journal of Applied Phycology*, *17*(6), 527-534. **https://doi.org/10.1007/s10811-005-9003-9**
28. Re, R., Pellegrini, N., Proteggente, A., Pannala, A., Yang, M., Rice-Evans, C. (1999). Antioxidant activity applying an improved ABTS radical cation decolorization assay. *Free Radical Biology and Medicine*, *26*(9-10), 1231-1237. **https://doi.org/10.1016/s0891-5849(98)00315-3**
29. Schols, H.A., Voragen, A.G.J. (1996). Complex pectins: Structure elucidation using enzymes. In J. Visser, A.G.J. Voragen (Eds.), *Progress in Biotechnology*, *vol. 14*, Elsevier, pp. 3-19. **https://doi.org/10.1016/S0921-0423(96)80242-5**
30. Shi, X., Zhang, X., Wang, L., Ge, Y., Chen, G. (2025). Comparative study of *Idesia polycarpa* Maxim cake meal polysaccharides: Conventional *versus* innovative extraction methods and their impact on structural features, emulsifying, anti-glycation, and hypoglycemic properties. *Food Chemistry*, *471*, art. no. 142745. **https://doi.org/10.1016/j.foodchem.2024.142745**
31. Stookey, L.L. (1970). Ferrozine – a new spectrophotometric reagent for iron. *Analytical Chemistry*, *42*(7), 779-781. **https://doi.org/10.1021/ac60289a016**
32. Synytsya, A., Čopíková, J., Matějka, P., Machovič, V. (2003). Fourier transform Raman and infrared spectroscopy of pectins. *Carbohydrate Polymers*, *54*(1), 97-106. **https://doi.org/10.1016/S0144-8617(03)00158-9**
33. Tadera, K., Minami, Y., Takamatsu, K., Matsuoka, T. (2006). Inhibition of α-glucosidase and α -amylase by flavonoids. *Journal of Nutritional Science and Vitaminology*, *52*(2), 149-153. **https://doi.org/10.3177/jnsv.52.149**
34. Uskoković, V. (2012). Dynamic light scattering based microelectrophoresis: Main prospects and limitations. *Journal of Dispersion Science and Technology*, *33*(12), 1762-1786. **https://doi.org/10.1080/01932691.2011.625523**
35. Voragen, A.G.J., Coenen, G.-J., Verhoef, R.P., Schols, H.A. (2009). Pectin, a versatile polysaccharide present in plant cell walls. *Structural Chemistry*, *20*(2), 263-275. **https://doi.org/10.1007/s11224-009-9442-z**
36. Wang, J., Wang, G., Wang, X., Qin, L., Xu, C., She, X., He, Y., Tan, D. (2022a). Chemical constituents and bioactivities of *Rosa roxburghii*: a systematic review. *Food Science and Technology*, *42*, art. no. 72722 **https://doi.org/10.1590/fst.72722**
37. Wang, L., Chen, C., Zhang, B., Huang, Q., Fu, X., Li, C. (2018a). Structural characterization of a novel acidic polysaccharide from *Rosa roxburghii* Tratt fruit and its α-glucosidase inhibitory activity. *Food & Function*, *9*(7), 3974-3985. **https://doi.org/10.1039/C8FO00561C**
38. Wang, L., Li, C., Huang, Q., Fu, X. (2020). Polysaccharide from *Rosa roxburghii* Tratt fruit attenuates hyperglycemia and hyperlipidemia and regulates colon microbiota in diabetic *db/db* mice. *Journal of Agricultural and Food Chemistry*, *68*(1), 147-159. **https://doi.org/10.1021/acs.jafc.9b06247**
39. Wang, L., Zhang, B., Xiao, J., Huang, Q., Li, C., Fu, X. (2018b). Physicochemical, functional, and biological properties of water-soluble polysaccharides from *Rosa roxburghii* Tratt fruit. *Food Chemistry*, *249*, 127-135. **https://doi.org/10.1016/j.foodchem.2018.01.011**
40. Wang, L., Zhang, P., Chen, J., Li, C., Tian, Y., Xu, F. (2023). Prebiotic properties of the polysaccharide from *Rosa roxburghii* Tratt fruit and its protective effects in high-fat diet-induced intestinal barrier dysfunction: A fecal microbiota transplantation study. *Food Research International*, *164*, art. no. 112400. **https://doi.org/10.1016/j.foodres.2022.112400**
41. Wang, L., Zhu, L., Gao, J., Zhang, F., Li, L., Yang, Y., Xu, Y. (2022b). Effect of dandelion root polysaccharide on structure, rheology and retrogradation properties of corn starch during storage. *International Journal of Food Science & Technology*, *57*(10), 6522-6530 **https://doi.org/10.1111/ijfs.15991**
42. Wang, L.-T., Lv, M.-J., An, J.-Y., Fan, X.-H., Dong, M.-Z., Zhang, S.-D., Wang, J.-D., Wang, Y.-Q., Cai, Z.-H., Fu, Y.-J. (2021). Botanical characteristics, phytochemistry and related biological activities of *Rosa roxburghii* Tratt fruit, and its potential use in functional foods: a review. *Food & Function*, *12*(4), 1432-1451. **https://doi.org/10.1039/d0fo02603d**
43. Wu, D., Zheng, J., Hu, W., Zheng, X., He, Q., Linhardt, R.J., Ye, X., Chen, S. (2020). Structure-activity relationship of Citrus segment membrane RG-I pectin against Galectin-3: The galactan is not the only important factor. *Carbohydrate Polymers*, *245*, art. no. 116526. **https://doi.org/10.1016/j.carbpol.2020.116526**
44. Zhang, Q., Huang, R., Chen, G., Guo, F., Hu, Y. (2025a). Effect of planting systems on the physicochemical properties and bioactivities of strawberry polysaccharides. *Foods*, *14*(2), art. no. 238. **https://doi.org/10.3390/foods14020238**
45. Zhang, Q., Huang, R., Wang, L., Ge, Y., Fang, H., Chen, G. (2025b). Comparative study on the effects of different drying technologies on the structural characteristics and biological activities of polysaccharides from *Idesia polycarpa* maxim cake meal. *Food Chemistry: X*, *26*, art. no. 102348. **https://doi.org/10.1016/j.fochx.2025.102348**
46. Zhang, Q., Wu, S., Dai, Q., Hu, P., Chen, G. (2024). Effects of different drying methods on the structural characteristics and multiple bioactivities of *Rosa roxburghii* Tratt fruit polysaccharides. *Foods*, *13*(15), art. no. 2417. **https://doi.org/10.3390/foods13152417**
47. Zhang, Y., Chen, Z., Huang, Z., Wu, Z., Xu, J., Wang, K. (2019). A comparative study on the structures of *Grifola frondosa* polysaccharides obtained by different decolourization methods and their *in vitro* antioxidant activities. *Food & Function*, *10*(10), 6720-6731. **https://doi.org/10.1039/c9fo01511f**
48. Zheng, Y., Bai, L., Zhou, Y., Tong, R., Zeng, M., Li, X., Shi, J. (2019). Polysaccharides from Chinese herbal medicine for anti-diabetes recent advances. *International Journal of Biological Macromolecules*, *121*, 1240-1253. **https://doi.org/10.1016/j.ijbiomac.2018.10.072**
49. Zor, T., Selinger, Z. (1996). Linearization of the Bradford protein assay increases its sensitivity: Theoretical and experimental studies. *Analytical Biochemistry*, *236*(2), 302-308. **https://doi.org/10.1006/abio.1996.0171**

ORIGINAL ARTICLE
http://journal.pan.olsztyn.pl

Polish Journal of Food and Nutrition Sciences
2026, Vol. 76, No. 3, 331–344
DOI: 10.31883/pjfns/235669
ISSN 1230-0322, e-ISSN 2083-6007

Evaluation of the Effect of Pretreatment Processes on the Bioactivity and Physicochemical Properties of Quince Slices Dried Using Vacuum-Combined Infrared Radiation

Serdar Uğurlu[1]*, Emre Bakkalbaşı[2]

[1]Department of Plant and Animal Production, Yüksekova Vocational School, Hakkari University, Hakkari, 30100, Türkiye
[2]Department of Food Engineering, Faculty of Engineering, Van Yüzüncü Yıl University, Zeve Campus, 65080 Van, Türkiye

This study investigated the effects of citric acid, ultrasound, ethanol solution, freeze-thawing, and blanching pretreatments and their combinations on quality parameters, phenolic profile, antioxidant activity, phenolic bioaccessibility, and α-glucosidase inhibitory activity of quince slices dried by vacuum-combined infrared radiation. Drying time was significantly shortened when pretreatments were applied, especially their combinations. The pretreatment combinations also resulted in a decreased rehydration ratio of the samples and high L^* values. The pretreatments increased the contents of chlorogenic, neochlorogenic, and cryptochlorogenic acids, decreased rutin content, and resulted in variable amounts of procyanidins B1 and B2. 5-Hydroxymethylfurfural was detected in dried quince slices pretreated with citric acid (61.3 mg/kg DM), ultrasounds (9.2 mg/kg DM), freezing-thawing (62.4 mg/kg DM), and blanching (4.3 mg/kg DM). The total phenolic, total flavonoid, and condensed tannin contents and antioxidant activity decreased after *in vitro* gastrointestinal digestion. Lower phenolic bioaccessibility was found especially in dried quince slices after pretreatment combinations. The α-glucosidase inhibitory activity of quince slices ranged from 17.94 to 24.84 mg/mL, which was higher than that of acarbose (26.79 mg/mL). The results showed that the pretreatments employed in quince drying can be used separately rather than in combination and that sample exposure to ultrasounds turned out to be be the most suitable pretreatment method.

Keywords: antioxidant potential, bioaccessibility, bioactive quality, α-glucosidase inhibitory activity, pretreatments

INTRODUCTION

Quince (*Cydonia oblonga* Miller) fruit is known for its micronutrient content, pleasant fragrance, and unique flavor. It is rich in ascorbic acid and minerals including calcium, potassium, and phosphorus [Sharma *et al.*, 2011]. However, it is particularly recognized as a dietary source of health-promoting compounds eliciting antioxidant and antimicrobial effects [Hajji *et al.*, 2020]. Phenolic compounds identified in quince fruit include 4-*O*-caffeolquinic acid, 3-*p*-coumaroylquinic acid, 5-*O*-caffeoylquinic acid, 5-*p*-coumaroylquinic acid, quercitin 3-*O*-glucoside, quercitin 3-*O*-rutinoside, kaempferol rutinoside, kaempferol hexoside, quercetin, catechin, epicatechin, and a procyanidin dimer [Baroni *et al.*, 2018].

Drying quince fruits is one possible method of storing them and preventing them from deterioration. Symilarly to other fruits, quince is perishable; therefore, drying is quite advantageous as it reduces the water activity of the material, thus reducing the microbiological activity to a level that prevents deterioration [Doymaz

*Corresponding Author:
E-mail: serdar_ugurlu_@hotmail.com, serdarugurlu@hakkari.edu.tr (S. Uğurlu)

Submitted: 13 April 2026
Accepted: 26 August 2026
Published on-line: 7 September 2026

et al., 2015]. The most commonly used drying method is hot-air convective drying, but this method has some disadvantages such as long processing time required and the use of high temperatures [Martins *et al*., 2022]. For food products, infrared drying is regarded as a promising drying method [Huang *et al*., 2021]. Novel combined infrared-vacuum drying is a new drying technique that has some advantages over conventional drying in terms of energy consumption, time savings, and high product quality [Topuz *et al*., 2023]. Nevertheless, any drying method influences the quality of the final dried products [Oliveira *et al*., 2016].

Various pretreatment techniques are, therefore, utilized to improve drying characteristics and/or dried product quality [Kriaa & Nassar, 2022]. These methods involve ultrasounds, high pressures, ethanol [Llavata *et al*., 2020], freeze-thawing, blanching, and pulsed electric field [Kriaa & Nassar, 2022]. Ethanol pretreatment is a simple and effective method, dissolving compounds in the cell wall and increasing its permeability [Llavata *et al*., 2020; Wang *et al*., 2019]. Wang *et al.* [2019] reported that ethanol pretreatment significantly reduced the drying time of scallion slices. These samples also exhibited better rehydration, odor, vitamin C content, and antibacterial effects. The principle of freeze-thawing pretreatment relies on ice crystallization, which is formed by free water penetrating to the cell wall during the expansion process of frozen water. This allows free water to overflow the cell and promote mass transfer [Xu *et al*., 2021]. Blanching is an important pretreatment in fruit and vegetable processing as it inactivates enzymes, enhances dehydration rate, removes pesticide residues, and reduces microbial load [Xiao *et al*., 2017]. Lagnika *et al.* [2019] found that blanching pretreatment of cashew apples led to medium quality results in terms of a rehydration rate and overall sensory quality, with substantial degradation of vitamin C. In turn, Chao *et al.* [2022] reported that ultrasound, blanching, and freeze-thawing pretreatments significantly accelerated the drying rate and that the seed-used pumpkin slices dried after blanching pretreatment exhibited the highest free phenolic content and total carotenoid content, which increased by 45% and 34%, respectively, compared to the untreated sample. In the studies, ethanol, freeze-thawing, and blanching pretreatments are used alone as well as in combination with ultrasounds. da Cunha *et al.* [2020] reported that the combination of ultrasounds and ethanol (50% and 100%) shortened the drying time of melon slices but negatively affected their quality parameters. Xu *et al.* [2021] investigated the effect of ultrasound, freeze-air thawing, freeze-water thawing, freeze-ultrasound thawing, and freeze-air ultrasound thawing pretreatments on the quality of dried okra and reported that all pretreatments shortened the drying time and that the freeze--air ultrasound thawing pretreatment yielded the most variable characteristics of dried okra quality. Xu *et al.* [2023] reported that thermoultrasound blanching resulted in more efficient drying by promoting tissue softening, moisture diffusion, microstructural changes, and microchannel formation compared to hot water blanching, which significantly reduced energy consumption and improved the overall quality of the dried sweet potatoes.

To the best of our knowledge, the effects of citric acid, ultrasounds, ethanol, freeze-thawing, blanching, and their various combinations as pretreatments on the vacuum-combined infrared radiation (VCIR) drying of quince have not been studied yet. Therefore, the aim of this study was to investigate the effects of ten different pretreatments on (i) drying time, color, and rehydration ratio; (ii) α-glucosidase inhibitory activity; (iii) phenolic composition; (iv) antioxidant activity; and (v) *in vitro* bioaccessibility of these phenolic compounds of quince slices dried by VCIR. These pretreatment combinations were expected to enhance the physical, chemical, and nutritional properties of quince.

MATERIALS AND METHODS

Sample preparation and drying procedure

Approximately 10 kg of fresh quince fruits (Eşme) were purchased at a local market in Van, a province of Türkiye. Before drying, quince fruits were peeled and cut into 5-mm thick slices with a manual fruit slicer (Hex, Istanbul, Türkiye). The slices were divided into 10 parts, each of which was subjected to a different pretreatment before drying, including immersion in a citric acid solution (CA), ultrasound and citric acid treatment (US), immersion in ethanol (ET), ethanol treatment with ultrasounds (ET+US), freezing-thawing (FT), freezing-thawing with ultrasounds and citric acid (FT+US), freezing-thawing with ethanol and ultrasounds (FT+ET+US), blanching with citric acid (BL), blanching with ultrasounds and citric acid (BL+US), and blanching with citric acid and then immersion in ethanol with ultrasounds (BL+ET+US). The conditions and details of each treatment are described in **Table 1**. Samples pretrated with ultrasounds were sonicated at 20 kHz and 200 W using a UW 3200 probe (Bandelin, Berlin, Germany) connected to an ultrasonic generator (HD 3200 Sonopuls, Bandelin). Ultrasound applications lasted 5 min, and temperature control (23±1°C) was provided with ice bags. Drying was carried out using a vacuum-combined infrared dryer (Uniterm, Ankara, Türkiye) with four 250 W infrared lamps both at the ceiling and the floor inside the oven, eqqupied by a vacuum pump (Pall Life Sciences, DOA-P730-BN, MI, USA). The distance between the samples and the lamps was adjusted to 12 cm. The samples were dried at 250 W infrared power and 40 kPa vacuum pressure. The initial moisture content of the quince fruits was 81.34±0.12 g/100 g, and the fruits were dried until they reached about 12 g/100 g. The moisture content of the samples was determined using the oven-drying method [AOAC, 2003].

Determination of color parameters

Color coordinates, including L^* (lightness), a^* (redness-greenness), and b^* (blueness-yellowness) of fresh and dried quinces, were measured by a CR-400 colorimeter (Konica Minolta, Tokyo, Japan). The instrument was calibrated using a white standard

Table 1. Pretreatment conditions of quince slices and sample codes.

Pretreatment	Code	Conditions
Citric acid (control)	CA	Quince slices were pretreated with 0.5% citric acid solution (1:4, *w/v*) at 20±1°C for 5 min.
Ultrasounds + citric acid	US	Quince slices were pretreated with 100% ultrasound amplitude for 5 min in 0.5% citric acid solution (1:4, *w/v*) at 20±1°C.
Ethanol	ET	Quince slices were immersed in ethanol (1:4, *w/v*) for 5 min at 20±1°C.
Ethanol + ultrasounds	ET+US	Quince slices were pretreated with 100% ultrasound amplitude for 5 min in ethanol (1:4, *w/v*) at 20±1°C.
Freezing-thawing	FT	Quince slices were frozen at −18°C for 12 h and then allowed to thaw at room temperature (22±1°C) for 3 h.
Freezing-thawing + ultrasounds + citric acid	FT+US	Quince slices were frozen at −18°C for 12 h. They were then immersed in 0.5% citric acid solution (1:4, *w/v*) and thawed using ultrasounds (100% amplitude) for 5 min.
Freezing-thawing + ethanol + ultrasounds	FT+ET+US	Quince slices were frozen at −18°C for 12 h. They were then immersed in ethanol (1:4, *w/v*) and thawed using ultrasounds (100% amplitude) for 5 min.
Blanching + citric acid	BL	Quince slices were blanched in hot water with 0.5% citric acid solution (1:4, *w/v*) at 80±1°C for 5 min.
Blanching + ultrasound + citric acid	BL+US	Quince slices were blanched in hot water with 0.5% citric acid solution (1:4, *w/v*) at 80±1°C for 5 min at 100% ultrasound amplitude.
Blanching + ultrasounds + citric acid + ethanol	BL+ET+US	Quince slices were blanched in hot water with 0.5% citric acid solution (1:4, *w/v*) at 80± 1°C for 5 min. They were then immersed in ethanol and treated using ultrasounds (100% amplitude) for 5 min.

according to the manufacturer's instructions. Based on the color coordinates, the total color difference (ΔE), chroma (C), and hue angle (h°) were calculated using Equations (1)–(3), respectively [Maskan, 2001]:

$$\Delta E = \sqrt{(L^* - L_0^*)^2 + (a^* - a_0^*)^2 + (b^* - b_0^*)^2} \quad (1)$$

$$C = \sqrt{a^{*2} - b^{*2}} \quad (2)$$

$$h° = tan^{-1}\left(\frac{b^*}{a^*}\right) \quad (3)$$

where coordinates with subscript "$_0$" refers to the color reading of fresh quinces.

Rehydration ratio

The dried quince samples (1 g) were immersed in pure water (50 mL) for 24 h at ambient temperature. Then, the surface water was removed using filter paper, and the samples were weighed. Rehydration ratio (RR) was determined as the ratio of weights of rehydrated sample slices to dried sample slices [Doymaz *et al.*, 2015].

Preparation of methanolic extracts

Fresh (5 g) and dried (1 g) quince fruits were stirred with 15 mL of methanol and a water mixture (80:20, *v/v*) at 150 rpm for 2 h at room temperature. The mixtures were centrifuged at 8,000×*g* for 10 min. After separation, the extraction was repeated using the residue and 10 mL of the same solvent. The supernatants were combined and reached a final volume of 25 mL with the solvent [Bakkalbaşı *et al.*, 2013]. Methanolic extracts were used to analyze phenolic compound composition and 5-hydroxymethylfurfural (HMF) content.

Total phenolic content determination

The total phenolic content (TPC) detemination of quince was carried out by Singleton & Rossi [1965] method. Briefly, 0.4 mL of the extract was mixed with 2 mL of the Folin-Ciocalteu reagent (Sigma-Aldrich, St. Louis, MO, USA) (1:10, *v/v*) and 1.6 mL of sodium carbonate (7.5%), and the mixture was kept in the dark at room temperature for 60 min. Absorbance was read at 765 nm using a spectrophotometer (8453, Agilent, Santa Clara, CA, USA). TPC was expressed as mg gallic acid equivalent (GAE)/kg quince dry matter (DM).

Total flavonoid content determination

The total flavonoid content (TFC) was determined as reported by Zhishen *et al.* [1999]. In brief, 1 mL of the extract, 5 mL of water, and 0.3 mL of $NaN0_2$ (5%) were mixed. After 5 min, 0.3 mL of $AlCl_3$ (10%) was added. After another 5 min, 2 mL of NaOH (1 M) was added, and the final volume of the solution was adjusted to 10 mL with water. Absorbance was read at 510 nm using a spectrophotometer (8453, Agilent). The TFC was expressed as mg quercetin equivalent (QE)/kg DM.

Condensed tannin content determination

Condensed tannin content (CTC) of quince samples was determined using the vanillin assay by Sun *et al.* [1998]. Four mixtures composed of: (1) extract (1 mL), 1% vanillin solution in methanol (2.5 mL), and 25% H_2SO_4 solution (2.5 mL); (2) methanol (1 mL), 1% vanillin solution in methanol (2.5 mL), and 25% H_2SO_4 solution (2.5 mL); (3) extract (1 mL), methanol (2.5 mL), and 25% H_2SO_4 soluton (2.5 mL); and (4) methanol (3.5 mL) and 25% H_2SO_4 solution (2.5 mL), were prepared in separate tubes and incubated at 30°C for 20 min. The absorbance of each mixture (A_s, A_b, A_c

and A_0, respectively) was measured at 500 nm with a spectrophotometer (8453, Agilent). A similar set of solutions was prepared and processed with catechin solutions at different concentrations instead of the extract to obtain a calibration curve.

Absorbance value (A) was calculated for each standard and sample solution using Equation (4):

$$A = (A_s - A_b) - (A_c - A_0) \quad (4)$$

Results were given as mg catechin equivalents (CE)/kg DM.

Antioxidant activity determination

The assay with 2,2-diphenyl-1-picrylhydrazyl (DPPH) radical (Sigma-Aldrich) was carried out according to the procedure described by Brand-Williams *et al*. [1995] with a minor modification. The extract (0.1 mL) and a DPPH radical solution (3.9 mL, 0.025 g/L in methanol) were mixed and reacted for 60 min at room temperature. Absorbance was read at 515 nm using a spectrophotometer (8453, Agilent).

The 2,2'-azino-bis(3-ethylbenzothiazoline-6-sulfonic acid) (ABTS) (Sigma-Aldrich) assay was performed according to Re *et al*. [1999] method. To generate the ABTS radical cation, a reaction was induced by incubating 7 mM ABTS and 2.45 mM potassium persulfate for 16 h at room temperature in a dark environment. The $ABTS^{\bullet+}$ solution was diluted with ethanol to obtain an absorbance of 0.700±0.05 at 734 nm. Then, the extract (20 µL) and the $ABTS^{\bullet+}$ solution (1,980 µL) were mixed and reacted in darkness for 6 min. The absorbance was measured at 734 nm.

$DPPH^{\bullet}$ and $ABTS^{\bullet+}$ scavenging activities were expressed as Trolox equivalents (mmol Trolox eq./g DM).

Determination of phenolic compound composition and 5-hydroxymethylfurfural content

Simultaneous analysis of phenolic compounds and HMF by high-performance liquid chromatography (HPLC) system (LC-20 AD, Shimadzu, Kyoto, Japan) was performed as reported by Colaric *et al*. [2005] with slight modifications. Separation was performed on a Symmetry C18 (250×4.6 mm id, particle size 5 µm) column (Waters, Milford, MA, USA) at 25°C. Acetic acid in water (2%, *v/v*) (A) and a mixture of acetonitrile with 0.5% (*v/v*) acetic acid in water (1:1, *v/v*) (B) were used as a mobile phase. The flow rate was 1.0 mL/min. The gradient program was as follows: 0 min, 90% A; 30 min, 80% A; 60 min, 65% A. Detection was made at 276 nm for HMF, 280 and 320 nm for phenolic acids, 280 nm for flavan-3-ols, and 360 nm for flavonols. The identification of the phenolic and HMF peaks on the chromatogram was carried out using retention time and spectrum of a commercial standard. Rutin, catechin, epicatechin, chlorogenic acid, neochlorogenic acid, and cryptochlorogenic acid standards were purchased from Sigma-Aldrich Co. Procyanidin B1 and procyanidin B2 standards were purchased from abcr GmbH (Karlsruhe, Germany). HMF standard was purchased from Carl Roth (Karlsruhe, Germany). Quantification was performed based on standard curves, and results were given as mg/kg DM.

Determination of phenolic bioaccessibility and antioxidant activity after *in vitro* digestion

Quince (1.5 g) was mixed with 30 mL of pure water and 1.5 mL of pepsin (20 g/L in 0.1 M HCl) [Vitali *et al*., 2009]. Mixture pH was adjusted to 2 using 6 M HCl, and the mixture was incubated at 37°C for 1 h in a shaking water bath. The pH of the mixture was then adjusted to 7.2 using 1 M $NaHCO_3$ to stop gastric digestion. Afterwards, 7.5 mL of a bile/pancreatin solution (2 g of pancreatin and 12 g of bile salt in 1 L of 0.1 M $NaHCO_3$) and 7.5 mL of an NaCl/KCl solution (120 mM NaCl and 5 mM KCl) were added to the mixture, which was then incubated at 37°C for 2.5 h in a shaking water bath. After incubation, the mixture was centrifuged at 8,000×*g* for 10 min, and the supernatant was used for TPC, TFC, CTC, and antioxidant activity analysis. Bioaccessibility of TPC, TFC, and CTC, and retention of antioxidant activity were expressed as the percentage ratio of the values in the digested content to the initial values before digestion.

α-Glucosidase inhibitory activity of quince

The α-glucosidase inhibitory activity (α-GIA) of fresh and dried quinces was determined according to the procedure previously used by Zhang *et al*. [2020] with minor modifications. An aliquot of 50 µL of α-glucosidase (from *Saccharomyces cerevisiae*, Sigma-Aldrich) (1 U/mL) in a phosphate buffer (0.1 M, pH 6.8) was mixed with 100 µL of extracts at different concentrations (5–40 mg/mL). The mixtures were preincubated at 37°C for 10 min, and 5 mM 4-nitrophenyl α-D-glucopyranoside (100 µL) was added as a substrate. Reaction was carried out at 37°C for 15 min. Then, 0.1 M Na_2CO_3 (750 µL) was added to terminate the reaction. Absorbance was measured at 405 nm, and results were given as the IC_{50} value, which was defined as the concentration of the extract required to inhibit 50% of the α-glucosidase activity. Acarbose was used as a positive control.

Statistical analysis

All samples were prepared in five replicates, and all analyses were performed three times for each sample. Data were presented as mean and standard deviation. SPSS 20.0 software (IBM Corp., Armonk, NY, USA) was used for multivariate analysis of variance. Differences among the means were determined using Duncan's multiple range tests and were considered significant at $p<0.05$. The JMP 13 package program (SAS Institute Inc., Cary, NC, USA) was used to carry out both correlation and principal component analysis (PCA).

RESULT AND DISCUSSION

Effect of pretreatment on drying time and physicochemical parameters of quince slices

The drying times of quince slices are given in **Table 2**. Pretreatments with ultrasounds (US), ethanol (ET), freezing-thawing (FT), and blanching (BL), as well as their combinations resulted in significantly shorter drying times of quince slices compared to those treated with citric acid (CA) for which it was180 min. The drying time was especially reduced when ET and US were used (alone

Table 2. Drying time, moisture content, rehydration ratio (RR), and color parameters of fresh and dried quince slices after different pretreatments.

Quince	Drying time (min)	Moisture (g/100 g)	RR	*L**	*a**	*b**	C	*h*°	Δ*E*
Fresh	–	81.34±0.12	–	64.80±1.48	−2.07±0.38	22.18±1.43	22.27±1.42	95.35±1.05	–
CA	180	12.39±0.31^{aA}	3.27±0.25^{aA}	60.98±2.66^{eB}	9.23±0.82^{aA}	23.24±2.00^{cB}	25.03±1.95^{dB}	68.26±2.20^{dD}	12.35±1.25^{aA}
US	160	11.98±0.94^{aA}	2.83±0.15^{bcB}	62.36±2.45^{deAB}	8.59±0.44^{abA}	24.15±1.85^{cB}	25.64±1.73^{cdB}	70.32±1.81^{dC}	11.47±0.61^{abcAB}
ET	138	12.58±0.39^{aA}	2.94±0.10^{bB}	64.16±1.40^{cdA}	7.82±0.52^{bcB}	26.60±1.32^{bA}	27.74±1.30^{abA}	73.55±1.16^{cB}	10.99±0.83^{bcB}
ET+US	112	12.12±0.07^{aA}	2.91±0.02^{bcB}	64.33±1.70^{cdA}	7.03±1.07^{cC}	27.25±1.67^{abA}	28.18±1.41^{abA}	76.22±1.96^{bA}	10.69±0.78^{cB}
FT	143	12.06±0.36^{aA}	2.64±0.22^{cdA}	60.98±2.26^{eB}	8.71±1.25^{abA}	23.47±2.86^{cB}	25.06±2.92^{dB}	69.59±2.63^{dB}	12.15±1.99^{abA}
FT+US	122	12.23±0.23^{aA}	2.72±0.05^{bcA}	67.00±1.02^{abA}	7.80±0.69^{bcAB}	27.56±0.97^{abA}	28.85±1.12^{abA}	73.94±1.34^{bcA}	11.37±0.92^{abcA}
FT+ET+US	105	12.13±0.14^{aA}	2.42±0.15^{deA}	68.57±0.49^{aA}	6.90±0.63^{cB}	27.74±0.07^{abA}	28.63±0.19^{abA}	75.75±1.34^{bcA}	10.84±1.10^{cA}
BL	142	11.98±0.18^{aA}	2.96±0.06^{bA}	64.58±2.34^{cB}	7.27±0.92^{cA}	27.44±1.38^{abB}	28.40±1.30^{abAB}	75.13±2.08^{bcB}	10.98±1.08^{bcA}
BL+US	138	11.95±0.07^{aA}	2.66±0.07^{cdB}	68.65±1.64^{aA}	5.33±0.83^{dB}	28.97±1.57^{aA}	29.47±1.50^{aA}	79.53±1.88^{aA}	10.91±1.36^{cA}
BL+ET+US	94	11.99±0.47^{aA}	2.23±0.12^{eC}	65.20±2.04^{bcB}	7.64±1.05^{cA}	26.07±1.62^{bB}	27.24±1.25^{bcB}	73.56±2.80^{cB}	10.78±0.55^{cA}

Values are given as mean ± standard deviation. Lowercase letters indicate the difference between the samples in the same column according to Duncan multiple comparison test, uppercase letters indicate the difference between the same group of pretreated samples ($p<0.05$). CA, citric acid; US, ultrasounds + citric acid; ET, ethanol; ET+US, ethanol + ultrasounds; FT, freezing-thawing; FT+US, freezing-thawing + ultrasounds + citric acid; FT+ET+US, freezing-thawing + ethanol + ultrasounds; BL, blanching + citric acid; BL+US, blanching + ultrasounds + citric acid; BL+ET+US, blanching + ultrasounds + citric acid + ethanol; *L**, lightness; *a**, redness-greenness; *b**, blueness-yellowness; C, chroma; h°, hue angle; Δ*E*, total color difference compared to fresh quince.

or in combination with other pretreatments such as blanching or freezing-thawing). Pore opening by ultrasound can improve dissolution of cell wall compounds by ethanol. Thus, during drying, the Marangoni flow effect is more intense than when ethanol is used alone [Miano *et al*., 2021]. Compared to the FT and US samples, the drying time for sample FT+US decreased by 14.68% and 23.75%, respectively (**Table 2**). A similar phenomenon was observed for plums by Li *et al*. [2025]. The highest reductions in drying time were 47.77% (for BL+ET+US), 41.66% (for FT+ET+US), and 37.77% (for ET+US) compared to the CA sample, demonstrating that the proposed approach of combining pretreatments for VCIR drying was effective in reducing processing time. The moisture content of quince samples after drying varied within a narrow range (11.95–12.58 g/100 g).

The RR values obtained for the quince slices dried after the ten different pretreatments are shown in **Table 2**. Among the pretreatments used, the highest and lowest rehydration ratios were 3.27 for CA and 2.23 for BL+ET+US, respectively. RR values of US, ET, and ET+US samples were found to be close to each other ($p \geq 0.05$), but were significantly ($p < 0.05$) lower than those of the CA sample. The microstructure of the sample was disrupted by US pretreatment. Thus, the water holding capacity of the cell was reduced, resulting in a lower RR [Ren *et al*., 2022]. Similar situation was also found in the samples treated with FT ($p \geq 0.05$). However, compared to US, ET, and ET+US samples, RR of the FT samples was lower. RR decreased with increasing pretreatment combinations in blanching samples ($p < 0.05$). This indicates that the damage caused to the structure by ultrasound or the combination of ethanol and ultrasound was higher compared to blanching.

After applying various pretreatments, a change in L^*, a^*, b^*, C, h°, and ΔE was observed compared to the fresh quince (**Table 2**). Generally, dried products exhibited higher a^* and b^* values than fresh quince, indicating browning during drying [Xu *et al*., 2021]. Among the pretreatments, the CA and FT resulted in the lowest L^* values of quince slices, indicating browning reactions [Ren *et al*., 2022]. The prolonged drying time for the CA sample may also have been important. The ET or ET+US pretreatment had a major impact on enhancing lightness and reducing browning (high L^* and b^* values and low a^* values) compared to CA and FT samples. This may be due to the decolorizing effect of alcohol which dissolved the pigments [Feng *et al*., 2019]. Moreover, after the FT pretreatment, the cellular structure of the samples is severely damaged, and the leakage of intracellular material can accelerate the browning reaction [Chao *et al*., 2022]. The FT quince slices were darker than the FT+US and FT+ET+US samples ($p < 0.05$). This may be due to the prolonged thawing time (3 h). Following freeze damage, the combination of US supported thawing, and a significantly shorter drying time effectively preserved the L^* values [Li *et al*., 2025]. L^* and b^* values of the BL samples were lower than those of the BL+US samples, and a^* value was higher ($p < 0.05$). The BL+ET+US sample was similar to the BL sample despite applying ultrasound and ethanol ($p \geq 0.05$). The BL+ET+US sample was first subjected to blanching (5 min) and then to ET+US pretreatment (5 min). The application of US and ET pretreatments after BL pretreatment did not result in a change in terms of color, on the contrary, it appeared to cause loss of time, solvent, and energy. The L^* values of the ET and BL samples were similar, but lower in the FT sample. This indicates that ET and BL preserve the brightness better than FT. Slight changes in C, h°, and ΔE were observed between pretreatments. The highest ΔE and lowest C and h° were detected in the CA and FT samples. It can be concluded that combinations of pretreatments positively affected limited color change. Generally, the L^* values of ethanol and combined pretreatment samples were found to be close to or higher than those of the fresh sample. In this case, it can be concluded that pretreatment combinations had a positive effect on the L^* color parameter of the samples.

Effects of pretreatment on the phenolic profile and 5-hydroxymethylfurfural content of quince slices

Procyanidins B1 and B2, chlorogenic acid, neochlorogenic acid, cryptochlorogenic acid, and rutin were detected in fresh and dried quince by HPLC method (**Table 3**). Chromatograms of separations of fresh and dried (US pretreatment) samples are given in **Figure 1**. Catechin and epicatechin were detected only in fresh samples (15.79±2.15 and 13.51±0.39 mg/kg DM) (not shown in the table). Similar results for catechin and epicatechin in pear were reported by Topuz *et al*. [2023]. In turn, da Silva *et al*. [2025] reported that epicatechin was not detected in pretreated (blanching, cooking, and combination with ethanol) and dried sweet potato samples. This could be due to the degradation of epicatechin during processing [da Silva *et al*., 2025]. In another study, the correlation between the polyphenol oxidase activity and catechin content was significant, and enzymatic degradation might have contributed to catechin losses [Zhu *et al*., 2022].

The procyanidin B1 content in the BL and BL+US samples, as well as the procyanidin B2 content in the CA and FT+US samples was similar to those determined in fresh quince slices (**Table 3**). CA, US, ET, and ET+US pretreatments did not differentiate the quince slices ($p \geq 0.05$) in terms of procyanidin B1 content; however, significantly decreased procyanidin B2 content ($p < 0.05$) in the following order: US < CA < ET < ET+US. In all freeze-thawed samples, the contents of procyanidins B1 and B2 were similar ($p \geq 0.05$). Among the blanched samples, procyanidin B1 content was significantly lower ($p < 0.05$) after pretreatment combination with ET and US compared to BL and BL+US. It has been reported that different pretreatment methods had varying effects on the procyanidin B2 content of apple samples [Zhu *et al*., 2022]; while the NaCl immersion and blanching pretreatments increased the procyanidin B2 content during air drying, it decreased when air drying with airborne sonication was applied.

It was found that chlorogenic acid was a major phenolic compound in all samples (**Table 3**). Chlorogenic acid, neochlorogenic acid, and cryptochlorogenic acid contents were higher in dried than in fresh quince slices ($p < 0.05$) and tended to be

Table 3. Content of phenolics and 5-hydroxymethylfurfural (HMF) of fresh and dried quince slices after different pretreatments (mg/kg dry matter).

Quince	HMF	Procyanidin B1	Procyanidin B2	Chlorogenic acid	Neochlorogenic acid	Cryptochlorogenic acid	Rutin
Fresh	n.d.	18.59±0.30	28.72±1.53	80.3±2.4	66±10	31.6±0.3	35.79±1.50
CA	61.3 ± 19^{aA}	19.26 ± 1.18^{abcA}	28.71 ± 0.15^{abB}	594 ± 156^{abcdA}	406 ± 51^{bcdB}	53.6 ± 1.0^{aA}	4.79 ± 0.16^{dB}
US	9.2 ± 5.8^{bB}	19.49 ± 0.04^{abcA}	29.41 ± 0.03^{aA}	724 ± 119^{aA}	623 ± 4^{aA}	57.0 ± 10.4^{aA}	6.16 ± 0.66^{aA}
ET	n.d.	17.37 ± 3.40^{bcdA}	27.03 ± 0.23^{cdeC}	655 ± 66^{abcdA}	415 ± 10^{bcB}	56.3 ± 10.2^{aA}	5.01 ± 0.08^{cdB}
ET+US	n.d.	17.09 ± 0.59^{cdA}	26.20 ± 0.00^{eD}	559 ± 65^{abcdA}	330 ± 7^{cdeC}	49.4 ± 4.3^{aA}	4.88 ± 0.05^{cdB}
FT	62.4 ± 1.4^{a}	20.67 ± 0.72^{abA}	27.59 ± 1.06^{bcdeA}	372 ± 197^{dA}	245 ± 97^{deA}	48.7 ± 12.4^{aA}	5.37 ± 0.18^{bcA}
FT+US	n.d.	21.26 ± 1.42^{aA}	28.20 ± 0.33^{abcA}	690 ± 147^{abA}	504 ± 173^{abA}	55.4 ± 2.5^{aA}	5.61 ± 0.26^{bA}
FT+ET+US	n.d.	20.41 ± 0.93^{abcA}	27.85 ± 0.91^{bcdA}	402 ± 23^{bcdA}	292 ± 0^{cdeA}	48.8 ± 1.3^{aA}	n.d.
BL	4.3 ± 2.8^{b}	18.24 ± 1.27^{abcA}	27.99 ± 0.33^{abcA}	693 ± 29^{aAA}	301 ± 25^{cdeA}	52.7 ± 2.1^{aA}	5.37 ± 0.00^{bc}
BL+US	n.d.	18.04 ± 0.25^{abcA}	27.90 ± 1.16^{abcA}	677 ± 42^{abcA}	266 ± 6^{cdeAB}	52.4 ± 0.0^{aA}	n.d.
BL+ET+US	n.d.	14.56 ± 0.36^{dB}	26.35 ± 0.64^{deA}	393 ± 110^{cdB}	228 ± 19^{eB}	51.2 ± 11.0^{aA}	n.d.

Values are given as mean ± standard deviation. Lowercase letters indicate the difference between the samples in the same column according to Duncan multiple comparison test, uppercase letters indicate the difference between the same group of pretreated samples ($p<0.05$). CA, citric acid; US, ultrasounds + citric acid; ET, ethanol; ET+US, ethanol + ultrasounds; FT, freezing-thawing; FT+US, freezing-thawing + ultrasounds + citric acid; FT+ET+US, freezing-thawing + ethanol + ultrasounds; BL, blanching + citric acid; BL+US, blanching + ultrasounds + citric acid; BL+ET+US, blanching + ultrasounds + citric acid + ethanol; n.d., not detected.

highest in the ultrasound-treated samples except for BL samples, where the amount of these compounds tended to decrease with increasing pretreatment combinations. However, significant ($p<0.05$) differences in chlorogenic acid content were only found between BL-treated samples, while significant ($p<0.05$) differences in neochlorogenic acid content were identified between CA, US, ET, and ET+US samples. The increase in phenolics following BL pretreatment was primarily caused by the inactivation of polyphenol oxidase at high temperatures and a decrease in enzyme-induced degradation [Chao *et al*., 2022]. Chlorogenic, neochlorogenic, and cryptochlorogenic acids were lower in the FT, FT+ET+US, and BL+ET+US samples. The FT samples were thawed at room temperature for 3 h, while the FT+ET+US and BL+ET+US samples were exposed to a combination of three pretreatments. This might have caused degradation/extraction of these compounds. Chlorogenic acid is sensitive to temperature and oxygen as it easily degrades at high temperatures and atmospheric conditions [Liu *et al*., 2015].

The rutin content of fresh quince slices was higher than that of the dried ones ($p<0.05$). Rutin was not detected in the samples pretreated with BL+US, BL+ET+US, and FT+ET+US (**Table 3**). This is thought to be due to the combined effect of multiple pretreatment applications. Irondi *et al*. [2017] reported that the amount of rutin decreased in the blanched *Adansonia digitata* leaves compared to fresh material. The high blanching temperature may have disrupted the cell walls and broken down the phenolics, causing them to leach into the blanching water [Irondi *et al*., 2017]. Rutin degradation does not directly relate to the denaturation of polyphenol oxidase, since its content decreases more quickly as temperature rises [Miletić *et al*., 2013]. In our study, the US and FT+US samples had the highest rutin contents. It can be concluded that the US pretreatment was effective in preserving phenolic compounds in combination with other pretreatments except ET. In contrast, in combination with ET, it caused greater loss of components. Ethanol pretreatment may cause the extraction of these compounds [da Cunha *et al*., 2020].

In general, the highest levels of phenolics were detected in the US sample compared to the samples exposed to the other pretreatment methods. Similar findings were reported by Wang *et al*. [2025] in quince peels subjected to different pretreatments (US, FT, and BL). This phenomenon can be attributed to the fact that bound phenolics become more liberated as a result of the ultrasound treatment [Topuz *et al*., 2025]. In summary, our results indicate that the US pretreatment was the most effective in preserving and increasing procyanidin B1, B2, chlorogenic acid, neochlorogenic acid, and cryptochlorogenic acid.

HMF does not occur naturally in food products. It is formed as a result of Maillard reactions under the influence of heat treatment and other factors (concentration of reducing sugar, type of sugar, storage time and temperature, *etc*.) [Shapla *et al*., 2018]. HMF content of quince slices dried after the different pretreatments varied between 0 and 62.4 mg/kg DM (**Table 3**). HMF was detected only in the CA, US, FT, and BL samples. Its content was significantly ($p<0.05$) higher in dried quince slices after CA

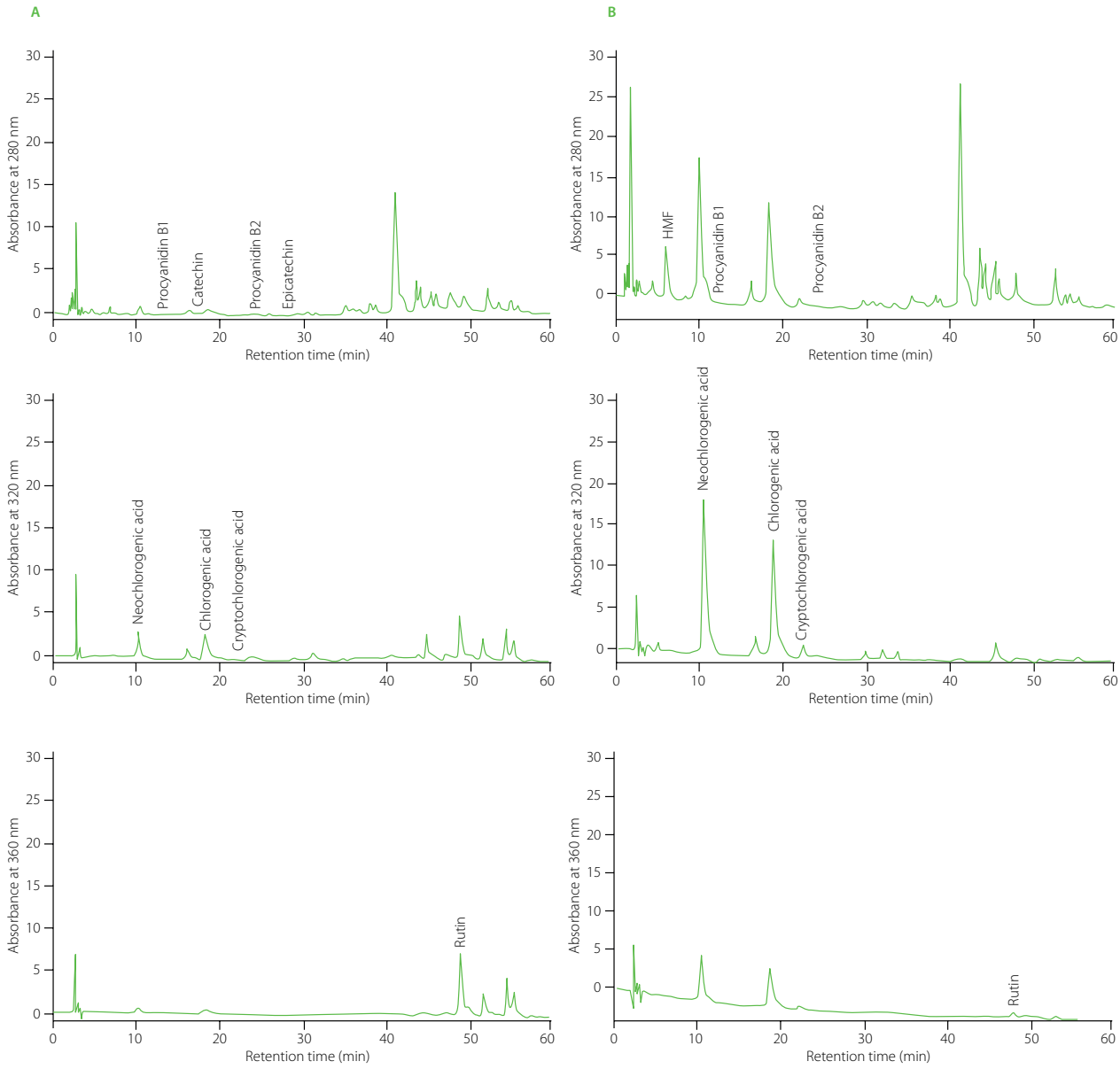

Figure 1. HPLC chromatograms of fresh quince slices (**A**) and dried after ultrasound pretreatment (**B**). HMF, 5-hydroxymethylfurfural.

and FT pretreatments than in the US and BL samples. The high HMF content in the FT sample shows that cell damage, rather than just drying time, contributes to nonenzymatic browning [Du *et al*., 2026]. In the CA sample, HMF content was similar ($p \geq 0.05$) to that in the FT sample, most likely due to the long drying time. Shorter drying times help reduce HMF accumulation [Du *et al*., 2026]. Compared to the CA sample, the HMF content of the US sample decreased by 85.04%. It can be concluded that the ultrasound pretreatment plays a significant role in preventing HMF formation. The substrates causing HMF formation may have been degraded or extracted by the effect of pretreatments via blanching or ultrasounds. It can, therefore, be concluded that HMF is not detected when ET or a combination of several pretreatments is used. This might be due to the shorter drying time of samples treated with ethanol and reduced heat exposure of the product. Therefore, it appears that the drying parameters were not the factors influencing the HMF content in the product.

- **Total phenolic content, total flavonoid content, condensed tannin content, and their bioaccessibility rates as well as antioxidant activity and its retention after *in vitro* digestion**

The TPC, TFC, and CTC of the quince slices are shown in **Table 4**, and their antioxidant activity (AA) (determined in DPPH and ABTS assays) is presented in **Table 5**. The TPC, TFC, DPPH$^{\bullet}$ scavenging activity and ABTS$^{\bullet+}$ scavenging activity of the dried quince slices were higher than those of the fresh sample (except for BL+ET+US sample for ABTS assay). However, CTC was higher in some dried samples (US, ET, BL, and BL+US). The highest TPC, TFC, CTC, and AA in both assays were detected in the US-pretreated

Table 4. Total phenolic content (TPC), total flavonoid content (TFC), and condensed tannin content (CTC) of fresh and dried quince slices after different pretreatments, and their bioaccessibility after *in vitro* gastrointestinal digestion (GID).

Quince	TPC (mg GAE/kg DM)	TPC-GID (mg GAE/kg DM)	Bioaccessibility (%)	TFC (mg QE/kg DM)	TFC-GID (mg QE/kg DM)	Bioaccessibility (%)	CTC (mg CE/kg DM)	CTC-GID (mg CE/kg DM)	Bioaccessibility (%)
Fresh	1,243±7	1,029±10	82.75±0.82	309±17	258±3	83.60±0.87	923±12	650±1	70.37±0.13
CA	4,132±24^{bB}	3,034±61^{cB}	73.40±1.48^{dB}	2,319±34^{bB}	1,722±17^{bB}	74.25±0.73^{bB}	845±42^{dBC}	459±7^{bB}	54.33±0.85^{bB}
US	4,379±104^{aA}	3,458±57^{aA}	78.97±1.31^{aA}	2,443±50^{aA}	1,963±13^{aA}	80.36±0.52^{aA}	1,517±2^{aA}	850±11^{aA}	56.01±0.70^{aA}
ET	3,570±145^{cC}	2,534±24^{dC}	70.98±0.67^{eC}	1,655±43^{eC}	1,199±14^{dC}	72.44±0.83^{cC}	1,037±18^{cB}	469±6^{bB}	45.22±0.56^{dC}
ET+US	3,235±74^{dD}	2,071±19^{fD}	64.03±0.59^{gD}	1,212±33^{gD}	844±4^{gD}	69.62±0.30^{dD}	645±178^{eC}	208±2^{fC}	32.23±0.32^{gD}
FT	3,008±38^{eA}	2,047±17^{fA}	68.05±0.57^{fA}	1,718±26^{deB}	1,124±13^{eB}	65.42±0.75^{eB}	229±3^{gC}	129±1^{hC}	56.36±0.30^{aA}
FT+US	2,709±22^{fB}	1,761±26^{gB}	64.99±0.97^{gB}	1,945±46^{cA}	1,376±21^{cA}	70.76±1.06^{dA}	753±25^{dA}	380±10^{dA}	50.42±1.34^{cB}
FT+ET+US	2,403±29^{gC}	1,472±21^{hC}	61.28±0.88^{hC}	1,224±60^{gC}	532±13^{iC}	43.41±1.07^{hC}	600±20^{eB}	192±1^{gB}	32.05±0.15^{gC}
BL	3,044±35^{eB}	2,289±13^{eB}	75.17±0.43^{cB}	1,767±33^{dA}	1,047±21^{fA}	59.26±1.18^{fA}	1,215±6^{bA}	434±6^{cA}	35.71±0.52^{eA}
BL+US	4,080±14^{bA}	3,144±28^{bA}	77.05±0.68^{bA}	1,491±67^{fB}	721±2^{hB}	48.32±0.16^{gB}	953±1^{cB}	323±3^{eB}	33.85±0.31^{fB}
BL+ET+US	1,282±55^{hC}	785±15^{iC}	61.26±1.20^{hC}	925±30^{hC}	392±13^{jC}	42.36±1.39^{hC}	482±18^{fC}	135±2^{hC}	27.93±0.39^{hC}

Values are given as mean ± standard deviation. Lowercase letters indicate the difference between the samples in the same column according to Duncan multiple comparison test, uppercase letters indicate the difference between the same group of pretreated samples ($p<0.05$). CA, citric acid; US, ultrasounds + citric acid; ET, ethanol; ET+US, ethanol + ultrasounds; FT, freezing-thawing; FT+US, freezing-thawing + ultrasounds + citric acid; FT+ET+US, freezing-thawing + ethanol + ultrasounds; BL, blanching + citric acid; BL+US, blanching + ultrasounds + citric acid; BL+ET+US, blanching + ultrasounds + citric acid + ethanol; DM, dry matter; GAE, gallic acid equivalent; QE, quercetin equivalent; CE, catechin equivalent.

Table 5. DPPH• and ABTS•+ scavenging activities of fresh and dried quince slices after different pretreatments, and their retention after *in vitro* gastrointestinal digestion (GID).

Quince	DPPH assay	DPPH-GID assay	Retention (%)	ABTS assay	ABTS-GID assay	Retention (%)
	(mmol Trolox eq./g DM)			(mmol Trolox eq./g DM)		
Fresh	6.12±0.21	5.78±0.03	94.35±0.63	32.76±0.86	30.45±0.38	92.96±1.18
CA	14.94 ± 0.89^{abAB}	10.43 ± 0.13^{cB}	69.86 ± 0.92^{bcB}	40.47 ± 0.09^{bB}	33.72 ± 0.26^{bB}	83.32 ± 0.65^{bB}
US	16.32 ± 0.24^{aA}	11.93 ± 0.07^{aA}	73.09 ± 0.44^{aA}	42.01 ± 0.66^{aA}	35.72 ± 0.32^{aA}	85.04 ± 0.76^{aA}
ET	14.58 ± 0.72^{bB}	9.99 ± 0.07^{dC}	68.55 ± 0.49^{cdC}	37.44 ± 0.65^{dC}	27.71 ± 0.03^{cC}	74.01 ± 0.10^{cC}
ET+US	11.86 ± 1.23^{cC}	7.62 ± 0.05^{gD}	64.24 ± 0.44^{eD}	33.55 ± 0.25^{gD}	23.84 ± 0.23^{fgD}	71.08 ± 0.68^{dD}
FT	15.29 ± 0.88^{abA}	10.92 ± 0.08^{bA}	71.41 ± 0.57^{bA}	38.23 ± 0.41^{cA}	26.53 ± 0.35^{dA}	69.41 ± 0.93^{eA}
FT+US	13.06 ± 1.32^{cB}	9.17 ± 0.10^{eB}	70.25 ± 0.82^{bcA}	34.85 ± 0.42^{fC}	24.06 ± 0.23^{fB}	69.05 ± 0.67^{eA}
FT+ET+US	11.86 ± 1.08^{cB}	8.27 ± 0.29^{fC}	69.73 ± 2.46^{bcA}	35.69 ± 0.23^{eB}	23.58 ± 0.06^{gC}	66.05 ± 0.17^{gB}
BL	12.17 ± 1.16^{cB}	7.39 ± 0.07^{hB}	60.70 ± 0.64^{fB}	34.50 ± 0.33^{fB}	22.21 ± 0.31^{hB}	64.38 ± 0.90^{hB}
BL+US	14.86 ± 0.28^{abA}	10.02 ± 0.20^{dA}	67.47 ± 1.36^{dA}	36.98 ± 0.61^{dA}	25.13 ± 0.39^{eA}	67.95 ± 1.07^{fA}
BL+ET+US	9.20 ± 0.28^{dC}	5.27 ± 0.10^{iC}	57.27 ± 1.15^{gC}	28.35 ± 0.51^{hC}	16.97 ± 0.09^{iC}	59.86 ± 0.34^{iC}

Values are given as mean ± standard deviation. Lowercase letters indicate the difference between the samples in the same column according to Duncan multiple comparison test, uppercase letters indicate the difference between the same group of pretreated samples ($p<0.05$). CA, citric acid; US, ultrasounds + citric acid; ET, ethanol; ET+US, ethanol + ultrasounds; FT, freezing-thawing; FT+US, freezing-thawing + ultrasounds + citric acid; FT+ET+US, freezing-thawing + ethanol + ultrasounds; BL, blanching + citric acid; BL+US, blanching + ultrasounds + citric acid; BL+ET+US, blanching + ultrasounds + citric acid + ethanol; DM, dry matter.

samples. US pretreatment enhanced the extractability of bioactive compounds and reduced their degradation [Wang *et al*., 2025]. ET and ET+US pretreatments resulted in a significant decrease in TPC, TFC, CTC, and AA ($p<0.05$). Dried quince slices after all FT pretreatments had lower TPC, TFC, CTC, and AA compared to those exposed to the US pretreatment because freeze-thawing damages the cell structure [Xu *et al*., 2021]. In addition, the thawing process has accelerated the breakdown of compounds that are sensitive to heat and oxidation [Li *et al*., 2025]. DPPH• scavenging activity decreased with increasing pretreatment combination in the freeze-thawed samples, and in both antioxidant assays, radical scavenging activity was highest in the FT sample ($p<0.05$). Furthermore, as indicated by data from **Table 4**, the TPC in the FT sample was higher than in the FT+US and FT+ET+US samples, which may be the main reason for the higher AA. Although blanching deteriorated quince quality, it was still better than that of the combined ethanol sample. Gonçalves *et al*. [2009] reported that blanching caused a significant reduction in the TPC of broccoli, probably due to thermal degradation and water leaching events. Additionally, BL pretreatment, likewise FT, can damage cell structures, increasing porosity and surface area. This may accelerate the release and subsequent degradation or oxidation of bioactive compounds during drying [Wang *et al*., 2025]. Among all blanched samples, the highest DPPH• and ABTS•+ scavenging activities and TPC were found in the BL+US sample ($p<0.05$). Xu *et al*. [2023] reported that thermoultrasound blanching significantly enhanced the inactivation efficiency of peroxidase and polyphenol oxidase compared to hot water blanching. Therefore, the TPC and antioxidant activity of the BL+US samples may be higher. The combination of blanching with ethanol and ultrasound as a pretreatment significantly affected TPC, TFC, CTC, and AA in ABTS and DPPH assays ($p<0.05$). This finding confirms that the combination of ET and US as a pretreatment decreased TPC, TFC, CTC, DPPH• scavenging activity, and ABTS•+ scavenging activity. The fact that the dried quince slices after the ET+US, FT+ET+US, and BL+ET+US pretreatments contained less bioactive compounds can be explained as follows: the use of ethanol pretreatment facilitates the extraction and thus the loss of phenolics [da Cunha *et al*., 2020]. As the increase in the combination of pretreatments would reduce the drying time, it caused a decrease in TPC, TFC, CTC, and antioxidant activity. In summary, US had a positive effect on the retention of bioactive compounds during the VCIR of quince.

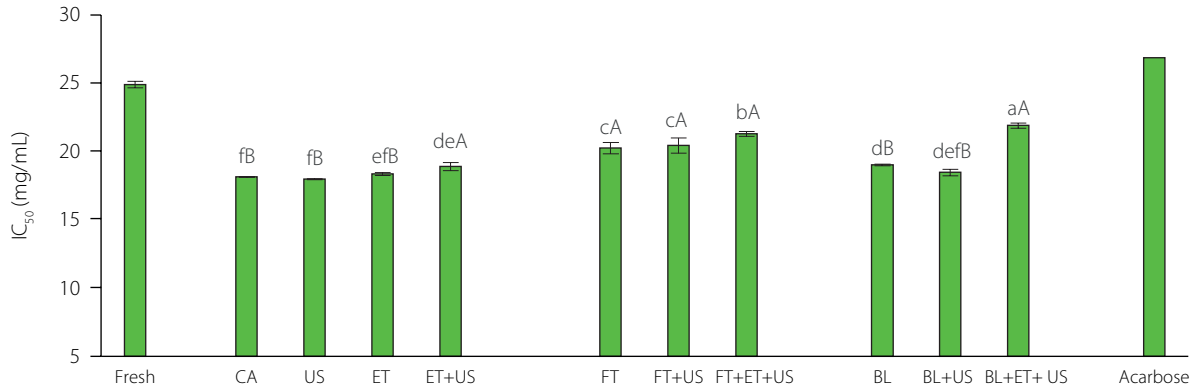

Figure 2. α-Glucosidase inhibitory activity of extracts from fresh and dried quince slices after different pretreatments. Values are given as mean ± standard deviation. Different lowercase letters indicate significant difference between samples, uppercase letters indicate difference between the same group of pretreated samples (p<0.05). CA, citric acid; US, ultrasounds + citric acid; ET, ethanol; ET+US, ethanol + ultrasounds; FT, freezing-thawing; FT+US, freezing-thawing + ultrasounds + citric acid; FT+ET+US, freezing-thawing + ethanol + ultrasounds; BL, blanching + citric acid; BL+US, blanching + ultrasounds + citric acid; BL+ET+US, blanching + ultrasounds + citric acid + ethanol; IC_{50}, concentration of the extract required to inhibit 50% of the α-glucosidase activity.

TPC, TFC, and CTC bioaccessibility, and antioxidant activity retention after gastrointestinal digestion (GID) in the fresh quince were higher than in the dried quince (**Tables 4** and **5**, respectively). TPC, TFC, CTC, and DPPH$^{\bullet}$ and ABTS$^{\bullet+}$ scavenging activities of the fresh and dried samples decreased after GID. This decrease may be related to the degradation of phenolics due to enzyme activity and increased pH [Ozdemirli & Kamiloglu, 2024]. CTC bioaccessibility was very low, especially in the dried samples (27.93–56.36%). Bouayed *et al*. [2012] reported that catechin, procyanidins B1, and B2 were not found in the intestinal phase. Therefore, CTC bioaccessibility may have been lower. TPC, TFC, and CTC bioaccessibility and AA retention of the US sample were higher than those of the CA, ET, and ET+US samples (p<0.05). TPC, DPPH$^{\bullet}$ scavenging activity, and ABTS$^{\bullet+}$ scavenging activity after GID, and their bioaccessibility/retention decreased with increasing pretreatment combination in freeze-thawing samples. This change was found to be insignificant only for DPPH$^{\bullet}$ scavenging activity retention (p≥0.05). In all freeze-thawed samples, the highest TFC-GID and CTC-GID values were found in the FT+US samples (p<0.05). In the blanched samples, TPC and AA after GID and their bioaccessibility/retention were highest in the BL+US sample, while TFC-GID and CTC-GID and their bioaccessibility started to decrease with increasing pretreatment combinations (p<0.05). Generally, all pretreatments were found to significantly reduce TPC, TFC, and CTC bioaccessibility, as their pretreatments may cause damage to the cell walls of the samples, while the ambient pH change during *in vitro* digestion may lead to degradation of phenolic compounds and reduce their AA.

Inhibitory effects on α-glucosidase activity

Antioxidants, including phenolics, can prevent the damage to β-cells by inhibiting the peroxidation chain reaction, potentially guarding against the onset of diabetes [Aslan *et al*., 2010]. They can improve β-cell function, stimulate insulin secretion, and improve adipose tissue metabolism [Lin *et al*., 2016]. Futhermore phenolics, particularly flavonoids, phenolic acids and tannins, possess the ability to inhibit α-glucosidase and α-amylase, which are responsible for digesting dietary carbohydrates into glucose, and thus can modulate carbohydrate and lipid metabolism [Lin *et al*., 2016]. The ability of extracts from fresh and dried quince to inhibit α-glucosidase is shown in **Figure 2**. The inhibitory activity of the samples against α-glucosidase expressed as IC_{50} values ranged from 17.94 to 24.84 mg/mL. Extracts from dried quince slices showed higher α-glucosidase inhibition activity than those from the fresh sample (p<0.05). Regardless of the method, the pretreatment process contributed to the increase in the antidiabetic activity. The inhibitory effect on α-glucosidase may be due to phenolic compounds present in the extracts [Irondi *et al*., 2017]. The α-GIA of the CA, US, and ET samples was similar (p≥0.05), but higher than that of the ET+US sample (p<0.05). α-Glucosidase inhibition decreased with increasing pretreatment combinations in the FT samples. However, this decrease was found to be insignificant (p≥0.05). The α-GIA of the CA, US, ET, ET+US, BL, and BL+US samples was higher than of all freeze-thawed samples (p<0.05). Contrary to our study, Irondi *et al.* [2017] reported that the inhibitory effect of *Adansonia digitata* leaf extract on α-glucosidase activity decreased due to blanching. In our study, this changed in proportion to the decrease in phenolic compound levels. Fresh and dried samples showed higher α-GIA than acarbose. Similar findings were reported by Uğurlu & Bakkalbaşı [2024] for apple chips. Due to their high content of bioactive compounds, both fresh and dried quince slices, especially the US sample, can be utilized as a food source with antidiabetic potential.

Principal component analysis results

PCA was performed using the correlation matrix to calculate the eigenvalues, percentages of variation, and load coefficients of the first three principal components for all the properties studied. The PCA results are presented in the form of a biplot (**Figure 3**). The first three principal components accounted for

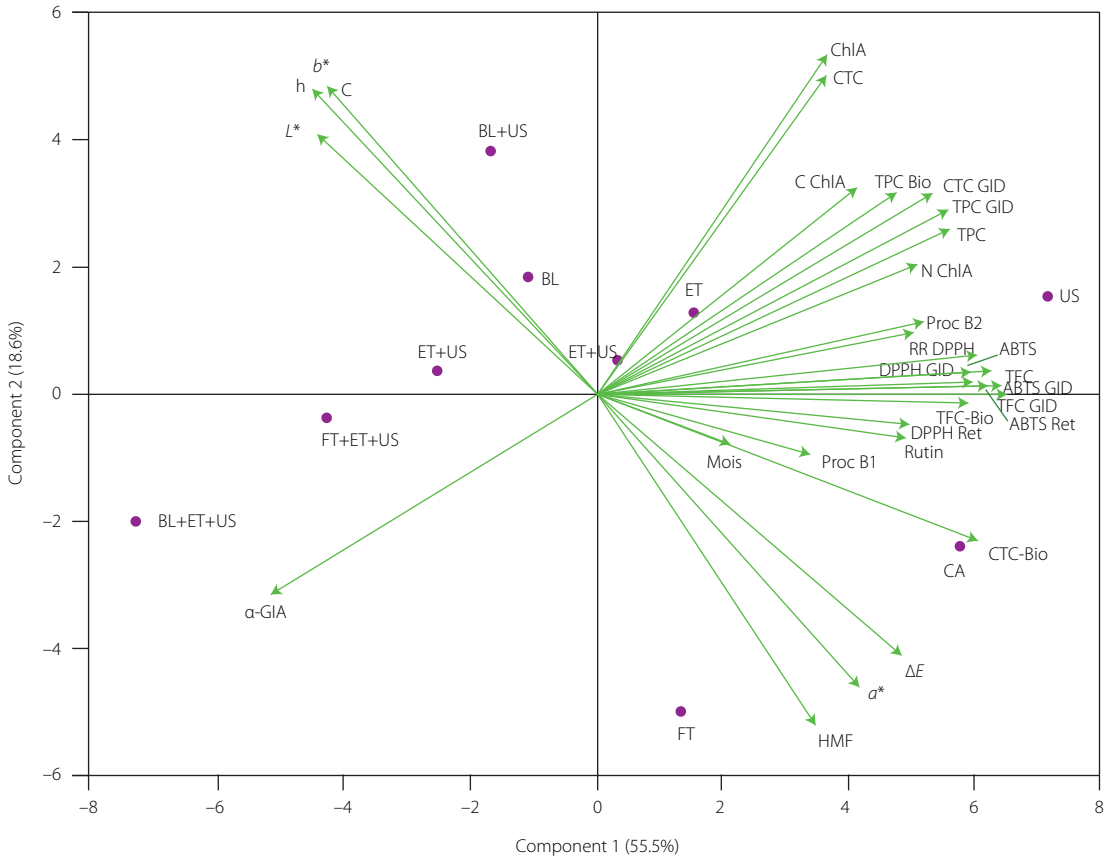

Figure 3. Biplot of principal component analysis. CA, citric acid; US, ultrasounds + citric acid; ET, ethanol; ET+US, ethanol + ultrasounds; FT, freezing-thawing; FT+US, freezing-thawing + ultrasounds + citric acid; FT+ET+US, freezing-thawing + ethanol + ultrasounds; BL, blanching + citric acid; BL+US, blanching + ultrasounds + citric acid; BL+ET+US, blanching + ultrasounds + citric acid + ethanol; ABTS, $ABTS^{\bullet+}$ scavenging activity; ABTS-Ret, retention of $ABTS^{\bullet+}$ scavenging activity; ABTS-GID, ABTS after gastrointestinal digestion; DPPH, $DPPH^{\bullet}$ scavenging activity; DPPH-Ret, retention of $DPPH^{\bullet}$ scavenging activity; DPPH-GID, $DPPH^{\bullet}$ scavenging activity after gastrointestinal digestion; TPC, total phenolic content; TPC-Bio, bioaccessibility of total phenolic content; TPC-GID, total phenolic content after gastrointestinal digestion; TFC, total flavonoid content; TFC-Bio, bioaccessibility of total flavonoid content; TFC-GID, total flavonoid content after gastrointestinal digestion; CTC, condensed tannin content; CTC-Bio, bioaccessibility of condensed tannin content; CTC-GID, condensed tannin content after gastrointestinal digestion; ProcB1, procyanidin B1; ProcB2, procyanidin B2; ChlA, chlorogenic acid; N-ChlA, neochlorogenic acid; C-ChlA, cryptochlorogenic acid; HMF, 5-hydroxymethylfurfural; α-GIA, α-glucosidase inhibitory activity; RR, rehydration ratio; Mois, moisture; *L**, lightness; *a**, redness-greenness; *b**, blueness--yellowness; C, chroma; h°, hue angle; Δ*E*, total color difference.

55.5, 18.6, and 8.0% of the total variation, respectively. The cumulative proportion of the variation approached 82.1% of the total variation. The traits contributing to this high variation in the first principal component (PC1) were RR, neochlorogenic acid, TPC, TPC-GID, TFC, TFC-GID, TFC bioaccessibility, CTC bioaccessibility, $ABTS^{\bullet+}$ scavenging activity, $ABTS^{\bullet+}$ scavenging activity after GID, and $ABTS^{\bullet+}$ scavenging activity retention. The effects of all these traits on variation were similar. Traits contributing to the second PCA component (PC2) were moisture, *L**, *a**, *b**, C, h°, Δ*E*, HMF, chlorogenic acid, TPC bioaccessibility, CTC, CTC GID, and α-GIA. The effects of α-GIA on the variation were less pronounced than others, and only the effects of *a**, ΔE, HMF, and α-glucosidase inhibitory activity were negative in PC2. As expected, a strong negative correlation was found between *L** and *a** and HMF. The third principal component (PC3) was primarily related to moisture, procyanidin B1 and B2, cryptochlorogenic acid, rutin, $DPPH^{\bullet}$ scavenging activity, $DPPH^{\bullet}$ scavenging activity after GID, and $DPPH^{\bullet}$ scavenging activity retention. The effect of procyanidin B1 and DPPH retention was stronger than of the other traits in PC3. *L** and HMF confirmed their inverse relationship by pointing in opposite directions on the graph. Additionally, the positions of the samples with FT and CA pretreatments on the biplot indicated their higher HMF content compared to the other samples. The position of the *a** value, indicating increased browning due to Maillard reactions, was consistent with treatments with longer drying times. The moisture content is located near the centre, indicating a moderate level of variation between applications and limited discriminating power in the PCA space. TPC, TFC, AA and their retention, along with phenolic compounds, contributed most significantly to the dispersion patterns of single pretreatments. A clear distinction was observed between single/ /double and triple pretreatment combinations. Compared to other pretreatments, the US pretreatment was clearly positioned above and to the right of the PC1 axis and exhibited a quality profile characterized by better preservation of certain sensitive bioactive compounds. The samples subjected to the triple pretreatment combination cover the lower left quadrant. This indicates that significant losses in phenolic compounds were associated with physicochemical changes such as extraction/ /degradation and exposure to oxygen.

CONCLUSIONS

This study investigated the effects of citric acid, ultrasound, ethanol, freeze-thawing, and blanching pretreatments and their various combinations on some physicochemical properties and bioactive compounds of dried quince. Pretreatment combinations caused a decrease in drying time. RR decreased significantly in the samples with more than two pretreatment combinations. CA and FT pretreatments were found to result in samples with darker appearance and the highest HMF content. The US pretreatment resulted in a higher phenolic content, AA, phenolic bioaccessibility, and α-GIA in dried samples than the combined pretreatments. Thus, pretreatments used alone are more effective than those applied in combination in reducing quality losses in products exposed to VCIR, and ultrasound was the most suitable pretreatment method. In this study, ultrasound was found to have a significant potential to improve product quality, either alone or in combination, in which it is included, thus paving the way for its inclusion in pretreatments to obtain healthy products in the food industry. *In vivo* studies are also required to fully understand the effect of these pretreatments on the bioaccessibility of phenolics and α-GIA of quince.

RESEARCH FUNDING

No funding was received for conducting this study.

CONFLICT OF INTERESTS

The authors declare that they have no conflict of interests.

ORCID IDs

E. Bakkalbaşı https://orcid.org/0000-0001-9913-1091
S. Uğurlu https://orcid.org/0000-0002-5785-9647

REFERENCES

1. AOAC (2003). *Official Methods of Analysis* (15th ed.). The Association of Official Analytical Chemists International, Washington, DC, USA.
2. Aslan, M., Orhan, N., Orhan, D.D., Ergun, F. (2010). Hypoglycemic activity and antioxidant potential of some medicinal plants traditionally used in Turkey for diabetes. *Journal of Ethnopharmacology*, *128*(2), 384–389. https://doi.org/10.1016/j.jep.2010.01.040
3. Bakkalbaşı, E., Yılmaz, Ö.M., Yemiş, O., Artık, N. (2013). Changes in the phenolic content and free radical-scavenging activity of vacuum packed walnut kernels during storage. *Food Science and Technology Research*, *19*(1), 105–112. https://doi.org/10.3136/fstr.19.105
4. Baroni, M.V., Gastaminza, J., Podio, N.S., Lingua, M.S., Wunderlin, D.A., Rovasio, J.L., Dotti, R., Rosso, J.C., Ghione, S., Ribotta, P.D. (2018). Changes in the antioxidant properties of quince fruit (*Cydonia oblonga* Miller) during jam production at industrial scale. *Journal of Food Quality, 2018*, art. no. 1460758. https://doi.org/10.1155/2018/1460758
5. Bouayed, J., Deußer, H., Hoffmann, L., Bohn, T. (2012). Bioaccessible and dialysable polyphenols in selected apple varieties following *in vitro* digestion *vs*. their native patterns. *Food Chemistry, 131*(4), 1466–1472. https://doi.org/10.1016/j.foodchem.2011.10.030
6. Brand-Williams, W., Cuvelier, M.E., Berset, C. (1995). Use of a free radical method to evaluate antioxidant activity. *LWT – Food Science and Technology, 28*(1), 25–30. https://doi.org/10.1016/S0023-6438(95)80008-5
7. Chao, E., Li, J., Fan, L. (2022). Enhancing drying efficiency and quality of seed-used pumpkin using ultrasound, freeze-thawing and blanching pretreatments. *Food Chemistry, 384*, art. no. 132496. https://doi.org/10.1016/j.foodchem.2022.132496
8. Colaric, M., Veberic, R., Solar, A., Hudina, M., Stampar, F. (2005). Phenolic acids, syringaldehyde, and juglone in fruits of different cultivars of *Juglans regia* L.. *Journal of Agricultural and Food Chemistry, 53*(16), 6390–6396. https://doi.org/10.1021/jf050721n
9. da Cunha, R.M.C., Brandão, S.C.R., de Medeiros, R.A.B., da Silva Júnior, E.V., da Silva, J.H.F., Azoubel, P.M. (2020). Effect of ethanol pretreatment on melon convective drying. *Food Chemistry, 333*, art. no. 127502. https://doi.org/10.1016/j.foodchem.2020.127502
10. da Silva, G.M., de Figueirêdo, R.M.F., de Melo Queiroz, A.J., de Vilela Silva, E.T., Moura, H.V., de França Silva, A.P., Santos, N.C., Buriti, F.C.A., de Brito Araújo Carvalho, A.J., dos Santos Lima, M. (2025). Blanching, cooking, and ethanol are effective strategies for preserving biofunctional compounds in purple-fleshed sweet potato powder. *Food and Bioproducts Processing, 150*, 118–130. https://doi.org/10.1016/j.fbp.2025.01.005
11. Doymaz, İ., Demir, H., Yıldırım, A. (2015). Drying of quince slices: Effect of pretreatments on drying and rehydration characteristics. *Chemical Engineering Communications, 202*(10), 1271–1279. https://doi.org/10.1080/00986445.2014.921619
12. Du, Y., Liu, K., Mi, S., Ding, J., Yuan, S., Yu, H., Guo, Y., Cheng, Y., Yao, W. (2026). Physical field pretreatments enhance drying efficiency and quality of goji berry. *Journal of Food Engineering, 403*, art. no. 112730. https://doi.org/10.1016/j.jfoodeng.2025.112730
13. Feng, Y., Zhou, C., Yagoub, A.E.A., Sun, Y., Owusu-Ansah, P., Yu, X., Wang, X., Xu, X., Zhang, J., Ren, Z. (2019). Improvement of the catalytic infrared drying process and quality characteristics of the dried garlic slices by ultrasound-assisted alcohol pretreatment. *LWT – Food Science and Technology, 116*, art. no. 108577. https://doi.org/10.1016/j.lwt.2019.108577
14. Gonçalves, E.M., Pinheiro, J., Alegria, C., Abreu, M., Brandão, T.R.S., Silva, C.L.M. (2009). Degradation kinetics of peroxidase enzyme, phenolic content, and physical and sensorial characteristics in broccoli (*Brassica oleracea* L. ssp. *Italica*) during blanching. *Journal of Agricultural and Food Chemistry*, *57*(12), 5370-5375. https://doi.org/10.1021/jf900314x
15. Hajji, W., Bellagha, S., Allaf, K. (2020). Efect of partial drying intensity, frozen storage and repeated freezethaw cycles on some quality attributes of dehydrofrozen quince fruit. *Journal of Food Measurement and Characterization, 14*, 353–365. https://doi.org/10.1007/s11694-019-00297-z
16. Huang, D., Yang, P., Tang, X., Luo, L., Sunden, B. (2021). Application of infrared radiation in the drying of food products. *Trends in Food Science & Technology*, *110*, 765–777. https://doi.org/10.1016/j.tifs.2021.02.039
17. Irondi, E.A., Akintunde, J.K., Agboola, S.O., Boligon, A.A., Athayde, M.L. (2017). Blanching influences the phenolics composition, antioxidant activity, and inhibitory effect of *Adansonia digitata* leaves extract on α-amylase, α-glucosidase, and aldose reductase. *Food Science & Nutrition, 5*(2), 233–242. https://doi.org/10.1002/fsn3.386
18. Kriaa, K., Nassar, A.F. (2022). Comparative study of pretreatment on microwave drying of Gala apples (*Malus pumila*): Effect of blanching, electric field and freezing. *LWT – Food Science and Technology, 165*, art. no. 113693. https://doi.org/10.1016/j.lwt.2022.113693
19. Lagnika, C., Amoussa, A.M.O., Sanni, A., Lagnika, L. (2019). Effect of blanching and ultrasound on drying time, physicochemical and bioactive compounds of dried cashew apple. *American Journal of Food Science and Technology, 7*(6), 227-233.
20. Li, X., Sun, J., He, Y., Zhang, J., Tang, W., Lai, F., Chen, G. (2025). Ultrasound and freeze-thaw pretreatments alter cell wall structure and water status to improve vacuum freeze-drying efficiency and quality attributes of plums. *Journal of Food Science, 90*(11), art. no. e70674. https://doi.org/10.1111/1750-3841.70674
21. Lin, D., Xiao, M., Zhao, J., Li, Z., Xing, B., Li, X., Kong, M., Li, L., Zhang, Q., Liu, Y., Chen, H., Qin, W., Wu, H., Chen, S. (2016). An overview of plant phenolic compounds and their importance in human nutrition and management of type 2 diabetes. *Molecules, 21*(10), art. no. 1374. https://doi.org/10.3390/molecules21101374
22. Liu, Y., Miao, S., Wu, J., Liu, J., Yu, H., Duan, X. (2015). Drying characteristics and modeling of vacuum far-infrared radiation drying of *Flos Lonicerae*. *Journal of Food Processing and Preservation, 39*, 338-348. https://doi.org/10.1111/jfpp.12237
23. Llavata, B., García-Pérez, J.V., Simal, S., Cárcel, J.A. (2020). Innovative pre-treatments to enhance food drying: A current review. *Current Opinion in Food Science, 35*, 20–26. https://doi.org/10.1016/j.cofs.2019.12.001
24. Martins, A.F.L., Vieira, É.N.R., de Leite Júnior, B.R.C., Ramos, A.M. (2022). Use of ultrasound and ethanol to improve the drying of yacon potato (*Smallanthus sonchifolius*): Effect of chemical and thermal bleaching. *LWT – Food Science and Technology, 162*, art. no. 113448. https://doi.org/10.1016/j.lwt.2022.113448
25. Maskan, M. (2001). Kinetics of colour change of kiwifruits during hot air and microwave drying. *Journal of Food Engineering, 48*(2), 169–175. https://doi.org/10.1016/S0260-8774(00)00154-0

26. Miano, A.C., Rojas, M.L., Augusto, P.E.D. (2021). Combining ultrasound, vacuum and/or ethanol as pretreatments to the convective drying of celery slices. *Ultrasonics Sonochemistry, 79*, art. no. 105779. **https://doi.org/10.1016/j.ultsonch.2021.105779**
27. Miletić, N., Mitrović, O., Popović, B., Nedović, V., Zlatković, B., Kandić, M. (2013). Polyphenolic content and antioxidant capacity in fruits of plum (*Prunus domestica* L.) cultivars "Valjevka" and "Mildora" as influenced by air drying. *Journal of Food Quality, 36*, 229–237. **https://doi.org/10.1111/jfq.12035**
28. Oliveira, S.M., Brandão, T.R.S., Silva, C.L.M. (2016). Influence of drying processes and pretreatments on nutritional and bioactive characteristics of dried vegetables: A review. *Food Engineering Reviews,* 8, 134–163. **https://doi.org/10.1007/s12393-015-9124-0**
29. Ozdemirli, N., Kamiloglu, S. (2024). Influence of industrial blanching, cutting, and freezing treatments on *in vitro* gastrointestinal digestion stability of orange (*Citrus sinensis* L.) and lemon (*Citrus limon* L.) peel polyphenols. *Journal of the Science of Food and Agriculture, 104*(4), 2165-2173. **https://doi.org/10.1002/jsfa.13101**
30. Re, R., Pellegrini, N., Proteggente, A., Pannala, A., Yang, M., Rice-Evans, C. (1999). Antioxidant activity applying an improved ABTS radical cation decolorization assay. *Free Radical Biology and Medicine*, *26*(9-10), 1231–1237. **https://doi.org/10.1016/S0891-5849(98)00315-3**
31. Ren, M., Ren, Z., Chen, L., Zhou, C., Okonkwo, C.E., Mujumdar, A.S. (2022). Comparison of ultrasound and ethanol pretreatments before catalytic infrared drying on physicochemical properties, drying, and contamination of Chinese ginger (*Zingiber officinale* Roscoe). *Food Chemistry, 386*, art. no. 132759. **https://doi.org/10.1016/j.foodchem.2022.132759**
32. Shapla, U.M., Solayman, M., Alam, N., Khalil, M.I., Gan, S.H. (2018). 5-Hydroxymethylfurfural (HMF) levels in honey and other food products: Effects on bees and human health. *Chemistry Central Journal, 12*, art. no. 35. **https://doi.org/10.1186/s13065-018-0408-3**
33. Sharma, R., Joshi, V.K., Rana, J.C. (2011). Nutritional composition and processed products of Quince (*Cydonia oblonga* Mill.). *Indian Journal of Natural Products and Resource, 2*(3), 354-357.
34. Singleton, V.L., Rossi, J.A. (1965). Colorimetry of total phenolics with phosphomolybdic-phosphotungstic acid reagents. *American Journal of Enology and Viticulture*, *16*(3), 144–158. **https://doi.org/10.5344/ajev.1965.16.3.144**
35. Sun, B., Ricardo-da-Silva, J.M., Spranger, I. (1998). Critical factors of vanillin assay for catechins and proanthocyanidins. *Journal of Agricultural and Food Chemistry*, *46*(10), 4267–4274. **https://doi.org/10.1021/jf980366j**
36. Topuz, F.C., Uğurlu, S., Bakkalbaşı, E. (2023). Comparison of a novel vacuum-combined infrared and hot-air convection methods for drying of deveci (*Pyrus communis* L.) pear slices. *Latin American Applied Research*, *53*(4), 317-325. **https://doi.org/10.52292/j.laar.2023.1200**
37. Topuz, F.C., Uğurlu, S., Bakkalbaşı, E. (2025). Investigation of the effect of immersion and ultrasound pretreatments on some quality characteristics of pears dried in vacuum-assisted double-sided infrared dryer. *Yuzuncu Yil University Journal of Agricultural Sciences, 35*(2), 188-204. **https://doi.org/10.29133/yyutbd.1608726**
38. Uğurlu, S., Bakkalbaşı, E. (2024). A comparison of phenolic compounds, antioxidant activity, and αglucosidase inhibitory activities of apple chips dried and fried by vacuum combined infrared radiation. *Journal of Food Measurement and Characterization, 18,* 3783–3792. **https://doi.org/10.1007/s11694-024-02453-6**
39. Vitali, D., Dragojević, I.V., Šebečić, B. (2009). Effects of incorporation of integral raw materials and dietary fibre on the selected nutritional and functional properties of biscuits. *Food Chemistry, 114*(4), 1462–1469. **https://doi.org/10.1016/j.foodchem.2008.11.032**
40. Wang, P., Lv, W., Wang, H. (2025). Effects of freeze-thawing, blanching, and ultrasound pretreatments on drying efficiency and quality of quince peels. *Journal of Food Science, 90*(2), art. no. e70024. **https://doi.org/10.1111/1750-3841.70024**
41. Wang, X., Feng, Y., Zhou, C., Sun, Y., Wu, B., Yagoub, A.E.A., Aboagarib, E.A.A. (2019). Effect of vacuum and ethanol pretreatment on infrared-hot air drying of scallion (*Allium fistulosum*). *Food Chemistry, 295*, 432-440. **https://doi.org/10.1016/j.foodchem.2019.05.145**
42. Xiao, H.W., Pan, Z., Deng, L.Z., El-Mashad, H.M., Yang, X.H., Mujumdar, A.S., Gao, Z.J., Zhang, Q. (2017). Recent developments and trends in thermal blanching – A comprehensive review. *Information Processing in Agriculture, 4*(2), 101–127. **http://dx.doi.org/10.1016/j.inpa.2017.02.001**
43. Xu, H., Guan, Y., Shan, C., Xiao, W., Wu, M. (2023). Development of thermoultrasound assisted blanching to improve enzyme inactivation efficiency, drying characteristics, energy consumption, and physiochemical properties of sweet potatoes. *Ultrasonics Sonochemistry, 101*, art. no. 106670. **https://doi.org/10.1016/j.ultsonch.2023.106670**
44. Xu, X., Zhang, L., Feng, Y., Zhou, C., Yagoub, A.E.A., Wahia, H., Ma, H., Zhang, J., Sun, Y. (2021). Ultrasound freeze-thawing style pretreatment to improve the efficiency of the vacuum freeze-drying of okra (*Abelmoschus esculentus* (L.) Moench) and the quality characteristics of the dried product. *Ultrasonics Sonochemistry, 70*, art. no. 105300. **https://doi.org/10.1016/j.ultsonch.2020.105300**
45. Zhang, Y., Yang, Z., Liu, G., Wu, Y., Ouyang, J. (2020). Inhibitory effect of chestnut (*Castanea mollissima* Blume) inner skin extract on the activity of α-amylase, α-glucosidase, dipeptidyl peptidase IV and *in vitro* digestibility of starches. *Food Chemistry, 324*, art. no. 126847. **https://doi.org/10.1016/j.foodchem.2020.126847**
46. Zhishen, J., Mengcheng, T., Jianming, W. (1999). The determination of flavonoid contents in mulberry and their scavenging effects on superoxide radicals. *Food Chemistry, 64*(4), 555–559. **https://doi.org/10.1016/S0308-8146(98)00102-2**
47. Zhu, R., Jiang, S., Li, D., Law, C.L., Han, Y., Tao, Y., Kiani, H., Liu, D. (2022). Dehydration of apple slices by sequential drying pretreatments and airborne ultrasound-assisted air drying: Study on mass transfer, profiles of phenolics and organic acids and PPO activity. *Innovative Food Science & Emerging Technologies, 75*, art. no. 102871. **https://doi.org/10.1016/j.ifset.2021.102871**

INSTRUCTIONS FOR AUTHORS

SUBMISSION. Original contributions relevant to food and nutrition sciences are accepted on the understanding that the material has not been, nor is being, considered for publication elsewhere. All papers should be submitted and will be processed electronically via Editorial Manager system (available from PJFNS web site: http://journal.pan.olsztyn.pl). On submission, a corresponding author will be asked to provide: Cover letter; Files with Manuscripts, Tables, Figures/Photos; and Names of two potential reviewers (one from the author's homeland – but outside author's Institution, and the other from abroad). All papers which have been qualified as relevant with the scope of our Journal are reviewed. All contributions, except the invited reviews are charged. Proofs will be sent to the corresponding author and should be returned within one week since receipt. No new material may be inserted in the text at proof stage. It is the author's duty to proofread proofs for errors.

Authors should very carefully consider the preparation of papers to ensure that they communicate efficiently, because it permits the reader to gain the greatest return for the time invested in reading. Thus, we are more likely to accept those that are carefully designed and conform the instruction. Otherwise, papers will be rejected and removed from the online submission system.

SCOPE. The Polish Journal of Food and Nutrition Sciences publishes original, basic and applied papers, and reviews on fundamental and applied food research, preferably these based on a research hypothesis, in the following Sections:

Food Technology:
- Innovative technology of food development including biotechnological and microbiological aspects
- Effects of processing on food composition and nutritional value

Food Chemistry:
- Bioactive constituents of foods
- Chemistry relating to major and minor components of food
- Analytical methods

Food Quality and Functionality:
- Sensory methodologies
- Functional properties of food
- Food physics
- Quality, storage and safety of food

Nutritional Research:
- Nutritional studies relating to major and minor components of food (excluding works related to questionnaire surveys)

"News" section:
- Announcements of congresses
- Miscellanea

OUT OF THE SCOPE OF THE JOURNAL ARE:
- Works which do not have a substantial impact on food and nutrition sciences
- Works which are of only local significance i.e. concern indigenous foods, without wider applicability or exceptional nutritional or health related properties
- Works which comprise merely data collections, based on the use of routine analytical or bacteriological methods (i.e. standard methods, determination of mineral content or proximate analysis)
- Works concerning biological activities of foods but not providing the chemical characteristics of compounds responsible for these properties
- Nutritional questionnaire surveys
- Works related to the characteristics of foods purchased at local markets
- Works related to food law
- Works emphasizing effects of farming / agricultural conditions / weather conditions on the quality of food constituents
- Works which address plants for non-food uses (i.e. plants exhibiting therapeutic and/or medicinal effects)

TYPES OF CONTRIBUTIONS. *Reviews*: (at least: 30 pages and 70 references) these are critical and conclusive accounts on trends in food and nutrition sciences; *Original papers*: (maximally: 30 pages and 40 references) these are reports of substantial research; *Reports on post and forthcoming scientific events, and letters to the Editor* (all up to three pages) are also invited (free of charge).

REVIEW PROCESS. All scientific contributions will be peer-reviewed on the criteria of originality and quality. Submitted manuscripts will be preevaluated by Editor-in-Chief and Statistical Editor (except for review articles), and when meeting PJFNS' scope and formal

requirements, they will be sent to a Section Editor who upon positive preevaluation will assign at least two reviewers from Advisory Board Members, reviewers suggested by the author or other experts in the field. Based on the reviews achieved, Section Editor and Editor-in--Chief will make a decision on whether a manuscript will be accepted for publication, sent back to the corresponding author for revision, or rejected. Once a manuscript is sent back to the corresponding author for revision, all points of the reviews should be answered or rebuttal should be provided in the Explanation letter. The revised manuscripts will be checked by Section Editor and by the original reviewers (if necessary), and a final decision will be made on acceptance or rejection by both Section Editor and Editor-in-Chief.

Polish Journal of Food and Nutrition Sciences uses CrossCheck's iThenticate software to detect instances of similarity in submitted manuscripts. In publishing only original research, PJFNS is committed to deterring plagiarism, including self-plagiarism.

COPYRIGHT LICENSE AGREEMENT referring to Authorship Responsibility and Acknowledgement, Conflict of Interest and Financial Disclosure, Copyright Transfer, are required for all authors, i.e. *Authorship Responsibility and Acknowledgement*: Everyone who has made substantial intellectual contributions to the study on which the article is based (for example, to the research question, design, analysis, interpretation, and written description) should be an author. It is dishonest to omit mention of someone who has participated in writing the manuscript ("ghost authorship") and unfair to omit investigator who have had important engagement with other aspects of the work. All contributors who do not meet the criteria for authorship should be listed in an Acknowledgments section. Examples of those who might be acknowledged include a person who provided purely technical help, writing assistance, or a department chairperson who provided only general support. Any financial and material support should also be acknowledged. *Conflict of Interest and Financial Disclosure*: Authors are responsible for disclosing financial support from the industry or other conflicts of interest that might bias the interpretation of results. *License to Publish*: All articles published on the website of Polish Journal of Food and Nutrition Sciences are available in the Open Access format, meaning they are freely accessible online without charge to anyone, anywhere.

Since volume 75, Authors publish their works under the Creative Commons Attribution 4.0 License (CC BY 4.0). Pursuant to the License terms, Authors retain the copyright and full publishing rights without restrictions. The License permits unrestricted use, distribution and reproduction, provided that the original work is cited. The specific license terms of use are available on https://creativecommons.org/licenses/by/4.0/

In volumes 64–74, Authors published their works under the Creative Commons Attribution-NonCommercial-NoDerivs Licenses (CC BY-NC-ND) 3.0 and 4.0, pursuant to which they retained the copyright, and other proprietary rights relating to the article, such as patent rights, to use the substance of the article in future own works, including lectures and books, to reproduce the article for own purposes, provided the copies are not intended for commercial re-use or for share of the adapted and derivative versions. The specific license terms of use are available on http://creativecommons.org/licenses/by-nc-nd/3.0 and http://creativecommons.org/licenses/by-nc-nd/4.0.

In earlier volumes (47–63), Authors published their works under Copyright Transfer License, pursuant to which they retained the right to revise, adapt, prepare derivative works, present orally, or distribute the work provided that all such use was for the personal noncommercial benefit of the author(s) and was consistent with any prior contractual agreement between the publisher and authors.

A manuscript will not be published once the signed form has not been submitted to the Editor with the manuscript revised after positive reviews.

CHANGES TO AUTHORHIP. Authors are expected to consider carefully the list and order of authors before submitting their manuscript and provide the definitive list of authors at the time of the original submission. Any addition, deletion or rearrangement of author names in the authorship list should be made only before the manuscript has been accepted and only if approved by the journal Editor. To request such a change, the Editor must receive the following from the corresponding author: (a) the reason for the change in author list and (b) written confirmation (e-mail, letter) from all authors that they agree with the addition, removal or rearrangement. In the case of addition or removal of authors, this includes confirmation from the author being added or removed.

ETHICAL APPROVAL OF STUDIES AND INFORMED CONSENT. For all manuscripts reporting data from studies involving human participants or animals, formal approval by an appropriate institutional review board or ethics committee is required and should be described in the Methods section. For those investigators who do not have formal approval from ethics review committees, the principles outlined in the Declaration of Helsinki should be followed. For investigations of humans, state in the Methods section the manner in which informed consent was obtained from the study participants (i.e., oral or written). Editors may request that authors provide documentation of the formal review and recommendation from the institutional review board or ethics committee responsible for oversight of the study.

UNAUTHORIZED USE. Unauthorized use of the PJFNS name, logo, or any content for commercial purposes or to promote commercial goods and services (in any format, including print, video, audio, and digital) is not permitted by IAR&FR PAS.

MANUSCRIPTS. A manuscript in English must be singlesided, preferably in Times New Roman (12) with 1.5-point spacing, without numbers of lines. The Editor reserves the right to make literary corrections and to make suggestions to improve brevity. English is the official language. The English version of the paper will be checked by Language Editor. Unclear and unintelligible version will be returned for correction.

Every paper should be divided under the following headings in this order: a **Title** (possibly below 150 spaces); the **Name(s)** of the author(s) in full. In paper with more than one author, the asterisk indicates the name of the author to whom correspondence and inquiries should be addressed, otherwise the first author is considered for the corre-spondence. Current full postal address of the indicated corresponding author or the first author must be given in a footnote on the title page; the **Place(s)** where the work was done including the institution name, city, country if not Poland. In papers originated from several institu-tions the names of the authors should be marked with respective superscripts; the **Key words** (up to 6 words or phrases) for the main topics of the paper; an **Abstract** (up to 250 words for regular papers and reviews) summarizing briefly main results of the paper, no literature references; an **Introduction** giving essential background by saying why the research is important, how it relates to previous works and stating clearly the objectives at the end; **Materials and Methods** with

sufficient experimental details permitting to repeat or extend the experiments. Literature references to the methods, sources of material, company names and location (city, country) for specific instruments must be given. Describe how the data were evaluated, including selection criteria used; **Results and Discussion** presented together (in one chapter). Results should be presented concisely and organized to supplement, but not repeat, data in tables and figures. Do not display the data in both tabular and graphic form. Use narrative form to present the data for which tables or figures are unnecessary. Discussion should cover the implications and consequences, not merely recapitulating the results, and it must be accomplished with concise **Conclusions**; **Acknowledgements** should be made to persons who do not fill the authorship criteria (see: Authorship forms); **Research funding** should include financial and material support; **Conflict of Interests**: Authors should reveal any conflicts of interest that might bias the interpretation of results; **Other information** including Generative AI use declaration and other important information (See Editorial Policy section for details on the journal website). **References** as shown below.

REFERENCES each must be listed alphabetically at the end of the paper (each should have an Arabic number in the list) in the form as follows: **Periodicals** – names and initials of all the authors, year of publication, title of the paper, journal title as in Chemical Abstracts, year of publication, volume, issue, inclusive page numbers, or article id.; **Books** – names and initials of all the authors, names of editors, chapter title, year of publication, publishing company, place of publication, inclusive page numbers; **Patents** – the name of the application, the title, the country, patent number or application number, the year of publication.

For papers published in language other than English, manuscript title should be provided in English, whereas a note on the original language and English abstract should be given in parentheses at the end.

The reference list should only include peer-reviewed full-text works that have been published or accepted for publication. Citations of MSc/PhD theses and works unavailable to international Editors, Reviewers, and Readers should be limited as much as possible.

References in the text must be cited by name and year in square parentheses (e.g.: one author – [Tokarz, 1994]; two authors – [Słonimski & Campbell, 1987]; more than two authors – [Amarowicz *et al*., 1994]). If more than one paper is published in the same year by the same author or group of authors use [Tokarz, 1994a, b]. Unpublished work must only be cited where necessary and only in the text by giving the person's name.

Examples:

Article in a journal:

Słonimski, B.A., Campbell, L.D., Batista, E., Howard B. (2008). Gas chromatographic determination of indole glucosinolates. Journal of Science and Food Agriculture, 40(5), 131–143.

Asher, A., Tintle, N.L., Myers, M., Lockshon, L., Bacareza, H., Harris, W.S. (2021). Blood omega-3 fatty acids and death from COVID-19: A pilot study. *Prostaglandins, Leukotrienes and Essential Fatty Acids, 166*, art. no. 102250.

Book: Weber, W., Ashton, L., Milton, C. (2012). Antioxidants – Friends or Foes? 2nd editition. PBD Publishing, Birmingham, UK. pp. 218–223.
Chapter in a book: Uden, C., Gambino, A., Lamar, K. (2016). Gas chromatography. In M. Queresi, W. Bolton (Eds.), CRC Handbook of Chromatography, CRC Press Inc., Boca Raton, Florida, USA, pp. 44–46.

ABBREVIATIONS AND UNITS. Abbreviations should only be used when long or unwieldy names occur frequently, and never in the title; they should be given at the first mention of the name. Metric SI units should be used. The capital letter L should be used for liters. Avoid the use of percentages (% g/g,% w/w; Mol%; vol%), ppm, ppb. Instead, the expression such as g/kg, g/L, mg/kg, mg/mL should be used. A space must be left between a number and a symbol (e.g. 50 mL not 50mL). A small x must be used as multiplication sign between numeric values (e.g. 5 × 102 g/mL). Statistics and measurements should be given in figures, except when the number begins a sentence. Chemical formulae and solutions must specify the form used. Chemical abbreviations, unless they are internationally known, Greek symbols and unusual symbols for the first time should be defined by name. Common species names should be followed by the Latin at the first mention, with contracting it to a single letter or word for subsequent use.

FIGURES should be submitted in separate files. Each must have an Arabic number and a caption. Captions of all Figures should be provided on a separate page "Figure Captions". Figures should be comprehensible without reference to the text. Self-explanatory legend to all figures should be provided under the heading "Legends to figures"; all abbreviations appearing on figures should be explained in figure footnotes. Three-dimensional graphs should only be used to illustrate real 3D relationships. Start the scale of axes and bars or columns at zero, do not interrupt them or omit missing data on them. Figures must be cited in Arabic numbers in the text.

TABLES should be submitted in separate files. They should be as few in number and as simple as possible (like figures, they are expensive and space consuming), and include only essential data with appropriate statistical values. Each must have an Arabic number and a caption. Captions of all Tables should be provided on a separate page "Table Captions". Tables should be self-explanatory; all abbreviations appearing in tables should be explained in table footnotes. Tables must be cited in Arabic numbers in the text.

PUBLICATION FEE. Since 16th December 2024, a standard publication fee has been established at the rate of 500 EUR (plus VAT if applicable, e.g. for private persons). For Polish Authors an equivalent fee was set at 1950 PLN +23%VAT. The fee applies irrespective of the number of pages and tables/figures in the manuscript. Payment instructions will be sent to Authors via e-mail with acceptance letter.

Information on publishing and subscription is available from:

Ms. Joanna Molga
Editorial Office of Pol. J. Food Nutr. Sci.
InLife Institute of Animal Reproduction and Food Research, Polish Academy of Sciences, Trylińskiego 18, 10-683 Olsztyn, Poland
phone (48 89) 500 32 45
e-mail: pjfns@pan.olsztyn.pl; http://journal.pan.olsztyn.pl

Nutrition